SEISMIC PERFORMANCE OF RE-CENTRING DUAL ECCENTRICALLY BRACED FRAMES WITH REMOVABLE LINKS

Teză destinată obţinerii
titlului ştiinţific de doctor inginer
la
Universitatea Politehnica Timişoara
în domeniul INGINERIE CIVILĂ
de către

Ing. Mirela Adriana Ioan

Conducător ştiinţific:	Prof.dr.ing. Dr.H.C. Dan Dubină M.C. al Academiei Române
Referenţi ştiinţifici:	Prof.univ.dr.ing. Andre Plumier Prof.univ.dr.ing. Dan Lungu Conf.univ.dr.ing. Aurel Stratan

Ziua susţinerii tezei: 26 Martie 2015

Seriile Teze de doctorat ale UPT sunt:

1. Automatică
2. Chimie
3. Energetică
4. Ingineria Chimică
5. Inginerie Civilă
6. Inginerie Electrică
7. Inginerie Electronică şi Telecomunicaţii
8. Inginerie Industrială
9. Inginerie Mecanică
10. Ştiinţa Calculatoarelor
11. Ştiinţa şi Ingineria Materialelor
12. Ingineria sistemelor
13. Inginerie energetică
14. Calculatoare şi tehnologia informaţiei
15. Ingineria materialelor
16. Inginerie şi Management

Universitatea Politehnica Timişoara a iniţiat seriile de mai sus în scopul diseminării expertizei, cunoştinţelor şi rezultatelor cercetărilor întreprinse în cadrul Şcolii doctorale a universităţii. Seriile conţin, potrivit H.B.Ex.S Nr. 14 / 14.07.2006, tezele de doctorat susţinute în universitate începând cu 1 octombrie 2006.

România, 300159 Timişoara, Bd. Republicii 9,
Tel./fax 0256 403823
e-mail: editura@edipol.upt.ro

Acknowledgements

The thesis was developed during my activity (2010 - 2015) within the Department of Steel Structures and Structural Mechanics (CMMC) and the Centre of Excellence in the Mechanics of Materials and Safety of Structures (CEMSIG), from the Politehnica University Timişoara.

First of all, I would like to thank my parents who guided me in the process of my education and loved me very much, helping me to become the person that I am today. I am very grateful for the support and patience that I have received from my husband throughout the years of the PhD studies.

I would like to express my gratitude towards my advisor and PhD coordinator, Prof. Dr. Ing. Dr. H.C. Dan Dubina, for sharing his knowledge and experience, and for his support and guidance throughout my research activity. I would also like to thank him for involving me in "DUAREM" research project – which represented the research framework of the thesis, and during which I have met remarkable personalities in the field and was able to work with researchers from all over Europe.

My deep gratitude to Assoc. Prof. Dr. Ing. Aurel Stratan for providing support when I needed it most during my work, and for taking such an interest in my overall personal growth and success.

My sincere thanks to ELSA-JRC research team: Martin Poljansek, Fabio Taucer, Pierre Pegon, Francisco-Javier Molina, Daniel Tirelli, Bernard Viaccoz, for their collaboration and support during the experimental programme, as well as to my younger colleague, Gabriel Sabău.

I would also like to thank Prof. Dr. Ing. Daniel Grecea, Prof. Dr. Ing. Florea Dinu, Prof. Dr. Ing. Viorel Ungureanu, Prof. Dr. Ing. Raul Zaharia, Assoc. Prof. Dr. Ing. Adrian Ciutina, for their observations and suggestions throughout the PhD stage. Thanks also to my colleagues, Cristi Vulcu, Carla Toduţ and Ionel Mărginean, for their help related to administrative aspects, and to Călin Neagu and Ovidiu Abrudan for their help related to laboratory work.

Timişoara, March 2015 ing. Mirela Adriana Ioan

This work was partially supported by the strategic grant POSDRU/159/1.5/S/137070 (2014) of the Ministry of National Education, Romania, co-financed by the European Social Fund – Investing in People, within the Sectorial Operational Programme Human Resources Development 2007-2013.

Ioan, Mirela Adriana

Seismic performance of re-centring dual eccentrically braced frames with removable links

(Performanţa seismică a structurilor în cadre duale contravântuite excentric cu bare disipative demontabile și capacitate de re-centrare)

Teze de doctorat ale UPT, Seria 5, Nr. 132, Editura Politehnica, 2015, 222 pagini, 234 figuri, 48 tabele.

ISSN: 1842-581X
ISBN: 978-606-554-929-6

Keywords:
eccentrically braced frames, dual structures, removable links, re-centring capability, seismic performance, experimental validation, numerical investigation.

Abstract:
The thesis research aims at reducing the repair costs and downtime of a structure hit by an earthquake, and consequently more rational design approach in the context of sustainability. These objectives are attained through removable dissipative members and re-centring capability of the structure. The concepts of removable dissipative members and re-centring capability are implemented in a dual structure, obtained by combining steel eccentrically braced frames with removable bolted links with moment resisting frames. The bolted links are intended to provide the energy dissipation capacity and to be easily replaceable, while the more flexible moment resisting frames would provide the necessary re-centring capability to the structure. The columns are realised from high strength steel, in order to keep these members in the elastic range even under strong seismic input.
The test structure was designed according to European codes and was numerically investigated. The validation of re-centring capability and link replacement procedure in a dual eccentrically braced structure, together with assessing its seismic performance, was realised through pseudo-dynamic tests of the full-scale experimental specimen performed at the European Laboratory for Structural Assessment (ELSA) facility at Joint Research Centre (JRC) in Ispra, Italy, where access was granted by FP7 SERIES Project „Full-scale experimental validation of dual eccentrically braced frame with removable links" (DUAREM). Other structural configurations of dual eccentrically braced frames with removable links were analysed in order to extend the experimental specimen behaviour to more general, current practice structures.

Table of contents

Notations, abbreviations & acronyms

Notations

Chapter 2

ρ_{PTE}	Initial cable prestressing ratio;
f_{yDE}	Dissipative Elements yielding stress;
δ_{pD}	Permanent displacement of dual system;
δ_{pr}	Permanent displacement of rigid system;
F_{pf}	Residual force of flexible subsystem;
F_{pr}	Residual force of rigid subsystem;

Chapter 3

q	Behaviour factor;
e	Length of seismic link;
e_s	Ratio used for classifying short seismic links;
$M_{p,link}$	Design value of plastic moment resistance of seismic link;
$V_{p,link}$	Design value of plastic shear force resistance of seismic link;
A_s*	Equivalent reduced shear area that accounts for the flexibility of bolted link;
γ	Bolted link web shear deformation;
γ_M	Bolted link bending deformation;
θ	Rotation of bolted link to beam connection;
Δ_s	Slip in bolted link to beam connection;
K_T^*	Equivalent stiffness of the removable link;
G	Transversal elasticity modulus;
K_γ	Shear stiffness of the link's web;
K_θ	Stiffness component due to the rotation in the link-beam connection;
K_s	Stiffness component due to the slip in the link-beam connection;
$V_{j,Ed}$	Design value of the shear force of link to beam connection;
$M_{j,Ed}$	Design value of the bending moment of link to beam connection;
γ_{ov}	Material over-strength factor;
Ω	Multiplicative over-strength factor;
G_k	Characteristic value of permanent action;
Q_k	Characteristic value of variable action;
Ψ_2	Factor for quasi-permanent value of a variable action;
δ_u	Ultimate shear deformation of seismic link;

a_{gr}	Reference peak ground acceleration;
a_g	Peak ground acceleration for a specific earthquake level;
D_t	Target displacement computed using N2 method;
T_C	Response spectrum control period;
T_1	Fundamental (first mode) period of the structure;
F_y^{MRF}	Yield strength of moment resisting frame;
F_y^{EBF}	Yield strength of eccentrically braced frame;
$M_{pl,b}$	Plastic moment resistance of moment resisting frame beam;
L	Frame span;
H	Frame height;
δ_u^{EBF}	Ultimate displacement of eccentrically braced frame;
$\gamma_{pl,u}$	Seismic link plastic deformation capacity;
δ_y^{MRF}	Yield displacement of moment resisting frame;
δ_y^{EBF}	Yield displacement of eccentrically braced frame;
δ_{pl}^{EBF}	Plastic displacement of eccentrically braced frame;
K^{EBF}	Eccentrically braced frame stiffness;
K_{link}^{EBF}	Eccentrically braced frame link's stiffness;
K_{br}^{EBF}	Eccentrically braced frame braces stiffness;
A_s	Seismic link shear area;
E	Young's modulus;
A	Eccentrically braced frame brace cross-section area;
l_{br}	Eccentrically braced frame brace length;
K^{MRF}	Moment resisting frame stiffness;
F_D	Nonlinear damping force;
c	Damping coefficient;
v	Velocity
α	Damping exponent.

Chapter 4

a_0	Steel sample thickness;
b_0	Steel sample width;
S_0	Steel sample cross-section area;
L_0	Original steel sample length;
L_c	Parallel steel sample length;
L_t	Total steel sample length;
f_y	Yield strength;
R_{eH}	Yield strength to product standards;
R_{p02}	Yield strength;
f_u	Ultimate strength;

R_m	Ultimate strength to product standards;
A	Elongation at fracture;
$M_{r,1}$	Reference torque value;
$F_{p,C}$	Normal minimum preloading force;
G_k	Total permanent load;
G_{ksm}	Self-weight of structural members;
G_{krc}	Self-weight of the reinforced concrete slab, including steel sheeting;
G_{ka}	Additional permanent load;
Q_k	Variable load;
a_{gr}	Reference peak ground acceleration (corresponding to 10% / 50 years earthquake);
a_g	Peak ground acceleration for a specific earthquake level;
M	Mass matrix;
a(t)	Internal (restoring) acceleration vector;
C	Viscous damping matrix;
v(t)	Internal (restoring) velocity vector;
r(t)	Internal (restoring) force vector;
f(t)	External force vector applied on the structure;
γ	Plastic deformation of link;
a	Vertical distance between the ends of link transducers;
b	Horizontal distance between the ends of link transducers;
θ_j	Beam to column joint zone rotation;
I_b	Rotation measured by the inclinometer placed on the beam;
$I_{s,u}$	Rotation measured by the inclinometer placed on the upper column;
$I_{s,l}$	Rotation measured by the inclinometer placed on the lower column;
V_{link}	Link shear force from experimental tests;
N_{br}	Axial force of the eccentrically braced frame braces;
α	Eccentrically braced frame braces angle with the vertical axis;
σ_{br}	Stress of the eccentrically braced frame braces;
A_{br}	Area of the eccentrically braced frame braces;
ε_{br}	Strain of the eccentrically braced frame braces measured with strain gauges;
E	Young modulus for steel;
H	Total height of the structure.

Chapter 5

q	Behaviour factor;
e	Length of seismic link;
e_s	Ratio used for classifying short seismic links;
$M_{p,link}$	Design value of plastic moment resistance of seismic link;

$V_{p,link}$	Design value of plastic shear force resistance of seismic link;
A_s*	Equivalent reduced shear area that accounts for the flexibility of bolted link;
γ	Bolted link web shear deformation;
γ_M	Bolted link bending deformation;
θ	Rotation of bolted link to beam connection;
K_T*	Equivalent stiffness of the removable link;
G	Transversal elasticity modulus;
K_γ	Shear stiffness of the link's web;
K_θ	Stiffness component due to the rotation in the link-beam connection;
a_{gr}	Reference peak ground acceleration;
a_g	Peak ground acceleration for a specific earthquake level;
D_t	Target displacement computed using N2 method;
T_C	Response spectrum control period;
T_1	Fundamental (first mode) period of the structure;
T_2	Second mode period of the structure;
F_y^{MRF}	Yield strength of moment resisting frame;
F_y^{EBF}	Yield strength of eccentrically braced frame;
$M_{pl,b}$	Plastic moment resistance of moment resisting frame beam;
L	Frame span;
H	Frame height;
δ_u^{EBF}	Ultimate displacement of eccentrically braced frame;
$\gamma_{pl,u}$	Seismic link plastic deformation capacity;
δ_y^{MRF}	Yield displacement of moment resisting frame;
K^{EBF}	Eccentrically braced frame stiffness;
K_{link}^{EBF}	Eccentrically braced frame link's stiffness;
K_{br}^{EBF}	Eccentrically braced frame braces stiffness;
E	Young's modulus;
A	Eccentrically braced frame brace cross-section area;
l_{br}	Eccentrically braced frame brace length;
K^{MRF}	Moment resisting frame stiffness;
λ	Seismic action amplifier;
q_d	Design behaviour factor;
λ_u	Seismic action amplifier corresponding to the ultimate link rotation;
λ_d	Seismic action amplifier corresponding to the level of seismic action used in design (in case of time-history analysis with 2% damping);
q	Effective behaviour factor;
λ_1	Seismic action amplifier corresponding to yield rotation in links;
$\lambda_{d,sp}$	Seismic action amplifier corresponding to the level of seismic action used in design (in case of spectral analysis with 5% damping);

$V_{s,SP}$	Design base shear force from spectral analysis (5% damping);
$V_{d,TH}$	Design base shear force from a linear time-history analysis (2% damping) with a 0.25 amplifier;
Ω_d	Design over-strength;
Ω_t	Total over-strength;
Ω_S	Structure's over-strength;
V_u	Base shear force corresponding to ultimate link rotation;
V_d	Design base shear force (from spectral analysis);
V_1	Base shear corresponding to yield rotation in links.

Abbreviations

MRF	Moment resisting frame;
EBF	Eccentrically braced frame;
CBF	Concentrically braced frame;
VFD	Viscous fluid damper;
VE	Viscoelastic;
ADAS	Added damping and stiffness (damper);
SMA	Shape memory alloy;
MR	Magnetorheological;
SASD	Semi-active stiffness damper;
TLCD	Tuned liquid column damper;
PZT	Piezoelectric;
SC-MRF	Self-centring moment resisting frame;
SC-CBF	Self-centring concentrically braced frame;
SCED	Self-centring energy-dissipative (device);
SSCD	steel self-centring device;
PT	Post-tensioned;
BRB	Buckling restrained braces;
SMRF	Special moment resisting frame;
SPSW	Steel plate shear walls;
PO	Pushover analysis;
TH	Time-history analysis;
IDA	Incremental Dynamic Analysis;
PGA	Peak ground acceleration;
FO	Full-operational state;
SLS	Serviceability limit state;
DL	Damage limitation state;
ULS	Ultimate limit state;

SD	Significant damage state;
NC	Near collapse state;
EC8	Eurocode 8 (EN1998);
MDOF	Multi-degree-of-freedom (system);
SDOF	Single-degree-of-freedom (system);
EPA	Effective peak ground acceleration;
EPV	Effective peak ground velocity;
2D	Two-dimensional;
3D	Three-dimensional.

Acronyms

DUAREM	"Full-scale experimental validation of dual eccentrically braced frame with removable links" – Research Project;
SERIES	Seismic Engineering Research Infrastructures for European Synergies Project;
ELSA	European Laboratory for Structural Assessment – facility of European's Commission JRC;
JRC	Joint Research Centre – Research Centre of the European Commission;
HSS-SERF	"High Strength Steel in Seismic Resistant Building Frames" – Research Project;
RFCS	Research Fund for Coal and Steel;
INERD	"INnovations for Earthquake Resistant Design" Project;
FUSEIS	"Dissipative devices for seismic resistant steel frames" Project
AISC	American Institute of Steel Construction (http://www.aisc.org/);
CEMSIG	Research centre for Mechanics of Materials and Structural Safety – CEMSIG is a RTD (Research and Technical Development) unit of the Politehnica University of Timisoara, at the faculty of Civil Engineering, Department of Steel Structures and Structural Mechanics;
FEMA	Federal Emergency Management Agency is an agency of the United States Department of Homeland Security (http://www.fema.gov/);
ECCS	European Convention for Constructional Steelwork;
NEHRP	National Earthquake Hazards Reduction Program of the United States.

List of figures

List of tables

REZUMAT

Pentru a reduce costurile de reparație și timpul de nefuncționare al unei structuri în urma unui cutremur și pentru a obtine, în consecință, o abordare de proiectare mai rațională în contextul dezvoltării durabile, conceptele elementelor disipative demontabile si al capacității de recentrare au fost implementate într-o structură dual, obținută prin combinarea cadrelor din oțel contravântuite excentric cu linkuri demontabile cu cadre necontravântuite. Linkurile prinse cu șuruburi sunt menite să asigure capacitatea de disipare a energiei, în timp ce cadrele necontravântuite mai flexibile asigură structurii capacitatea necesară de revenire. Așadar, cu scopul de a evalua performanța seismică a cadrelor duale contravântuite excentric cu linkuri demontabile și a valida capacitatea de recentrare a acestora, cât și procedura de înlocuire a linkurilor, s-au realizat ample investigații numerice în cadrul centrului de cerectare CEMSIG al Universității Politehnica Timișoara și un complex program de încercări experimentale pe o structură la scară reală în cadrul laboratorului ELSA al JRC, din Ispra, Italia. Teza prezintă rezultatele încercărilor experimentale și a analizelor numerice, precum și concluziile principalele ale cercetării şi contribuţiile autorului.

Capitolul 1: Introducere

În primul capitol se face o introducere în tema de cerceare abordată. Sunt prezentate scopul și obiectivele tezei de doctorat, precum și cadrul în care s-a realizat cercetarea, acesta fiind reprezentat de un proiect FP7/2007-2013 al Comunității Europene, din cadrul proiectului SERIES, intitulat DUAREM („Full-scale experimental validation of dual eccentrically braced frame with removable links”).

Capitolul 2: Sisteme structurale care concentrează deformația plastică în elemente de siguranță seismică

Pot fi utilizate diferite strategii în scopul de a reduce deteriorarea structurilor supuse unor cutremure moderate sau puternice. Soluţiile cele mai radicale sunt izolarea bazei şi diferite implementări ale controlului structural activ şi semi-activ. Alte strategii se bazează pe amortizarea suplimentară oferită structurii prin diverse dispozitive bazate pe amortizori vâscoși, de frecare sau de curgere. Mai mult sau mai puţin eficiente pentru reducerea avarierii structurii, toate aceste soluţii au dezavantajul de a necesita cunoştinţe de specialitate în faza de proiectare și in timpul execuției, de a avea nevoie de o întreţinere atenta şi cost initial ridicat. De asemenea, există soluții care asigură autocentrarea structurii, dar sunt exigente din punct de vedere tehnic (toroane post-tensionete, dispozitive cu aliaje de memorie a formei, etc.)

Alternativ, proiectarea convențională poate fi folosită, dar cu elementele disipative realizate ca fiind detașabile (de exemplu, prin îmbinări cu şuruburi), permițând înlocuirea elementelor disipative deteriorate în urma a unui cutremur moderat sau puternic, reducând costurile de reparație. Pentru a putea repara structura, pe lângă concentrarea deformațiilor inelastice în elementele disipative demontabile, deplasările permanente (reziduale) relative de nivel ar trebui să fie eliminate. Această soluție asigură capacitate de recentrare (spre deosebire de

autocentrare), prin intermediul elementelor disipative demontabile și a configurației structurale duale (rigid-flexibil).

Capitolul 3: Proiectarea seismică și investigarea numerică a specimenului experimental

Capitolul trei tratează proiectarea unei structuri prototip duale în cadre contravântuite excentric cu linkuri demontabile. Linkurile din cadrele contravântuite excentric au fost concepute ca elemente disipative demontabile (prinse cu șuruburi) fiind menite să asigure capacitatea de disipare a energiei și să fie ușor de înlocuit. Cadrele necontravântuite care sunt mai flexibile oferă structurii capacitatea necesară de recentrare. Având în vedere că pe direcția transversală sistemul care preia forțele laterale este situat doar perimetral în structura prototip, și pentru a reduce costul specimenului experimental, acesta din urmă este alcătuit doar din cele două cadre marginale. Proiectarea bazată pe capacitate s-a realizat în conformitate cu standardele europene.

În continuare, este evaluată performanța seismică a specimenului experimental prin analize statice și dinamice neliniare folosind modelul numeric descris, verificând de asemenea capacitatea de recentrare, obiectivul de proiectare fiind reprezentat de prevenirea curgerii în alte elemente decât cele disipative demontabile, până la atingerea capacității de deformare ultime a elementului disipativ demontabil. Procesul de înlocuire a linkurilor este investigat și validat numeric, oferind soluții tehnice pentru procedura și ordinea eliminării linkurilor. În cadrul laboratorului de încercări experimentale s-au ivit preocupări pentru posibilitatea apariției unei eliberări bruște de forțe tăietoare din linkuri în timpul eliminării acestora, care ar putea fi periculoasă pentru personalul laboratorului. În consecință, s-a propus folosirea unor sisteme de contravântuiri temporare alcătuite din contravântuiri și disipatori, în timpul eliminării linkurilor, soluția fiind investigată numeric.

Capitolul 4: Evaluarea experimentală a cadrelor duale contravântuite excentric cu link demontabil si capacitate de recentrare

Acest capitol prezintă în prima parte efectuarea a două serii de încercări la tracțiune pe materiale. Prima serie s-a realizat pe 9 seturi de câte trei epruvete metalice și a doua, pe 6 ansambluri șurub+piuliță+șaibe. Toate materialele încercate au fost primite de la ELSA, provenind din aceleași loturi cu materialele folosite la execuția specimenului experimental. Aceste încercări s-au efectuat pentru a evalua caracteristicile materialelor din care s-au realizat elementele structurale și șuruburile îmbinărilor link-grindă. Proprietățile obținute ale materialelor s-au folosit în continuare pentru calibrarea modelului numeric al specimenului folosit în viitoare simulări numerice.

Încercările experimentale pe specimenul la scară reală sunt tratate în continuare. Programul de încercări experimentale este compus din încercări „snap-back", încercări pseudo-dinamice și încercări pushover. Sunt prezentate date despre montajul experimental pentru fiecare categorie de teste. Sunt descrise încărcările verticale (gravitaționale) și orizontale (accelerograma naturală) folosite la încercările pseudo-dinamice. Este descrisă, de asemenea, instrumentarea folosită pentru măsurarea și observarea deplasărilor și deformațiilor locale și globale ale structurii. În continuare, este prezentat programul experimental propus, care este împarțit în trei mari categorii de încercări experimentale: testele Stării Limită de Serviciu (SLS),

în urma cărora specimenul a suferit deteriorări moderate și au rezultat drifturi reziduale mici, testele Stării Limită Ultime (SLU), în urma cărora s-au obținut drifturi reziduale mai mari și testele Stării Limită Prevenirea Colapsului, în urma cărora s-au observat deteriorări la nivelul întregii structuri, aceasta nemaiavând capacitatea de recentrare din cauza curgerii celorlalte elemente înafară de linkuri.

După testele SLS, a fost validată experimental procedura de înlocuire a linkurilor și capacitatea de recentrare prin eliminarea likurilor prin deșurubare fără utilizarea contravântuirilor cu disipatori ca sistem de siguranță. După testele SLU, în urma cărora au rezultate drisfturi reziduale mai mari, eliminarea linkurilor s-a realizat prin tăierea cu flacără atât a inimii linkurilor cât și a tălpilor, de asemenea fără a utiliza sistemele de siguranță cu disipatori. În cazul ambelor proceduri de înlocuire a linkurilor s-a observat o foarte bună recentrare a specimenului experimental după eliminarea linkurilor deteriorate și înlocuirea lor cu unele noi.

Capitolul 5: Validarea metodologiei de proiectare a cadrelor duale contravântuite excentric cu linkuri demontabile

În acest capitol, sunt analizate alte configurații structurale ale cadrelor duale contravântuite excentric cu linkuri demontabile, pentru a extinde numeric comportamentul specimenului experimental unor structuri aplicabile în practică. Două structuri diferite cu câte șase etaje au fost proiectate: prima, la fel ca specimenul experimental, având un cadru contravântuit situat central și două cadre necontravântuite marginale și a doua având un cadru necontravântuit situat central și două cadre contravântuite excentric marginale. Rezultatele încercărilor experimentale au fost folosite pentru calibrarea modelului numeric folosit în viitoare simulări numerice. S-a evaluat performanța seismică a celor două structuri prin analize neliniare statice și dinamice. S-a realizat în continuare o serie de simulări numerice pentru a valida capacitatea de recentrare a celor două structuri și pentru a studia diferite soluții de eliminare a linkurilor în cadrul unui etaj și pe înălțimea structurii, alegând-o pe cea mai potrivită pentru a fi recomandată.

Spre finalul capitolului sunt prezentate rezultatele analizelor incremental dinamice folosite pentru a calcula factorul de comportare și supra-rezistența celor după structuri, pentru diferite stări limită corespunzătoare standardelor European și American.

Capitolul 6: Concluziile tezei de doctorat. Contribuții ale autorului. Activități viitoare de cercetare

Ultimul capitol prezintă concluziile tezei de doctorat, principalele contribuții ale autorului și diseminarea rezultatelor. De asemenea, sunt prezentatate și activități viitoare de cercetare.

Anexele

În anexe, sunt prezentate informații suplimentare cu privire la execuția specimenului experimental (vederi, planuri și detalii de execuție), instrumentarea specimenului experimental (captori de deplasare locali și globali, inclinometer și timbre tensiometrice) și rezultate suplimentare ale programului de încercări pseudo-dinamice.

SUMMARY

To reduce the repair costs and downtime of a structure hit by an earthquake and consequently obtain more rational design approach in the context of sustainability, the concepts of removable dissipative members and re-centring capability are implemented in a dual structure, obtained by combining steel eccentrically braced frames with removable bolted links with moment resisting frames. The bolted links are intended to provide the energy dissipation capacity and to be easily replaceable, while the more flexible moment resisting frames would provide the necessary re-centring capability to the structure. Therefore, with the aim to evaluate the seismic performance of dual eccentrically braced frames with removable links and to validate their re-centring capability and link replacement procedure, extensive numerical investigations were carried out at the CEMSIG Research Centre from Politehnica University of Timisoara, Romania and full-scale experimental research was performed at the European Laboratory for Structural Assessment of the Joint Research Centre in Ispra, Italy. The thesis summarises the experimental and numerical investigations and presents the main conclusions of the research.

Chapter 1: Introduction

In the first chapter, an introduction is made in relation to the research topic. The scope and the objectives of the thesis are shown as well as the research framework which was represented by the European Community's Seventh Framework Programme [FP7/2007-2013], relating to the Transnational Access Use SERIES Project titled DUAREM („Full-scale experimental validation of dual eccentrically braced frame with removable links").

Chapter 2: Seismic resistant structural systems which constrain plastic deformations in safety fuses

Different strategies can be employed in order to reduce damage to structures under moderate to strong earthquakes. The most radical solutions are base isolation and various implementations of active and semi-active structural control. Other strategies rely on supplemental damping conferred to the structure through various devices based on viscous, friction, or yielding dampers. More or less efficient for reduction of structural damage, all these solution have the disadvantage of requiring specialised knowledge at the design stage and during erection, need for careful maintenance and high initial cost. Also, solutions providing self-centring of the structure exist, but are technically demanded (post-tensioned strands, shape memory alloy devices, etc.).

Alternatively, a conventional design can be employed, but with the dissipative members realised to be removable (e.g. through bolted connections), allowing replacement of the dissipative elements damaged as a result of a moderate to strong earthquake, and reducing the repair costs. For the structure to be repairable, in addition to constraining inelastic deformations to removable dissipative members, the permanent (residual) drifts should be eliminated. This

solution provides re-centring capability (as opposed to self-centring), through removable dissipative members and dual (rigid-flexible) structural configuration**.**

Chapter 3: Structural design and numerical investigation of experimental specimen

The third chapter deals with the design of a dual eccentrically braced frame with removable links prototype structure. The links from eccentrically braced frames (EBFs) were conceived as removable (bolted links) dissipative elements because they are intended to provide the energy dissipation capacity and to be easily replaceable. The more flexible moment resisting frames provide the necessary re-centring capability to the structure. Considering that in the transversal direction the lateral force resisting system is located on the perimeter frames only, and in order to reduce the cost of the experimental mock-up, the latter is composed of the two end frames of the prototype only. The capacity design was carried out according to European standards.

Afterwards, the seismic performance of the test specimen is assessed through static and dynamic non-linear analyses on a described numerical model, checking also the re-centring capability, the design objective consisting in preventing yielding in members other than removable dissipative ones, up to the ultimate deformation capacity of the removable dissipative member. The link replacement procedure is numerically investigated and validated, giving technical solutions for the link removal procedure and order. There are concerns that a sudden release of link shear force may occur during link elimination that might be dangerous to the operating personnel. Consequently, some temporary bracing system consisting of tension braces and dampers were proposed to be used during the link removal.

Chapter 4: Experimental evaluation of re-centring dual eccentrically braced frames with removable links

Chapter four firstly presents two series of material tensile tests. The first series was performed on 9 sets of three steel samples each and the second one on 6 bolt+nut+washers assemblies, all of them being prepared from additional material corresponding to elements of the tested specimen. These tests were performed in order to evaluate the material characteristics of the main structural elements and the bolts from the link connection. The obtained material properties were further used (see Chapter 5) to calibrate the numerical model of the specimen.

Full-scale specimen testing is treated next. The experimental programme in composed of snap-back, pseudo-dynamic and push-over tests. Data about the experimental set-up for each type of test are presented. Vertical (gravity) and horizontal (seismic record) loading for the pseudo-dynamic tests are described. The instrumentation used to measure and observe the structural local and global behaviour is described. The proposed testing sequence is presented, having three main test sections: Serviceability Limit State (Damage Limitation) tests which produce moderate damage of the specimen, with low residual drifts, Ultimate Limit State (Significant Damage) tests which produce larger residual drifts and Near Collapse tests that produce extensive damage throughout the structure, the re-centring capability being lost due to the yielding of members other than the links.

After SLS tests, the link replacement procedure and re-centring capability were validated by removing links by simply unbolting without using safety braces with dampers. After ULS tests, which produce larger residual drifts, the link removal

was done by flame cutting both the web and flanges of links, also without use of damper braces. A very good re-centring of the specimen was observed after removing the damaged links and replacing them with new ones, in case of both replacement procedures.

Chapter 5: Numerical validation of design methodology for dual eccentrically braced frames with removable links

In this chapter, other structural configurations of dual eccentrically braced frames with removable links were analysed in order to check if the experimental specimen behaviour can be extended to more general, current practice structures. Two different 6 storey structures were designed: the first, like in the case of the experimental specimen, having a central EBF and two side MRFs and the second having a central MRF and two side EBFs. The experimental tests results were used to calibrate a numerical model that was employed in further numerical simulations. The seismic performance of the two structures was assessed by means of nonlinear static (pushover) and dynamic (time-history) analyses. A series of numerical simulations were performed next, in order to validate the re-centring capability of the two structures and to study different solutions for removing links within a storey and per height of the structure and choose the most suitable one in order to be recommended.

Incremental dynamic analyses were performed in order to compute the behaviour factor and the over-strength of dual eccentrically braced frames with removable links, for different limit states associated to both European standard and American one.

Chapter 6: Conclusions of PhD study. Contributions of author. Future research activities

The last chapter presents the conclusions of the PhD study, as well as the main contributions of the author and dissemination of results. Future research activities are also presented.

Annexes

In the annexes, additional information is shown in relation to specimen erection views, plans and details, specimen instrumentation using local and global displacement transducers, inclinometers and strain gauges and supplementary results from PsD tests of the carried experimental programme.

1. INTRODUCTION

1.1. Scope

The thesis research aims at reducing the repair costs and downtime of a structure hit by an earthquake, and consequently more rational design approach in the context of sustainability. These objectives are attained through removable dissipative members and re-centring capability of the structure. The concepts of removable dissipative members and re-centring capability are implemented in a dual structure, obtained by combining steel eccentrically braced frames with removable bolted links with moment resisting frames. The bolted links are intended to provide the energy dissipation capacity and to be easily replaceable, while the more flexible moment resisting frames would provide the necessary re-centring capability to the structure. The columns are realised from high strength steel, in order to keep these members in the elastic range even under strong seismic input.

Past numerical and experimental research on removable link assemblies and eccentrically braced frames with removable links showed that this is a feasible solution for earthquake resistant construction. However, there are two critiques to the removable link solution. The first one concerns permanent (residual) deformations of the structure after a damaging earthquake, which can lead to difficulties in replacing removable links. The second one is related to interaction between the removable link and the concrete slab, which was not addressed in previous studies. On one hand, the concrete slab can affect the link shear capacity, as well as the behaviour of the link-beam connection. On the other hand, large link deformations can damage the concrete slab, which violates the principle that plastic deformations (damage) are constrained to removable links only.

The first issue can be solved by realising a structure as a dual one, by combining eccentrically braced frames (EBFs) with moment-resisting frames (MRFs). The elastic response of the flexible subsystem (MRF) can provide the re-centring capability to the structure, once the links damaged during an earthquake are removed. For this principle to be efficient, the flexible subsystem should remain in the elastic range. A possible way to favour this is to realise some members from high-strength steel. The second issue can be addressed in two ways. One possible solution is to disconnect the removable link from the reinforced concrete slab, by extending the slab only up to an additional secondary beam placed in parallel with the beam containing the link. Another possible solution is to use a conventional reinforced concrete slab, connected or not with shear studs to the removable link, and to accept damage to the slab. In this situation, it would be necessary to repair locally the slab after a damaging earthquake, in addition to replacing the removable link. It is expected that only the concrete would be damaged in the link region, while the reinforcement and corrugated steel sheet used as formwork would retain the integrity due to larger flexibility. The repair procedure would consist in removing the crushed concrete and casting of new concrete over affected area.

While the concept of re-centring in an idealized dual system due to elastic action of the flexible subsystem following removal of damaged dissipative members

in the rigid subsystem is simple, numerical analysis is difficult due to the elements that are removed from the system. Full-scale experimental validation is believed to be crucial in proving the practical applicability of the concept. Considering the large scale of the test, it is believed that the optimum solution for testing is a pseudo-dynamic test. On the other hand, eccentrically braced frames are widely used in seismic regions, including Romania, as they provide a convenient balance between stiffness and ductility, in comparison with the alternative MRFs (lacking stiffness) or concentrically braced frames (CBFs – with moderate ductility). One of the advantages of using removable links relies in the greater flexibility in tuning their strength along the building height, in order to satisfy the stringent requirements from EN 1998-1 [1] in this respect. Assessment of global seismic of EBFs in general, and with removable links in particular is thus of increased interest. A large scale pseudo-dynamic test would provide valuable data on extending the provisions of EN 1998-1 to EBFs with removable links.

1.2. Objectives

Most of the structures designed to modern code procedures would experience inelastic deformations even under moderate seismic action, with permanent (residual) displacements after the earthquake. Repair is difficult in such cases. The proposed research suggests a solution that provides re-centring capability, through removable dissipative members and dual (rigid-flexible) structural configuration.

The objectives of the thesis are the following:

- Assess (numerically and experimentally) the global seismic performance of dual EBFs with removable links;
- Investigate numerically and validate experimentally the link removal technology;
- Investigate numerically and validate experimentally the re-centring capability of dual structures with removable dissipative members;
- Investigate the interaction between the concrete slab and the steel structure in the link region.
- Calibrate a numerical model based on experimental tests and use it in further numerical simulations;
- Assess seismic performance and extend the numerical investigation of link replacement procedure on current practice structures.

1.3. Research framework

The removable dissipative link concept was developed and experimentally validated in detail in 2003 by Stratan [2], at CEMSIG Research Centre from Politehnica University Timisoara, Romania. It was further experimentally validated on a portal frame in 2010 by Stratan et al. [3] also at CEMSIG Research Centre from Politehnica University Timisoara.

The research leading to achieving the objectives states above has received funding from the European Community's Seventh Framework Programme [FP7/2007-2013] for access to the European Laboratory for Structural Assessment of the European Commission – Joint Research Centre under grant agreement n°

227887, relating to the Transnational Access Use SERIES Project titled DUAREM („Full-scale experimental validation of dual eccentrically braced frame with removable links").

The partnership for the project was composed of Politehnica University Timisoara (Romania) as a coordinator and University of Liege (Belgium), University of Napoli „Federico II" (Italy), University of Ljubljana (Slovenia) and University of Coimbra (Portugal).

The main objectives of the DUAREM Project were:

- Validate experimentally the re-centring capability of dual structures with removable dissipative members.
- Investigate the interaction between the concrete slab and the steel structure in the link region.
- Assess global seismic performance of dual EBFs with removable links, including replacement of damaged links.

The main activities of the project were the following:

- Design and assessment of seismic performance of experimental specimen;
- Numerical simulations on investigating link replacement procedure;
- Investigations on practical solutions of link removal order;
- Investigation of the safety of link removal process;
- Validate experimentally the studied solution.

The validation of the proposed solution was realised through a pseudo-dynamic testing programme of a full-scale model of a dual eccentrically braced structure. The research demonstrated the feasibility of the proposed concept (re-centring capability of dual structures with removable dissipative members), clearing the route toward implementation into design practice. Additionally, the overall seismic performance of dual eccentrically braced frames was validated. Full-scale test provided valuable information on the interaction between the steel frame and the reinforced concrete slab in the link region.

The framework for the DUAREM Project was represented by grant agreement n° RFSR-CT-2009-00024 "High strength steel in seismic resistant building frames" (HSS-SERF Project) of the European Community's Research Fund for Coal and Steel (RFCS). The project aim was to observe the behaviour and to characterise in terms of stiffness, capacity and ductility, the seismic performance of welded beam-to-column joints for multi-storey building frames of concrete filled tubes high strength steel columns and mild carbon steel beams.

2. SEISMIC RESISTANT STRUCTURAL SYSTEMS WHICH CONSTRAIN PLASTIC DEFORMATIONS IN SAFETY FUSES

2.1. Introduction

Different strategies can be employed in order to reduce damage to structures under moderate to strong earthquakes. The most radical solutions are base isolation and various implementations of active and semi-active structural control. Other strategies rely on supplemental damping conferred to the structure through various devices based on viscous, friction, or yielding dampers. More or less efficient for reduction of structural damage, all these solution have the disadvantage of requiring specialised knowledge at the design stage and during erection, need for careful maintenance and high initial cost. Also, solutions providing self-centring of the structure exist, but are technically demanded (post-tensioned strands, shape memory alloy devices, etc.).

Alternatively, a conventional design can be employed, but with the dissipative members realised to be removable (e.g. through bolted connections), allowing replacement of the dissipative elements damaged as a result of a moderate to strong earthquake, and reducing the repair costs. For the structure to be repairable, in addition to constraining inelastic deformations to removable dissipative members, the permanent (residual) drifts should be eliminated. This solution provides re-centring capability (as opposed to self-centring), through removable dissipative members and dual (rigid-flexible) structural configuration.

2.2. Specialized dissipative devices systems

Conventionally, structures have been designed to resist natural hazards (earthquakes, strong winds) through a combination of strength, deformability, and energy absorption. Their behaviour may be satisfactory well beyond the elastic limit in the case of a severe earthquake. These structures may remain intact due to their ability to deform inelastically, as this deformation results in increased flexibility and energy dissipation. Unfortunately, this deformation also results in local damage to the structure, as the structure itself must absorb much of the earthquake input energy.

Alternatively, some types of structural protective systems may be implemented to mitigate the damaging effects of environmental forces. These systems work by absorbing or reflecting a portion of the input energy that would otherwise be transmitted to the structure itself. As a result of this approach, many new and innovative concepts for structural protection have been advanced and are at various stages of development. These concepts can be divided into three main categories, namely passive control systems, semi-active control systems, and active control systems. The first two categories are presented in the following.

2.2.1. Passive energy dissipation systems

Passive energy dissipation systems for seismic applications have been under development for a number of years being widely implemented starting in the mid-1990s. The principal function of a passive energy dissipation system is to reduce the inelastic energy dissipation demand on the framing system of a structure ([4], [5]). The result is reduced damage to the framing system.

Passive control devices require no external power. They use the relative deformation between the attachment points of the device to the structure to dissipate energy. Many types and multiple configurations of passive energy dissipation devices exist. Two categories of passive devices are rate-independent and rate-dependent [6]. Rate-independent devices dissipate energy through mechanisms that depend only on the displacement in the device. Examples of these include metallic yielding and friction dampers. The energy dissipation capacity of rate-dependent devices depends on the velocity across the device. These devices include viscous fluid dampers (VFD) and viscoelastic (VE) solid dampers. Depending on which VE materials are utilized, the magnitude of the displacement can have an effect on the energy dissipation capacity, making the energy dissipation capacity of VE dampers dependent upon both the velocity and the displacement.

2.2.1.1. Metallic yielding dampers

Metallic yielding devices use the ductility of metals to dissipate energy. Mild steel is the standard in these devices. One major category of metallic dampers is represented by added damping and stiffness (ADAS) dampers [6].

ADAS devices use a series of parallel plates typically connected to a chevron brace at the bottom and the structural frame at the top, as shown in Fig. 2-1. The plates are tapered to match the shape of the moment diagram such that the yielding occurs throughout the plate to achieve the most energy dissipation per volume of steel. The plates are subject to bending about the weak axis.

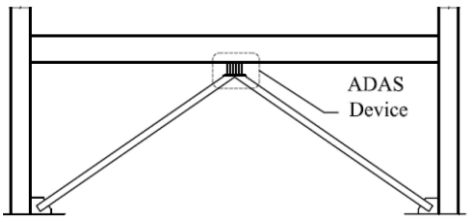

Fig. 2-1. Chevron Brace Configuration for ADAS Device [6]

The initially used shape was hourglass or X-shaped plate. Both ends of the plates were clamped, resulting in double curvature bending. Because of the hourglass shape of the plate, it yields uniformly over its height. Fig. 2-2 illustrates the ADAS devices' plate geometry.

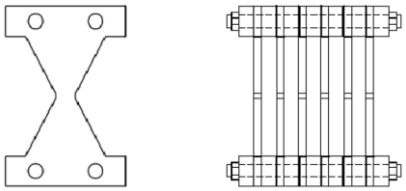

Fig. 2-2. Additional Damping and Stiffness (ADAS) Device [6]

Other metallic yielding dampers are Shape Memory Alloy (SMA) devices. SMAs are special metal alloys which can deform up to large strain levels (up to 10%) with no residual deformation. The qualities beneficial to seismic protection systems include energy dissipation, super-elastic deformation, low-cycle fatigue resistance and re-centring capabilities. Various applications of SMAs include beam-column connections, diagonal braces, and as an element of an isolation system ([7], [8]).

The disadvantage of these dampers are that they may be damaged after an earthquake and may require replacement and to assess the nonlinear behaviour, nonlinear analyses could be necessary.

2.2.1.2. Friction dampers

Friction dampers dissipate energy via sliding friction across the interface between two solid bodies. They rely on the same system as automobile brakes to dissipate energy. They are similar to metallic yielding devices in that they add only stiffness to the structure until the forces in the dampers reach the slip level. Upon slipping, they begin to dissipate energy through heat. A critical aspect to frictional dampers is the ability of the friction surface to maintain a constant frictional coefficient. When this occurs, the hysteresis loops are rectangular and stable [6].

The proposed device for use in the middle of cross-bracing was shown through analytical means to effectively dissipate energy without damaging the structural frame [9]. A schematic of this device is shown in Fig. 2-3.

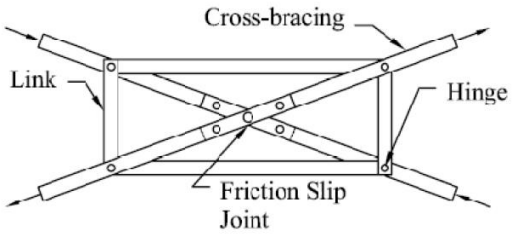

Fig. 2-3. Friction Device for Frames [9]

This friction damping system was later tested experimentally in a scaled nine-story structure. The results verified the benefit of the devices in providing significant energy dissipating capacity to the structure.

Friction dampers were applied to seismic retrofit one wing of Monterey County Government Centre from Monterey County, California and the Patient Tower from Seattle [10] (see Fig. 2-4).

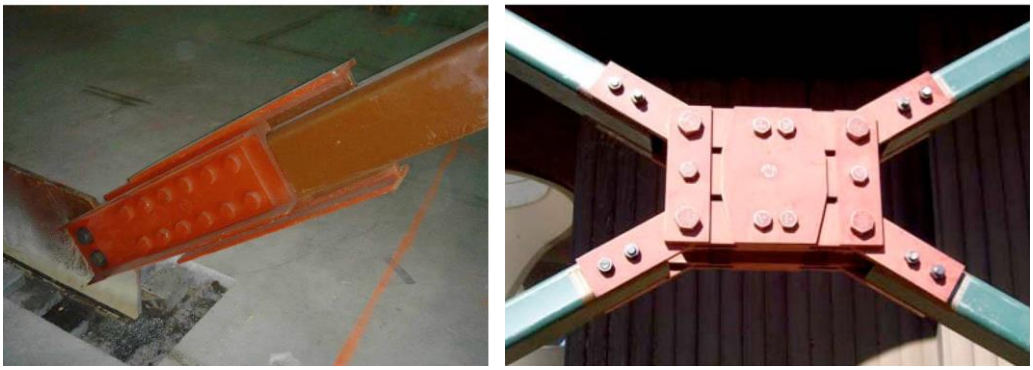

Fig. 2-4. Installed friction dampers on Monterey County Government Centre [11] and on Patient Tower [12]

Friction dampers have large energy dissipation per cycle, but have the disadvantage that permanent displacements may occur if no restoring force mechanism is provided.

2.2.1.3. Viscous fluid dampers (VFD)

VFD dissipate energy through deformation of viscous fluids. This is accomplished through a piston-type device with orifices in the face of the piston. As the piston head moves through the fluid inside the sealed cylinder, the deformations of the fluid dissipate energy. The configuration of the openings in the piston determines whether the device will be linear or nonlinear. These devices typically add little or no stiffness to the structure at low frequency levels (below 4 Hz) and do not modify the fundamental modes of the structure. A true viscous damper does not add significant additional base shear to the structure while it remains elastic because the force in the damper is out of phase with the structure [6]. A schematic of a VFD is presented in Fig. 2-5.

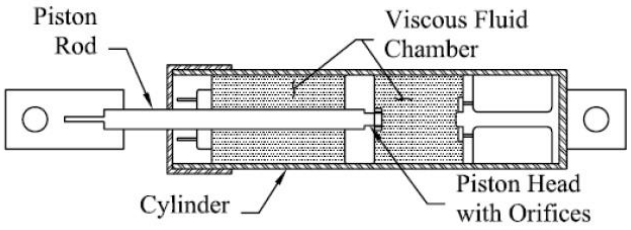

Fig. 2-5. Schematic Diagram of VFD [6]

Viscous fluid dampers were applied in the final design of Torre Mayor Tower from Mexico City, Mexico [10] (see Fig. 2-6).

Fig. 2-6. Installed viscous fluid dampers on Torre Mayor Tower [10]

Viscous fluid dampers are activated at low displacements and exhibit minimal restoring force.

2.2.1.4. Viscoelastic (VE) solid dampers

Viscoelastic solid devices are dampers which use VE materials sandwiched between steel plates. Two typical configurations of VE dampers (VED) are shown in Fig. 2-7. VE materials dissipate energy when they are deformed in shear. Unlike viscous dampers, VEDs add stiffness to the structure initially, although not to the same degree as metallic yielding devices. Unlike metallic or friction dampers, VE materials dissipate energy for all deformation levels [6].

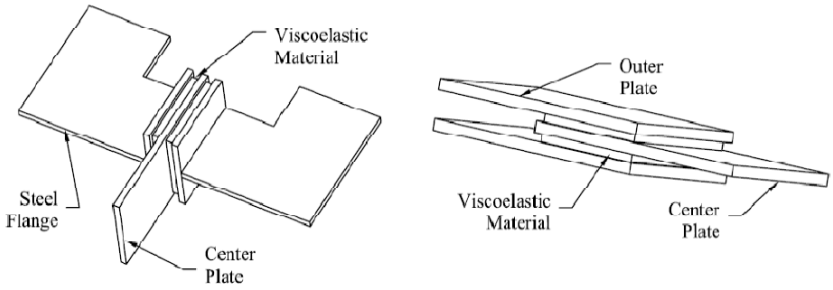

Fig. 2-7. Typical configurations for VE devices [6]

VE solid dampers were applied in the retrofitting of Hotel Stockton in California, of LAPD Recruit Training Centre in Los Angeles and San Mateo County Hall of Justice in Redwood City, California [10] (see Fig. 2-8).

Fig. 2-8. Installed VE solid dampers on Hotel Stockton, LAPD Recruit Training Centre and San Mateo County Hall of Justice [10]

VE solid dampers are activated at low displacements and provide restoring forces to the systems they are installed in, but have limited deformation capacity.

2.2.2. Semi-active control systems

A semi-active control device has properties that can be adjusted in real time but cannot inject energy into the controlled system [13]. Frequently, such devices are referred to as controllable passive dampers.

Because they offer the adaptability of active control devices without requiring large power sources, semi-active control systems have attracted a great deal of attention in recent years. Many of these systems can operate on battery power alone, proving advantageous during seismic events when the main power source to the structure may fail. Also, because semi-active devices cannot inject energy into the structural system, they do not have the potential to destabilize the system. Recent work by several researchers has indicated that semi-active control systems, when appropriately implemented, achieve significantly better results than passive control systems; in fact, they may even outperform fully-active control systems, demonstrating significant potential for controlling structural responses to a wide variety of dynamic loading conditions [14].

Some of these devices are discussed below.

2.2.2.1. Magnetorheological (MR) fluid dampers

One method of semi-active control is the use of MR fluid dampers. These dampers employ MR fluids which produce large damping forces in a piston-cylinder system that can be controlled by varying the current to the damper in real time. In the event of power loss, the MR fluid dampers act as passive dampers, thus maintaining some protection [15].

In general, MR dampers work in one of these modes: Flow or valve mode, shear mode, squeeze mode or a combination of them. Schematics of these operation modes are shown in Fig. 2-9 [16].

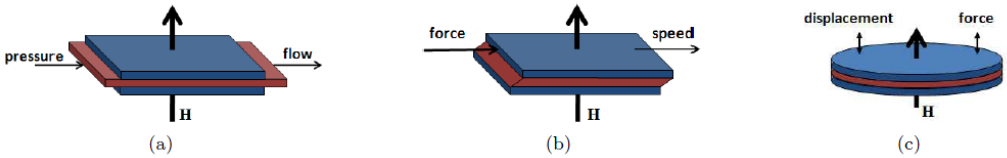

Fig. 2-9. MR damper operation modes: (a) flow or valve mode, (b) shear mode, (c) squeeze mode [16]

Research on MR dampers has demonstrated that the device possesses a significant potential for full-scale structural control implementation ([17], [18]). Since the early 2000s, MR damper has been gradually accepted by the construction industry in some countries.

To experimentally evaluate the effectiveness of semi-active control strategies using an MR damper, a structural vibration control experiment of a three-story model building subjected to seismic excitation was conducted in the SDC/EEL at the University of Notre Dame ([19], [20]). Fig. 2-10 shows a schematic of the experimental setup.

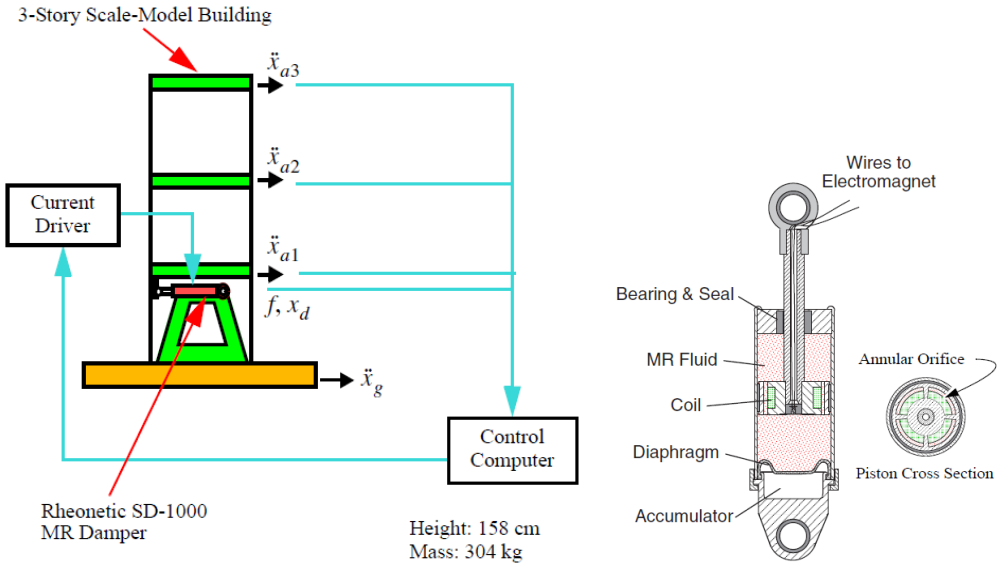

Fig. 2-10. Experimental setup of model building structural vibration control using MR dampers and MR fluid damper used [14]

The effectiveness of the proposed semi-active control strategy was clearly seen through a peak third-floor displacement reduction and a peak third-floor acceleration reduction [14].

2.2.2.2. Semi-active stiffness dampers

Semi-Active Stiffness Dampers (SASD) consist of a fluid filled cylinder, a piston and a motor controlled valve. The motor regulates the opening of the valve,

thus controlling the flow of the viscous fluid (most commonly oil) and adjusting the damping coefficient in real time [15].

With the purpose of evaluating the effectiveness of SASD against structure type and varying earthquake inputs, a study of a SASD in two building models of five-stories under four benchmark earthquake records is reported [21] (see Fig. 2-11).

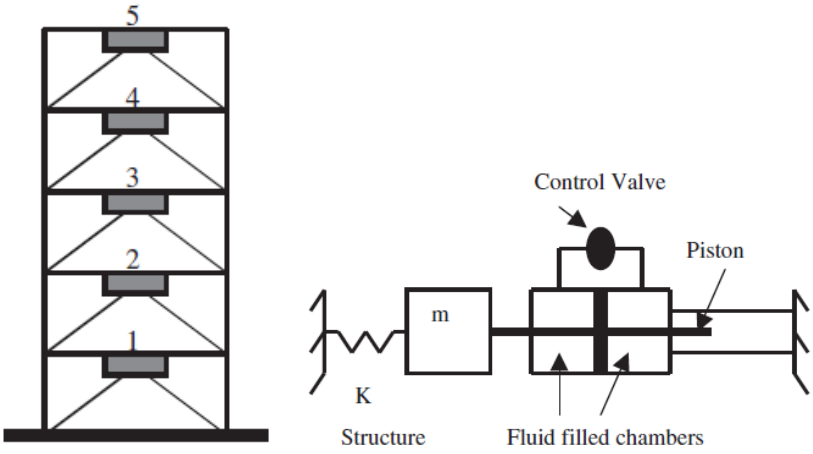

Fig. 2-11. Installation of the SASD in the bracing system and schematic diagram of SASD [21]

Results show that the use of a SASD is effective in reducing seismic responses, more precisely, floor displacements.

2.2.2.3. Semi-active tuned liquid column dampers

In a tuned liquid column damper (TLCD) system, the solid mass is replaced by liquid (commonly water) and control forces are based on the motion of a liquid column through an orifice in a U-like container to counteract the forces acting on the structure [15].

In order to examine the performance of a prototype semi-active TLCD, experiments were conducted to determine the dynamic characteristics of a coupled structure-TLCD system [22]. A schematic diagram of the experimental setup is shown in Fig. 2-12a. It consists of a model of a single story structure fixed on a shaking table. A TLCD consisting of a U-shaped tube made of PVC material with an electro-pneumatically actuated ball valve at the centre of the tube is attached to the model (Fig. 2-12b).

The semi-active system provided an additional 15–25% reduction in response over a passive system. A design example was presented to demonstrate the application of semi-active TLCDs to tall buildings under wind loads. The semi-active TLCD reduced the acceleration at the building top by 45% at all wind speeds.

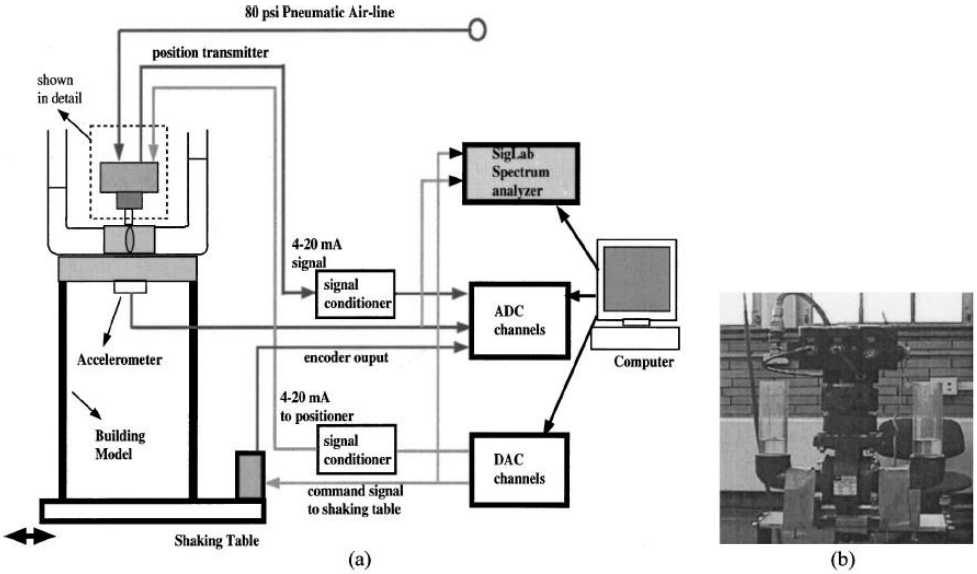

Fig. 2-12. (a) Schematic diagram of experimental setup and (b) photograph of electro-pneumatic actuator [22]

2.2.2.4. Piezoelectric dampers

Piezoelectric (PZT) dampers utilize PZT materials (most commonly ceramic or crystalline in structure) that react to the application of electric current and generate a significant amount of strain/stress, the level of which can be adjusted through the level of current applied. These materials are utilized as stack actuators (an actuator consisting of a stack of PZT material that provides displacement when current is applied) or in active struts (linear actuators with variable stiffness) [15].

A study was performed, where the performance of piezoelectric dampers as part of a smart structural system for buildings was evaluated [23]. Fig. 2-13 shows a schematic of a piezoelectric damper.

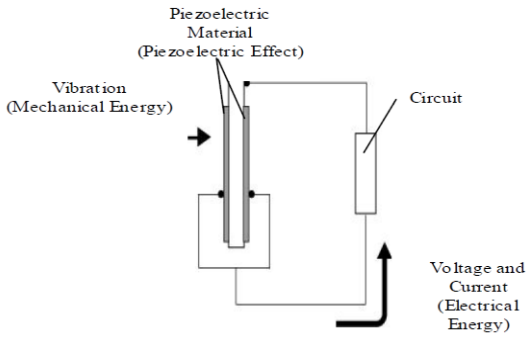

Fig. 2-13. Schematic of a piezoelectric damper [23]

The piezoelectric dampers installed in the 30 stories test building were composed of piezoelectric material, a resistor, and an inductor. The layout of piezoelectric dampers installed in beams and columns in the tests are presented in Fig. 2-14.

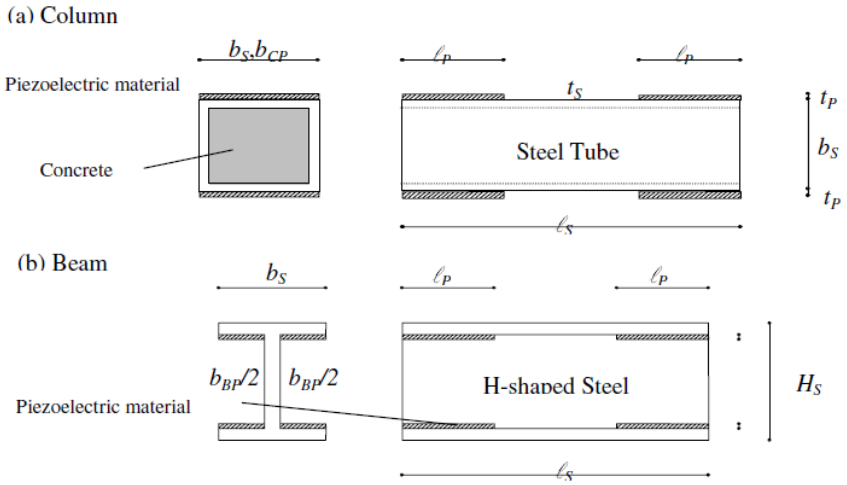

Fig. 2-14. Layout of piezoelectric material [23]

Habitability of the building frame was improved economically and effectively by installing piezoelectric material along 30% of the length from the end of the beams and columns.

2.3. Self-centring seismic systems

Buildings designed according to modern seismic codes are expected to develop a controlled ductile inelastic response during major earthquakes, implying extensive structural damage after a design level earthquake, along with possibly substantial residual deformations. To address this drawback of traditional yielding systems, self-centring seismic systems have been developed.

2.3.1. SC-MRFs (Self-centring moment-resisting frames) systems

Recent development of performance-based design recommendations for SC-MRFs [24] was motivated by results obtained in the last decade in experimental and analytical investigations of these systems for seismic applications (e.g., [25]–[32]). Research shows that these ductile systems resist structural damage after repeated inelastic response cycles under design-level earthquakes. Due to posttensioning that enables self-centring, residual drift after an earthquake is eliminated. Supplemental connection elements are designed to minimize structural damage in the main frame elements at inelastic levels of cyclic loading, and to provide stable energy dissipation (ED) through yielding (e.g., top-and-seat angles in Garlock et al. [33], steel bars in Christopolous et al. [29], or reduced flange plates in Chou et al. [28]), or through

friction-based damping(as in Rojas et al. [34], Lin et al. [35], and Kim and Christopoulos [36]).

The behaviour of connections in SC-MRFs under cyclic loading includes opening and closing of a horizontal gap at the beam–column interface. This gap is quantified by the relative rotation, θ_r, between the beam tension flange and the column flange, as shown in Fig. 2-15a. An idealized moment–rotation behaviour of the connection, reflecting key events in a hysteretic cycle under seismic load, is seen in Fig. 2-15b. At decompression, the horizontal gap opens, after which θ_r increases with continued loading, and the connection stiffness reflects the stiffness of the ED (energy dissipation) device and the PT (post-tensioned) strands. If unloading occurs prior to the yielding of PT strands, a reverse load-deformation hysteretic path reaches the zero-moment and zero-rotation point, when the connection self-centres. The axisymmetric hysteretic curve indicates the connection behaviour following a full reversal of moment [37].

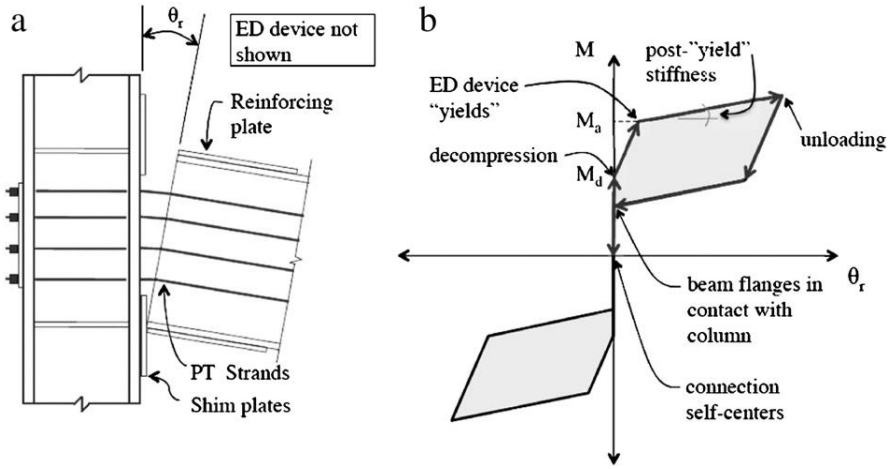

Fig. 2-15. PT Connection: (a) deformation at decompression; and (b) idealized moment–rotation behaviour [37].

The PT (post-tensioned) column base connection (Fig. 2-16a) is designed to eliminate structural damage at column bases in self-centring moment resisting frames (SC-MRFs) under seismic loading; the softening behaviour at the connection is provided by gap opening and elongation of PT bars rather than yielding in the column. Additional shear resistance is provided by bolted keeper plates; additional energy dissipation is provided by buckling restrained steel (BRS) plates (Fig. 2-16b) [38].

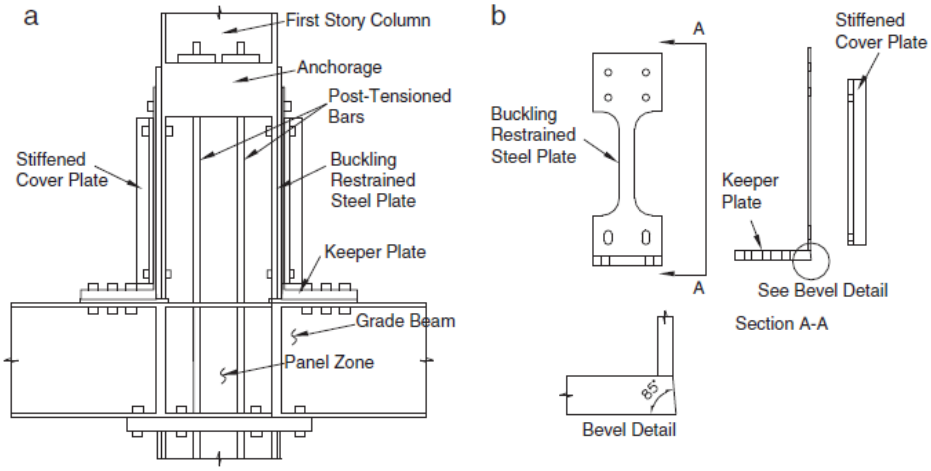

Fig. 2-16. (a) Configuration of PT column base connection; (b) BRS and keeper plates [38].

2.3.2. SC-CBFs (Self-centring concentrically-braced frames) systems

SC-CBF systems have been developed with increased drift capacity prior to initiation of damage. SC-CBF systems are intended to minimize structural damage and residual drift under the design basis earthquake. The behaviour of SC-CBF system differs from that of a conventional CBF system in that the SC-CBF columns are designed to uplift from the foundation at a specified level of lateral loading, initiating a rigid body rotation (rocking) of the frame (Fig. 2-17b). Vertically-aligned post-tensioning bars resist uplift and provide a restoring force to return the SC-CBF columns to the foundation (self-centring the system) [39]. The SC-CBF system is shown schematically in Fig. 2-17a.

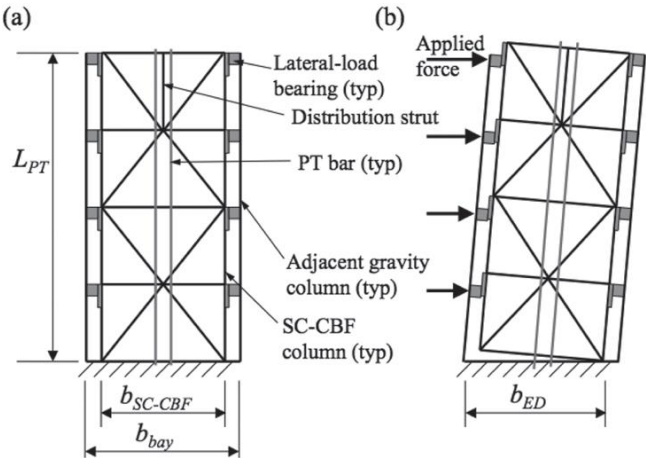

Fig. 2-17. SC-CBF concept: (a) configuration; (b) rocking behaviour [39].

2.3.3. SCED (self-centring energy dissipative) bracing systems

A new bracing system that can undergo large axial deformations without structural damage while providing stable energy dissipation capacity and a restoring force has also recently been developed [40]. The SCED system is a bracing member that is mountable to frame structures similarly to traditional steel bracing or specialized damping devices. As shown in the illustrative sketch of Fig. 2-18, the system consists of two bracing members, a tensioning system, an energy dissipation system, and a series of guiding elements. The bracing member exhibits a repeatable flag-shaped hysteretic response with full re-entering capabilities, therefore eliminating residual deformations.

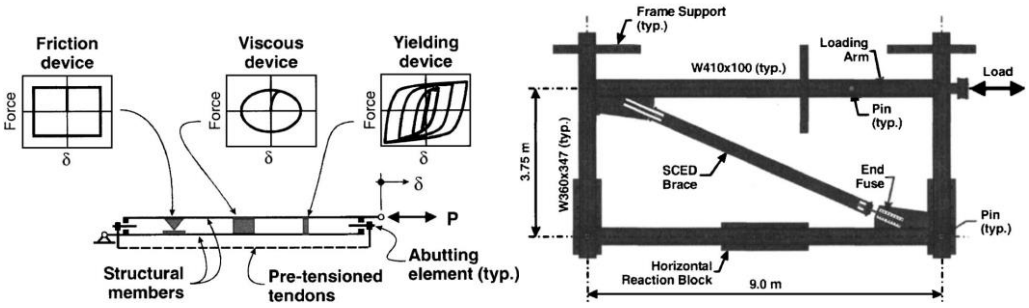

Fig. 2-18. Concept of SCED system and testing setup [40]

Experimental results confirm the expected self-centring behaviour of the self-centring energy dissipative (SCED) bracing system within the target design drift. It is concluded that the proposed SCED concept can represent a viable alternative to current braced frame systems because of its attractive self-centring property and because the simplicity of the system allows it to be scaled to any desired strength level.

2.3.4. SSCD (steel self-centring device) systems

The proposed hysteretic device exhibits two technical features essential to protecting structures against the effects of an earthquake: re-centring and recovery of the structure's original dissipative resources (Dissipative Elements) after a seismic event.

Based on the SCED proposed by Christopoulos et al. [40], a SSCD was developed, being made completely of steel and being easily fashioned by a steelworks [41]. The dissipative system is made up of steel fuses that are easy to replace after use. The proposed SSCD is made up of three groups of elements, each with specific functions: the Skeleton, the Dissipative Elements and the Pretension Elements (Fig. 2-19). The Skeleton serves to transmit and distribute any external forces between the Dissipative Elements and the Pretension Elements. The Internal Sliding Frame is positioned within the External Carter. The Carter has guide elements that allow the Internal Sliding Frame to move only in the axial direction and, at the same time, serve as stops for the Endplates in the longitudinal direction. The endplates are located in correspondence to the ends of the Internal Sliding Frame. The Dissipative Elements, located within the skeleton, are made up of dog

bone shaped steel elements linked to the Internal Carter and the Endplates. They are equipped with a lateral buckling restraining system. The Pretension Elements, made with Prestressing Cables, are located within the Skeleton and linked at both their extremities to the Endplates.

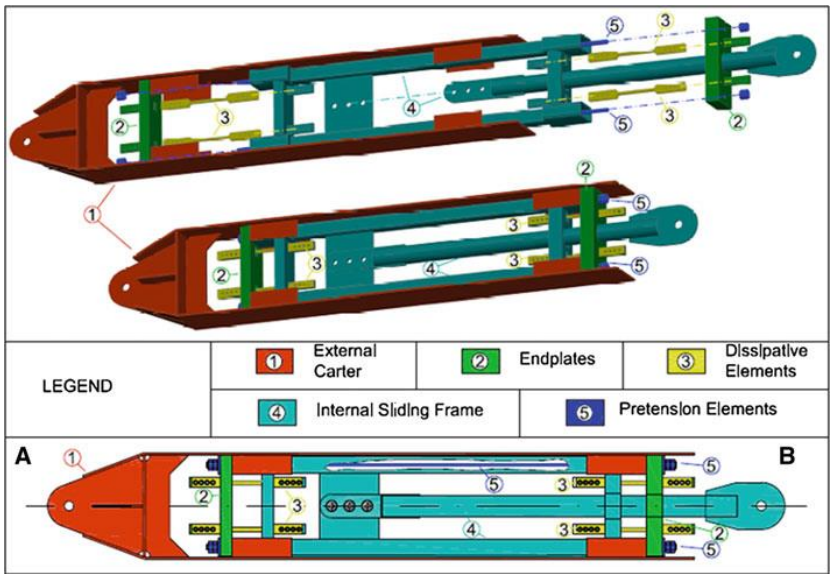

Fig. 2-19. Main members of SSCD [41]

The preliminary design of the SSCD was made with the intent of retrofitting an isolated frame of a concrete building located in Assisi, Italy (see Fig. 2-20).

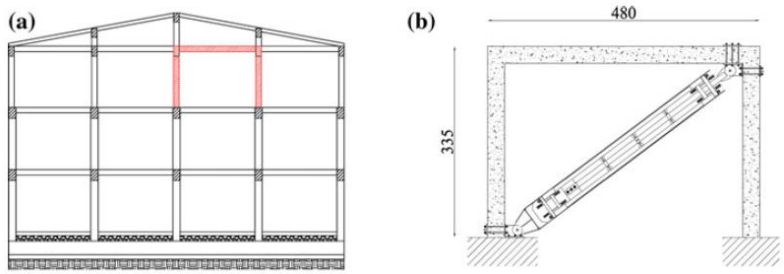

Fig. 2-20. (a) Location of the isolated frames within the building and (b) main dimensions of the frame [41]

The dissipative capacity and re-centring ability of the SSCD are strictly related to the geometrical and mechanical characteristics of the Dissipative Elements and Prestressing Cables. It was concluded that: high values of the initial prestressing ratio, ρ_{PTE}, ensure good re-centring capacity, but reduce overall displacement ductility and the equivalent viscous damping factor; values of the yielding stress, f_{yDE}, of the Dissipative Elements below approximately 500 MPa ensure good re-centring capacity and displacement ductility; the higher the

Dissipative Elements' yielding stress, f_{yDE}, the greater the initial prestressing ratio should be.

2.4. Removable dissipative components systems

Modern seismic codes allow for inelastic deformations in dissipative zones during design earthquakes, accepting damage to a certain extend in the relevant structural parts. As past experience shows, repair works are needed after strong earthquakes, either less or larger than the design one. Structural systems that are easily repairable-replaceable, while maintaining the benefits of high ductility, are therefore beneficial in seismic regions. For the structure to be repairable, in addition to constraining inelastic deformations to removable dissipative members (safety seismic fuses), the permanent (residual) drifts should be eliminated. Therefore innovation in developing new seismic resistant systems is highly appreciated.

In the following some removable dissipative components systems are presented.

2.4.1. INERD connections

An innovation of the INERD Project consists in using dissipative connections for diagonals of frames with concentric bracings. Two types of connections are studied: the "pin" connections, made of bent rounded or rectangular bars, and "U-device" connection, made of plates bent in U. The innovation demonstrates a higher capacity to dissipate energy [43].

a) Pin connections (Fig. 2-21)

The pin connections consist of two external eye-bars welded or bolted to the adjacent member (column or beam), two internal eye-bars welded to the brace and a pin running through the eye-bars (Figure 2.1). In this type of connection the pin exhibits inelastic bending deformations and dissipates energy due to the fact that the eye-bars are placed at some distance between each other.

b) U-connections (Fig. 2-22)

The U-connections consist of one or two bent, U-shaped thick plates that connect the brace to the adjacent member (Figure 2.2). Here again, energy dissipation takes place in the bent plate(s).

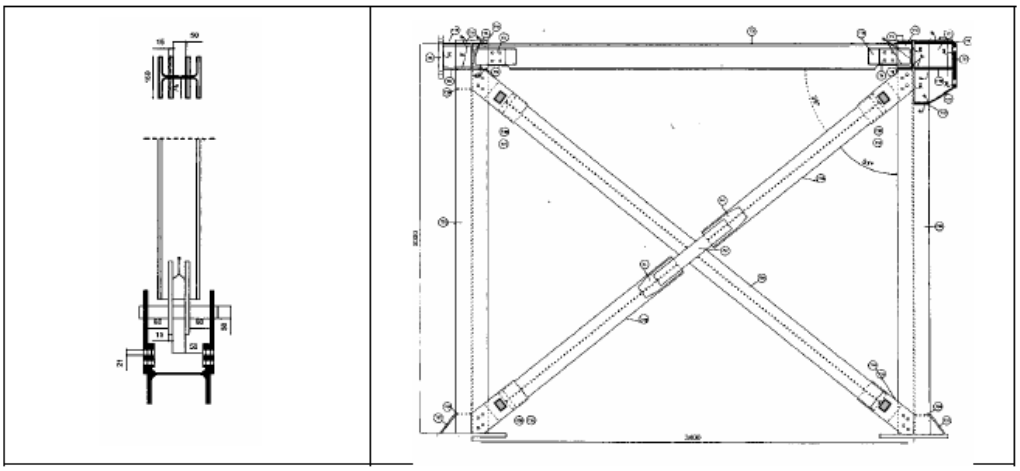

Fig. 2-21. INERD pin connections [43]

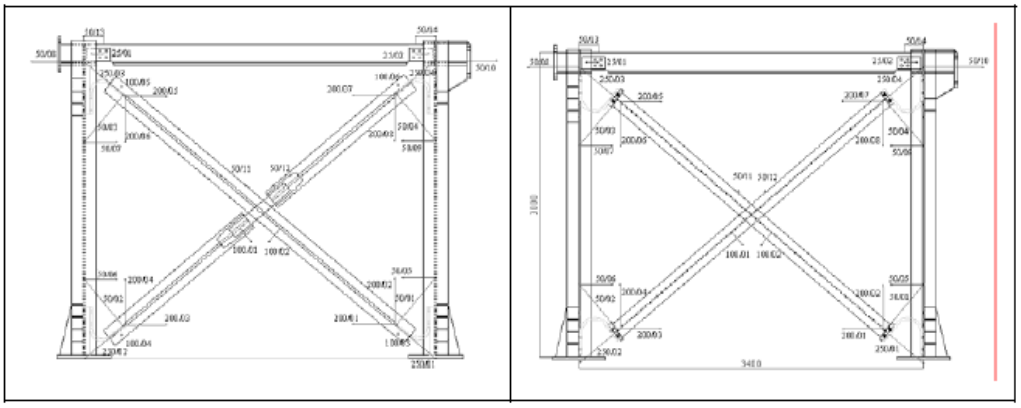

Fig. 2-22. INERD U-connections [43]

The advantage of these connections is that, by appropriate sizing, inelastic deformations are limited within exactly predetermined zones, the pins or the U-plates, whereas the adjacent parts remain elastic. Consequently, braces are protected from buckling and damage is restricted in the pins or the U-plates. These are small parts that may be easily replaced if they are largely deformed, after an unusually strong earthquake.

2.4.2. FUSEIS dissipative devices

a) FUSEIS 1

FUSEIS 1 is an innovative seismic resistant system composed of two closely spaced strong columns, rigidly connected to multiple beams. The beams run from column to column (FUSEIS 1- 1) or alternatively are interrupted and connected by short pins (FUSEIS 1-2) (Fig. 2-23) [44].

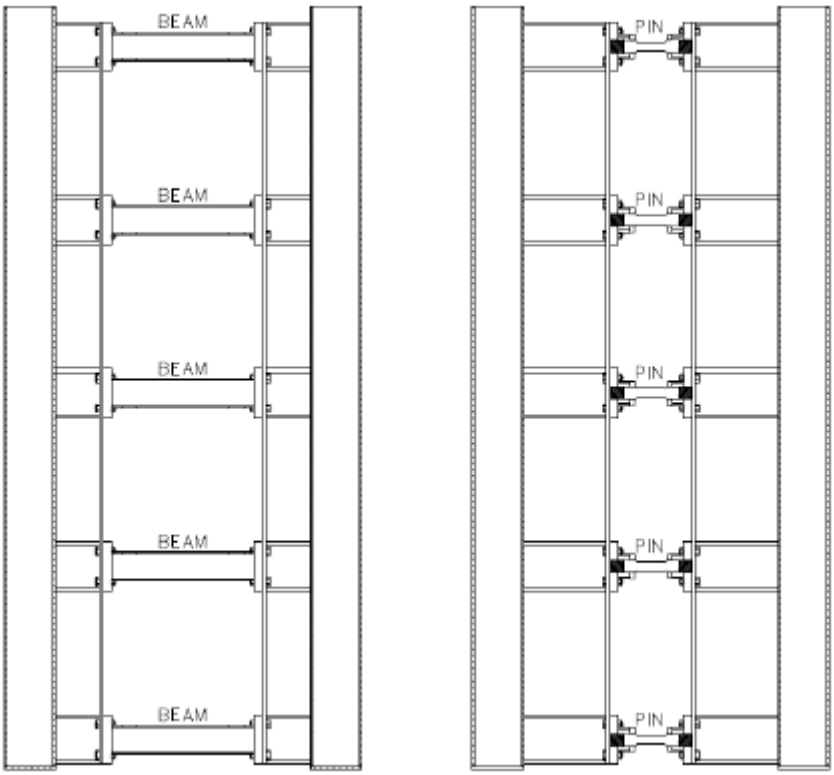

Fig. 2-23. FUSEIS 1-1 and FUSEIS 1-2 systems [44]

FUSEIS 1 has the advantages that inelastic deformations are strictly limited to the dissipative elements (beams or pins) and the dissipative elements are easily replaceable if they are plastically deformed or damaged after a strong seismic event, since they are small and are not part of the gravity loading resistant system.

b) FUSEIS 2

FUSEIS2 devices are seismic fuses for steel and composite steel-concrete moment resisting frames that provide good seismic performance and easiness in repair work (Fig. 2-24) [44].

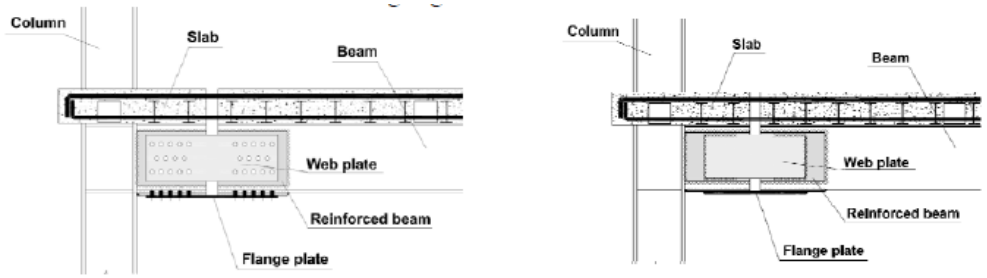

a) bolted device *b) welded device*

Fig. 2-24. FUSEIS 2 system [44]

The FUSEIS2 fuse devices consist in a cross-sectional weakening located at the beam ends at a certain distance from the beam-to-column connections, avoiding this way potential brittle failures at the welds. They act as dissipative seismic fuses, forcing the plastic hinge to develop at the fuse device trough concentration of inelastic behaviour, preventing the spreading of damage into the beams and columns, concentrate all the damage efficiently and are easily replaceable, so that repair work after an earthquake is limited to replacing the fuses by new ones.

2.4.3. Buckling restrained braces (BRBs)

In traditional braced frames, braces are the structural fuses. They yield in compression and tension and absorb energy. However, buckling in compression leads to a sudden loss of stiffness and a progressively degrading behaviour which limits the amount of energy dissipation [45]. Several attempts have been made in order to solve the buckling problem. However, these were unsuccessful until Wada, whose team developed the Unbonded Brace™ [46]. The buckling of the central steel core is prevented by encasing it over its length in a steel tube filled with mortar, concrete or different aggregates. The term "Unbonded Brace™" derives from the need to provide a slip surface or unbonding layer between the steel core and the surrounding concrete, so that axial loads are taken only by the steel core.

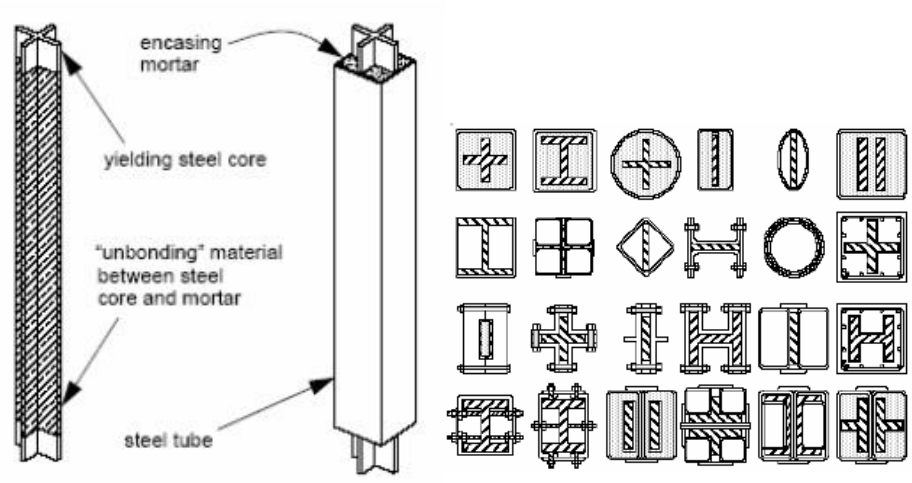

Fig. 2-25. Components of a BRB and cross-section types [47]

BRBs were originally designed for seismic rehabilitation of structures, but their use later extended to new structures (Fig. 2-26).

Fig. 2-26. Osaka International Convention Centre, Japan b) UC Davis Plant & Environmental Facility, California [45]

Fig. 2-27. Wallace F. Bennett Federal Building Before Retrofitting and After Retrofitting [48]

The main advantage of the BRB system is based on good stiffness, especially in the case of V or inverted V systems and also very good ductility compared with the conventional centric braces. That is why the importance of BRB systems is increasing, especially for existent RC frame buildings with a small strength capacity to respond earthquake action. The adoption of BRB systems assures the fulfilment of strength, stiffness and ductility simultaneously [49].

Some experimental tests on BRBs were made at the Politehnica University Timisoara - CEMSIG Research Centre [49]. In order to study the behaviour of the BRB element, a unit test has been performed. The test was carried out according to AISC 2005 [50] recommendations. Fig. 2-28 shows the test setup. Also, a RC frame designed for gravity loads was tested with and without the BRB retrofitting system (Fig. 2-29). The two types of frames were tested monotonically and cyclically.

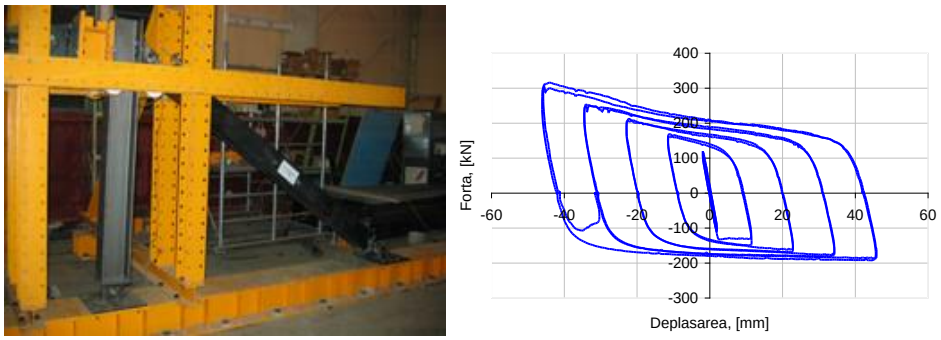

Fig. 2-28. Experimental tests on BRBs: test setup and hysteretic curve [49]

Fig. 2-29. Experimental tested frame view and connection detail [49]

Tests showed a very good behaviour of the retrofitted structure. The ductility of the structure was very much improved and the failure was caused by the failure of the steel brace in tension. The connections between the BRB and the RC elements performed very well.

Energy input by a strong earthquake is greatly dissipated by these devices, and if they are damaged they make the rehabilitation easy after the earthquake, since these devices are designed to be replaceable.

In addition to component tests and developments of new configurations of BRBs, research has also been concentrated on the performance of braces within a structural system. One of the drawbacks of a BRB-only system was residual deformation [51]. To improve this behaviour, they recommend installing BRBs with a special moment-resisting frame (SMRF) as a dual system. They analysed three and six story frames and found that the ductility demand on the braces was not significantly reduced but the story drift and residual displacement were.

2.4.4. Steel plate shear walls (SPSWs)

First studies on steel plate shear wall structures began in the 1970s. Since then, many experimental and analytical studies were conducted all over the world, to demonstrate the structural efficiency and cost competitiveness of this new lateral resisting system [52] - [59].

The idea of using steel plates to resist lateral loads is based on the fact that buckling of a plate with a stiff boundary frame does not necessarily represent the limit of plate capacity in shear.

For the first structural applications of shear walls in Japan and United States the shear panels were designed with a considerable number of stiffeners and thickness to prevent local and global buckling from shear forces that appear even under low lateral excitations and to increase their shear resistance. Numerous studies were conducted on shear panels since then which indicated a good behaviour of simple, unstiffened, thin steel panels mostly because of their high inelastic deformation capacity. In current practice most of the shear walls used are made from thinner steel panels without stiffeners. The design concept allows local buckling of the panel under shear and diagonal tension zones are formed that dissipate energy through successive yield under cyclic loads. Stress distribution for shear panels with one or more stiffeners is presented in Fig. 2-30.

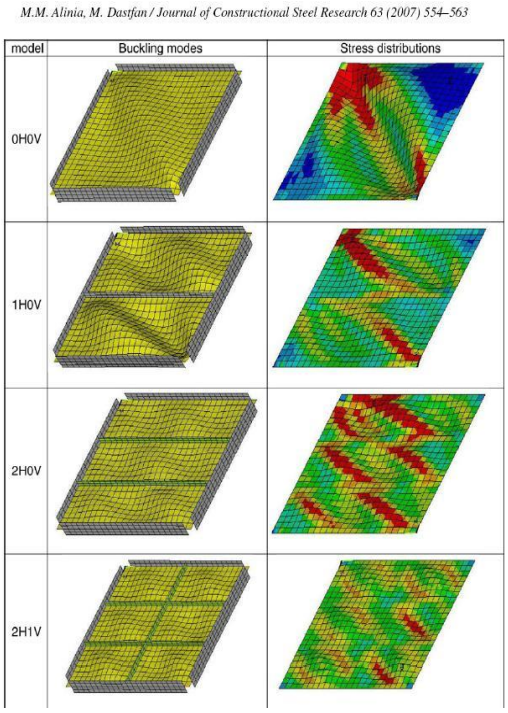

Fig. 2-30. Stress distribution for shear panels with one or more stiffeners [60]

Applications of steel plate shear walls systems can be found all over the world: in USA, Canada, Japan, China, Mexico.


Fig. 2-31. SPSW buildings in USA: Olive View Hospital in Sylmar [61], California and US Federal Courthouse in Seattle [62]


Fig. 2-32. SPSW buildings in Japan: Nippon Steel Building in Tokyo and Shinjuku Nomura Building [62]

Some experimental tests on the influence of boundary members and their connections on the performances of dual SPSW systems were made at the Politehnica University Timisoara - CEMSIG Research Centre (Fig. 2- 33, Fig. 2-34) [62].

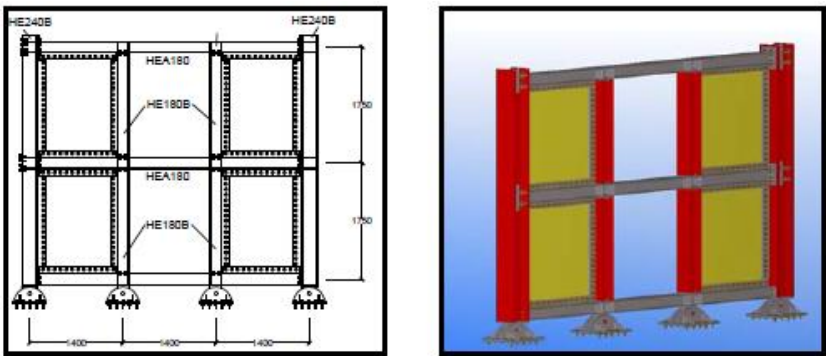

Fig. 2- 33. Experimental frames [62]

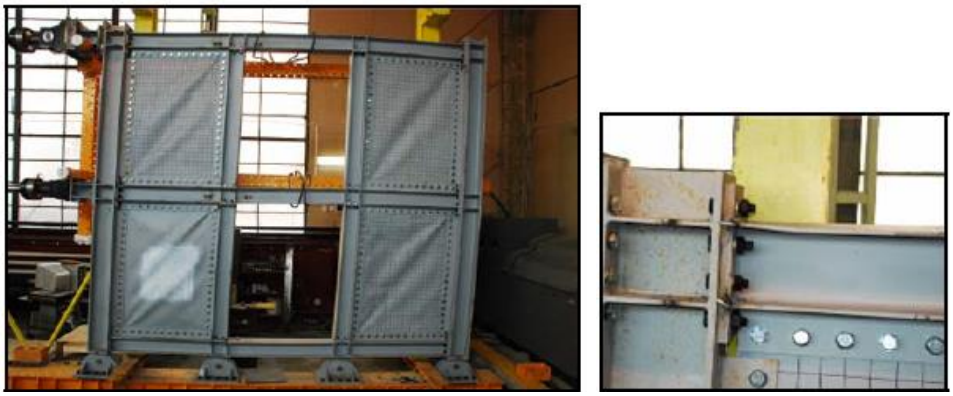

Fig. 2-34. Tested specimen and connection detail [62]

All specimens showed appropriate behaviour during the tests and the use of thin plate made of lower strength steel made the plates manifest good energy absorption with the maximum displacement [62].

The behaviour of a self-centring steel plate shear wall (SC-SPSW) that consists of replaceable thin steel web panels as the primary lateral load resistance and energy dissipation elements, and post-tensioned (PT) beam-to-column rocking connections that provide system re-centring capabilities, has been analytically and experimentally investigated at the University at Buffalo and the University of Washington, in the USA, and at the National Centre for Research in Earthquake Engineering, in Taiwan, as part of a collaborative research effort [63]. SC-SPSW should be attractive in situations where high structural stiffness, strength, and system self-centring after an earthquake are desired features. As such, it is an innovative technology worth the consideration of engineers interested in implementing damage-avoidance technology, with the understanding that yielding plates act as structural fuses that would need to be replaced following a large earthquake. Architectural finishes providing easy access to the SC-SPSW, without obstructions by difficulty to move non-structural components, should be designed to facilitate such replacement in those situations.

2.5. Eccentrically braced frames with removable links and re-centring capability

Eccentrically braced frames are widely used in seismic regions, as they provide a convenient balance between stiffness and ductility, in comparison with the alternative MRFs (lacking stiffness) or concentrically braced frames (CBFs – with moderate ductility).

Eccentrically braced steel frames (EBFs) dissipate energy induced by earthquake loading through the inelastic deformations of beam segments called links. These segments should be preferably short and centrally placed to promote the shear yielding and avoid possible problems related to the connections between the beam and the column. Design procedures are based on capacity design principles and aim to produce frames with stable inelastic response of links and elastic behaviour of all other frame members. To achieve this behaviour, links are selected to have adequate inelastic resistance for factored seismic loads while columns, braces and outer beam segments are sized for the forces generated by fully-yielded and strain-hardened links. Verification of link inelastic rotations completes the ductility phase of design. Selected sections are also checked for the ultimate and serviceability limit states for all relevant load combinations, including wind and earthquake [64].

2.5.1. Applicability and seismic performance of EBFs

Applications of eccentrically braced frames can be found all over the world (Fig. 2- 35, Fig. 2- 36).

Fig. 2- 35. Eccentrically braced steel frame under construction, New Zealand (A. Charleson) [65]

Fig. 2- 36. İstanbul Bilgi University, Prep School Building [66]

A research program combining an experimental and analytical investigation has been conducted at the University of Texas at Austin to study the performance of link-column connections in seismic-resistant EBFs. Link-column specimens were tested with four different connection types, designated as the PN-, MW-, FF- and NA-types. The PN-connection featured detailing and construction typical of the pre-Northridge practice. The MW connection adopted the modifications in welding which are currently widely accepted for moment connections. The FF- and NA- connections were designed based on the free flange moment connection developed by Choi et al. [67] and the no weld access hole ("non-scallop") connections developed in Japan, respectively. Based on extensive literature review, these two connections were selected as the most promising for application to EBF link-column connections [68].

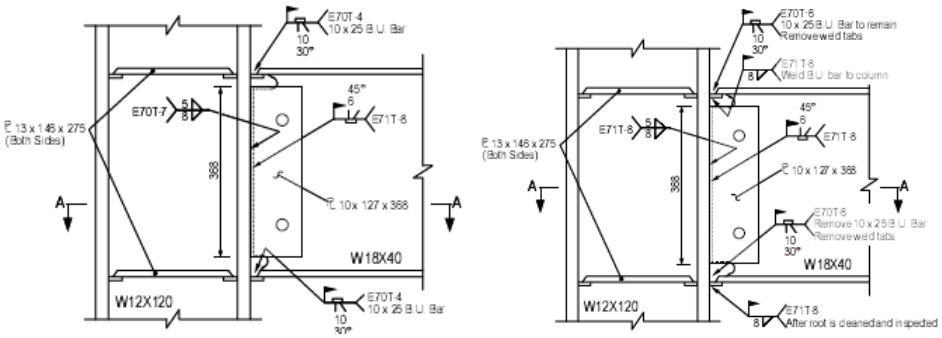

Fig. 2-37. The PN and MW connections [68]

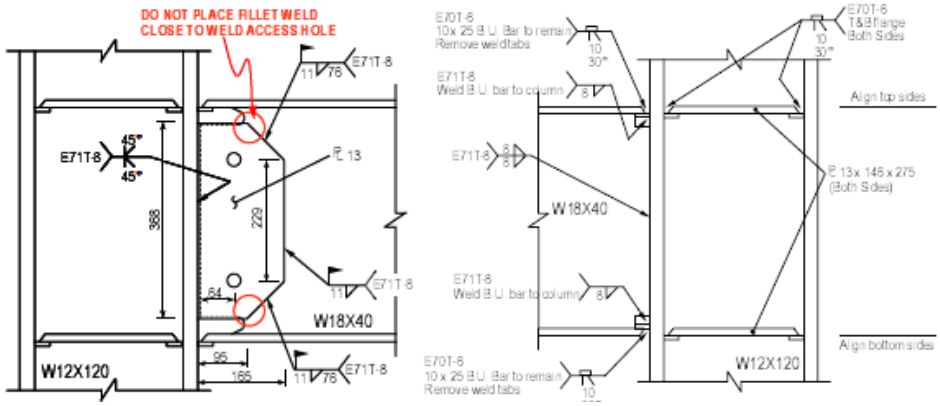

Fig. 2-38. The FF and NA connections [68]

Link-column specimens with four different connection types and three different link lengths, ranging from a short shear yielding link to a long flexure yielding link were tested. The performance of the link-column connection depended strongly on the link length, with the inelastic link rotation capacity decreasing significantly with increase in the link length. The test results suggest that link-column connections in EBFs are prone to premature and abrupt failure due to fracture of the link flanges.

The seismic performance of multi-storey eccentrically braced frames was observed also in Christchurch during the earthquake series of 2010 to 2011 [69]. The EBFs performed well during this earthquake series, inelastic deformations being less than what would have been expected given the severity of the recorded strong motions.

Two recently designed and built multi-storey buildings in the Central Business District (CBD) had eccentrically braced frames as part of their lateral load resisting system, these being the 22-storey Pacific Residential Tower (see Fig. 2-39) in Christchurch's CBD, completed in 2010, and the Club Tower building (see Fig. 2-40), completed in 2009.

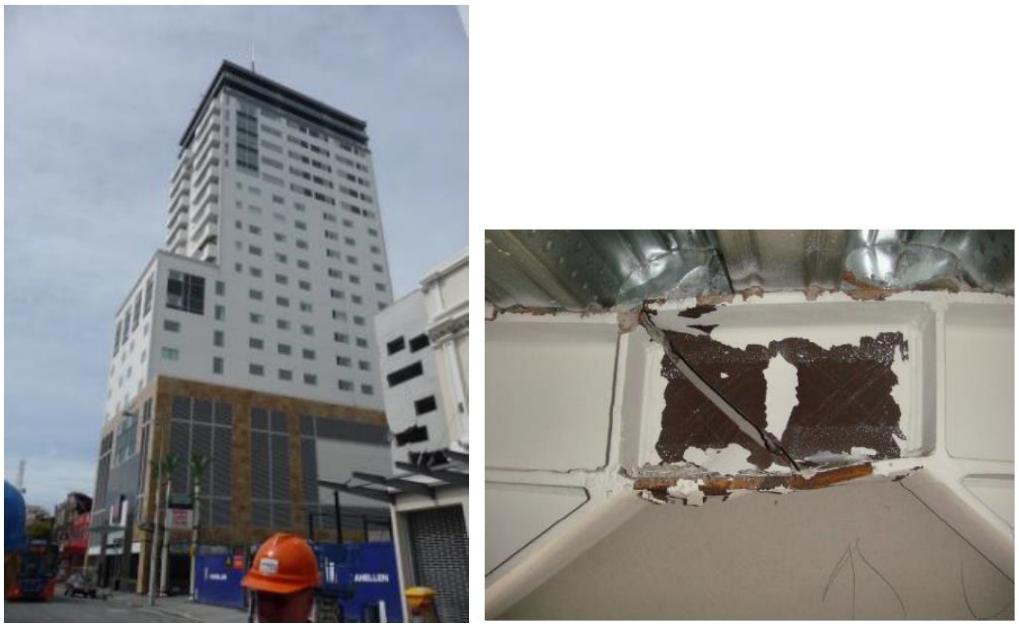

Fig. 2-39. Pacific Tower global view and fractured EBF active link [69]

Fig. 2-40. Club Tower global view and paint peeling of EBF link [69]

Both buildings were green-tagged following the earthquake, indicating that they were safe to occupy even if they will require some minor repairs. In the first case this includes at least one active link replacement (Fig. 2-39). Temporary strap

cross-bracing was welded to the active link frame to provide lateral load resistance while a repair strategy was implemented, which comprised cutting out the damaged link, welding on an endplate system to each collector beam/brace face and replacing with a site bolted endplate active link.

Some link fractures were also observed in EBFs of a hospital parking garage closer to the epicentre of Darfield Earthquake of September 4, 2010 in New Zeeland [70]. The fractures (Fig. 2-41) were of particular concern as these were the first fractures recorded in EBFs worldwide (the Pacific Tower fracture as mentioned above was discovered later). The fracture plane indicated a ductile overload failure rather than a brittle fracture, this being explained by the offset of the brace flange from the stiffener.

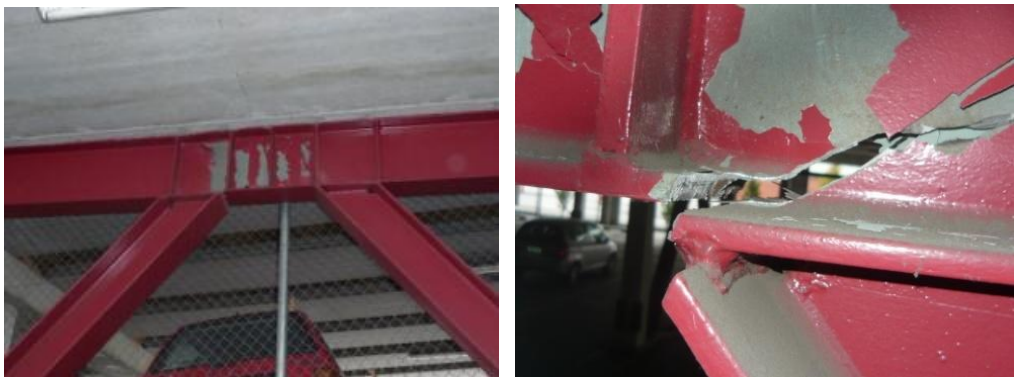

Fig. 2-41. Parking garage evidence of EBF link yielding and fractured link at lower level EBF [70]

The fractured active links have been cut out and replaced to bring the building back into service.

2.5.2. Removable dissipative elements applied to EBFs

The concept of removable dissipative members can be applied to eccentrically braced frames (EBFs), plastic deformations being constrained to removable (bolted) seismic links only that act as safety fuses.

Optimizing the design of an EBF is a process in which the design of the shear link is central. Therefore, de-coupling the link from the remaining structural elements by using replaceable links, allows for an independent control of strength, stiffness and ductility of the EBF system [71].

Therefore, several solutions for making links in EBFs removable were studied over time and are shortly presented further on.

2.5.2.1. Bolted link-column connections

Bolted extended end-plate connections for eccentrically braced frames with link-column connection configuration were previously investigated experimentally by

Ghobarah and Ramadan [72]. Their inelastic performance was found to be similar to fully-welded connections.

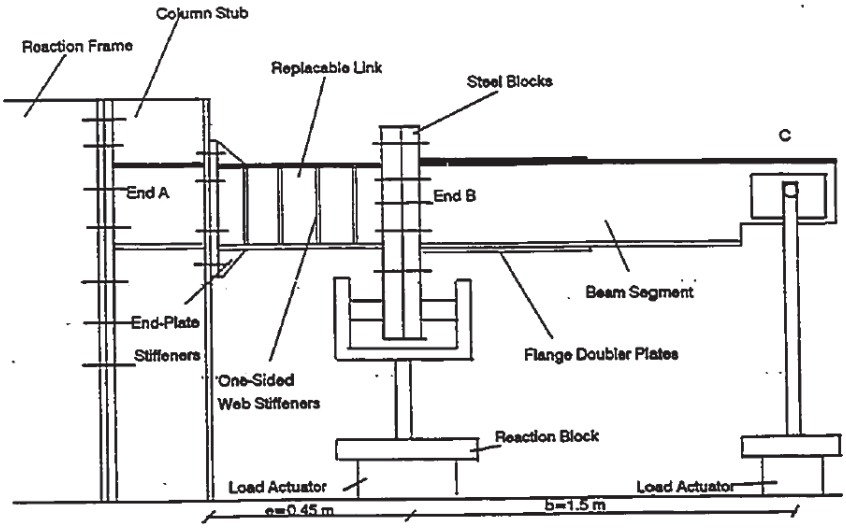

Fig. 2-42. Schematic of test setup [72]

Balut and Gioncu [73] suggested a replaceable solution for links in eccentrically braced frames, and investigated more in detail two replaceable "dog-bone" solutions in moment-resisting frames: one using an I-beam extended endplate bolted connection, and another one consisting of two channels bolted using high-strength friction grip bolts to the beam.

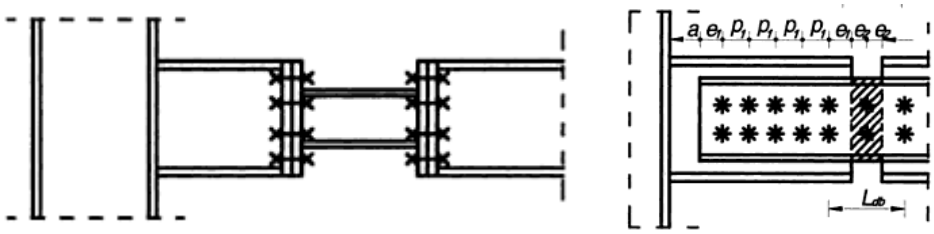

Fig. 2-43. „Dog-bone" solutions [73]

2.5.2.2. Bolted link-beam connections

Two series of experimental tests on removable link assemblies were carried out at the Politehnica University Timisoara – CEMSIG Research Centre in order to determine cyclic performance of bolted links and to check the feasibility of the removable link solution [74], [75]. The first series of tests was realised on isolated links (Fig. 2-44), while the second one on almost full-scale model of a single bay and single storey eccentrically braced frame with removable link (Fig. 2-44). Tests on links showed an important influence of the connection on the total response of the bolted link, in terms of stiffness, strength and overall hysteretic response.

Shorter links were found to be suitable for the bolted solution, as plastic deformations were constrained to the link, while the connection response was almost elastic, allowing for an easy replacement of the damaged link. At the frame level, the experimental tests showed that the removable link solution is feasible. Inelastic deformations were constrained to the removable links alone, all other frame members and connections remaining in the elastic range. Additionally, it was possible to replace the damaged removable links with new elements.

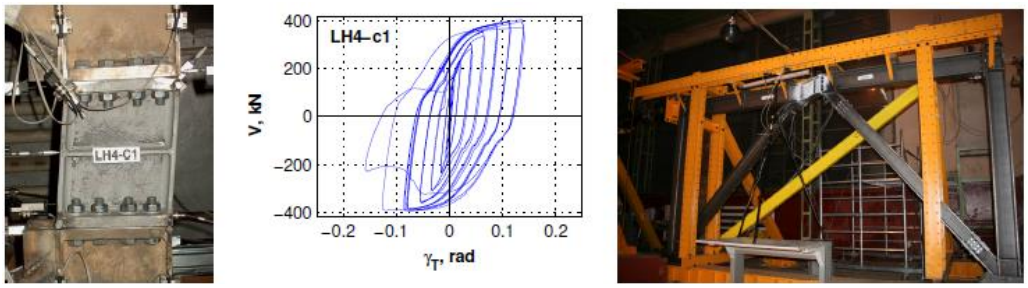

Fig. 2-44. Experimental test on removable bolted link – LH4-c1 specimen, force-deformation relationship V-γ_T of the same specimen and tests on almost full-scale frame with bolted links [74], [75]

Mansour studied different link options that can be divided into two main categories: i) replaceable links fabricated from a W-section with end-plate connections, and ii) replaceable links fabricated from a C-section with web-bolted and web-welded connections [71].

The first link option that was investigated was one where the link section is comprised of a wide flange beam section of length e, as shown in Fig. 2-45. The link is welded to end plates on either side to form one unit, which in turn is connected to the beam section through bolted end-plate connections. The connections must be able to transfer and sustain the maximum forces that can be delivered by the fully yielded and strain hardened link.

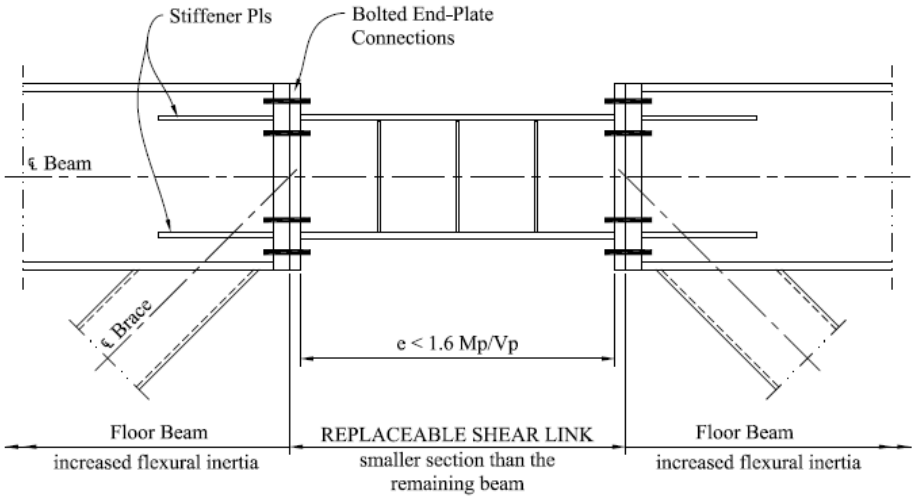

Fig. 2-45. Shear replaceable link with end plate connection [71]

A second option is the one where the link section consists of 2 channels back-to-back, connected to the beam through eccentrically loaded web-bolted connections, as shown in Fig. 2-46. The web bolted link-to-beam connections are deemed easier, quicker and cheaper than the welded end-plate connections. This is due to saving in steel material as the considerably thick end-plates are not needed, and fillet welds instead of complete joint penetration welds are used in the web connections.

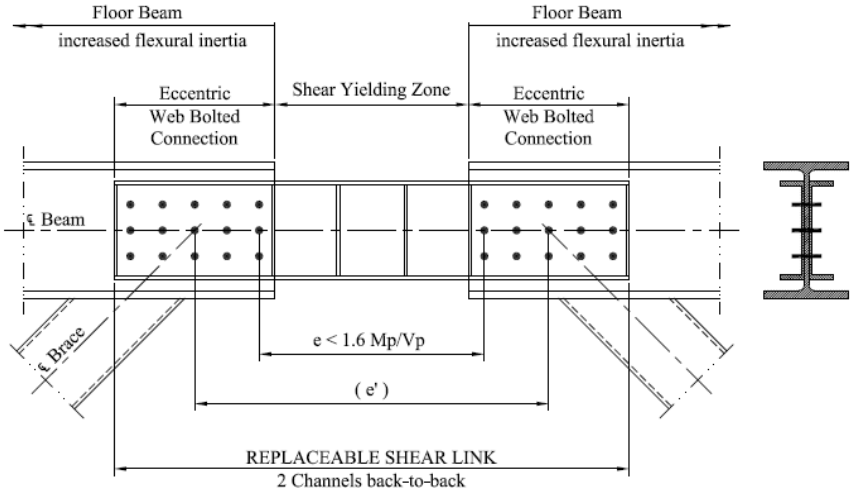

Fig. 2-46. Shear replaceable link with eccentrically loaded web-bolted connection [71]

The third option consists on the link that is comprised of 2 built-up channel sections, back-to-back, as shown in Fig. 2-47. It is very similar in principal to the link described in the second option, but it differs in the manner in which the link is connected to the floor-beam. The moment is transferred through top and bottom flange bolts, while the shear is transferred through concentric web-bolted connections.

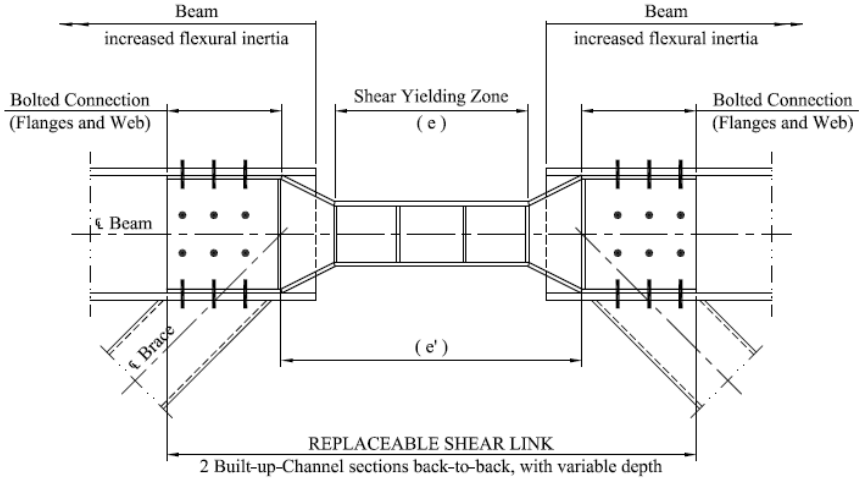

Fig. 2-47. Shear replaceable link with web and flange connection [71]

Two of the suggested replaceable link options were tested at the University of Toronto [71]: replaceable shear links with end-plate connections and replaceable shear links with web-bolted and web-welded connections. The behaviour of the end-plate connected links closely resembled that of traditional chevron EBFs. The response of the web connected links was different from that of the end-plate connected links. The connection rotations due to the localized plate bearing around the bolt holes influenced the total link rotation.

Full-scale frame experimental program conducted at École Polytechnique in Montreal (EPM) [71] was performed on an eccentrically braced frame with ductile replaceable shear links (see Fig. 2-48) to evaluate the global performance of EBFs equipped with replaceable links and to assess various replacement techniques under conditions similar to what would be encountered in a real building.

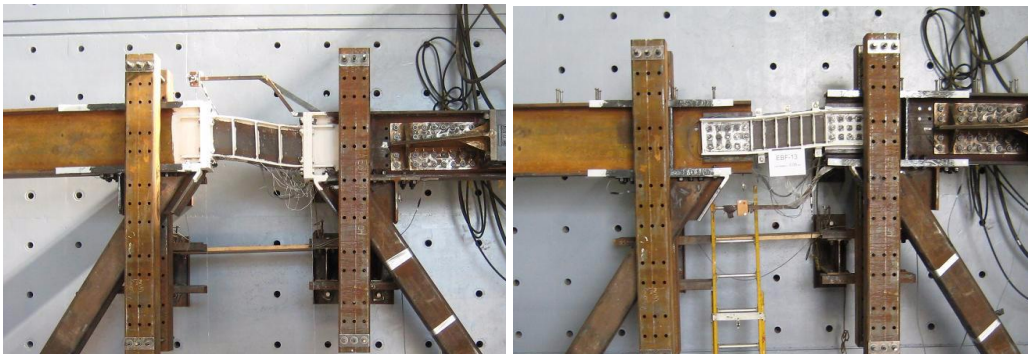

Fig. 2-48. EBF tests with links with end-plate connections and with web-bolted connections [71]

The behaviour of the end-plate and web connected links were similar to those observed in the tests conducted at University of Toronto. The rotation of the web bolted connection was shown to influence the total link rotation of the web bolted links. Two link replacement techniques were investigated: bolted web connections and welded web connections. While both procedures proved feasible, the welded technique provided greater flexibility and ease to position the replacement link.

2.5.3. Re-centring capability of EBFs with removable links

As mentioned in Chapter 2.4, in removable dissipative components systems, a conventional design can be employed, but with the dissipative members realised to be removable (e.g. through bolted connections), allowing replacement of the dissipative elements damaged as a result of a moderate to strong earthquake, and reducing the repair costs. For the structure to be repairable, in addition to constraining inelastic deformations to removable dissipative members, the permanent (residual) drifts should be eliminated.

Structural systems that aim at reducing structural damage by isolating plastic deformations in removable or "repairable" fuses, and have the ability to return to the initial un-deformed shape after an earthquake have received much attention.

Vargas and Bruneau [76] investigated a design approach aiming to concentrate damage on removable and easy to repair structural elements ("structural fuses"), with the main structure designed to remain elastic or with minor inelastic deformations. A systematic procedure was proposed to design buildings with metallic structural fuses. Kiggins and Uang [77] showed that even if buckling restrained braced frames exhibit a favourable energy-dissipating mechanism, the low post-yield stiffness of the braces leave the system vulnerable to unfavourable behavioural characteristics such as large permanent drift. The potential benefit of using buckling-restrained braces in a dual system to minimize permanent deformations was investigated and shown to reduce significantly residual story drifts.

As proposed by Stratan and Dubina [74], [75], in order to provide the re-centring capability of a structure with eccentrically braced frames with removable dissipative members, it was suggested to use dual structural configurations, obtained by combination of EBFs and moment resisting frames (MRFs). If the more flexible MRFs are kept elastic (a possible way to favour this is to realise some members from high-strength steel), they would provide the restoring force necessary to re-centre the structure upon removal of damaged removable links.

An idealized dual system consisting of two inelastic springs connected in parallel is shown in Fig. 2-49a. In order to provide the re-centring capability, the flexible subsystem should be kept in the elastic range up to the displacements at which the rigid subsystem attains its ultimate plastic deformation capacity. However, a conventional dual system that satisfies this condition will not return to the initial position following deformations into the inelastic range, even if permanent displacements δ_{pD} in the dual system are smaller than the ones that would be obtained in a rigid system alone δ_{pr} (Fig. 2-49b). Permanent deformations can be eliminated if the rigid subsystem is realised to be removable. Upon unloading of the dual system, there is a permanent displacement δ_{pD}, and corresponding residual forces in the flexible (F_{pf}) and rigid (F_{pr}) subsystems. Once removable dissipative members are dismantled, stiffness and strength of the system is provided by the flexible subsystem alone (F_{pr}=0). If the flexible subsystem is still in the elastic range, it will return the system to the initial position, implying zero permanent deformations (Fig. 2-49c).

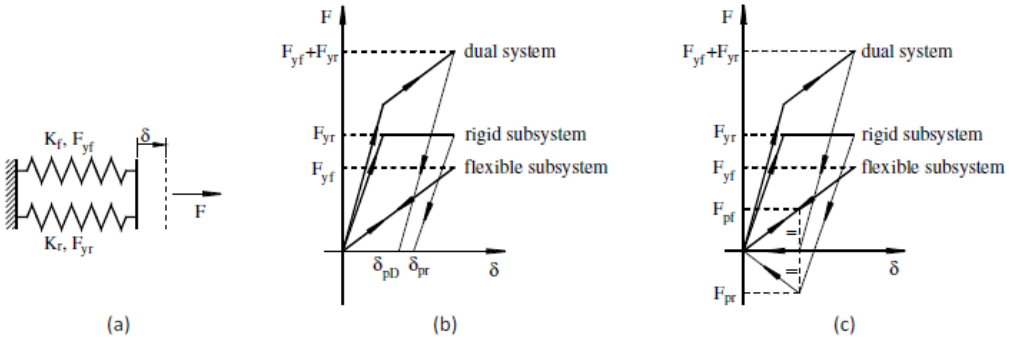

(a) (b) (c)

Fig. 2-49. Simplified model of a generalized dual system (a), and permanent deformations in a conventional dual system (b) and in a dual system with removable dissipative members (c)

2.6. Concluding remarks

Conventionally, structures have been designed to resist natural hazards (earthquakes, strong winds) through a combination of strength, deformability, and energy absorption. Their behaviour may be satisfactory well beyond the elastic limit in the case of a severe earthquake. These structures may remain intact due to their ability to deform inelastically, as this deformation results in increased flexibility and energy dissipation. Unfortunately, this deformation also results in local damage to the structure, as the structure itself must absorb much of the earthquake input energy.

Alternatively, some types of structural protective systems may be implemented to mitigate the damaging effects of environmental forces. These systems work by absorbing or reflecting a portion of the input energy that would otherwise be transmitted to the structure itself. As a result of this approach, many new and innovative concepts for structural protection have been advanced and are at various stages of development. These concepts can be divided into three main categories, namely passive control systems, semi-active control systems, and active control systems.

Passive control devices require no external power. They use the relative deformation between the attachment points of the device to the structure to dissipate energy. Many types and multiple configurations of passive energy dissipation devices exist. Two categories of passive devices are rate-independent and rate-dependent. Rate-independent devices dissipate energy through mechanisms that depend only on the displacement in the device. Examples of these include metallic yielding and friction dampers. The energy dissipation capacity of rate-dependent devices depends on the velocity across the device. These devices include viscous fluid dampers (VFD) and viscoelastic (VE) solid dampers. Depending on which VE materials are utilized, the magnitude of the displacement can have an effect on the energy dissipation capacity, making the energy dissipation capacity of VE dampers dependent upon both the velocity and the displacement.

Because they offer the adaptability of active control devices without requiring large power sources, semi-active control systems have attracted a great deal of attention in recent years. Many of these systems can operate on battery power alone, proving advantageous during seismic events when the main power source to the structure may fail. Also, because semi-active devices cannot inject energy into the structural system, they do not have the potential to destabilize the system. Recent work by several researchers has indicated that semi-active control systems, when appropriately implemented, achieve significantly better results than passive control systems; in fact, they may even outperform fully-active control systems, demonstrating significant potential for controlling structural responses to a wide variety of dynamic loading conditions. Some examples of semi-active control systems are: magnetorheological fluid dampers, semi-active stiffness dampers and semi-active tuned liquid column dampers.

Buildings designed according to modern seismic codes are expected to develop a controlled ductile inelastic response during major earthquakes, implying extensive structural damage after a design level earthquake, along with possibly substantial residual deformations. To address this drawback of traditional yielding systems, self-centring seismic systems have also been developed.

Modern seismic codes allow for inelastic deformations in dissipative zones during design earthquakes, accepting damage to a certain extend in the relevant

structural parts. As past experience shows, repair works are needed after strong earthquakes, either less or larger than the design one. Structural systems that are easily repairable-replaceable, while maintaining the benefits of high ductility, are therefore beneficial in seismic regions. For the structure to be repairable, in addition to constraining inelastic deformations to removable dissipative members (safety seismic fuses), the permanent (residual) drifts should be eliminated. Therefore innovation in developing new seismic resistant systems is highly appreciated.

The concept of removable dissipative members can be applied to eccentrically braced frames (EBFs) that are widely used in seismic regions, as they provide a convenient balance between stiffness and ductility, in comparison with the alternative MRFs (lacking stiffness) or concentrically braced frames (CBFs – with moderate ductility). Plastic deformations are constrained to removable (bolted) seismic links only that act as safety fuses. Optimizing the design of an EBF is a process in which the design of the shear link is central. Therefore, de-coupling the link from the remaining structural elements by using replaceable links, allows for an independent control of strength, stiffness and ductility of the EBF system. Bolted link-column and link beam connections have been studied.

In order to provide the re-centring capability of a structure with eccentrically braced frames with removable dissipative members, it was suggested to use dual structural configurations, obtained by combination of EBFs and moment resisting frames (MRFs). If the more flexible MRFs are kept elastic (a possible way to favour this is to realise some members from high-strength steel), they would provide the restoring force necessary to re-centre the structure upon removal of damaged removable links.

One of the advantages of using removable links relies in the greater flexibility in tuning their strength along the building height, in order to satisfy the stringent requirements from EN1998 in this respect. Assessment of global seismic of EBFs in general, and with removable links in particular is thus of increased interest. A large scale pseudo-dynamic test would provide valuable data on extending the provisions of EN1998 to EBFs with removable links.

3. STRUCTURAL DESIGN AND NUMERICAL INVESTIGATION OF EXPERIMENTAL SPECIMEN

3.1. Introduction

The first part of the chapter deals with the design of a dual eccentrically braced frame with removable links prototype structure. Considering that in the transversal direction the lateral force resisting system is located on the perimeter frames only, and in order to reduce the cost of the experimental mock-up, the latter is composed of the two end frames of the prototype only.

The second part of the chapter investigates the seismic performance of the test specimen through static and dynamic non-linear analyses on a described numerical model. It also treats the investigation of the link replacement procedure, giving technical solutions for the link removal procedure and order. There are concerns that a sudden release of link shear force may occur during link elimination that might be dangerous to the operating personnel. Consequently, some temporary bracing system consisting of tension braces and dampers were proposed to be used during the link removal.

3.2. Design of the prototype structure

In order to achieve the objectives presented in Chapter 1, a dual frame (eccentrically braced frames with removable bolted links combined with moment resisting frames) prototype structure was firstly conceived, designed and analysed. The links from eccentrically braced frames (EBFs) were conceived as removable (bolted links) dissipative elements because they are intended to provide the energy dissipation capacity and to be easily replaceable. The more flexible moment resisting frames provide the necessary re-centring capability to the structure.

This structure has 3 spans of 6 meters and 5 bays of 6 meters, and 3 storeys of 3.5 meters each. The main lateral load resisting system is composed of eccentrically braced frames. Additionally, there are 4 moment resisting frames on transversal direction and 10 moment resisting frames on longitudinal direction, to assure the restoring forces after an earthquake (Fig. 3-1). The main features of the structure can be summarised as follows (Fig. 3-2): columns realised from high strength steel; braces, beams and removable links realised from mild carbon steel; composite secondary beams; reinforced concrete floor cast in place on corrugated steel sheet.

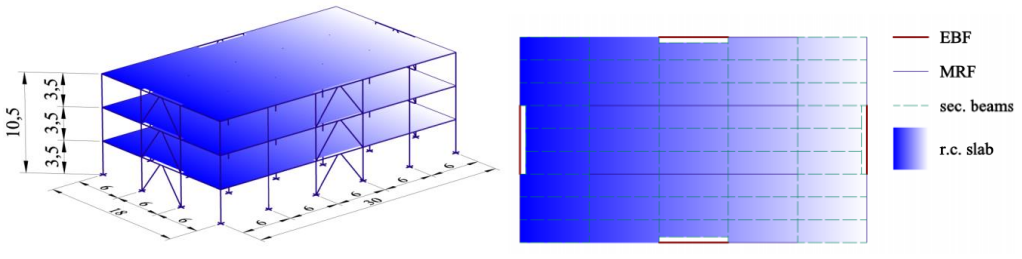

(a) (b)

Fig. 3-1. 3D view (a) and plan layout (b) of the prototype structure.

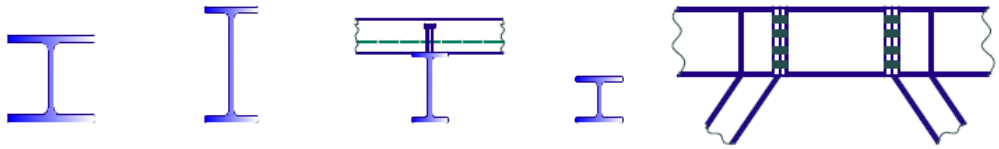

Steel column; high-strength steel

Steel main beams in MRFs; mild carbon steel

Composite steel concrete secondary beams; mild carbon steel

Steel braces; mild carbon steel

Bolted links; mild carbon steel

Fig. 3-2. Typical structural members

The capacity design of the structure was carried out according to EN1990 [78], EN1991 [79], EN1992 [80], EN1993 [81], EN1994 [82] and EN1998 [1]. A 4.9 kN/m^2 dead load and 3.0 kN/m^2 live load were considered. The building was analysed for stiff soil conditions (Eurocode 8 - EC8 type 1 spectrum for soil type C), characterised by 0.19g peak ground acceleration. A behaviour factor q=4 (ductility class medium) and inter-storey drift limitation of 0.0075 of the storey height are used.

The Ultimate Limit State (ULS) design was performed according to Eurocode 8 [1] rules. The links were designed from the seismic design situation combination for dissipative elements [78], with a length of e=400mm, as short links ($e<e_s=1.6M_{p,link}/V_{p,link}$) which dissipate energy by yielding in shear [1], in order to ensure the practical over-strength of the link's flush end plate connection. In the global analysis, a reduced equivalent shear area A_s* was used for the links in order to account for the more flexible behaviour of bolted links, arising from the following sources [83] (see Fig. 3-3):

- the link web shear deformation (γ)
- the link bending deformation (γ_M)
- the rotation from the link to beam connection (θ)
- the slip in the link to beam connection (Δ_s).

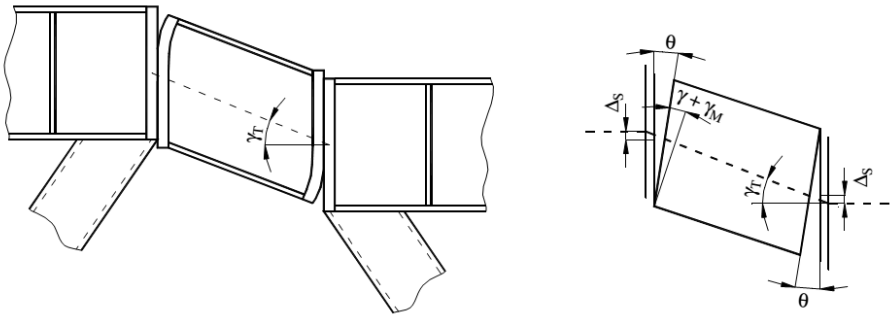

Fig. 3-3. Removable link deformation sources [83]

The bending stiffness of the link is explicitly modelled in the global analysis, therefore, the following formulas were used:

$$A_s^* = \frac{K_T^* e}{G} \quad (3\text{-}1)$$

$$K_T^* = \frac{1}{\frac{1}{K_\gamma} + \frac{1}{K_\theta} + \frac{1}{K_s}} \quad (3\text{-}2)$$

where:
K_T* is the equivalent stiffness of the removable link;
e is the link's length;
G is the transversal elasticity modulus;
K_γ is the shear stiffness of the link's web;
K_θ is the stiffness component due to the rotation in the link-beam connection;
K_s is the stiffness component due to the slip in the link-beam connection.

The MRFs beams were designed from the persistent design situation ULS combinations [78], while braces, beams from EBFs (eccentrically braced frames) and columns were designed from the seismic design situation combination for non-dissipative elements [78].

For the Serviceability Limit State (SLS), overall horizontal displacement over the building height and beams deformations were checked from the fundamental SLS combinations [78], while the inter-storey drifts were checked from the seismic SLS combination [78].

The geometry of the designed elements is presented in Table 3-1.

Table 3-1. Elements sections

Element	Section	Height	Flange width	Flange thickness	Web thickness
Column	welded	230	240	12	8
MRF Beam	IPE 240	240	120	9.8	6.2
EBF Beam	HE 240 A	230	240	12	8
Brace	HE 200 B	200	200	15	9
Link L1 & L2	welded	230	170	12	8
Link L3	welded	230	120	12	4

Steel structural components were designed in S355 grade steel, with two exceptions (Fig. 3-4). Grade S460 steel was used for columns, in order to obtain a larger capacity without increasing the stiffness. This approach helps promoting the capacity design rules. Links were designed from S235 steel grade (which was replaced during fabrication with equivalent DOMEX 240 YP B) mainly due to coping with available actuator capacities.

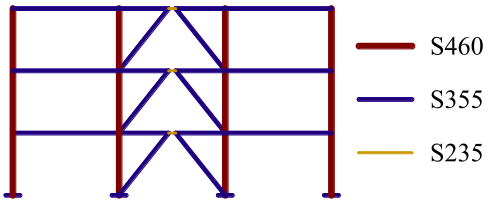

Fig. 3-4. Specimen materials

Mechanical characteristics of steel components according to quality certificates (and in some cases from independent tests as well) are presented in Table 3-2.

Table 3-2. Mechanical characteristics of steel components

Element	Component	Steel grade	f_y, N/mm^2	f_u, N/mm^2	f_u/f_y	A, %
Columns	Web t=8mm	S460NL	512	651	1.271	25.5
	Flange t=12 mm	P460NH	503	650	1.292	25.0
	Base plate t=30 mm	S355J2+N	387	536	1.385	30.9
Links (independent tests)	Web storey III t=4 mm	DOMEX 240 YP B	303	391	1.290	39.3
	Web storey I,II t=8 mm	DOMEX 240 YP B	293	380	1.297	34.8
	Flanges t=12 mm	DOMEX 240 YP B	250	361	1.444	39.0
	Stiffeners t=10 mm	DOMEX 240 YP B	282	377	1.337	39.3
Links (quality certificates)	Web storey III t=4 mm	DOMEX 240 YP B	282 326	380 389	1.348 1.193	37.0 36.0
	Web storey I,II t=8 mm	DOMEX 240 YP B	308 307	387 393	1.256 1.280	32.0 29.0
	Flanges t=12 mm	DOMEX 240 YP B	263 267	369 367	1.403 1.375	34.0 35.0
	Stiffeners t=10 mm	DOMEX 240 YP B	265 276	378 383	1.426 1.388	34.0 33.0
Link end plate	t=25 mm	S355J2+N	351	543	1.547	29.9

Element	Component	Steel grade	f_y, N/mm^2	f_u, N/mm^2	f_u/f_y	A, %
EBF braces	HEB200	S355J2+M	405	492	1.215	33.69
	Splice connection web plate t=6 mm	S355J2+N	373	495	1.327	26.8
	Splice connection flange plate t=8 mm	S355J2+N	378	533	1.410	24.3
EBF beam	HEA240	S355J0+M	384 385	541 490	1.409 1.273	32.0 30.89
	Splice connection web plate t=6 mm	S355J2+N	373	495	1.327	26.8
	Splice connection flange plate t=8 mm	S355J2+N	378	533	1.410	24.3
MRF beam	IPE240	S355J2+AR	425	553	1.301	29.0
	Haunch web t=6 mm	S355J2+N	373	495	1.327	26.8
	Haunch flange t=16 mm	S355J2+N	382	526	1.377	28.2
	End plate t=20 mm	S355J0+N	460	561	1.220	26.0
Sec. beams	IPE220	S355J0+AR	416	568	1.365	30.0

For the bolted links to be replaceable, the flush end plate connection (Fig. 3-5) was designed to remain in the elastic range (considering an elastic distribution of the internal bolt rows forces), the design bending moment and shear force for this connection being computed as follows [83]:

$$V_{j,Ed} = \gamma_{ov}\omega V_{pl,link}, \text{ where } \begin{cases}\gamma_{ov} = 1.25\\ \omega = 1.5\end{cases} \quad (3\text{-}3)$$

$$M_{j,Ed} = \frac{V_{j,Ed}e}{2} \quad (3\text{-}4)$$

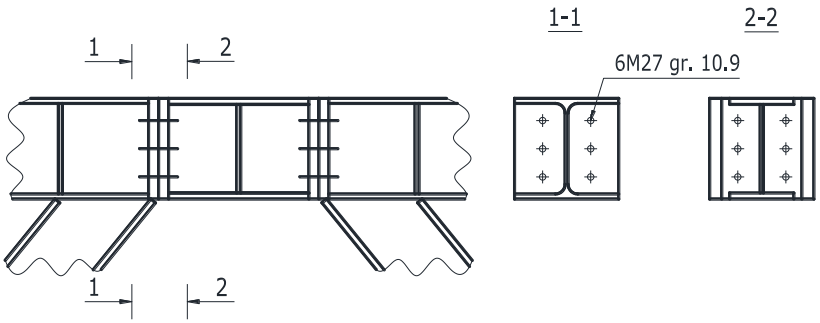

Fig. 3-5. Link flush end plate connection

The extended full-strength end plate MRF beam to column connection (Fig. 3-6) was designed to resist efforts larger than the ones corresponding to the formation of plastic hinges at the ends of the beam.

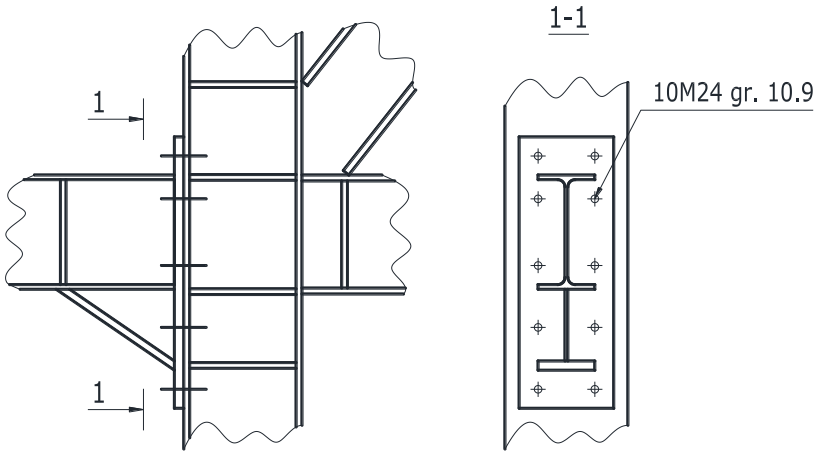

Fig. 3-6. Beam to column connection

The columns are fixed at the bottom part, the base connection being described in the following chapter.

3.3. Description of the test specimen

Considering that in the transversal direction of the prototype structure the lateral force resisting system is located on the perimeter frames only, and in order to reduce the cost of the experimental mock-up, the latter is composed of the two end frames only (Fig. 3-7) with columns fixed at the base.

The experimental mock-up has 3 spans of 6 meters, 1 bay of 6 meters and 3 stories of 3.5 meters each. The lateral force resisting system is composed of two dual steel frames (eccentrically braced and moment resisting frames), to each frame being assigned the masses corresponding to half of the prototype structure, computed from the following load combination, according to EN1990 [78]:

$$G_k + \Psi_2 \times Q_k \quad (3\text{-}5)$$

where:
G_k is the permanent load;
Q_k is the variable load;
Ψ_2 is the factor for quasi-permanent value of a variable action (considered 0.3).

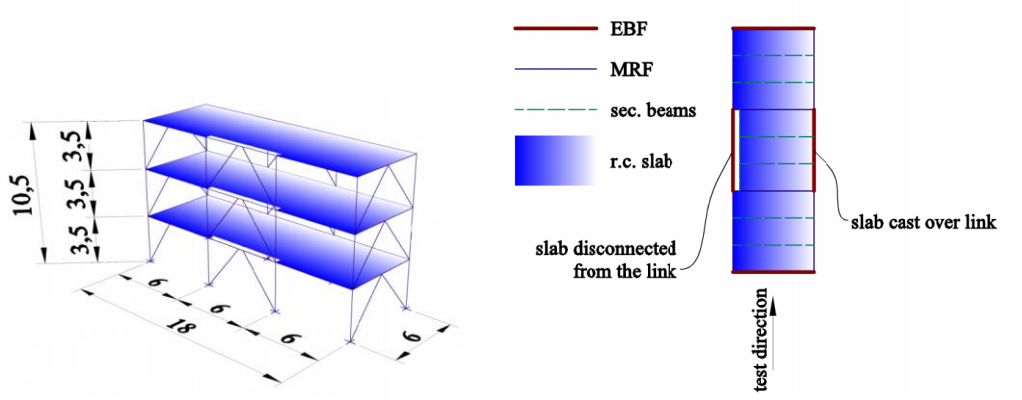

(a) (b)

Fig. 3-7. 3D view (a) and plan layout (b) of the experimental mock-up.

In case of the base connection, the 30 mm thickness base plate welded to the column steel section is bolted to a 100 mm thickness plate by 7 M36 10.9 HV bolts (4 M36 for the corner columns). The 100 mm thickness plate is anchored to the reaction floor using four Dywidag bars (Fig. 3-8) at a distance of 1.00 m between them. 20 mm thick stiffeners were welded to both the column flanges and the steel base plate.

The M36 bolts are tightened with 500 Nm torque and the 30 mm base plate is welded to the 100 mm thick plate on all four sides.

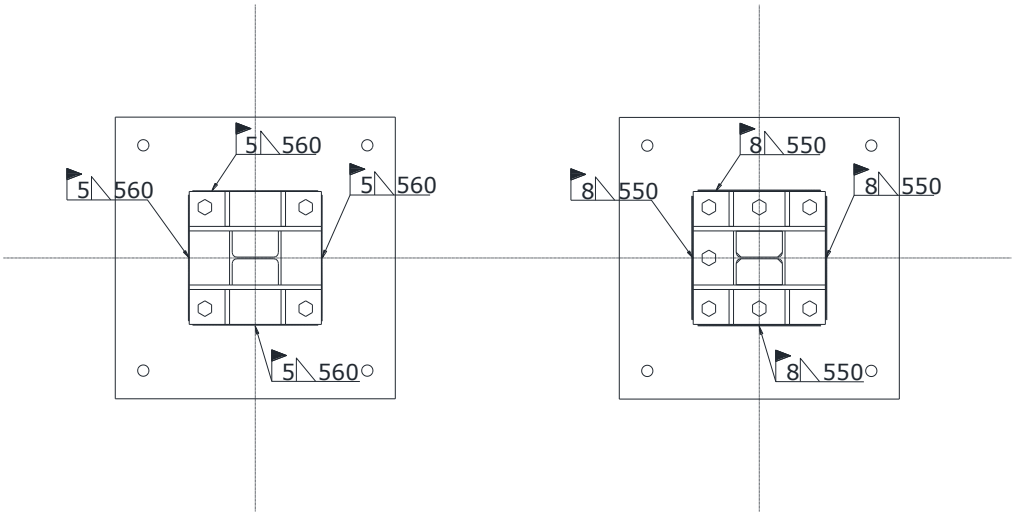

(a) (b)

Fig. 3-8. Base connections for: (a) corner and (b) central columns.

The floor layout is conceived in a manner that allows investigation of two different solutions of interaction between the removable link and the reinforced

concrete slab (Fig. 3-9). One of the two eccentrically braced frames is realised so that the beam containing the removable link is totally disconnected from the reinforced concrete slab (the south frame). It is expected that this solution will prevent any damage to the reinforced concrete slab. In the other EBF (the north frame) the beam containing removable links is connected to the slab in a conventional way. It is expected that some damage will occur in the reinforced concrete slab at the interface with the removable link, needing local repair after a strong earthquake.

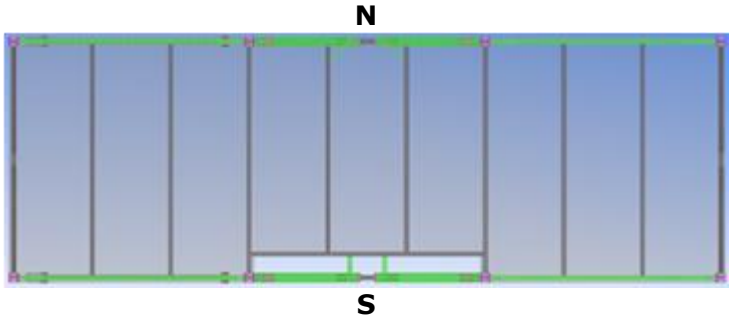

Fig. 3-9. Floor layout

The reinforced concrete slab was designed as a one way slab, on the longitudinal direction. The 90 mm thickness slab is made from C25/30 concrete, reinforced with ϕ8/130 mm 610HD independent bars, cast over 0.8 mm thickness, 55 mm high, A55-P600 G5 corrugated steel sheeting used as formwork.

The ends of the links are fixed at the upper side by the slab, in the north frame, and at the lower side by L fly-braces and at both sides by L braces in the south frame (Fig. 3-10).

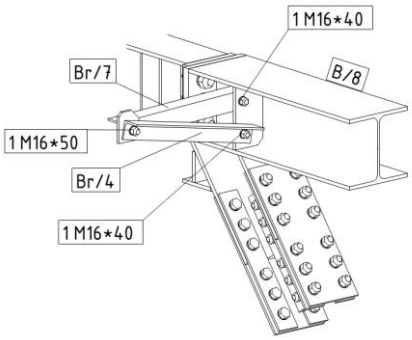

Fig. 3-10. Link end braces

In order to transfer the horizontal loads imposed by the actuators to the structure, there is used, at each level, a transverse, very stiff, C25/30 concrete beam reinforced with B450-C steel bars (Fig. 3-11).

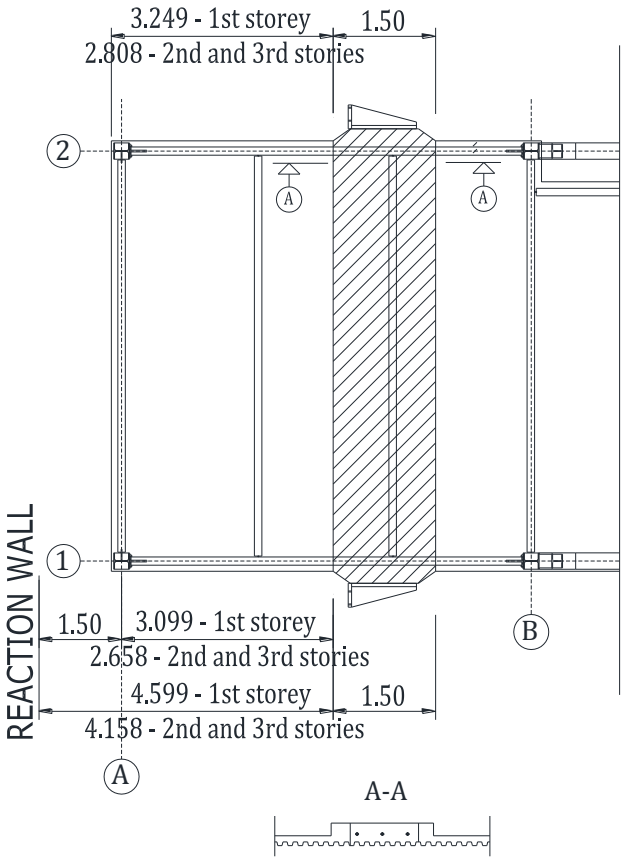

Fig. 3-11. RC loading beam position

The secondary beams are pinned composite beams. Shear studs are present on the main beams, except the zones near the joints and over the links (Fig. 3-12) and there is a 50 mm gap between the reinforced concrete slab and the steel columns, ensured by strips of polystyrene board in order to prevent transferring of forces between slab and columns (Fig. 3-13).

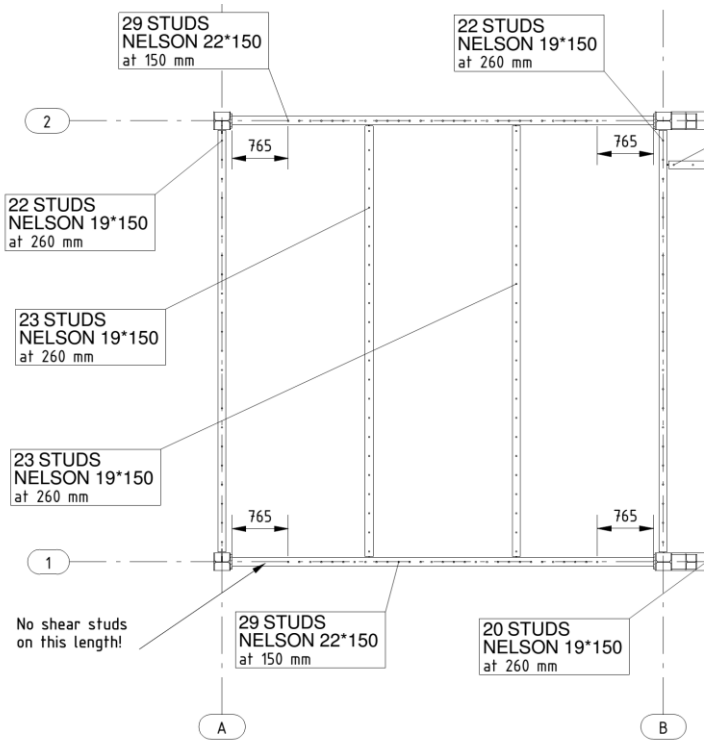

Fig. 3-12. Shear studs arrangement

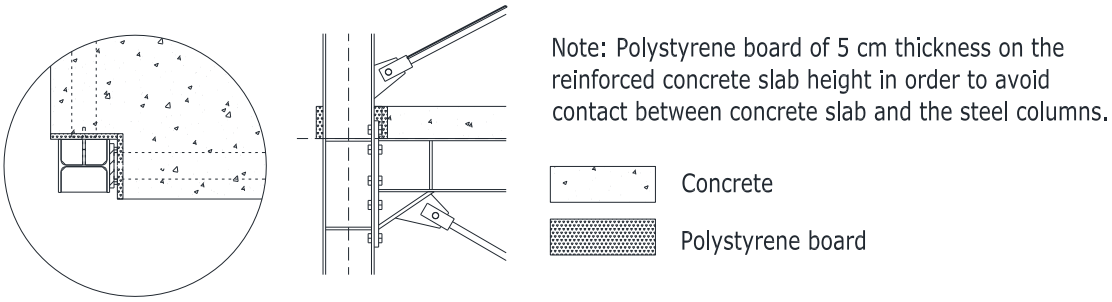

Fig. 3-13. Details of gap between r.c. slab and steel columns.

3.4. Numerical evaluation and investigation of the test specimen

3.4.1. Numerical model

In order to assess the structural performance and to validate the feasibility of the link removal procedure, numerical analyses were made on a model of the test structure using SeismoStruct program [84]. Due to the fact that during testing of

the experimental model the pseudo-dynamic procedure will be applied on the south frame (with links disconnected from the slab), and the obtained displacements enforced on the north frame (with slab casted over links), a 2D numerical model of the south frame was used (see Fig. 3-14).

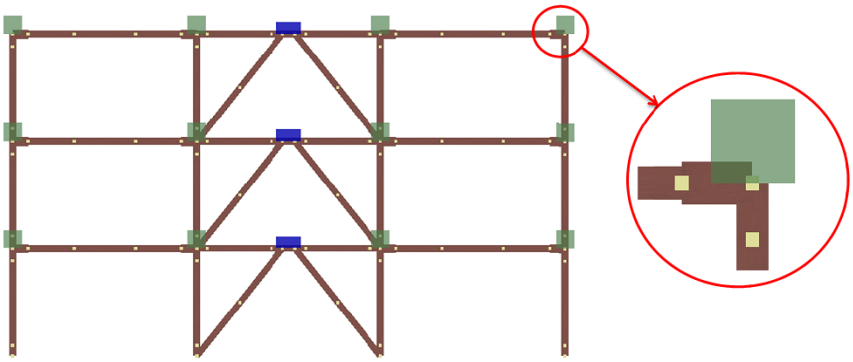

Fig. 3-14. 2D numerical model of the specimen

Force-based plastic hinge elements for beams and columns were used (plastic hinges being at the end of elastic haunches in the MRF beams). For braces, the physical theory model is used (two force based plastic hinge elements per brace; initial out-of-plane member imperfection). Bolted links were modelled using a force-based inelastic beam with two rotational springs at the end. The former was used in order to model the flexural stiffness of the link, while the latter were used in order to account for shear stiffness of the link, as well as rotational deformations and slip in the bolted connection (Fig. 3-15). The rotational springs are modelled using multi-linear curve link elements that can simulate the deteriorating behaviour of strength, stiffness, and pinching.

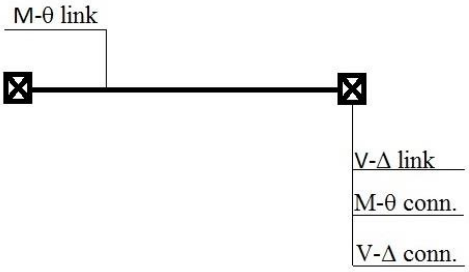

Fig. 3-15. Bolted link model

Material characteristics obtained from quality certificates were used (Table 3-2). The masses corresponding to half of the prototype structure, computed as described in Chapter 3.1, were assigned to nodes.

In order to obtain the numerical model of the removable links, a calibration was made using the experimental results obtained from removable links tests at Politehnica University Timisoara - CEMSIG Research Centre [85]. In order to calibrate the numerical model of the link, there were chosen the experimental results of the cyclic test on the link with the length of 400 mm (the LH5 link),

because it is of the same length and has a more closer values of the $e_s=1.6M_{p,link}/V_{p,link}$ ratio as the DUAREM structure links.

The backbone curve used to define the multi-linear rotational springs is defined in Fig. 3-16. The initial stiffness is the one computed with equation (3-2) (accounting for shear of the link and rotational deformations and slips in the bolted connections), the ratio between the ultimate force and the yield force is 1.4 and the ultimate shear deformation $\gamma_u=0.15$ rad.

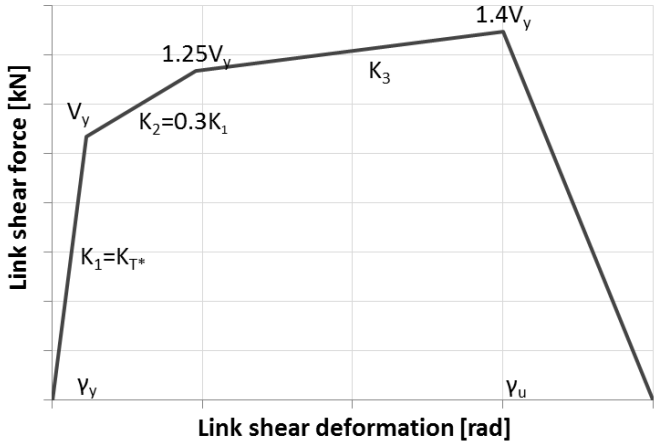

Fig. 3-16. Multi-linear link element backbone curve

A static nonlinear time-history analysis was made, where there were applied the cyclic experimental test displacements and there was observed a good correlation between the experimental results and the numerical simulation (Fig. 3-17). The calibrated numerical model was adopted for the DUAREM links and introduced in the numerical model of the test structure.

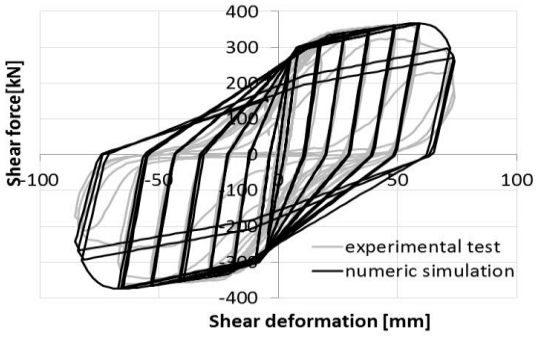

Fig. 3-17. Shear force – displacement relationship for the LH5 link

3.4.2. Evaluation of seismic performance

In order to evaluate the seismic performance of the specimen in the inelastic domain, static nonlinear analyses were performed together with using the N2 method, as well as dynamic nonlinear analyses.

3.4.2.1. Static nonlinear analysis (Pushover analysis)

Static pushover analyses were made on the model described above in order to evaluate the seismic performance of the test specimen, considering two lateral force distributions: modal (inverted triangular) and uniform, determined according to EN1998 [1].

The N2 method developed by Fajfar [86] is a method used to evaluate the seismic performance of structures designed by code methods (i.e. spectral analysis). This method combines the pushover analysis of a multi-degree-of-freedom (MDOF) model with the response spectrum analysis of an equivalent single-degree-of-freedom (SDOF) system, being computed a „target displacement" that represents the maximum displacement to be experienced during the design earthquake.

Structural performance was evaluated for the limit states shown in Table 3-7, where a_{gr} is the reference peak ground acceleration of 0.19g and a_g represents the peak ground acceleration for a specific earthquake level.

Table 3-3. Limit states and corresponding scaling factors for seismic input

Limit state	Return period, years	Probability of exceedance	a_g/a_{gr}	a_g/g
Damage Limitation (DL / SLS)	95	10% / 10 years	0.59	0.112
Significant Damage (SD / ULS)	475	10% / 50 years	1.00	0.190
Near Collapse (NC)	2475	2% / 50 years	1.72	0.327

The target displacements (D_t) were computed using the N2 method for each of the three limit states above. For each limit state, the link rotation at the target displacement was compared to the FEMA356 [87] acceptance criteria for shear links (0.005 rad at DL, 0.11 rad at SD and 0.14 rad at NC):

Table 3-4. Seismic performance assessment in case of uniform distribution pushover

	N2		FEMA acc. criteria	
PO uniform	D_t [mm]	Link rotation at D_t [rad]	Link rotation [rad]	Corresponding top displacement
DL/SLS	43,30	0,079	0,005	6,00
SD/ULS	73,30	0,127	0,11	61,20
NC	126,30	0,322	0,14	80,70

Table 3-5. Seismic performance assessment in case of modal distribution pushover

	N2		FEMA acc. criteria	
PO modal	D_t [mm]	Link rotation at D_t [rad]	Link rotation [rad]	Corresponding top displacement
DL/SLS	45,70	0,052	0,005	7,20
SD/ULS	77,30	0,097	0,11	83,70
NC	133,10	0,295	0,14	86,40

Using the N2 method approach, it can be concluded that the performance objectives are not accomplished in case of the uniform distribution pushover and are accomplished only for the SD/ULS in case of the modal distribution pushover (see Table 3-4 and Table 3-5).

The pushover curves presented below (Fig. 3-18) illustrate the seismic performance of the specimen discussed above:

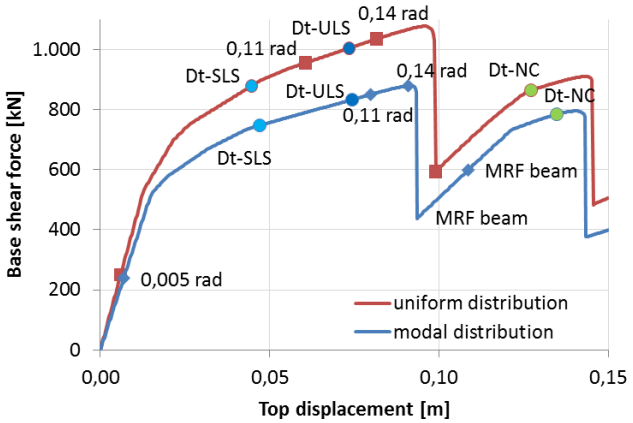

Fig. 3-18. Pushover curves

Although the performance objectives are not satisfied for SLS and NC using the N2 approach, the objective of having no yielding in the MRFs before the attainment of the ULS deformation in the removable links (0.11 rad) of the EBFs is accomplished, representing the basic design requirement for dual frames with removable dissipative members [88]. MRFs provide the re-centring of the specimen even until after the links ultimate deformation (0.14 rad).

3.4.2.2.Dynamic non-linear analysis (Time-history)

Seven recorded accelerograms were used for seismic performance assessment of the test structure using nonlinear time-history analysis. Recorded accelerograms were selected from the RESORCE database (http://www.resorce-portal.eu/, [89]). Records fulfilling the following criteria were used only: magnitude Mw ≥ 5.8, free-field or structure-related free-field instrument location, peak ground acceleration PGA ≥ 1.0 m/s^2. Accelerograms having closest matching with the target spectrum (EN 1998-1 type 1 elastic spectrum for soil type C) in terms of control

period T_C (0.6 s), effective peak ground acceleration (EPA), and effective peak ground velocity (EPV) were then selected. Characteristics of ground motion records are given in Table 3-6.

Individual accelerograms were first scaled to the target spectrum (EN 1998-1:2004 type 1, soil type C, a_g = 0.19g) in the $0.2T_1$ – $2T_1$ range using the equal area rule. The average spectrum was scaled to the target spectrum using EN 1998-1:2004 criteria. Response spectra of as scaled accelerograms are shown in Fig. 3-19 and Fig. 3-20, while acceleration time-histories can be observed in Fig. 3-21.

Pre-test nonlinear dynamic simulations were performed on the 2D model of the experimental mock-up described in 3.4.1, using the selected ground motion records.

Table 3-6. Characteristics of ground motion records selected for performance assessment.

Record code	Earthquake name	Date	Station name	Station country	Magnitude Mw
00385_H1	Alkion	24.02.1981	Xylokastro-O.T.E.	Greece	6.6
14336_H1	Montenegro (Aftershock)	24.05.1979	Bar-Skupstina Opstine	Montenegro	6.2
15613_H2	Izmit (Aftershock)	13.09.1999	Yarimca (Eri)	Turkey	5.8
15683_H2	Izmit (Aftershock)	13.09.1999	Usgs Golden Station Kor	Turkey	5.8
16035_H2	Faial	09.07.1998	Horta	Portugal	6.1
16889_H1	L'Aquila Mainshock	06.04.2009	L'Aquila - V. Aterno - Aquil Park In	Italy	6.3
17167_H1	Aigion	15.06.1995	Aigio-OTE	Greece	6.5

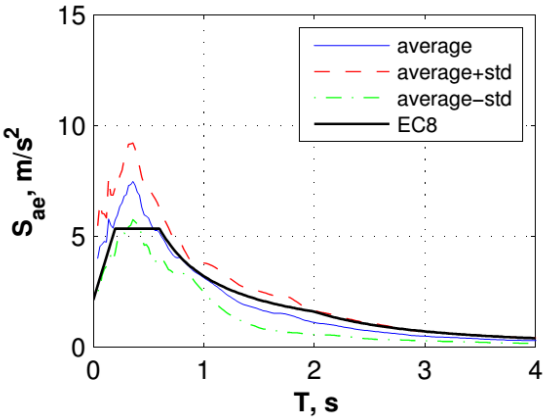

Fig. 3-19. Average and average +/- one standard deviation response spectra of selected records (as scaled) versus target spectrum.

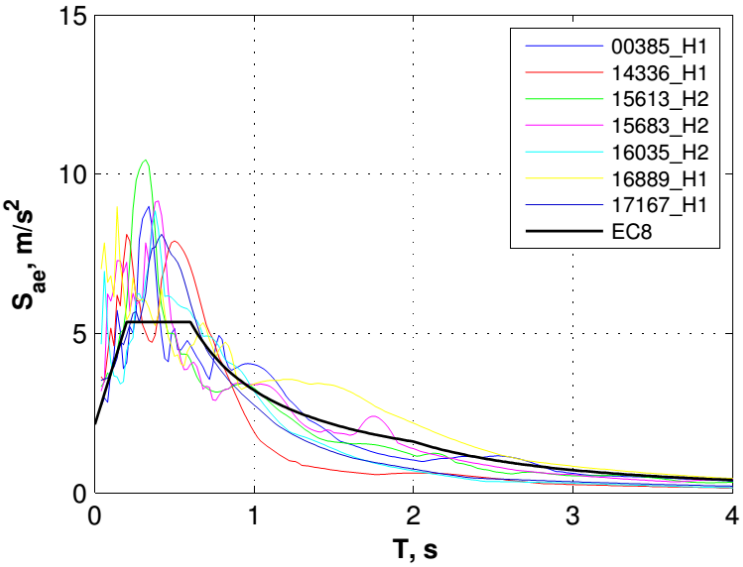

Fig. 3-20. Response spectra of selected records (as scaled) versus target spectrum

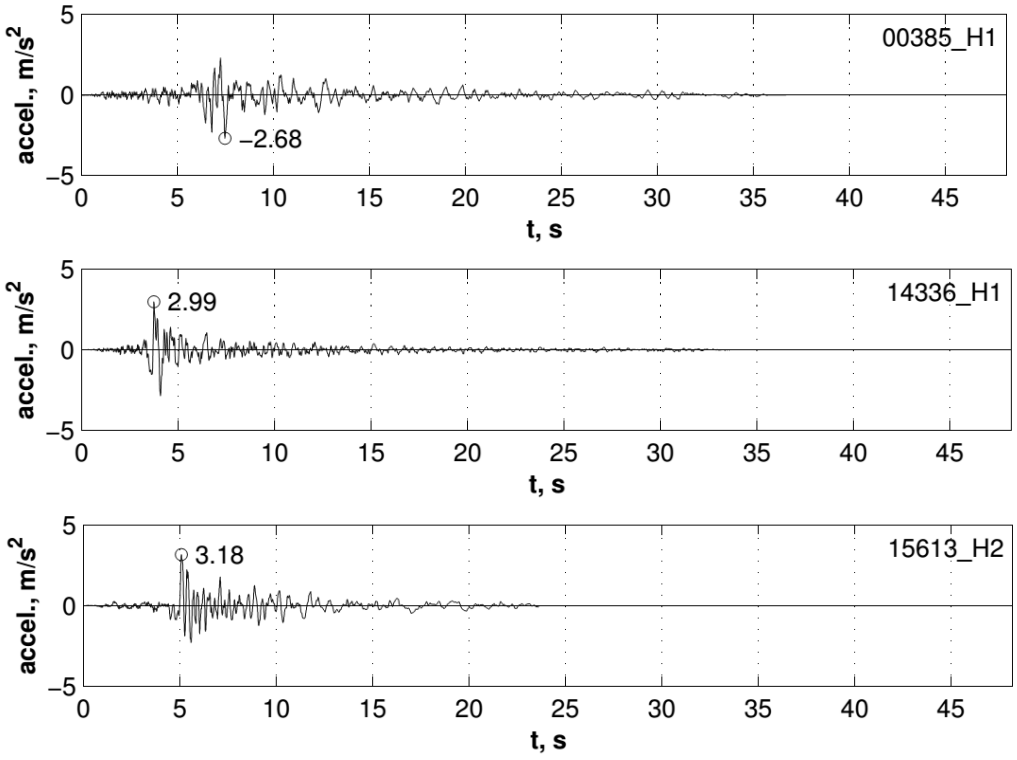

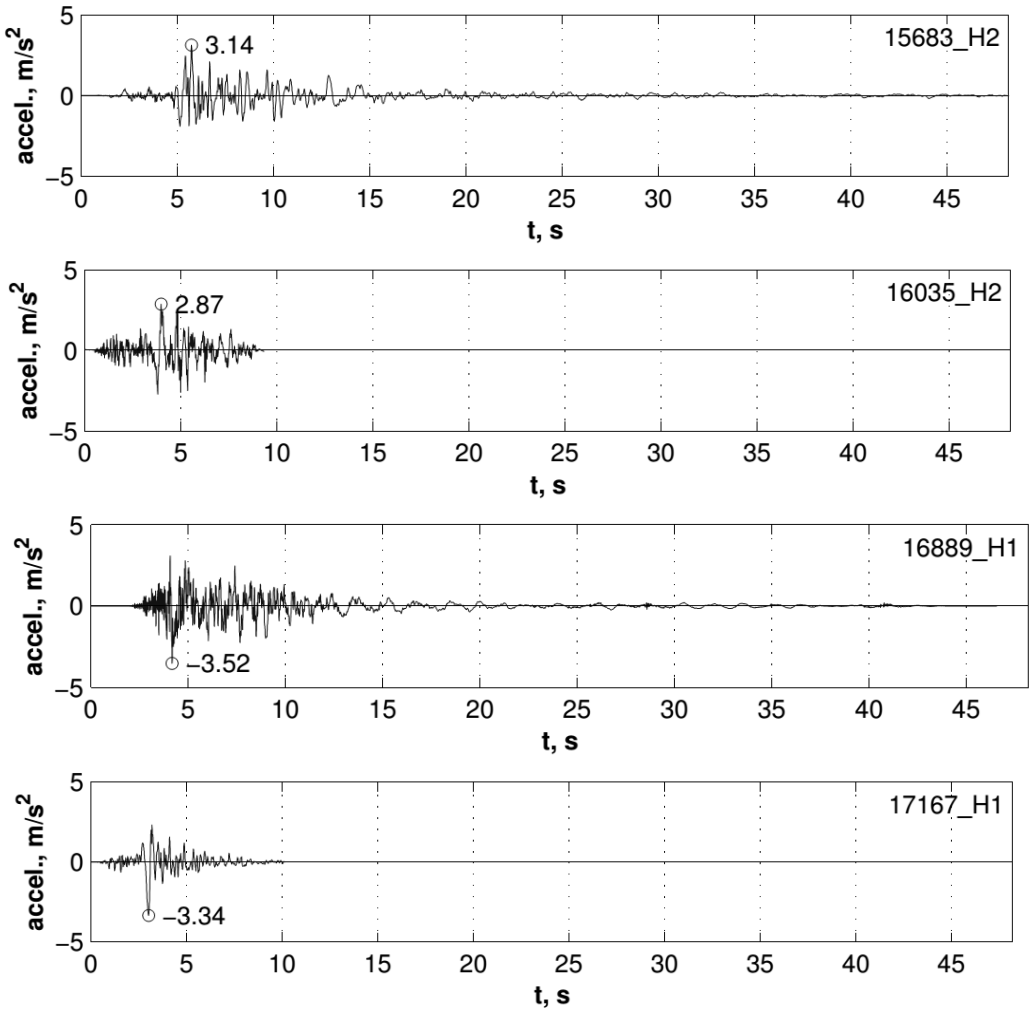

Fig. 3-21. Acceleration time histories of selected records.

Structural performance was evaluated for the limit states shown in Table 3-7, where a_{gr} is the reference peak ground acceleration (corresponding to 10% / 50 years earthquake) and a_g represents the peak ground acceleration for a specific earthquake level.

Table 3-7. Limit states and corresponding scaling factors for seismic input

Limit state	Return period, years	Probability of exceedance	a_g/a_{gr}
Damage Limitation (DL / SLS)	95	10% / 10 years	0.59
Significant Damage (SD / ULS)	475	10% / 50 years	1.00
Near Collapse (NC)	2475	2% / 50 years	1.72

The key parameters of structural response at the limit states considered are shown in Table 3-8. Acceptance criteria for shear links were considered those from FEMA 356 [87] (0.005 rad at DL, 0.11 rad at SD and 0.14 rad at NC).

At the Damage Limitation (DL) limit state all structural components except links are in the elastic range. Shear deformations in links exceed the FEMA 356 [87] limits, but this is normal, since the design carried out according to EN1998 did not impose any limitation on yielding of structural members at DL limit state. Even so, permanent inter-storey drifts are very low (0.007 % or 0.2 mm in average, and a maximum value of 0.028 % or 0.98 mm) and peak inter-storey drifts are within the limits imposed (<0.75%). In these conditions, the advantage of the proposed system is obvious, since the damaged dissipative members (links) can be replaced easily due to negligible permanent drifts. Even if some structural damage is present, it can be repaired easily by replacing the bolted links.

At the Significant Damage (SD) limit state damage is still constrained to links only, which exhibit plastic deformation demands in the range of 0.11 rad, which is very close to the acceptable 0.11 rad. Permanent drifts are only slightly larger than at the DL limit state, the average values being about 0.011 % or 0.4 mm, and the maximum ones of 0.033 % or 1.2 mm. Due to low permanent drifts, the structure is easily repairable at this limit state as well.

At the Near Collapse (NC) limit state the structural damage is widespread. Shear deformations in links are well over acceptable values (0.432 rad compared to 0.14 rad). However, due to moment resisting frames, the overall performance of the structure can be considered acceptable for this limit state, average transient drifts being of the order of 2.73%. Plastic deformation demands are present in moment resisting frames (beams and columns) and braces. Even so, permanent inter-storey drifts are not very large (average of 0.15% or 5.1 mm). However, repairing of the structure is considered not to be feasible and desirable at these large levels of seismic input.

Table 3-8. Key parameters of response

	Peak transient inter-storey drift, %			Permanent inter-storey drift, %			Shear deformation in links, rad		
Record	DL	SD	NC	DL	SD	NC	DL	SD	NC
00385_H1	0.45	0.86	2.82	0.001	0.001	0.155	0.054	0.108	0.432
14336_H1	0.46	0.76	1.68	0.003	0.005	0.016	0.056	0.093	0.256
15613_H2	0.43	0.76	2.87	0.003	0.003	0.154	0.051	0.101	0.441
15683_H2	0.40	0.91	3.06	0.028	0.011	0.128	0.046	0.123	0.169
16035_H2	0.51	0.86	2.14	0.004	0.002	0.125	0.058	0.108	0.327
16889_H1	0.39	0.72	3.69	0.006	0.025	0.238	0.044	0.094	0.570
17167_H1	0.56	1.17	2.82	0.006	0.033	0.199	0.069	0.155	0.429
mean	**0.46**	**0.86**	**2.73**	**0.007**	**0.011**	**0.145**	**0.054**	**0.108**	**0.432**

3.4.3. Re-centring capability of the specimen

The issue of permanent (residual) deformations of the structure after a damaging earthquake, which can lead to difficulties in replacing removable links can be solved by realising a structure as a dual one, by combining eccentrically braced frames (EBFs) with moment-resisting frames (MRFs) [74], [75]. If the more flexible MRFs are kept elastic (a possible way to favour this is to realise some members from high-strength steel) and the plastic deformations are constrained to removable dissipative members only (see Chapter 3.4.2.1), the MRFs would provide the

restoring force necessary to re-centre the structure upon removal of damaged removable links.

A requirement that EN1998 [1] does not mention about dual structures can be found in other codes (e.g. NEHRP [92], P100-1 [93]): the MRFs should be able of resisting at least 25% of the total seismic force.

Using an approach studied by Stratan et al. [88], the yield strength of the EBF (F_y^{EBF}), as well as the yield strength of the two MRFs (F_y^{MRF}) were computed using the following formulas:

$$F_y^{EBF} = \frac{L}{H} V_{p,link} \quad (3\text{-}6)$$

where $V_{p,link}$ is the shear strength of the link.

$$F_y^{MRF} = \frac{4M_{pl,b}}{H} \quad (3\text{-}7)$$

where $M_{pl,b}$ is the beam plastic moment.

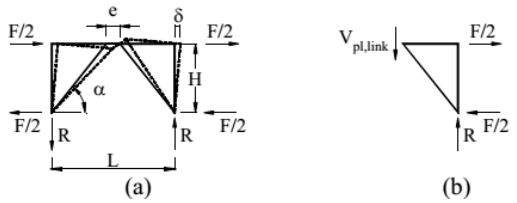

Fig. 3-22. Basic one-storey EBF component [88]

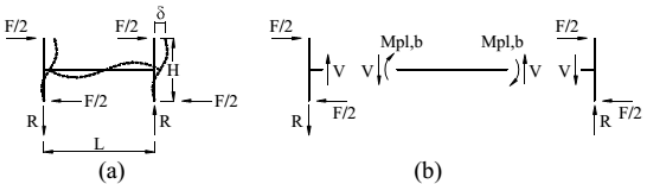

Fig. 3-23. Basic one-storey MRF component [88]

The yield strength of the MRFs represents 27% for the first 2 levels and 42% for the 3rd one from the total yield strength of the system, the specimen being considered a dual structure.

Moreover, the ultimate displacement of the EBF (δ_u^{EBF}) at ULS (where the plastic deformation capacity of the link $\gamma_{pl,u}$ is considered to be 0.11 rad) is smaller than the yield displacement of the MRFs (δ_y^{MRF}), meaning the yielding in MRFs is prevented up to the attainment of ultimate deformation capacity in the EBF with removable links. This was checked analytical using the formulas below and numerical in Chapter 3.4.2.1 (uniform distribution pushover).

$$\delta_u^{EBF} = \delta_Y^{EBF} + \delta_{pl}^{EBF} = \frac{F_y^{EBF}}{K^{EBF}} + \frac{e}{L-e} \cdot H \cdot \gamma_{pl,u} \quad (3\text{-}8)$$

where δ_y^{EBF} is the yield displacement of the EBF, δ_{pl}^{EBF} is the plastic displacement of the EBF, K^{EBF} is the EBF stiffness and *e, L, H* are shown in Fig. 3-22.

$$K^{EBF} = \frac{K_{link}^{EBF} \cdot K_{br}^{EBF}}{K_{link}^{EBF} + K_{br}^{EBF}} \quad (3\text{-}9)$$

where K_{link}^{EBF} is the link's stiffness and K_{br}^{EBF} is the braces stiffness.

$$K_{link}^{EBF} = \frac{L}{H^2} \cdot (L-e) \cdot \frac{G \cdot A_s}{e} \quad (3\text{-}10)$$

$$K_{br}^{EBF} = 2 \cdot \frac{E \cdot A}{l_{br}} \cdot \cos^2 \alpha \quad (3\text{-}11)$$

where *G* is the shear modulus, A_s is the link shear area, *E* is the Young's modulus, *A* is brace cross-section area, l_{br} is the brace length.

$$\delta_y^{MRF} = \frac{F_y^{MRF}}{K^{MRF}} \quad (3\text{-}12)$$

where K^{MRF} is the MRFs stiffness.

$$K^{MRF} = \frac{4}{H^2 \cdot \left(\frac{L}{6 \cdot E \cdot I_b} + \frac{H}{12 \cdot E \cdot I_c} \right)} \quad (3\text{-}13)$$

where L and H are shown in Fig. 3-23.

Table 3-9. Comparison of analytical and numerical predictions of storey displacements

	δ_u^{EBF}, mm	δ_y^{MRF}, mm	$\delta_y^{MRF}/\delta_u^{EBF}$
Analytical	29.4	54.6	1.86
Numerical	28,9	49.6	1.72

Table 3-8 presents a comparison of yield displacements in the MRFs and ultimate displacements in the EBF for the first storey, where largest demands are present. Acceptable agreement can be observed between analytical and numerical results, observing a difference of only 8%.

3.4.4. Link replacement investigation

Residual forces and deformations are present in the links after they have experienced plastic excursions during an earthquake. Removing a damaged link involves redistribution of residual forces to other parts of the structure, more precisely from eccentrically braced frame to moment resisting ones. The technically easiest way to release the residual forces in links is believed to be by flame cutting the web and flanges of the link. This operation is necessary only if large permanent deformations are present in the link. Direct unbolting might be feasible if permanent deformations are small.

There are concerns that a sudden release of link shear force may occur during flame cutting of the link that might be dangerous to the operating personnel. Consequently, the solution was improved by introducing a temporary bracing system consisting of tension braces and dampers. During removal of links through flame cutting, the forces locked in the links are transferred to the temporary bracing system and smoothly released through the dampers. Investigations underlying the process of link removal through flame cutting and use of safety braces are detailed in section 3.4.4.1.

Link removal procedure is performed on a storey-by-storey basis. Once all links from a storey are removed, all structural components from that storey are in the elastic range of response. Therefore, as brace forces are released through dampers, the structure recovers its initial (plumb) position, becoming free of any locked-in forces and new link can be installed. Additional information on link removal order and replacement procedure is given in section 3.4.4.2.

3.4.4.1.Technical solution for link removal

Tests were performed in the past at Politehnica University Timisoara - CEMSIG Research Centre, on a one storey – one span eccentrically braced frame with removable link (see Fig. 3-24), in order to check the feasibility of link removal through flame cutting [94]. It was found out that removing the link web by oxy-fuel cutting is not enough for eliminating the residual forces in the link, due to the fact that flanges have an important contribution to the ultimate shear strength of the link, so both the web and flanges have to be flame cut in order to allow easy replacement of the links.

(a) (b)

Fig. 3-24. One storey frame: (a) experimental setup and (b) flame cutting of the link.

Though no sudden displacements or vibrations in the experimental mock-up were observed during link removal, there was a concern that such phenomena might be present in the larger DUAREM mock-up. Therefore, solutions were sought that would guarantee a safe link removal procedure.

A simplified single degree of freedom (SDOF) system was analysed, representative for the elimination of the links from the first storey. The elastic structure was modelled by a vertical cantilever with a height equal to the DUAREM structure storey height and the same stiffness of the reference structure with all shear links removed (see Fig. 3-26a). The mass was then computed in order to obtain the same period of vibration in the SDOF model and the reference multi degree of freedom (MDOF) model (with shear links removed). A value of 2% Rayleigh damping was used.

A time history analysis was performed, under a horizontal force at the top of the cantilever with the load pattern below (see Fig. 3-25). The amplitude of the force was equal to the one generating the obtained displacement in the 3D model of the test structure from the step just before the elimination of the last link from the first storey, at the time the force is suddenly dropped to zero. As can be observed in Fig. 3-26d, large vibrations are present in the reference case (no braces), assuming there is a sudden release of forces in the link due to instantaneous drop of link shear capacity.

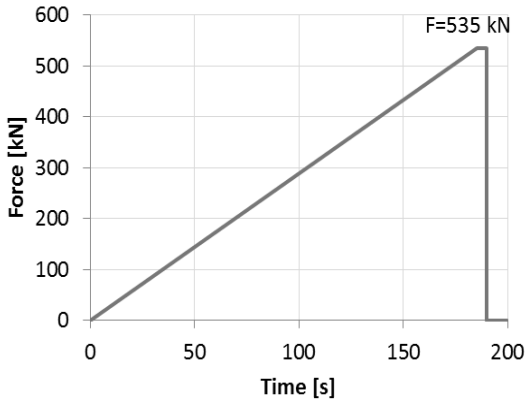

Fig. 3-25. Time history function definition

Two solutions that would alleviate these vibrations were investigated. In the first case, a tension brace that releases force through manual or hydraulic de-tensioning (see Fig. 3-26b) was analysed, while in the second one a bracing system composed of a brace in series with a damper (see Fig. 3-26c) was employed. Damper properties were selected so as to provide a damping coefficient c close the critical one. Damper response was modelled using the law: $F_D=cv^a$, with $a=1$. It can be observed (see Fig. 3-26d) that the top displacement amplitude decreases by adding the tension brace but the structure still vibrates. Moreover, there is an important amplification (about 2) of the force in the brace with respect to the static force. However, when using a brace in series with a damper, it can be observed that the structure doesn't vibrate, meaning that this is the best solution from safety

considerations. The brace force is very close to the force obtained from static linear analysis.

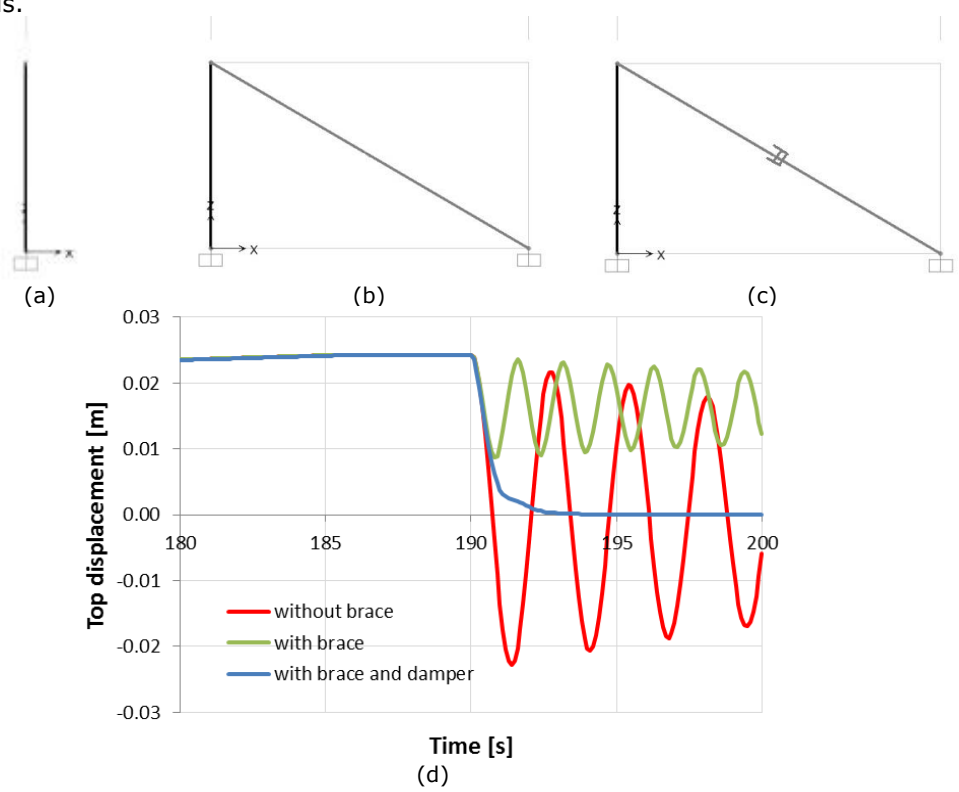

Fig. 3-26. Vertical cantilever (a); vertical cantilever with brace (b); vertical cantilever with brace and damper (c); vibrations chart (d).

Consequently, two safety braces with dampers (Fig. 3-27) were fabricated, in order to be used during removal of links in the experimental mock-up, one for each eccentrically braced frame.

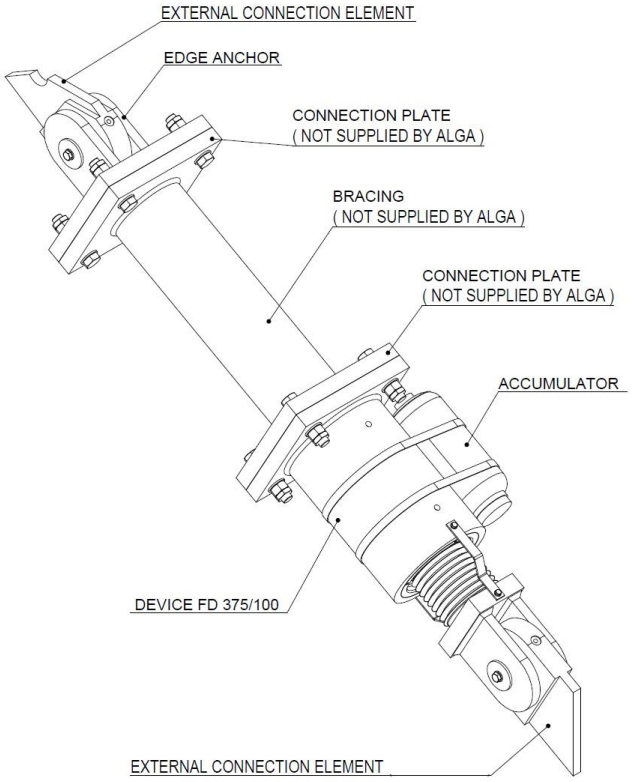

Fig. 3-27. Braces with dampers

3.4.4.2.Link removal order and replacement procedure

Numerical simulations were performed in order to investigate the link replacement procedure following significant inelastic deformations [3]. Nonlinear static analysis was used, considering that there is no possibility of dynamic effects, especially when safety braces are used. It was found out that there is negligible redistribution of forces among storeys (an increase of link shear force smaller than 10%). Therefore, the link removal procedure can be performed on a storey by storey basis, starting from the least loaded to the most loaded one (from the upper storey toward the lower one, see Fig. 3-28), in parallel for both frames of the experimental mock-up.

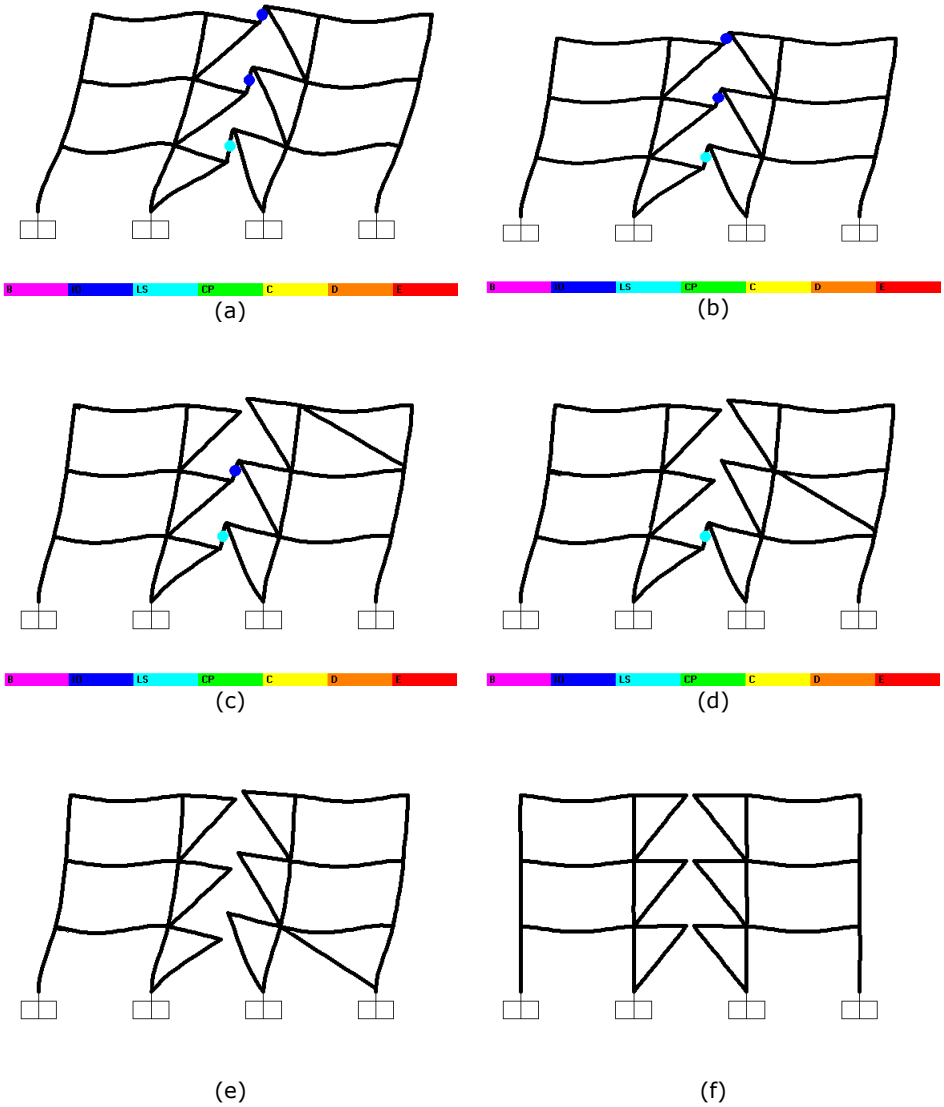

Fig. 3-28. Height-wise link removal order.

Once all links have been removed, and the last safety brace was eliminated, the structure should recover its initial (plumb) position. The new (replacement) links should be installed at this stage. To simplify the mounting of new links, the latter were fabricated slightly shorter (by 2 mm) with respect to the original ones. Shims (1 mm and 2 mm) were made available in order to fit possible gaps between end plates. Additionally, a manually operated hydraulic jack of 400 kN capacity was used to slightly put apart the beam end plates before installing new links. Special

supports for the hydraulic jack were foreseen on the braces just under the links (see Fig. 3-29).

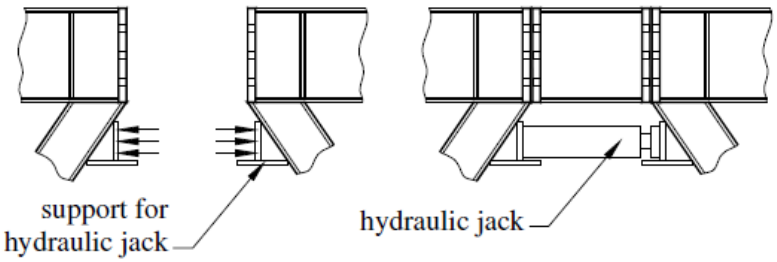

Fig. 3-29. The supports for hydraulic jack (a) and the hydraulic jack used to facilitate removal of existing links and fitting new ones (b).

The test procedure to be used during pseudo-dynamic tests that include link replacement is outlined in the following:

- Gravity loading is applied using water tanks and concrete blocks placed on the reinforced concrete floor.
- Earthquake action is simulated on the test structure using the pseudo-dynamic procedure (see Fig. 3-29a).
- Actuators are disconnected from the mock-up, while instrumentation is still in operation. Permanent deformations will be present in this state (see Fig. 3-29b).
- Two bracing systems are installed in the last (third) storey by connecting them to the gusset plates available in one moment resisting span.
- One of the links from the third storey is flame cut (see Fig. 3-29c). First the central panel of the web is cut out, then, the flanges. The bolts are then removed by untightening. A hydraulic jack is placed in a special support below the link and is used to apply a force of maximum 400 kN in order to slightly push apart the end plates, removing the link. The brace forces are released through braces with dampers.
- The same procedure is repeated for the other link from the third storey and the two bracing systems are removed.
- The previous three steps are repeated for storey 2 (see Fig. 3-29d) and storey 1 (see Fig. 3-29e). The structure should recover its plumb position at this stage (see Fig. 3-29f).
- New links are installed in the first storey.
- The previous step is repeated for storey 2 and 3.

3.5. Concluding remarks

In order to achieve the objectives of the DUAREM project, a dual frame (eccentrically braced frames with removable bolted links combined with moment resisting frames) prototype structure was firstly conceived, designed and analysed. The links from eccentrically braced frames (EBFs) were conceived as removable (bolted links) dissipative elements because they are intended to provide the energy

dissipation capacity and to be easily replaceable. The more flexible moment resisting frames provide the necessary re-centring capability to the structure.

Considering that in the transversal direction of the prototype structure the lateral force resisting system is located on the perimeter frames only, and in order to reduce the cost of the experimental mock-up, the latter is composed of the two end frames only with columns fixed at the base.

To evaluate the seismic performance of the specimen in the inelastic domain, static nonlinear analyses were performed together with using the N2 method, as well as dynamic nonlinear analyses. Although the performance objectives are not satisfied for SLS and NC using the N2 approach, the objective of having no yielding in the MRFs before the attainment of the ULS deformation in the removable links (0.11 rad) of the EBFs is accomplished, representing the basic design requirement for dual frames with removable dissipative members. MRFs provide the re-centring of the specimen even until after the links ultimate deformation (0.14 rad). Pre-test nonlinear dynamic simulations were performed on the 2D model of the experimental mock-up, using the seven selected ground motion records. Structural performance was evaluated for the limit states: DL (SLS), SD (ULS) and NC.

At the Damage Limitation (DL) limit state all structural components except links are in the elastic range. Shear deformations in links exceed the FEMA 356 limits, but this is normal, since the design carried out according to EN1998 did not impose any limitation on yielding of structural members at DL limit state. Even so, permanent inter-storey drifts are very low and peak inter-storey drifts are within the limits imposed. In these conditions, the advantage of the proposed system is obvious, since the damaged dissipative members (links) can be replaced easily due to negligible permanent drifts. Even if some structural damage is present, it can be repaired easily by replacing the bolted links.

At the Significant Damage (SD) limit state damage is still constrained to links only, which exhibit plastic deformation demands very close to the acceptable 0.11 rad. Permanent drifts are only slightly larger than at the DL limit state. Due to low permanent drifts, the structure is easily repairable at this limit state as well.

At the Near Collapse (NC) limit state the structural damage is widespread. Shear deformations in links are well over acceptable values. However, due to moment resisting frames, the overall performance of the structure can be considered acceptable for this limit state. Plastic deformation demands are present in moment resisting frames (beams and columns) and braces. Even so, permanent inter-storey drifts are not very large. However, repairing of the structure is considered not to be feasible and desirable at these large levels of seismic input.

Residual forces and deformations are present in the links after they have experienced plastic excursions during an earthquake. Removing a damaged link involves redistribution of residual forces to other parts of the structure, more precisely from eccentrically braced frame to moment resisting ones. The technically easiest way to release the residual forces in links is believed to be by flame cutting the web and flanges of the link. This operation is necessary only if large permanent deformations are present in the link. Direct unbolting might be feasible if permanent deformations are small.

There are concerns that a sudden release of link shear force may occur during flame cutting of the link that might be dangerous to the operating personnel. Consequently, the solution was improved by introducing a temporary bracing system consisting of tension braces and dampers. During removal of links through

flame cutting, the forces locked in the links are transferred to the temporary bracing system and smoothly released through the dampers.

Link removal procedure is performed on a storey-by-storey basis. Once all links from a storey are removed, all structural components from that storey are in the elastic range of response. Therefore, as brace forces are released through dampers, the structure recovers its initial (plumb) position, becoming free of any locked-in forces and new link can be installed.

4. EXPERIMENTAL EVALUATION OF RE-CENTRING DUAL ECCENTRICALLY BRACED FRAMES WITH REMOVABLE LINKS

4.1. Introduction

The first part of the chapter presents two series of material tensile tests. The first series was performed on 9 sets of three steel samples each and the second one on 6 bolt+nut+washers assemblies, all of them being prepared from additional material corresponding to elements of the tested specimen. These tests were performed in order to evaluate the material characteristics of the main structural elements and the bolts from the link connection. The obtained material properties were further used (see Chapter 5) to calibrate the numerical model of the specimen.

Full-scale specimen testing is treated next. The experimental programme in composed of snap-back, pseudo-dynamic and push-over tests. Data about the experimental set-up for each type of test are presented. Vertical (gravity) and horizontal (seismic record) loading for the pseudo-dynamic tests are described. The proposed testing sequence is presented, having three main test sections: Serviceability Limit state (Damage Limitation), Ultimate Limit State (Significant Damage) and Near Collapse tests sets. The instrumentation used to measure and observe the structural local and global behaviour is described. The last and most consistent part of the chapter presents the results of the performed tests, in terms of evaluating the seismic performance, validating the link removal procedure and re-centring capability and observing the influence of the concrete slab over the links.

4.2. Material tests

4.2.1. Steel samples

In order to evaluate the material characteristics from tensile tests at Politehnica University Timisoara (CEMSIG Research Centre), samples were prepared (see Fig. 4-1) from the additional material received from JRC (profiles and plates) associated to each structural member of the test specimen, according to ISO 6892-1 [96].

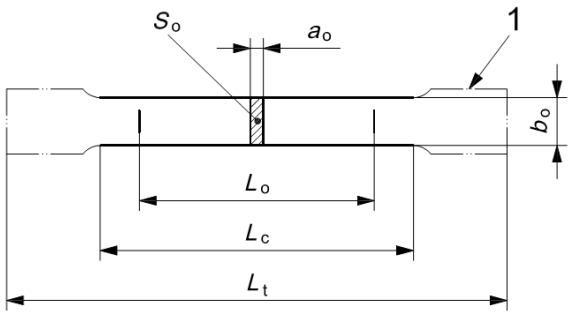

Fig. 4-1. Machined test piece of rectangular cross-section [96].

The geometrical properties of the obtained steel samples are summarised in Table 4-1.

Table 4-1. Geometric properties of steel samples

Element	Sample	Steel grade	Pieces	Thickness a_0 [mm]	Width b_0 [mm]	Parallel length L_c [mm]	Original length L_o [mm]	Total length L_t [mm]
Columns (welded)	CW (web)	S460NL	3	8.38	55	150	120	590
	CF (flange)	P460NH	3	12.64	40	160	125	600
Links (welded)	LW3 (web)	DOMEX 240 YP B	3	4.00	60	115	90	555
	LW12 (web)	DOMEX 240 YP B	3	8.38	55	150	120	590
	LF (flange)	DOMEX 240 YP B	3	12.64	40	160	125	600
EBF braces HEB200	CVW (web)	S355J2+M	3	8.82	35	130	100	450
	CVF (flange)	S355J2+N	3	14.18	20	125	100	445
MRF beam IPE240	MBW (web)	S355J2+AR	3	6.75	50	125	100	435
	MBF (flange)	S355J2+N	3	10.22	30	125	100	435

The tensile tests on steel samples were performed using a 1000 kN INSTRON 8805 hydraulic testing machine (see Fig. 4-2 and Fig. 4-3). The strain was measured using a video extensometer.

Fig. 4-2. Tensile test on steel sample

Fig. 4-3. Tested steel samples

The main test characteristics: the upper yield limit f_y (R_{eH} and R_{p02}), the ultimate strength f_u (R_m), the ratio f_u/f_y and the ultimate strain A are presented in Table 4-2. The values from the table are the average between three tests. Some stress-strain characteristic curves are shown in Fig. 4-4.

Table 4-2. Tensile test results

Element	Sample	Steel grade	f_y, N/mm^2		f_u (R_m), N/mm^2	f_u/f_y		A, %
			R_{eH}	R_{p02}		(R_m /R_{eH})	(R_m /R_{p02})	
Columns (welded)	CW	S460NL	489.1	479.8	632.4	1.293	1.318	23.2
	CF	P460NH	493.9	486.7	641.5	1.299	1.318	24.5

Element	Sample	Steel grade	f_y, N/mm²		f_u (R_m), N/mm²	f_u/f_y		A, %
			R_{eH}	R_{p02}		(R_m /R_{eH})	(R_m /R_{p02})	
Links (welded)	LW3	DOMEX 240 YP B	304.0	296.5	387.7	1.275	1.308	35.6
	LW12	DOMEX 240 YP B	302.5	291.8	381.6	1.261	1.308	35.4
	LF	DOMEX 240 YP B	261.9	258.6	359.7	1.373	1.391	37.9
EBF braces HEB200	CVW	S355J2+ M	398.7	390.8	492.3	1.235	1.260	28.6
	CVF	S355J2+ N	379.7	373.5	492.7	1.298	1.319	35.6
MRF beam IPE240	MBW	S355J2+ AR	460.8	456.5	563.2	1.222	1.234	32.0
	MBF	S355J2+ N	-	390.4	566.0	-	1.450	27.7

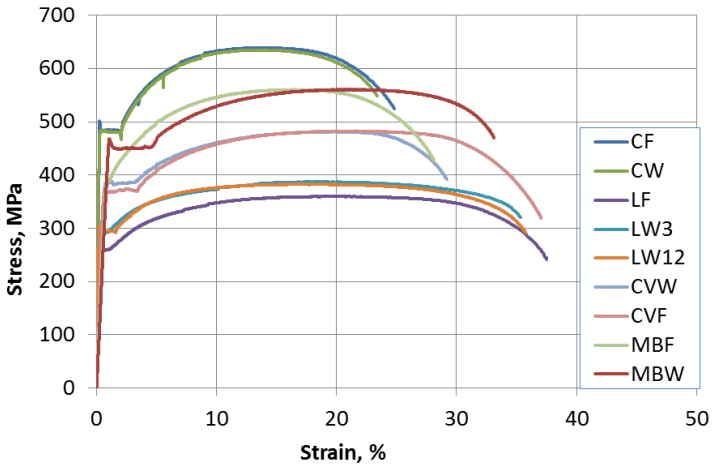

Fig. 4-4. Characteristic stress-strain curves

All the materials have fulfilled the product standards demands (see Table 4-3), higher strength being observed.

Table 4-3. Nominal material characteristics

Steel grade	f_y, N/mm²	f_u (R_m), N/mm²	A, %
S460NL	460	540	17
P460NH	460	570	17
DOMEX 240 YP B	240	360	28
S355J2	355	470	22

4.2.2. Bolts

Further on, 6 sets of bolts+nuts+washers assemblies (see Fig. 4-5), the same as the ones used in the test specimen at the link connections, were sent from

JRC to Steel Structures Department laboratory for strength testing. Their geometry is shown in Fig. 4-6 and summarised in Table 4-4 and Table 4-5.

Fig. 4-5. The tested bolt assemblies

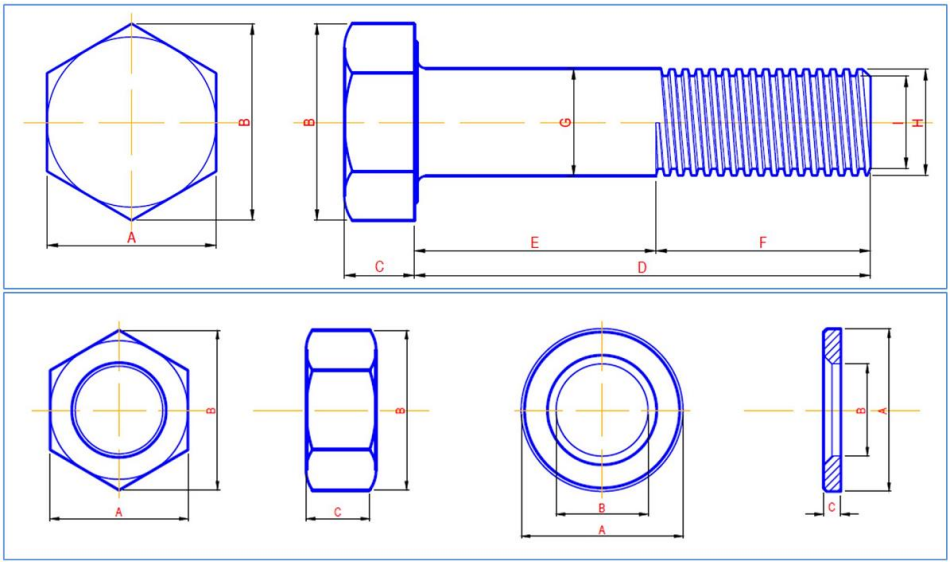

Fig. 4-6. Bolt geometry

Table 4-4. Bolt geometry

	specimen	Bolt dimensions [mm]								
		A	B	C	D	E	F	G	H	I
BOLT M27 gr 10.9	1	45,41	51,82	17,05	100,50	53,61	46,8	26,77	26,60	23,73
	2	45,44	51,84	16,99	100,27	53,40	46,58	26,76	26,54	23,35
	3	45,46	51,82	17,01	100,45	53,78	46,52	26,81	26,54	23,35
	4	45,42	51,90	16,98	100,20	53,47	46,8	26,83	26,64	23,30
	5	45,45	51,86	17,07	100,22	53,73	46,66	26,86	26,51	23,44
	6	45,36	51,81	16,90	100,47	53,22	47,13	26,81	26,35	23,36

Table 4-5. Nuts and washers geometry

	specimen	Nut dimensions [mm]			Washer dimensions [mm]		
		A	B	C	A	B	C
BOLT M27 gr 10.9	1	45,34	51,80	21,34	48,90	28,16	4,69
					49,23	28,91	4,63
	2	45,42	51,76	21,42	49,13	28,34	4,75
					49,34	28,13	4,62
	3	45,38	51,73	21,26	49,29	28,11	4,64
					49,02	28,92	4,70
	4	45,29	51,79	21,35	49,29	28,13	4,71
					49,19	28,00	4,75
	5	45,36	51,78	21,30	49,29	28,17	4,61
					49,02	28,90	4,77
	6	45,26	51,79	21,30	49,40	28,15	4,66
					49,32	28,09	4,59

The tensile tests on the 6 bolt assemblies were performed using the same 1000 kN INSTRON 8805 hydraulic testing machine with two metallic cylinders used to fix the bolt assemblies into the machine grips (see Fig. 4-7). The strain was measured using a video extensometer.

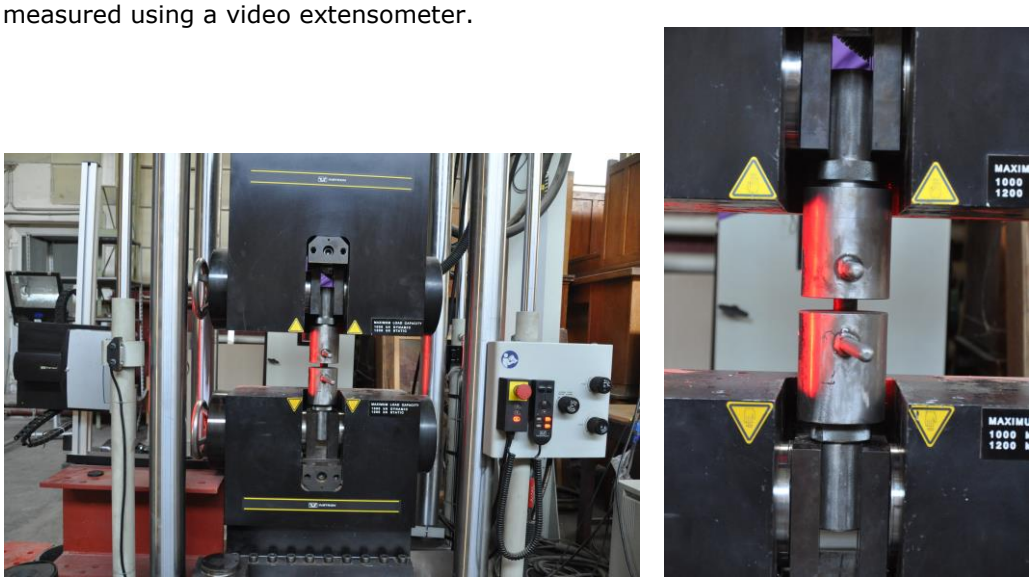

Fig. 4-7. Tensile tests on bolts

The first specimen has failed by thread stripping, while all the other five specimens have failed by thread fracture (see Fig. 4-8).

Fig. 4-8. Bolt failure modes

The main test characteristics: the upper yield limit f_y (R_{p02}), the ultimate strength f_u (R_m), the ratio f_u/f_y and the ultimate strain A are presented in Table 4-6. Some stress-strain characteristic curves are shown in Fig. 4-9.

Table 4-6. Tensile tests on bolts results

Bolt assembly	Diameter I [mm]	f_y (R_{p02}), N/mm^2	f_u (R_m), N/mm^2	f_u/f_y (R_m /R_{p02})	A, %
1	23,7	930,0	1156,2	1,243	26,22
2	23,4	1080,0	1182,8	1,095	14,23
3	23,4	1111,0	1174,9	1,057	15,4
4	23,3	1170,0	1189,2	1,016	14,17
5	23,4	1138,0	1165,0	1,024	14,77
6	23,4	1163,0	1196,6	1,029	13,54
mean	23.4	1098.7	1177.4	1.077	16.39

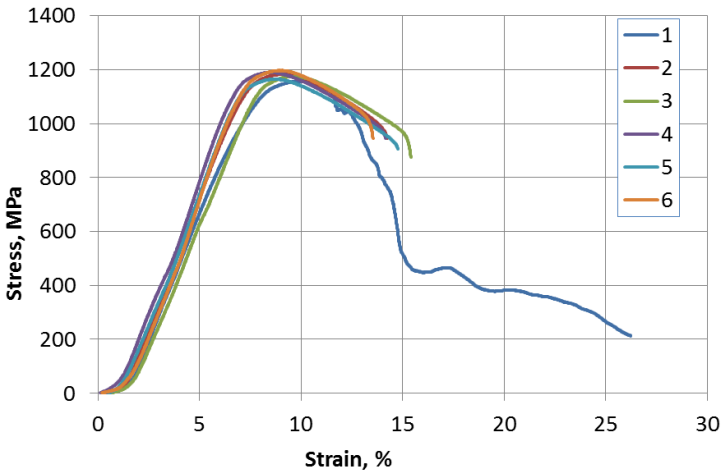

Fig. 4-9. Stress-strain characteristic curves for bolt assemblies

All the bolts have fulfilled the product standards demands (f_y=900 N/mm^2 and f_u=1000 N/mm^2), higher strength being observed.

4.3. Full-scale specimen testing

The validation of re-centring capability and link replacement procedure in a dual eccentrically braced structure, together with assessing its seismic performance, was realised through pseudo-dynamic tests of a full-scale structure (see Fig. 4-10) performed at the European Laboratory for Structural Assessment (ELSA) facility at JRC in Ispra, Italy.

Fig. 4-10. Full-scale experimental specimen

Some structural details are illustrated in the Fig. 4-11. It can be seen that in the South frames the links are disconnected from the concrete slab (see Fig. 4-11a), the ends of the links being fixed with L braces both at the upper and lower sides. In the North frame the slab is continuous over the links (see Fig. 4-11b), the ends of the links being fixed with L braces at the lower side and by the slab at the upper side. Different beam to column connections were applied (see Fig. 4-11c): haunch end plate bolted connection for the MRFs beams, welded connection for the EBF

beam and pinned connection for the secondary composite beams. The column are fixed at the base to the strong floor of the testing facility (see Fig. 4-11d).

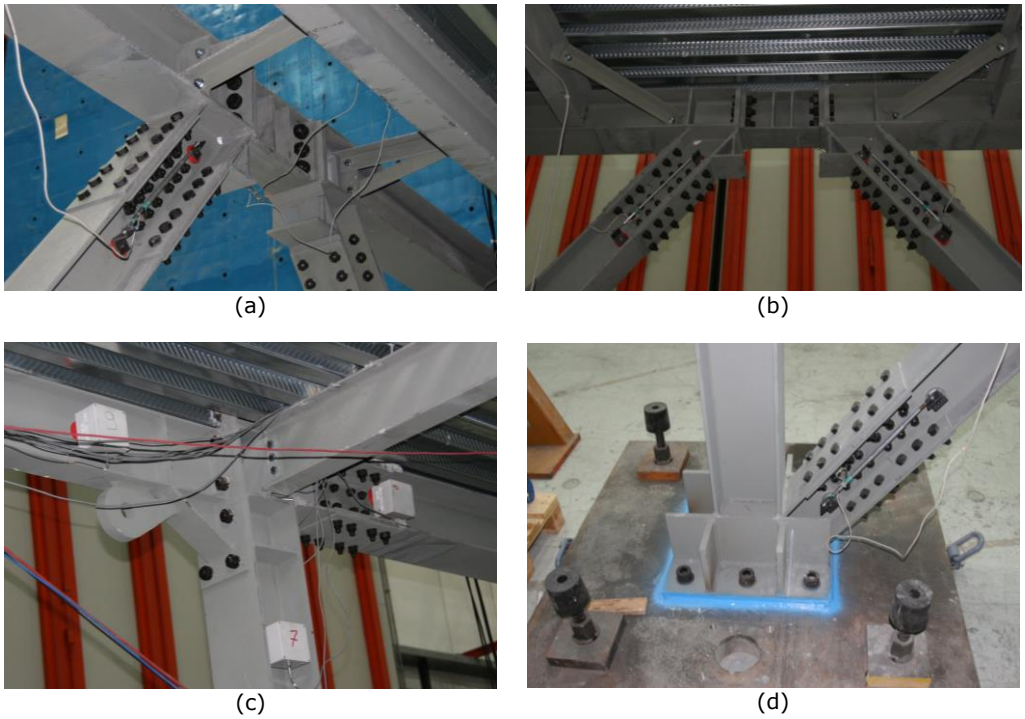

(a) (b)

(c) (d)

Fig. 4-11. Structural details: (a) South frame link, (b) North frame link, beams to column connection and (d) column base connection.

After the structure was erected, out of plumb measurements were made to check the verticality of the structure, compared to the required tolerances. The measurement was done using a plumb-line placed at the top of each column and stretched downwards and measured above the footings [97]. The initial out of plumb shape for the three stories is presented in Fig. 4-12 to Fig. 4-14.

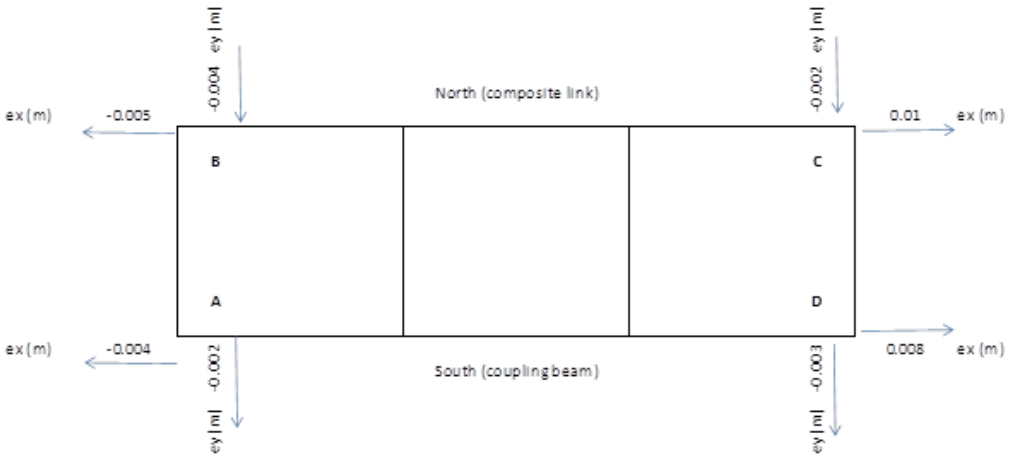

Fig. 4-12. Out of plumb shape for the 1st floor [97]

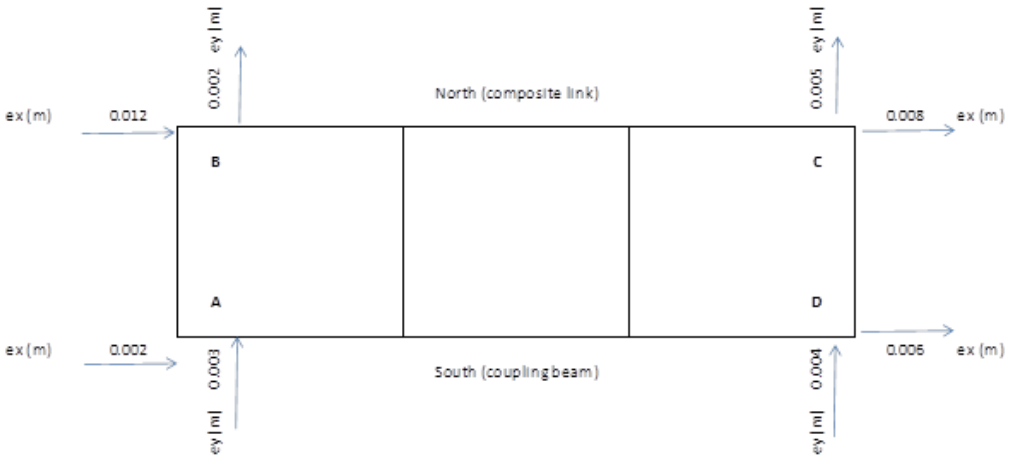

Fig. 4-13. Out of plumb shape for the 2nd floor [97]

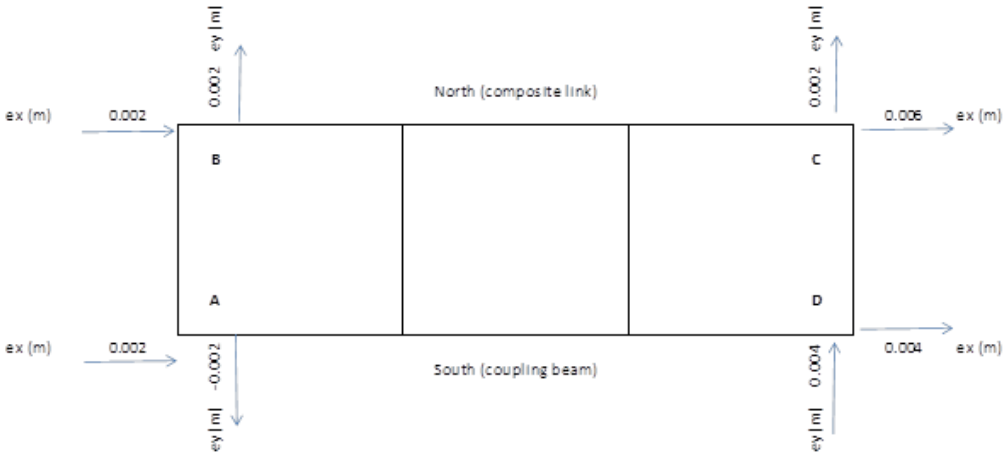

Fig. 4-14. Out of plumb shape for the 3rd floor [97]

The out of plumb measurements were within the limits of elevation tolerances (*H*/300) defined in EN 1090-2 [98].

4.3.1. Snap-back tests

The experimental set-up differed from one test to another. For the snap-back test, a small piston was connected with four bolts, placed on the column closest to the reaction wall on the northern side (Fig. 4-15), to simulate the snap due to a sudden release of forces. This was done prior to the instalment of the actuators which were used for the pseudo-dynamic tests.

In order to run the snap-back tests, the links were removed from the structure. A hydraulic jack (with the maximum capacity of 500 kN at 700 bar) was used to push apart the structure to generate enough gap to remove the links. In the N frame, because of the presence of the reinforced concrete slab over the links, it was more difficult to push apart the ends of the EBFs beams, using the maximum capacity of the jacks and having to force out the links. The forces applied in order to remove the links are present in Table 4-7.

Table 4-7. Pressure and Forces Applied at Link Removal (Snap-back)

Position	**Bar**	**kN**	**Observation**
Set A Links - 1st replacement			
S L3	359.8	257	removed
S L2	599.2	428	removed
S L1	499.8	357	removed
N L3	700	500	removed
N L2	700	500	removed
N L1	700	500	removed

The snap-back test consisted in pulling the structure towards the reaction wall with an increasing force until the connection snapped, thus releasing the structure in a very short time. The piston was used to pull the structure to reach a

target force; the displaced position was locked in with a nut. Afterwards the piston continued to generate an internal force measured by a loading cell applied on an M27 (with an 18.6 mm notch) bolt which was designed to resist a force of about 150 kN. When the bolt snapped the structure was released and left to vibrate freely.

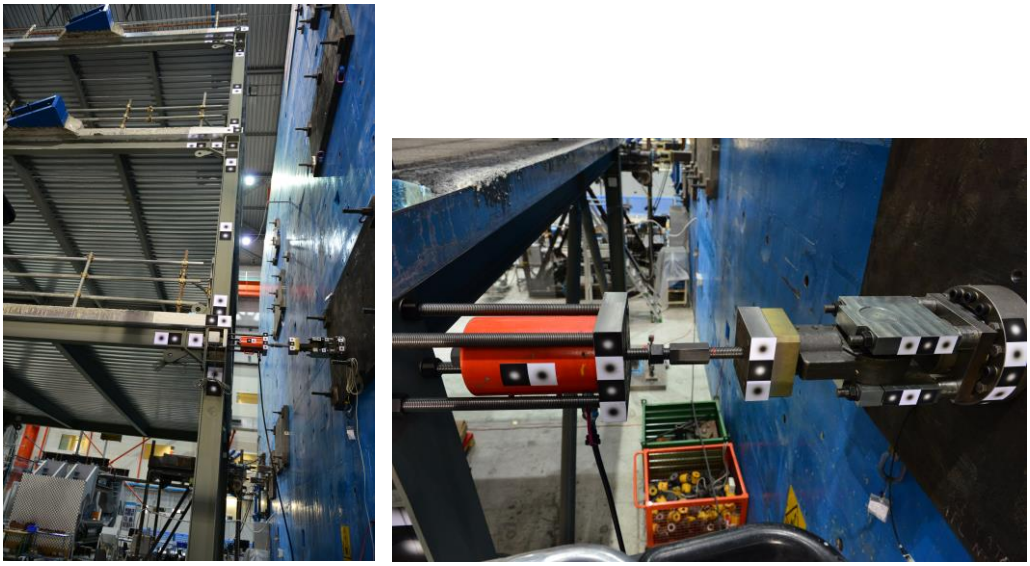

Fig. 4-15. Snap-back test set-up

The loading function of the test was similar to the one presented in the numeric models for assessing removal of the last seismic link at the first floor (where according to numerical simulation is when the highest forces are locked into the seismic links) (Fig. 3-25), but scaled to a value where the force would not damage the structure's elements (Fig. 4-16). This force was considered to be 150 kN, equal to the bolt's resistance.

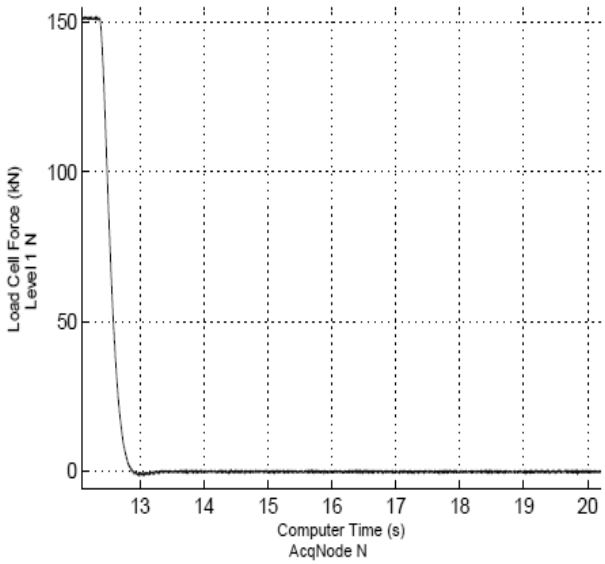

Fig. 4-16. Applied force at level 1 N [97]

A set of two dampers constructed by Alga SpA (Fig. 4-17) were designed with the purpose of preventing the structure to snap due to a sudden release of force during removal of the link. The snap-back tests were designed to assess on one side the amplitude of the free vibrations, and on the other side the effectiveness of dampers in limiting such vibrations; for this, two configurations were considered: with and without the dampers.

Fig. 4-17. Braces with dampers

The time histories of displacements in the longitudinal direction at the third, second and first floors for the north and south frames are shown in Fig. 4-18 and Fig. 4-19 without and with the ALGA dampers, respectively. The results show a maximum displacement of 2 mm and confirm that the dampers were not activated due to the small size of displacements imposed on the frame. The transverse displacements were also small, with a maximum value of 1 mm.

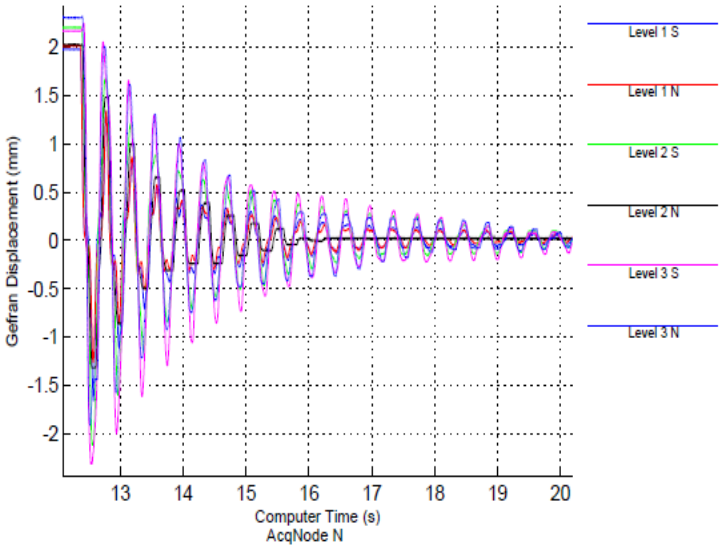

Fig. 4-18. Time history of longitudinal displacements (at all levels N and S frame) – snap-back test without ALGA dampers [97]

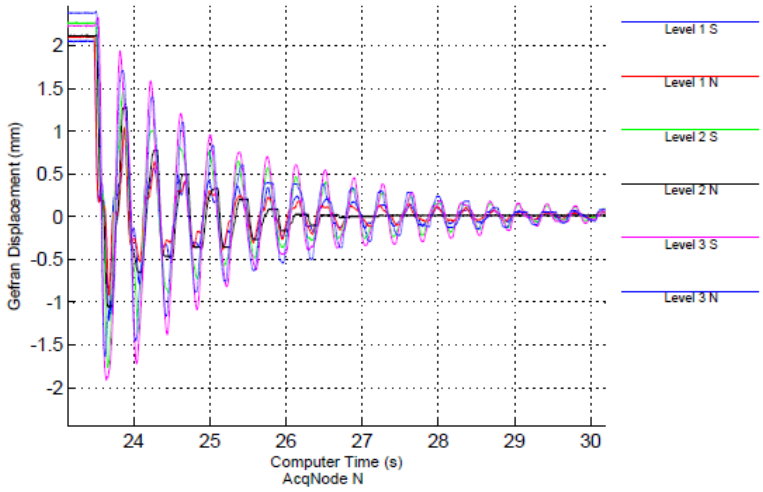

Fig. 4-19. Time history of longitudinal displacements (at all levels N and S frame) – snap-back test with ALGA dampers [97]

More results about modal shapes and frequencies obtained after the snap-back tests are presented in Annex C.1.

4.3.2. Experimental set-up for Pseudo-dynamic and Push-over tests

In order to proceed with the pseudo-dynamic tests, the links had to be mounted back into the structure. The installation of the links after the snap-back tests arose some difficulties due to irregularities in the concrete slab and at the welding in the links.

The links that initially fitted in the structure could not be mounted back because they were too long to fit. The lengths of the links provided by the manufacturer (399 mm to 402 mm) were slightly larger than the ones from the design project (398 mm and 400 mm). Therefore, the links have been machined precision of ±0.5 mm according to class M tolerance of ISO 2768-1, Table 1 [99], to total lengths of 396 (one set) and 398 mm (second set).

The preloading of the bolts from the links of the N frame raised some difficulties also. The method applied for preloading consisted in tightening the bolts with a torque of $0.75M_{r,1}$, where $M_{r,1}$ is the reference torque value to be used for a normal minimum preloading force $F_{p,C}$, then turning the dynamometric key another 60° as stated in EN 1090-2 [98]. This was difficult because of the limited space between the slab and additional masses, presence of link stiffeners, small distance between bolts and between first bolt row and flanges.

For the pseudo-dynamic (PsD) and push-over tests, four actuators were connected on each frame (N and S) of the specimen, two actuators with a capacity of 500 kN each on the first floor (Fig. 4-20) and the other two actuators with a capacity of 1000 kN each on the second and third floors. The actuators were connected to the reaction strong wall using an end plate and a loading reinforced concrete beam on the structure. To facilitate the concomitant action of the first floor actuators, a connection was designed to transfer the forces from the actuators to the loading beam [97].

Fig. 4-20. First storey actuators

Two reference frames were installed on the side opposite from the wall (eastern side) on which Heidenhain transducers were positioned to measure the longitudinal and transverse displacement (Fig. 4-21).

Fig. 4-21. Test set-up

4.3.3. Loading for the PsD tests

Gravity loads were determined based on the provisions of EN 1991 [79]. The prototype structure was designed for permanent and variable loads on floors amounting to 4.9 kN/m^2 (not including self-weight of structural members) and 3.0 kN/m^2, respectively. The load combination applied on the specimen prior to pseudo-dynamic testing was:

$$1.00\ G_k + 0.30\ Q_k \quad (4\text{-}1)$$

Where:
G_k is the total permanent load = $G_{ksm} + G_{krc} + G_{ka}$;
G_{ksm} is the self-weight of structural members;
G_{krc} is the self-weight of the reinforced concrete slab, including steel sheeting (3.14kN/m^2);
G_{ka} is the additional permanent load (1.76kN/m^2);

Q_k is the variable load (3.0 kN/m^2).

Therefore, the additional gravity load per floor that needs to be placed on the structure amounts to:

$$1.00 \times 1.76 \text{ kN/m}^2 + 0.30 \times 3.00 \text{ kN/m}^2 = 2.66 \text{ kN/m}^2 \quad (4\text{-}2)$$

which was reached by placing water tanks of maximum capacity of 1 ton (1 m^3) each, with plan dimensions of 1.0 x 1.2 m, and concrete blocks of 2.7 tonnes (0.87x1.0x1.25m). The water tanks and concrete blocks were placed above the transversal beams, except where the actuator beam is found (not being necessary any additional loads on this strip). The exact placement of the water tanks and concrete blocks, as well as the level to which the tanks need to be filled (in mm) and the necessary volume of water (in m^3) are sketched in Fig. 4-22 to Fig. 4-24 and illustrated in Fig. 4-25.

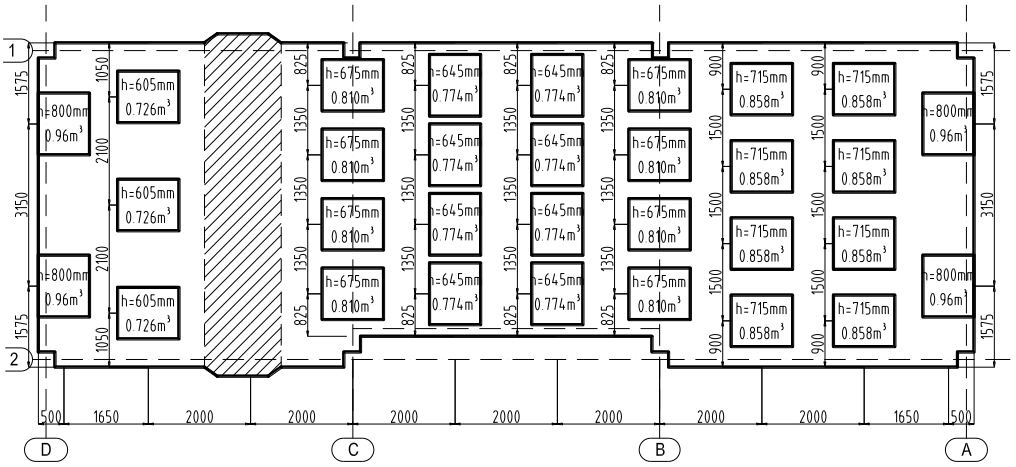

Fig. 4-22. Water tanks on the specimen at the 1st story

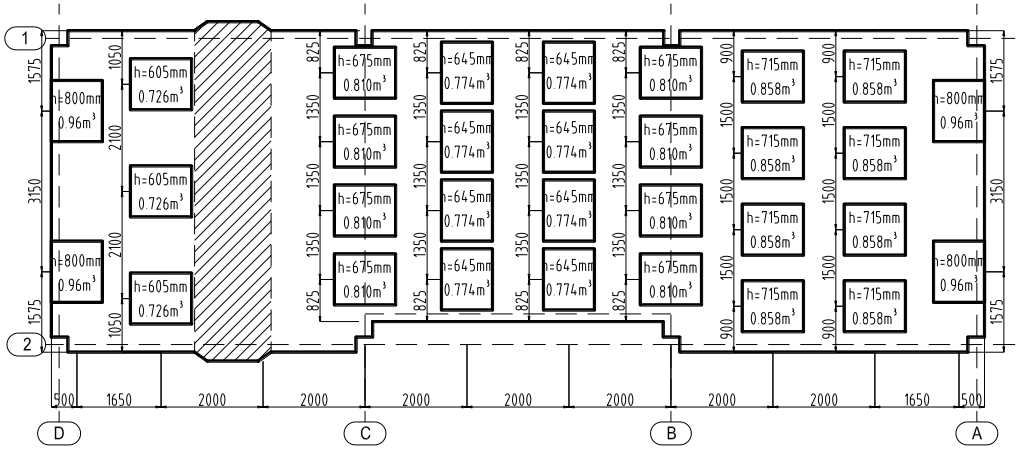

Fig. 4-23. Water tanks on the specimen at the 2nd story

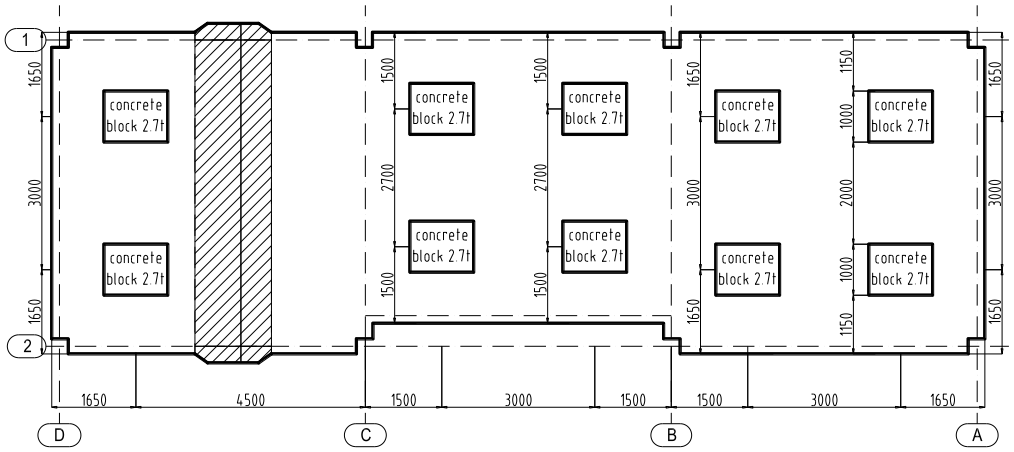

Fig. 4-24. Concrete blocks on the specimen at the 3rd story

Fig. 4-25. Arrangement of water tanks and concrete blocks on the specimen

Pre-test nonlinear dynamic simulations were performed on the 2D model of the experimental mock-up, using the selected ground motion records (see Chapter 3.4.2.2). The record that provided a response closest to the mean response, in terms of top displacement, inter-storey drift, and shear deformation in the links, was 15613_H2 (see Fig. 4-26). This record was up-sampled to a 0.005s time interval, to produce a convenient volume of data regarding all the signals to be recorded and analysed.

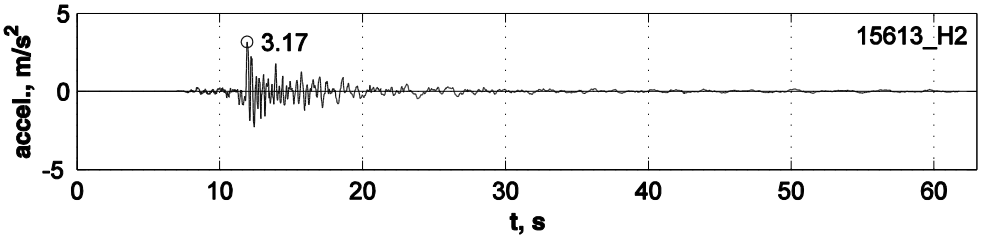

Fig. 4-26. Acceleration time history for 15613_H2 record

Table 4-8 lists several seismic input levels for the 15613_H2 record, which were chosen to be used in the pseudo-dynamic tests in order to evaluate the structural performance of the test structure, where a_{gr} is the reference peak ground acceleration (corresponding to 10% / 50 years earthquake) and a_g represents the peak ground acceleration for a specific earthquake level.

Table 4-8. Limit states and corresponding scaling factors for seismic input

Limit state	Return period, years	Probability of exceedance	a_g/a_{gr}	a_g/g
Full Operation (FO)	-	-	0.062	0.020
Damage Limitation (DL / SLS)	95	10% / 10 years	0.59	0.191
Significant Damage (SD / ULS)	475	10% / 50 years	1.00	0.324
Near Collapse (NC)	2475	2% / 50 years	1.72	0.557

4.3.4. Testing programme

As described by ELSA personnel ([97] and [100]), in a pseudo-dynamic (PsD) test, on-line computer numerical models are combined with actual measurements of the properties of a structure. To simulate the response of a structure under seismic loading the computer running the PsD simulation takes an accelerogram as an input. For the test campaign the accelerogram mentioned in the previous chapter was used.

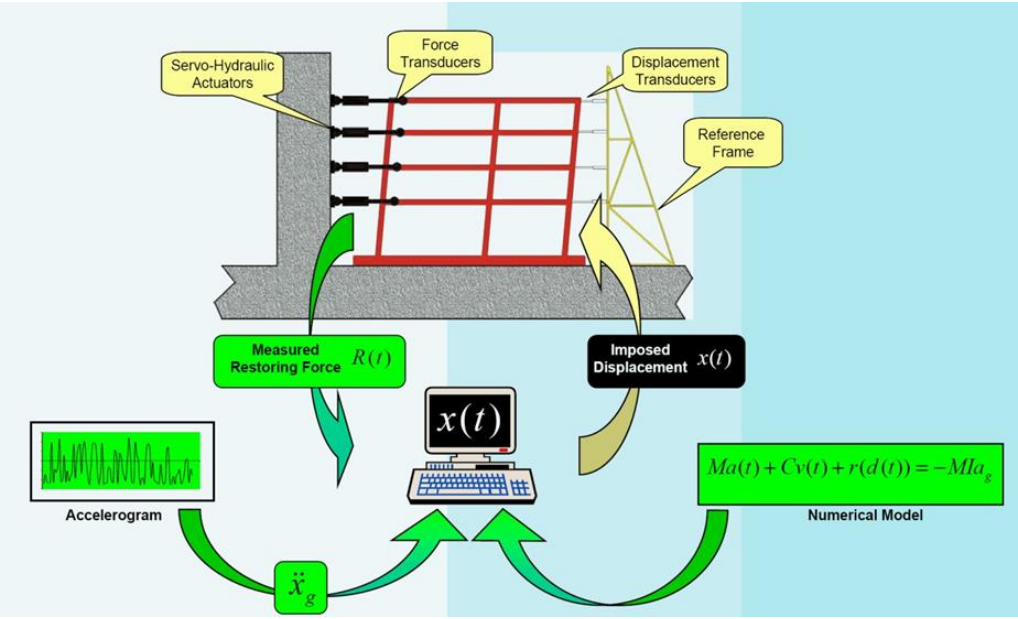

Fig. 4-27. Illustration of pseudo-dynamic testing method (www.ct.upt.ro/centre/cemsig)

In a PsD test it is assumed that the response of a structure can be determined by a discrete model with a limited number of degrees of freedom (DoF). In this test campaign three DoFs were selected: the horizontal displacements of each storey with the assumption that all the mass is concentrated at the selected DoFs (i.e., the floor slabs). The equations of motion for such an idealized system are second order differential equations which can be expressed in matrix form:

$$M \cdot a(t) + C \cdot v(t) + r(t) = f(t) \quad (4\text{-}3)$$

where *M* is the mass matrix, *C* is the viscous damping matrix, *r(t)* is the internal (restoring) force vector and *f(t)* is the external force vector applied on the structure. Horizontal displacements of the controlled DoFs were solved for a prototype time step of $0.005/1000=5\times10^{-6}$ s using the explicit Newmark time integration method. To guarantee optimal control of structure response the equation of motion was solved for the north frame and the resulting displacements were applied to both the north and south frame. Displacements were then applied by horizontal actuators at each storey at a laboratory time step of 0.005 s corresponding to the sampling rate of the controllers. The forces measured by the load cells in the actuators, following the application of the controlled displacements, represent the restoring forces that are fed back to the computer and that are used in the next time step of the calculation. Restoring forces are thus obtained from the specimen's response and reflect its state of damage.

Since the inertial and viscous damping forces are modelled in the computer, the test does not have to run in the real time scale. The hysteretic damping is automatically accounted for through inelastic deformation and damage progression of the test structure; consequently no viscous damping matrix was used. During the PsD test campaign the equation of motion was solved for restoring forces coming from the south frame only (calculated from static equilibrium of the load cell force measurements at each floor) and multiplied by a factor of two (the south frame is considered equal to the north frame in the numerical model). Equal displacements were applied to the two frames, in order to avoid rotation of the structure around the vertical axis. The PsD test method used for the test campaign was continuous, which reduces problems of material relaxation and avoids load over-shoot.

Restoring forces in the PsD model were 1.09 times those of the South actuators, minus 0.09 times those of the North actuators (the distance between actuators was 7.080 m, while the frames were distanced at 6.000 m).

The mass used in the equations of motion of the PsD test corresponded to the total mass of the prototype structure, equal to 165 tons for the first two floors and 168 tons for the last floor, assuming the internal frames provide a negligible stiffness (they have no bracing) in the direction of the lateral, seismic forces.

In order to assess the seismic performance of the full-scale specimen and validate the link replacement procedure, a PsD testing programme was proposed, composed of the sequence of the following tests:

- Damage Limitation/ Serviceability Limit State (DL/SLS) tests:
  - Full-operation (FO1) earthquake (a_g = 0.02 g) – to assess the elastic response of the structure and calibrate the numerical model of the test structure;
  - DL earthquake (a_g = 0.191 g) – to produce moderate damage, with low residual drift; subsequently, the first set of links will be replaced (LR1).
- Significant Damage/ Ultimate Limit State (SD/ULS) tests:

- Full-operation (FO2) earthquake (a_g = 0.02 g) – to assess the elastic response of the structure with the new (second) set of links installed;
- SD earthquake (a_g = 0.324 g) – to produce large drift, but possibly small residual drift;
- Pushover (PO1) test (monotonic, with a displacement of 55 mm) – to produce a larger residual drift than that of the SD test; the second set of links will then be replaced (LR2).

– Near Collapse (NC) tests:

- Full-operation (FO3) earthquake (a_g = 0.02 g) – to assess the elastic response of the structure with another new (third) set of links installed;
- NC earthquake (a_g = 0.557 g) – to produce extensive damage throughout the structure; the re-centring capability is lost due to the yielding of members other than the links;

4.3.5. Instrumentation

The two frames of the specimen were instrumented, Grid 1 being the frame with slab over links (northern side according to the laboratory position, see Fig. B-2 from ANNEX B) and Grid 2 being the frame where the slab is disconnected from the links (southern side, see Fig. B-3 from ANNEX B.

A number of 6 Heidenhain transducers (Fig. 4-28) were used to measure the global longitudinal displacement of the specimen, 3 in longitudinal N frame – D1A-H1(2,3) (Fig. B-2 from ANNEX B) and 3 in longitudinal S frame – D2A-H1(2,3) (Fig. B-3 from ANNEX B), one per storey, installed on the farthest column line from the reaction wall;

Fig. 4-28. Heidenhain transducers

A total of 38 local displacement transducers were used to monitor different relative deformations or displacements between different components. 12 displacement transducers (±50 mm stroke) were used to monitor the link rotation, 2 for each of the 6 links of the specimen (D1BC-LD11(2,3) and D1BC-LD21(2,3) in the N frame and L2BC-LD11(2,3) and L2BC-21(2,3) in the S frame) (see Fig. 4-29). 24 displacement transducers (±12.5 mm stroke) were used to check the slip in the splice connections of every EBF brace, 2 for each of the 12 braces of the specimen (D1BC-BRLB1(2,3) and D1BC-BRLT1(2,3) at the bottom and top of the left braces and D1BC-BRRB1(2,3) and D1BC-BRRT1(2,3) at the bottom and top of the right braces from the N frame and D2BC-BRLB1(2,3) and D2BC-BRLT1(2,3) at the bottom and top of the left braces and D2BC-BRRB1(2,3) and D2BC-BRRT1(2,3) at the bottom and top of the right braces from the S frame) (see Fig. 4-30). 2 displacement transducers (±12.5 mm stroke) were used to check the slip in the splice connection of the EBF beams from the 1st story of the S frame (D2BC-BL1 in the left beam and D2BC-BR1 in the right beam) (see Fig. 4-30).

Another 3 global transversal displacement transducers (±25 mm stroke) were used to measure the global transversal displacement of the specimen (installed on the farthest transversal frame from the reaction wall, one per storey) (D2A-HT1(2,3)) (see Fig. B-1. from ANNEX B);

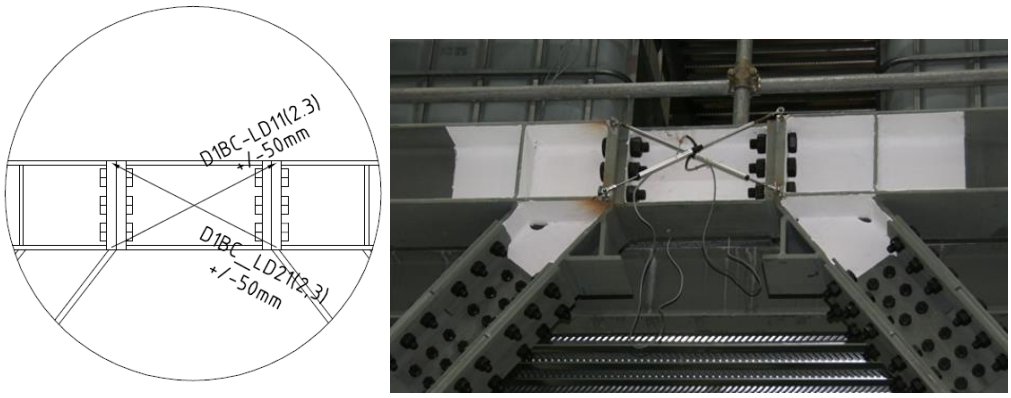

Fig. 4-29. Link displacement transducers

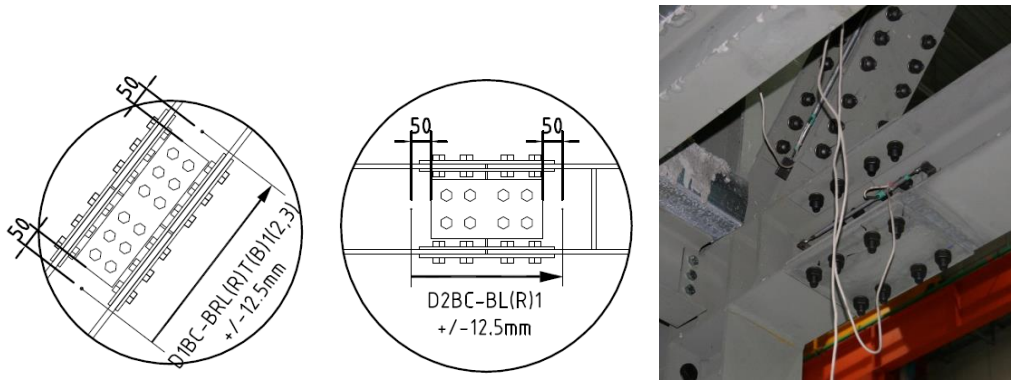

Fig. 4-30. EBF braces and EBF beams at 1st story in the S frame displacement transducers

22 inclinometers (see Fig. 4-31 and Fig. 4-32) were installed on web of the beams and columns from the beam to column and base joints in order to monitor their deformation (1-I(1 to 11) in the N frame and 2-I(1 to 11) in the S frame);

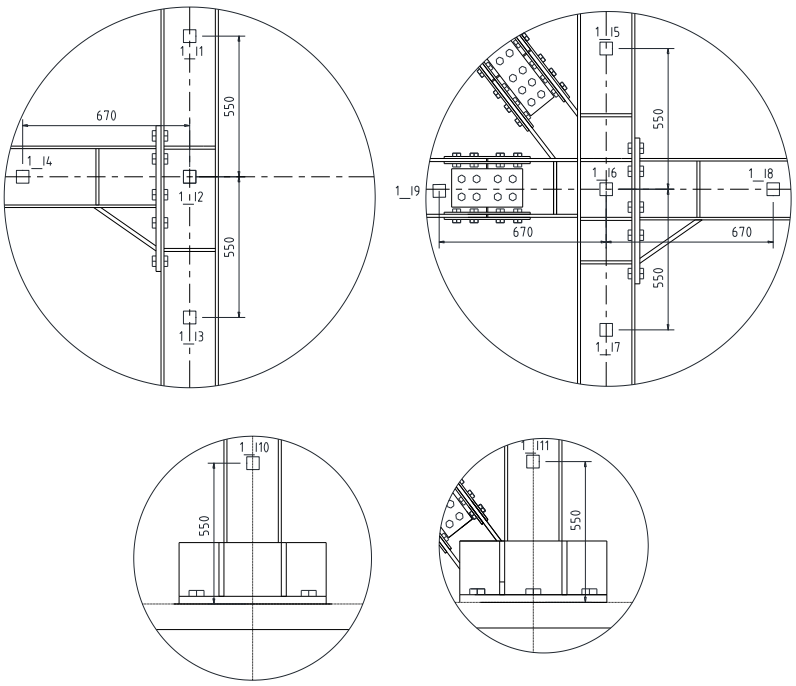

Fig. 4-31. Inclinometers arrangement

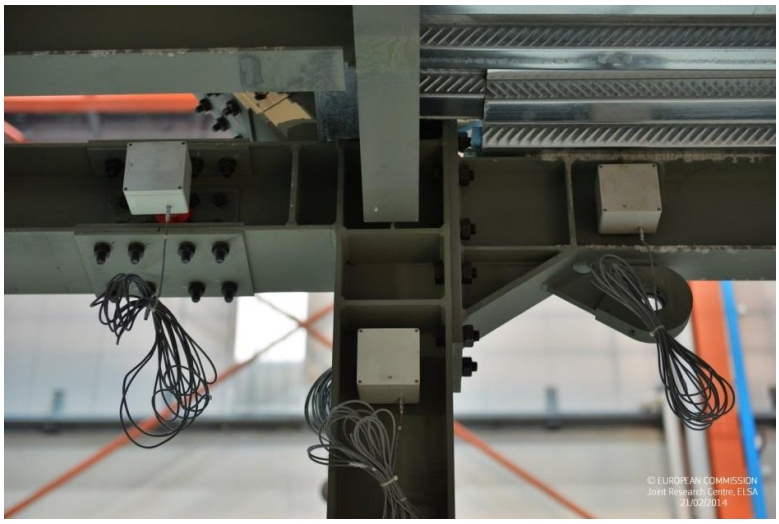

Fig. 4-32. Inclinometers on specimen

An additional 28 strain gauges were proposed (see Fig. B-4 and Fig. B-5 from ANNEX B and Fig. 4-35) to monitor element elongations (in order to observe yielding in elements). 24 of them were mounted at the 12 EBF braces of the specimen (at the middle of the HEB200 bar, in the middle of the external face of the flange) to monitor their elongation (G1BC1(2,3)-BR1(2,3,4) in the N frame and G2BC1(2,3)-BR1(2,3,4) in the S frame) (see Fig. 4-33). The other 4 were proposed for the damper braces (at the middle of the CHS bar) from the 1st story of the N and S frames to monitor their elongation (G1CD-BR1(2) in the N frame and G2CD-BR1(2) in the S one) (see Fig. 4-33). After the DL test, another 8 strain gauges were added at the ends of the beams (two on each lower flange) from the first floor of the eastern MRFs from both the N and S frames (G1AB1-MB1(2)i(e) in the N frame and G2AB1-MB1(2)i(e) in the S frame) to monitor their yielding (see Fig. 4-34).

Fig. 4-33. Strain gauges position on EBF braces and an damper braces

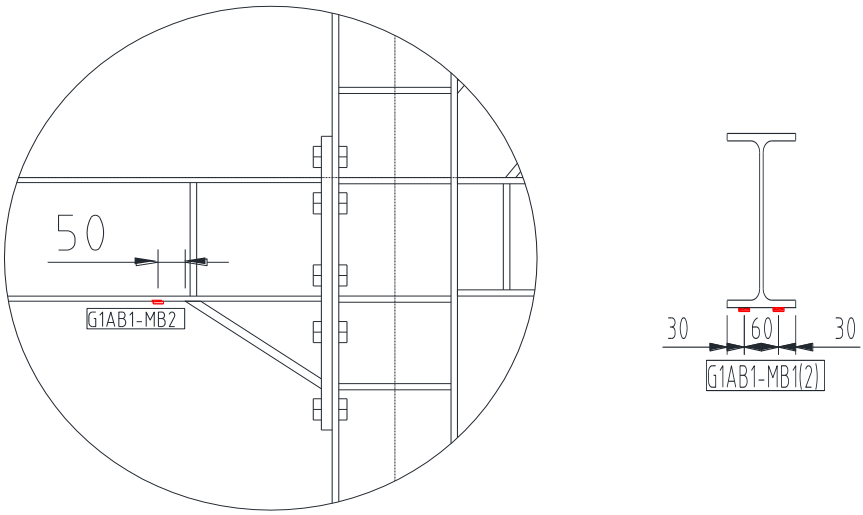

Fig. 4-34. Strain gauges position on MRF beams

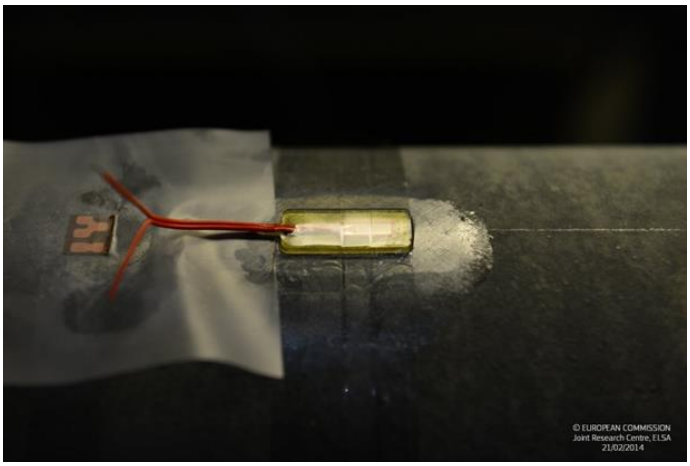

Fig. 4-35. Strain gauge

In order to monitor visually the presence of possible yielding in the beam to column, link to beam and base joints and parts of the EBF braces, potential dissipative areas (both web and flanges) with length equal to the height of the corresponding steel profile were white-washed (Fig. 4-29).

4.4. PsD tests results

4.4.1. DL tests set

During the first FO1 test, the structure manifested an elastic response, in the non-dissipative elements, as well as in the dissipative ones (including the links). This means that there were no residual top displacements or any inter-storey drift in the structure, while the maximum top displacement was also small, at 5.7 mm in both frames (see Fig. 4-36).

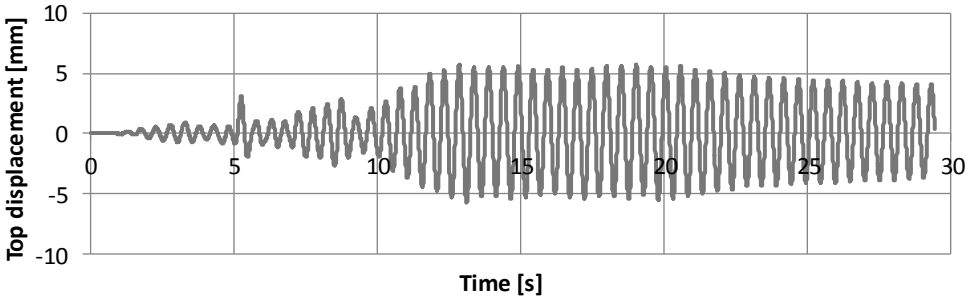

Fig. 4-36. Top displacement time history for FO1 test

Taking into account that both frames were in displacement control they both had the same displacement with a different force input. The maximum base shear

forces were -341 kN and 321 kN, and -289 and 293 kN, for the north and south frames, respectively. These results show the difference in stiffness between the two frame configurations due to the presence of the slab above the links in the N frame.

The damage limitation (DL) test was then performed. During this test, no yield was observed in the elements outside the links. Small maximum plastic deformations occurred in the links (see Fig. 4-37a and Fig. 4-40), the highest being 0.032 rad (with the maximum residual deformation being 0.014 rad).

The plastic deformations of the links were determined using the equation below [2], where *DD1* and *DD2* are the displacements measured by the two transducers placed diagonally on the link (Fig. 4-29), *a* and *b* being the vertical and horizontal distance between the ends of the transducers.

$$\gamma = \frac{\sqrt{a^2 + b^2} \cdot (DD2 - DD1)}{2 \cdot a \cdot b} \quad (4\text{-}4)$$

No slip occurred in the EBF braces or beam splice connections (the displacement transducers showed deformations of < 1 mm in these elements). The beam to column and column base joint zones exhibited small rotations, amounting to a maximum of 9 mrad. Minor cracks were observed in the concrete slab (see Fig. 4-37b).

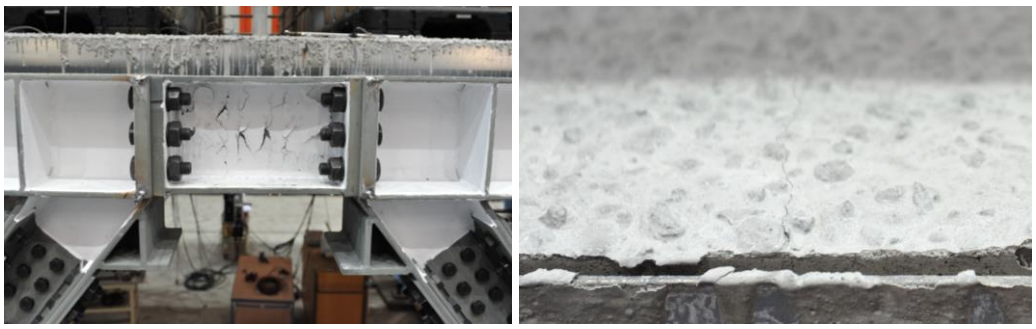

(a) (b)

Fig. 4-37. Link behaviour (a) and concrete slab state (c) at the end of DL test

The beam to column joint zone rotations (θ_j) were computed using the formula below:

$$\theta_j = I_b - \frac{I_{s,u} + I_{s,l}}{2} \quad (4\text{-}5)$$

where I_b is the rotation measured by the inclinometer placed on the beam, $I_{s,u}$ is the rotation measured by the inclinometer placed on the upper column and $I_{s,l}$ is the rotation measured by the inclinometer placed on the lower column.

The structure exhibited a low residual top displacement of 5.3 mm in the S frame and 5.8 mm in the N frame (0.05%, respectively 0.06%), the maximum top displacement being 32 mm (see Fig. 4-38) for both frames. Also, a low residual inter-storey drift amounting to a maximum of 3 mm (less than 0.1%) was observed (Fig. 4-39).

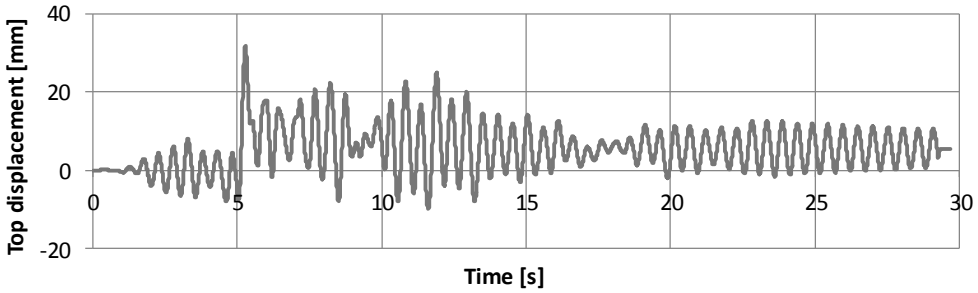

Fig. 4-38. Top displacement time history for DL test

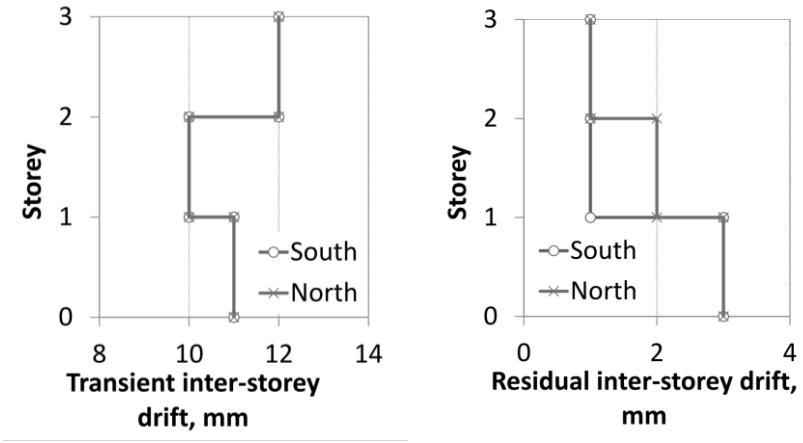

Fig. 4-39. Transient and residual inter-storey drifts for DL test

The link hysteresis curves, corresponding to the levels of the inter-storey drift illustrated in Fig. 4-39, are shown in Fig. 4-40.

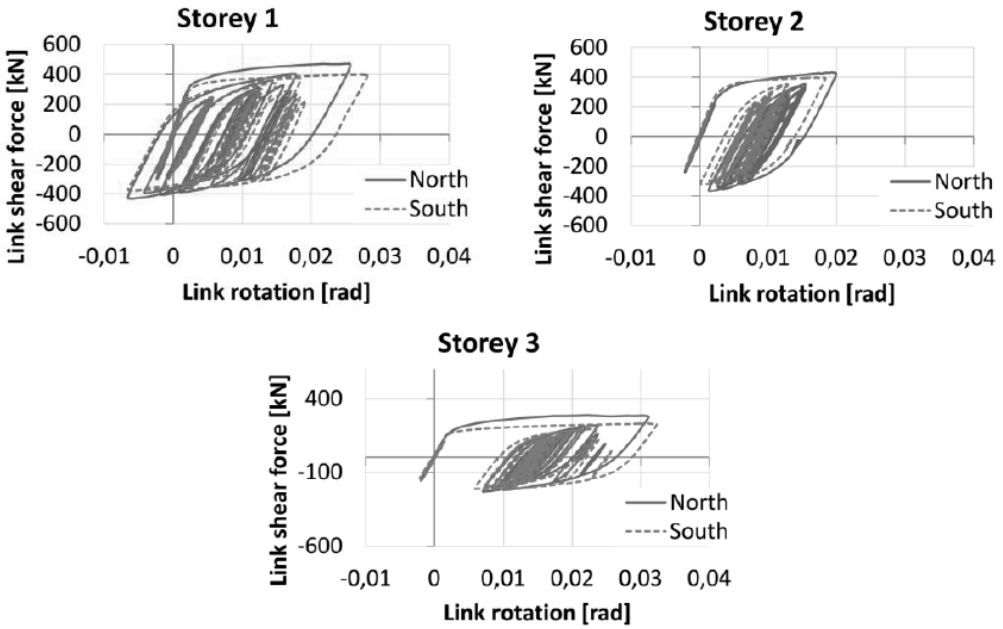

Fig. 4-40. Links behaviour during DL test

The link shear forces (V_{link}) were obtained employing the strains registered in the EBFs braces by strain gauges, using the following formula:

$$V_{link} = N_{br} \cdot \cos\alpha = \sigma_{br} \cdot A_{br} \cdot \cos\alpha = \varepsilon_{br} \cdot E \cdot A_{br} \cdot \cos\alpha \quad (4\text{-}6)$$

where: N_{br} is the axial force of the EBF brace, α is the EBF braces angle with the vertical axis, σ_{br} is the stress of the EBF brace, A_{br} is the area of the EBF brace, ε_{br} is the strain of the EBF brace measured with strain gauges and E is Young modulus for steel.

Additional test results obtained during the FO1 and DL/SLS tests are presented in Annex C.2, C.3 and C.9.

After the DL test, the first set of damaged links was removed (LR1) and replaced with a new (second) set of unused links. This process is described in the following.

4.4.2. First link replacement

Because the structure exhibited a low residual top displacement after the DL test and low residual drift was observed, the decision was made to remove the first set of damaged links, by simply removing the bolts (see Fig. 4-41), one level at a time, starting from the lower level. The dampers where not installed because a smooth transition of forces from the link to the frame was expected.

(a) (b)

Fig. 4-41. Link removal by unscrewing bolts

During replacement of the links the Heidenhains were recording the displacement of the structure. It can be seen that the low value of the residual top displacement at the end of the DL test decreased after the elimination of the damaged links (1 mm for the south frame and 4 mm for the north frame) (see Fig. 4-42). In fact, better re-centring was observed in the south frame, where the link is not connected to the concrete slab.

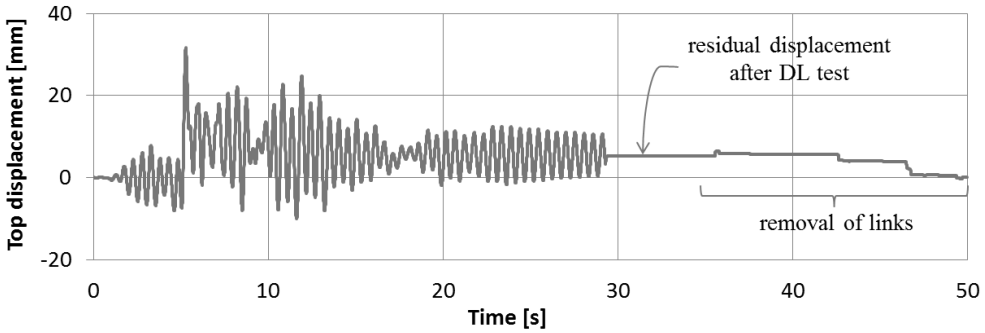

Fig. 4-42. Top displacement time history for south frame during first link removal process

Link removal by unbolting proved more difficult in the north frame than in the south frame, due to the limited available space. To address this issue, a solution whereby the beam containing the removable link is totally disconnected from the reinforced concrete slab (south frame) would be more suitable.

After the bolts had been unscrewed, a hydraulic jack had to be used to push the braces apart so that the links could be pulled out. The pressure applied by the hydraulic jack and the forces supplied are shown in Table 4-9.

Table 4-9. Pressure and forces applied at LR1

Position	bar	kN	Observation
N 1st storey	400	2861	movement[a]
	500	357	removed
S 1st storey	500	357	movement[a]
	600	429	removed

Position	bar	kN	Observation
N 2nd storey	550	393	movement[a]
	600	429	removed
S 2nd storey	500	357	movement[a]
	600	429	removed
S 3rd storey	600	429	removed
N 3rd storey	600	429	removed

[a]Movement – the link could be moved but not removed due to geometric irregularities

No bending occurred in the endplates after removal of the links, therefore there was no relative rotation between the beam and the link during the test.

A new set of unused links was then installed in the structure, thus readying the structure for the next upper input level of the seismic record. An additional low re-centring was also verified during the replacement of the links (2 mm remaining for both frames) (see Fig. 4-43).

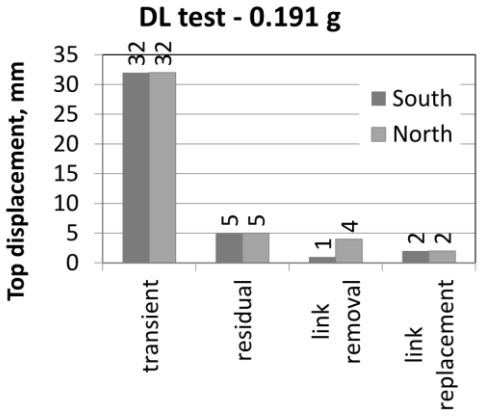

Fig. 4-43. Top displacement during first link replacement process

At the end of the LR1 procedure, a very small residual drift (H/5250 for both frames) that is lower than the erection tolerance (H/300) was observed, the structure being almost re-centred.

4.4.3. SD tests set

During the FO2 test, the structure behaved similarly to the FO1 test. This means that the structure exhibited an elastic response, in the non-dissipative elements, as well as in the dissipative ones (including the links) and there were no residual top displacements or inter-storey drifts of the structure, the maximum top displacement also being small at 5 mm.

The significant damage (SD) test was then performed. During this test, no yield was observed in the elements outside the links. Moderate maximum plastic deformations occurred in the links (see Fig. 4-44a and Fig. 4-47), the highest being 0.061 rad (with the residual deformation amounting to a maximum of 0.022 rad) with no slips occurring in the EBF braces or beam splice connections (displacement transducers showed deformations of < 1 mm in these elements). The beam to

column and column base joint zones exhibited slightly larger rotations, amounting to a maximum of 13 mrad. Moderate cracks were observed in the concrete slab (see Fig. 4-44b).

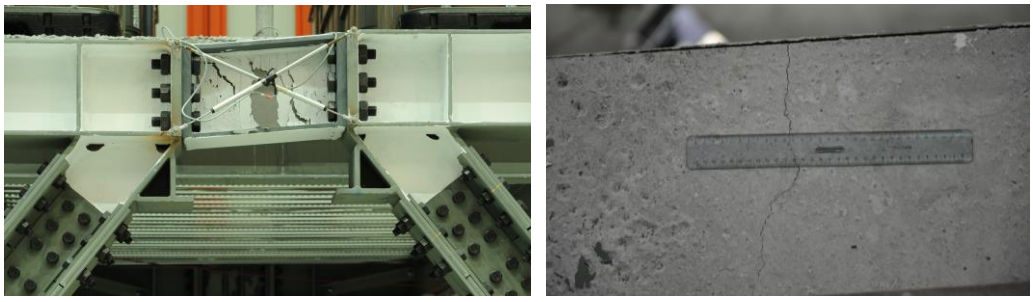

(a) (b)

Fig. 4-44. Link behaviour a) and concrete slab state b) at end of SD test

The structure nevertheless continued to exhibit a low residual top displacement of 13 mm (0.12%), the maximum top displacement being 50 mm (see Fig. 4-45). Also low residual inter-storey drifts having a maximum of 5 mm (0.14%) were observed (Fig. 4-46).

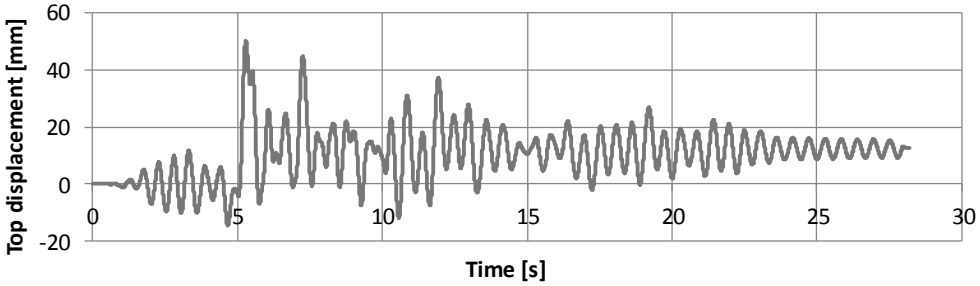

Fig. 4-45. Top displacement time history for SD test

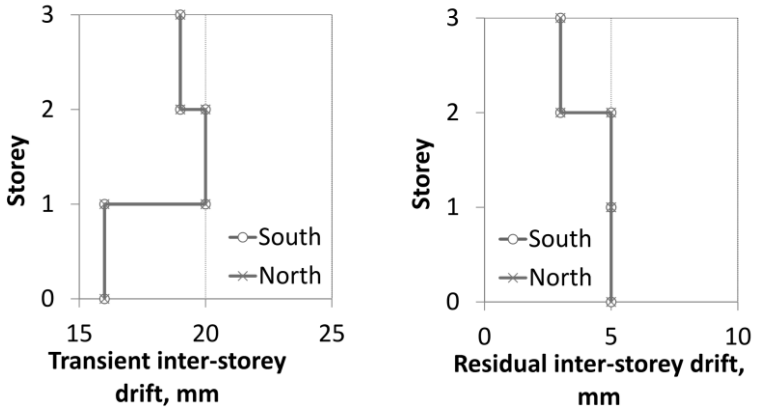

Fig. 4-46. Transient and residual inter-storey drift for SD test

The link hysteresis curves, corresponding to the levels of the inter-storey drifts illustrated in Fig. 4-46, are presented in Fig. 4-47.

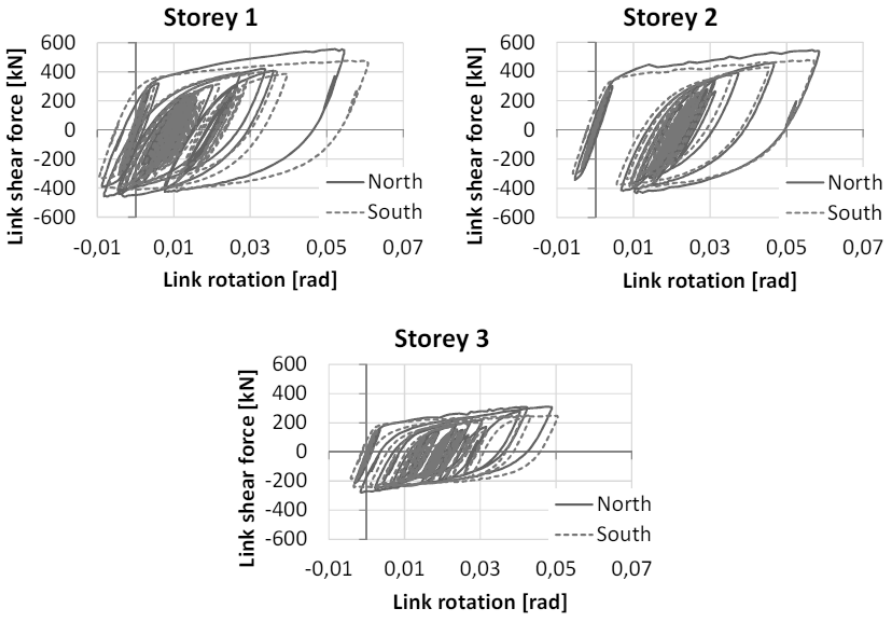

Fig. 4-47. Links behaviour during SD test

Given that, after the SD test, the residual displacement was still small, a monotonic pushover test (using as input a target displacement of 55 mm) (PO1) was performed, starting from the end of the SD test position. This was done to obtain a larger residual displacement than would be necessary to validate the feasibility of the link removal process and re-centre the structure. The PO1 test was started after the actuators' release of force from the previous test (SD) and was conducted under displacement control on the third floor with an inverted triangular distribution of forces at the south frame and equal displacements at both frames.

The test was stopped before reaching the target displacement, after slipping of the base of the central columns at a base shear in the north frame equal to 1088 kN. The slippage of columns took place between the base plate and the strong floor, as the horizontal forces exceeded the static friction force between these two elements.

During this test, no yield was observed in the elements outside the links. Higher maximum plastic deformations occurred in the links (see Fig. 4-48a and Fig. 4-51), the highest being of 0.075 rad (with the residual deformation amounting to a maximum of 0.066 rad) and no slip occurred in the EBF braces or beam splice connections (displacement transducers showed deformations of < 1 mm in these elements). The beam to column and column base joint zones exhibited larger rotations, amounting to a maximum of 20 mrad. More visible cracks were observed in the concrete slab (see Fig. 4-48b).

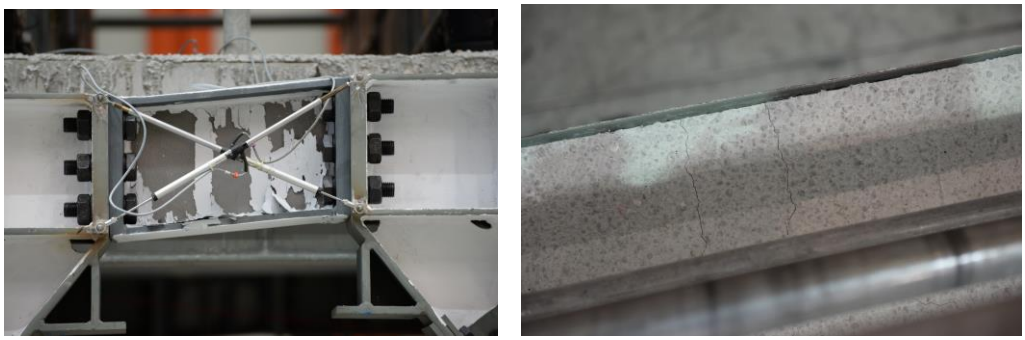

(a) (b)

Fig. 4-48. Link behaviour a) and concrete slab state b) at end of PO1 test

After the completion of this test, the structure exhibited a significantly larger residual top displacement of 45 mm (0.43%), the maximum top displacement being 68 mm (the sum of the residual displacement from the previous test and the applied displacement of the current test) (see Fig. 4-49). Larger residual inter-storey drift amounting to a maximum of 18 mm (0.5%) was observed (Fig. 4-50).

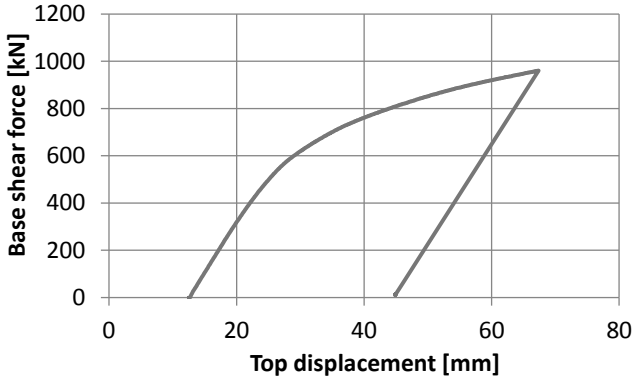

Fig. 4-49. Pushover curve for PO1 test

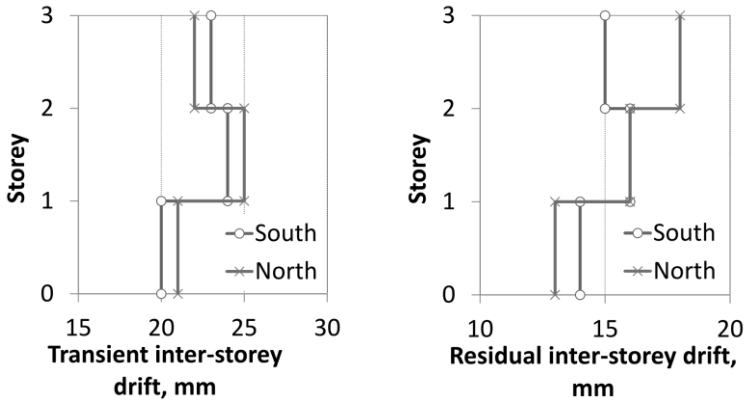

Fig. 4-50. Transient and residual inter-storey drift for PO1 test

The link response during the PO1 test, are presented in Fig. 4-51.

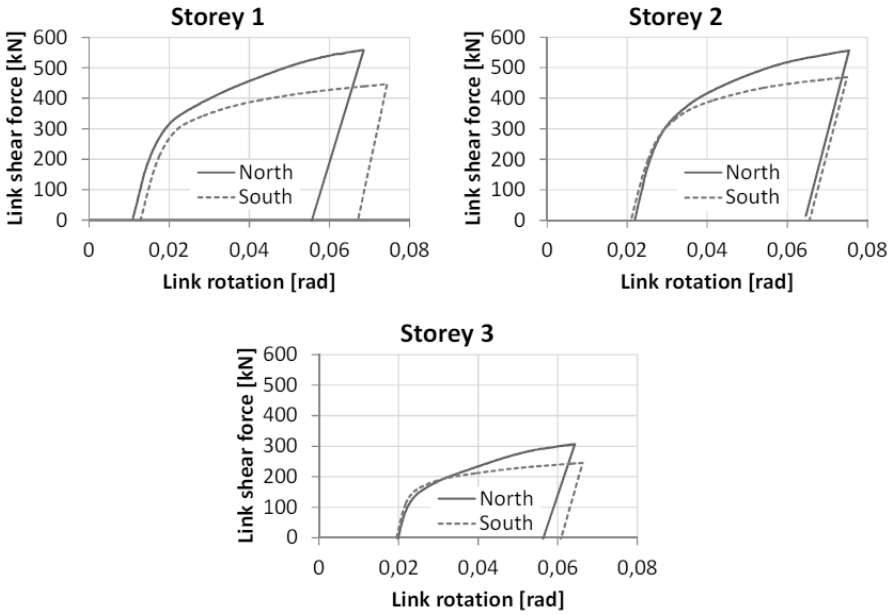

Fig. 4-51. Link behaviour during PO1 test

Additional test results obtained during the SD/ULS and PO1 tests are presented in Annex C.4, C.5 and C.9.

After the PO1 test, the second set of damaged links was removed (LR2) and replaced with another new (third) set of unused links. This process is described in the following.

4.4.4. Second link replacement

After the SD test, the structure continued to exhibit a low residual top displacement of 13 mm (0.12%), the maximum top displacement being 50 mm. Then, the PO1 test was proposed, which caused the structure to exhibit a significantly larger residual top displacement. In this case, removal of the links required that they be flame cut (see Fig. 4-52) (firstly the link web and after, the flanges), from the top storey downwards.

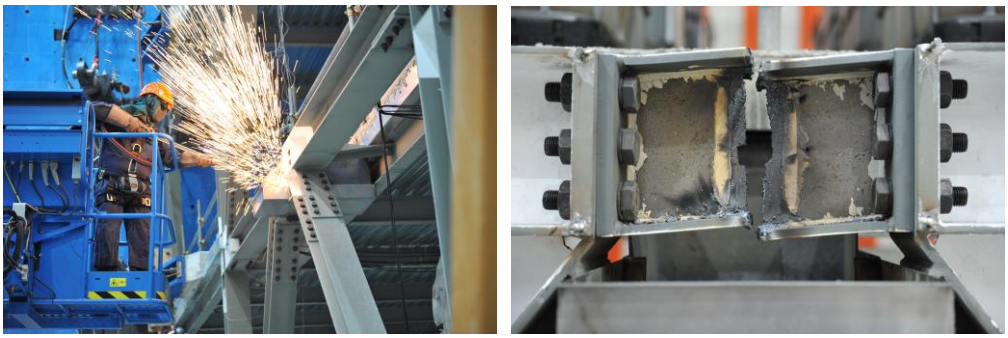

(a) (b)

Fig. 4-52. Link removal by flame cutting and unscrewing bolts

During removal of the links and the following 48 hours, the Heidenhains remained connected and the acquisition system continued to record the displacement of each floor. As there was no oil pressure, the actuator followed the displacements of the structure with negligible reaction force.

The residual top displacement at the end of the PO1 test was reduced after the elimination of the damaged links (10 mm in the south frame and 19 mm in the north frame) (see Fig. 4-53). Again, better re-centring was observed in the south frame, where the link is not connected to the concrete slab.

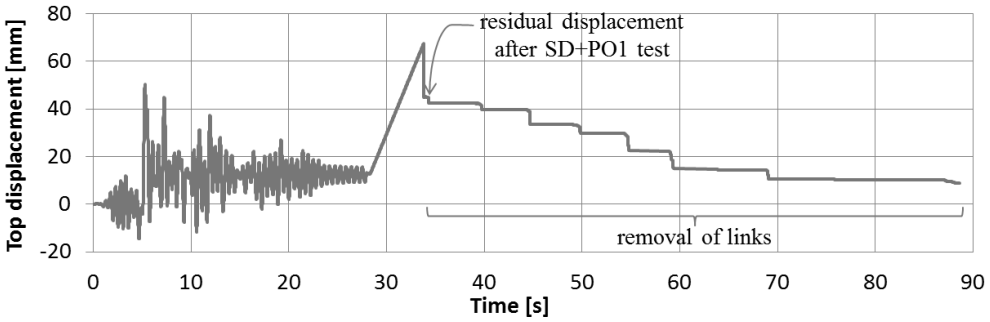

Fig. 4-53. Top displacement time history for south frame during second link removal process

Although it was not necessary to use a hydraulic jack to remove the links, it was needed to place the new set of links in the structure. The forces used for fixing the links are listed in Table 4-10, below.

Table 4-10. Pressure and forces applied to link insertion

Position	bar	kN	Observation
S 3rd storey	500	357	everything
N 3rd storey	400	286	started moving
	680	486	to fix bolts
S 2nd storey	400	286	everything
N 2nd storey	300	214	started moving
	400	286	to fix bolts
S 1st storey	500	357	everything
N 1st storey	200	143	everything

A new set of unused links was then mounted into the structure, thus readying the structure for the next upper input level of the seismic record. An additional low re-centring was also observed after the replacement of the links (2 mm remaining for the south frame and 6 mm for the north one), see Fig. 4-54.

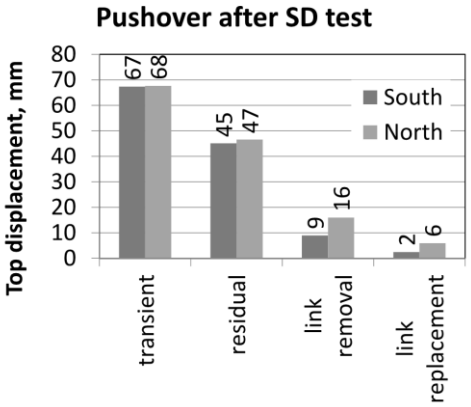

Fig. 4-54. Top displacement during second link replacement process

At the end of the LR2 procedure, a small residual drift (H/5250 for the south frame and H/1750 for the north frame) that was lower than erection tolerance (H/300) was observed, the structure being mostly re-centred.

Before continuing with the next tests, two sets of two square hollow section steel elements, secured with four prestressed Dywidag bars where placed between and welded to the footing plates of the columns of each of the frames (Fig. 4-55), with the purpose of preventing any relative displacements between the columns and the reaction floor.

Fig. 4-55. Additional fixing of the columns

During this stage a second and third out-of-plumb measurements were done, in order to compare the current geometry of the structure with the initial one. The results are shown in Fig. 4-56 to Fig. 4-60. The second measurement was done before the installation of the links, while the third measurement was done after placement of the links.

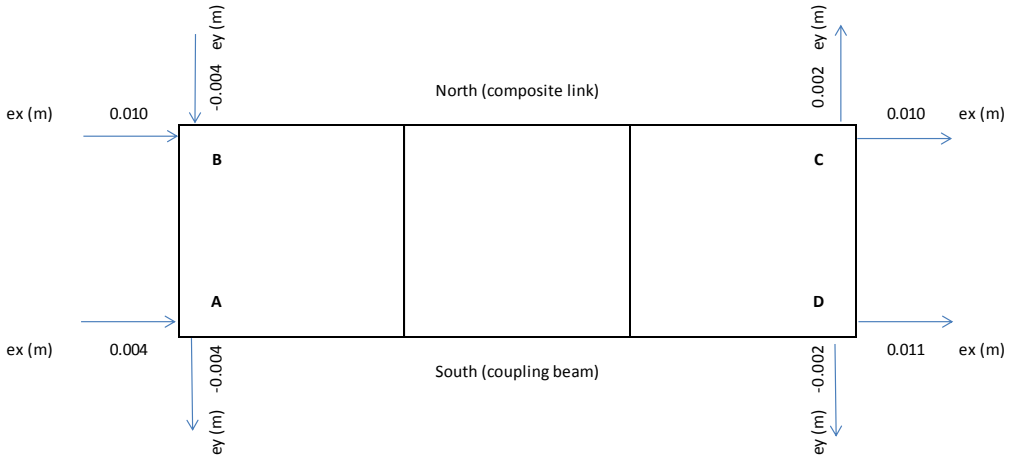

Fig. 4-56. Out of plumb, 2nd measurement, 1st floor

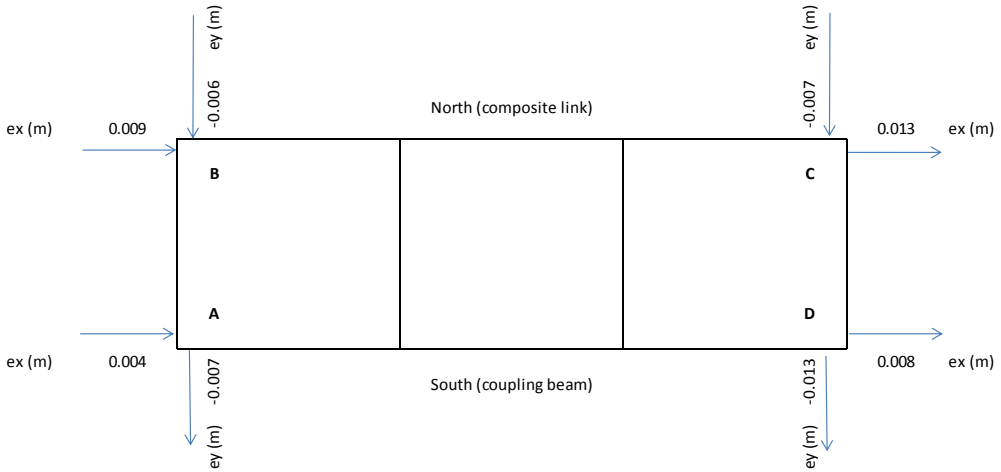

Fig. 4-57. Out of plumb, 2nd measurement, 2nd floor

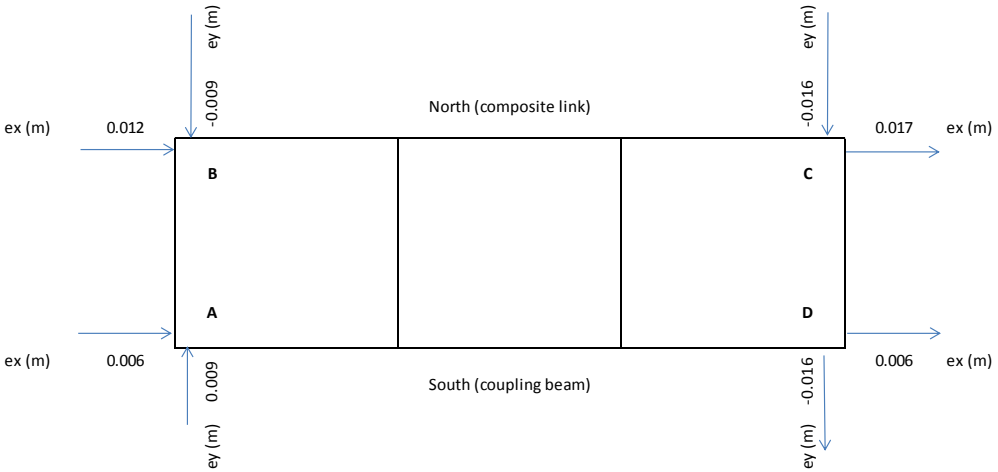

Fig. 4-58. Out of plumb, 2nd measurement, 3rd floor

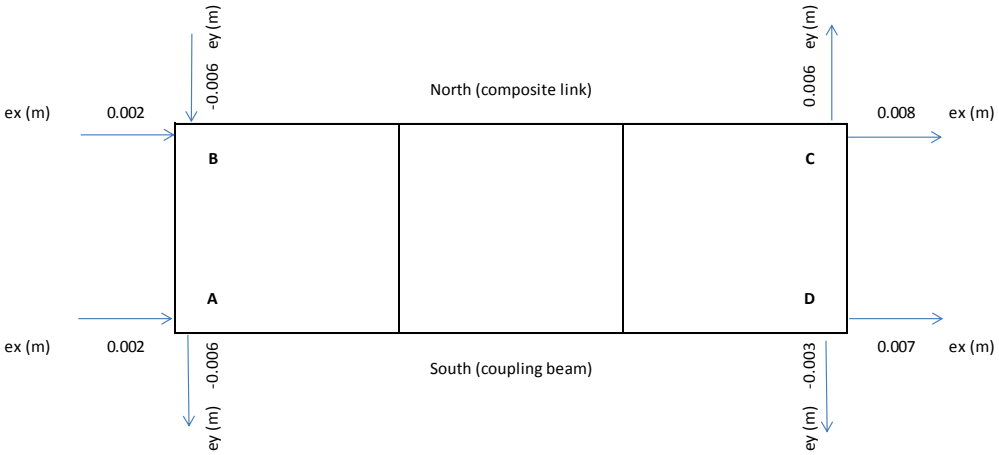

Fig. 4-59. Out of plumb, 3rd measurement, 1st floor

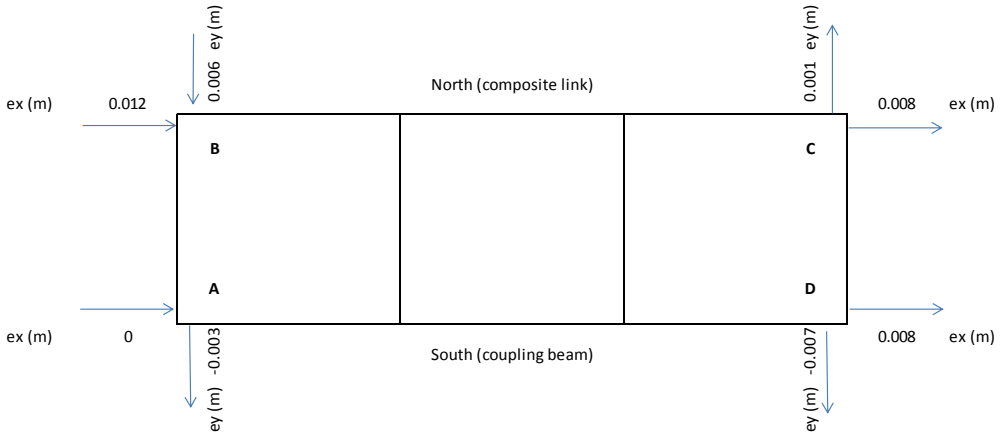

Fig. 4-60. Out of plumb, 3rd measurement, 2nd floor

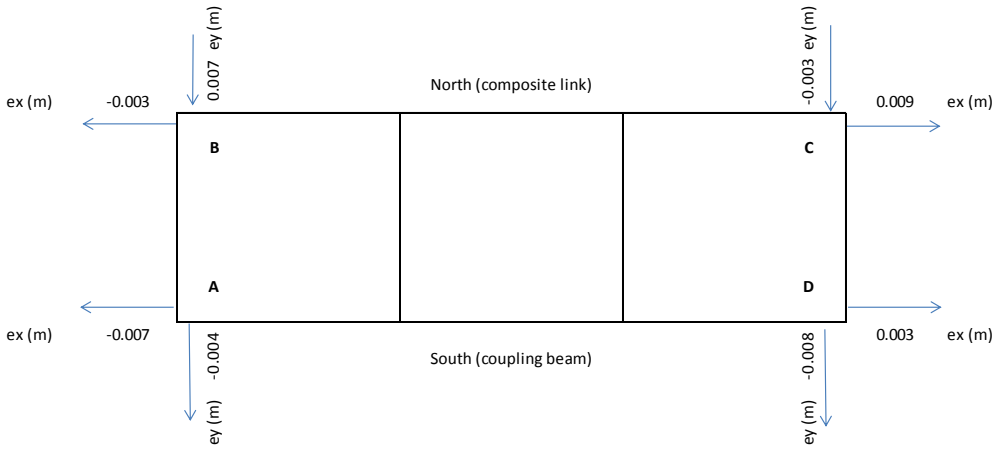

Fig. 4-61. Out of plumb, 3rd measurement, 3rd floor

4.4.5. NC tests set

During the FO3 test, the structure exhibited a similar behaviour to that in the first two FO tests. The structure exhibited an elastic response in the non-dissipative elements, as well as in the dissipative ones outside the links, as well as a very small residual deformation in the links (amounting to a maximum of 0.001 rad). There was no residual top displacement or inter-storey drift in the structure, while the maximum top displacement was also small at 5 mm.

While the near collapse (NC) test was being performed, an alarm was triggered following a difference exceeding 10 mm between the displacement recorded by the actuator displacement transducers and those recorded by the external displacement transducers (a sign of high force close to saturation of the actuator). This test had to be stopped prematurely because the available actuator

capacity (1000 kN per frame at every floor) was not sufficient to execute the test with the imposed null torsion at every floor (see Fig. 4-62). This corresponded to a situation where the actuators from the first floor were acting in a direction opposite to that of the actuators of the second and third floors. The maximum displacement recorded at the top of the structure was 118.1 mm. The seismic links reached high deformations, exceeding the maximum limit of the transducers (± 25 mm) placed across the links of the first two floors.

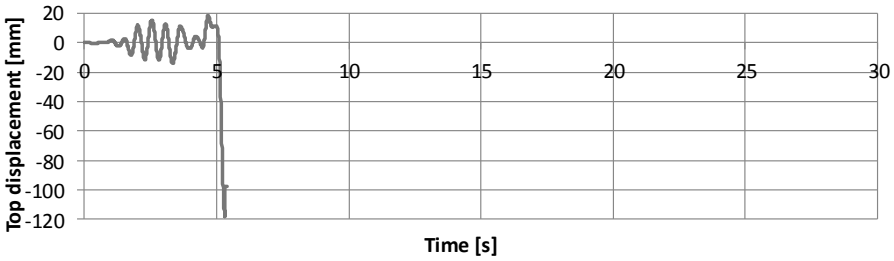

Fig. 4-62. Top displacement time history for NC test

Since the whole accelerogram was not completed, including passing through the PGA of the record, it was decided to continue with a push-over test (PO2) with an inverted triangle distribution of forces. Equal displacements (using as input a target displacement of 150 mm) between the north and south frames were imposed at the third floor, the actuators of the first and second floors were under force control. Although equal displacements were imposed on the north and south frames of the third floor, the two lower floors rotated along the horizontal plane due to the different stiffness between the two frames. The test was stopped at 231.6 mm displacement at the top floor.

A final cyclic push-over test (PO3) was carried out under displacement control (with a target amplitude of 400 mm) considering uniform distribution of forces. To avoid the saturation of the actuator forces, for these pushover tests, the torsion would be null only at the second floor. Maximum displacements at the third floor were recorded at 405 and 499.4 mm on the north and south frames respectively.

The last test produced extensive plastic behaviour throughout the entire structure. First of all, very large maximum plastic deformations occurred in the links, specifically, 0.15 – 0.38 rad for the first two levels and 0.09 – 0.13 rad for the third level (see Fig. 4-63b), with failure occurring inside the link element very close to the welding with the end plate and also between the webs and flanges of the first two levels (see Fig. 4-63a). At the point of maximum displacements the links from the first two floors had already failed and fallen down. The first link to fall was the one from the first floor on the south frame, followed by the link on the opposite frame.

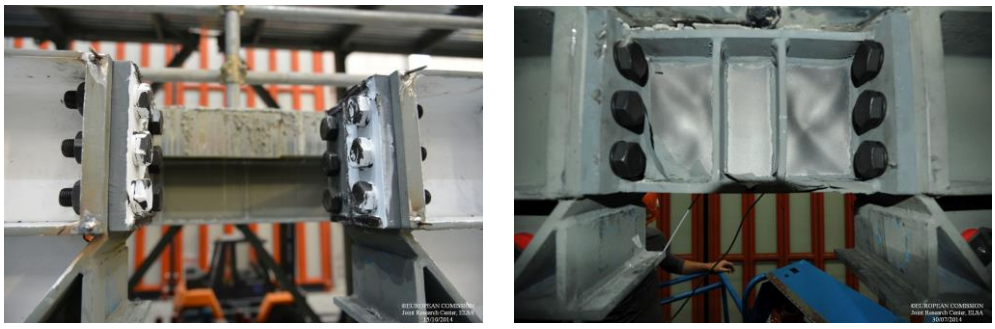

(a) (b)

Fig. 4-63. State of links from first two stories (a) and from the third storey (b) at the end of the experimental programme

Significant damage was also observed in the column bases zones (see Fig. 4-64a) and at the end of the MRF beams (with a strain three times greater than the yield value), just outside the haunch (see Fig. 4-64b). The beam to column and column base joint zones exhibited very large rotations, amounting to a maximum of 90 mrad. The concrete slab was heavily compromised in the north frame (see Fig. 4-64c).

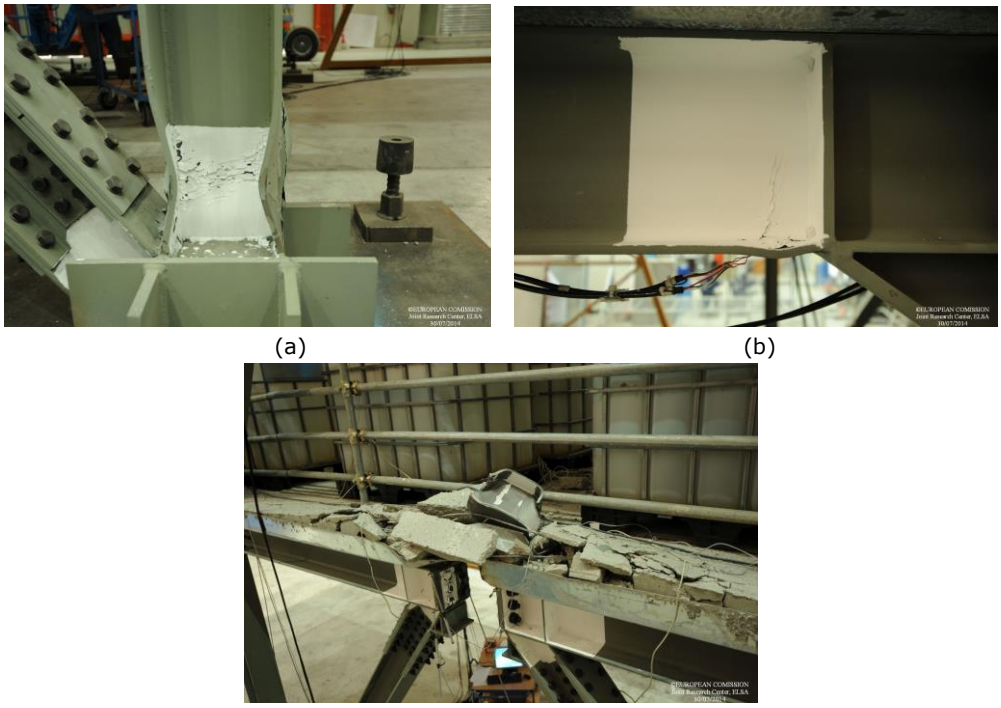

(a) (b)

(c)

Fig. 4-64. State of elements outside links: column base (a) and moment resisting frame beam (b) and concrete slab (c) at the end of the experimental programme

Additional test results obtained during the NC, PO2 and PO3 tests are presented in Annex C.6, C.7, C.8 and C.9.

4.5. Influence of concrete slab

One of the critiques to the removable link solution is related to the interaction between the removable links and the concrete slab. The floor layout of the test specimen was designed to allow the investigation of two different solutions to the interaction between a removable link and the reinforced concrete slab. The solution for the south frame involved disconnecting the removable link from the reinforced concrete slab, by extending the slab only up to an additional secondary beam placed in parallel with the beam containing the link. The solution for the north frame involved using a conventional reinforced concrete slab (not connected to the link with shear studs) such that it would accept damage to it.

After obtaining the results of the tests, on one hand, it could be seen that the concrete slab increases the link's shear capacity, (the shear capacity is larger for the link in the north frame than for that in the south frame) (Fig. 4-65).

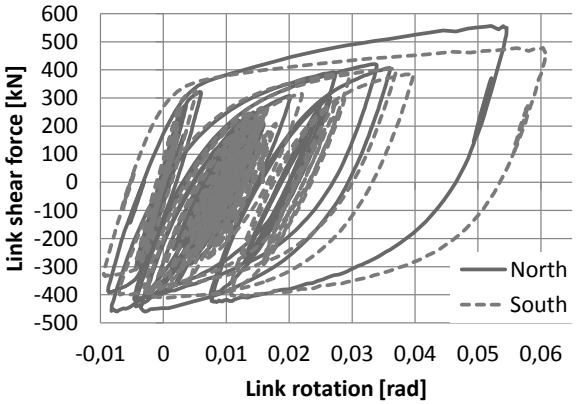

Fig. 4-65. First storey link rotation – shear force for SD test

On the other hand, large link deformations can damage the concrete slab, which violates the principle that plastic deformation (damage) should be constrained to the removable links. However the SD seismic input level and the following PO (for which the maximum link rotation was 75 mrad), caused only minor to moderate cracking (Fig. 4-37b, Fig. 4-44b, Fig. 4-48b) of the concrete slab. These can be repaired locally, while the reinforcement and corrugated steel sheet used as the formwork retain their integrity due to their greater flexibility.

Furthermore, due to the presence of the slab over the links, the north frame is more rigid and has a larger capacity than the south frame (Fig. 4-66). This makes re-centring of the north frame more difficult than in the case of the south frame (Fig. 4-54), but the residual drift was still lower than the erection tolerances.

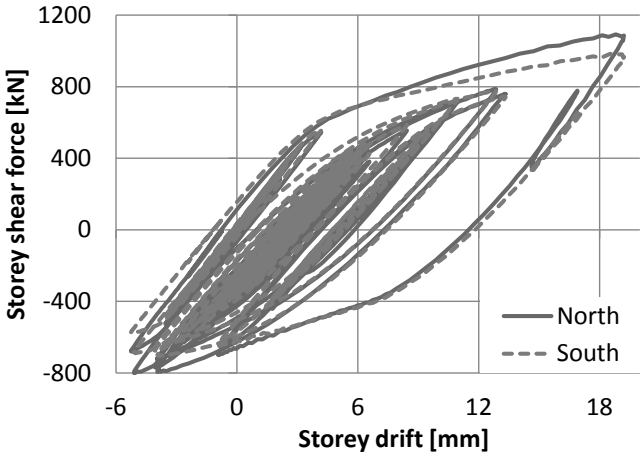

Fig. 4-66. First storey drift – shear force for the SD test

4.1. Concluding remarks

Tests on material samples

In order to evaluate material characteristics, tensile tests were performed at Politehnica University Timisoara (CEMSIG Research Centre), on steel samples prepared from the additional material received from JRC associated to each structural member of the test specimen and link-beam connection bolts. All the materials have fulfilled the product standards demands.

Tests on full-scale specimen

The validation of re-centring capability and link replacement procedure in a dual eccentrically braced structure, together with assessing its seismic performance, was realised through a pseudo-dynamic testing programme of a full-scale model performed at the European Laboratory for Structural Assessment (ELSA) facility at JRC in Ispra, Italy.

The first set of tests were represented by the snap-back tests. These were performed to simulate the snap due to a sudden release of forces, prior to the instalment of the actuators which were used for pseudo-dynamic tests, assessing on one side the amplitude of the free vibrations, and on the other side the effectiveness of dampers in limiting such vibrations. The results show a very small maximum displacement and confirm that the dampers were not activated due to the small size of displacements imposed on the frame. The transverse displacements were also small.

In order to assess the seismic performance of the full-scale specimen and validate the link replacement procedure, a pseudo-dynamic testing programme was proposed, composed of the sequence of the following tests: DL/SLS tests (Full-operation FO1 earthquake and DL earthquake), followed by the first set of links replacement, SD/ULS tests (Full-operation FO2 earthquake, SD earthquake and a

pushover test), followed by the second set of links replacement and NC tests (Full-operation FO3 earthquake and NC earthquake).

DL tests

The structure manifested an elastic response, in the non-dissipative elements, as well as in the dissipative ones (including the links), during the first FO1 test. This means that there were no residual top displacements or any inter-storey drift in the structure, while the maximum top displacement was also small.

During DL test, no yield was observed in the elements outside the links. Small maximum plastic deformations occurred in links. Minor cracks were observed in the concrete slab. The structure exhibited a low residual top displacement of in the S frame and slightly higher in the N frame. Also, a low residual inter-storey drift was observed.

First link replacement

Because the structure exhibited a low residual top displacement after the DL test and low residual drift was observed, the removal of the first set of damaged links was performed by simply unscrewing the bolts, one level at a time, starting from the lower level. The dampers where not installed because a smooth transition of forces from the link to the frame was expected. The low value of the residual top displacement at the end of the DL test decreased after the elimination of the damaged links. Better re-centring was observed in the south frame, where the link is not connected to the concrete slab. An additional low re-centring was also verified during the replacement with a new set of unused links A very small residual drift that is lower than the erection tolerance was observed at the end of this procedure, the structure being almost re-centred.

SD tests

The structure behaved similarly to the FO1 test, during the FO2 test. This means that the structure exhibited an elastic response, in the non-dissipative elements, as well as in the dissipative ones (including the links) and there were no residual top displacements or inter-storey drifts of the structure.

Because after the SD test, the residual displacement was still small, a monotonic pushover test was performed, starting from the end of the SD test position. This was done to obtain a larger residual displacement than would be necessary to validate the feasibility of the link removal process and re-centre the structure. During this test, no yield was observed in the elements outside the links. Higher maximum plastic deformations occurred in the links. More visible cracks were observed in the concrete slab. After the completion of this test, the structure exhibited a significantly larger residual top displacement. Larger residual inter-storey drift was observed.

Second link replacement

Because the PO1 test caused the structure to exhibit a significantly larger residual top displacement, removal of the links required that they be flame cut (firstly the link web and after, the flanges), from the top storey downwards. The

residual top displacement at the end of the PO1 test was reduced after the elimination of the damaged links. Again, better re-centring was observed in the south frame, where the link is not connected to the concrete slab. A new set of unused links was then mounted into the structure, thus readying the structure for the next upper input level of the seismic record. An additional low re-centring was also observed after the replacement of the links. A small residual drift that was lower than erection tolerance was observed, the structure being mostly re-centred.

NC tests

The structure behaved similarly to the first two FO tests, during the FO3 test. The structure exhibited an elastic response in the non-dissipative elements, as well as in the dissipative ones outside the links, as well as a very small residual deformation in the links. There was no residual top displacement or inter-storey drift in the structure.

The NC test was started, but had to be stopped prematurely because the available actuator capacity was not sufficient to execute the test with the imposed null torsion at every floor. It was then decided to continue with pushover tests.

The last pushover test produced extensive plastic behaviour throughout the entire structure. First of all, very large maximum plastic deformations occurred in the links, specifically, with failure occurring inside the link element very close to the welding with the end plate and also between the webs and flanges of the first two levels. At the point of maximum displacements the links from the first two floors had already failed and fallen down. The first link to fall was the one from the first floor on the south frame, followed by the link on the opposite frame. Significant damage was also observed in the column bases zones and at the end of the MRF beams, just outside the haunch. The concrete slab was heavily compromised in the north frame.

Concrete slab influence

One of the critiques to the removable link solution is related to the interaction between the removable links and the concrete slab. The floor layout of the test specimen was designed to allow the investigation of two different solutions to the interaction between a removable link and the reinforced concrete slab. The solution for the south frame involved disconnecting the removable link from the reinforced concrete slab, by extending the slab only up to an additional secondary beam placed in parallel with the beam containing the link. The solution for the north frame involved using a conventional reinforced concrete slab (not connected to the link with shear studs) such that it would accept damage to it.

The concrete slab increases the link's shear capacity. Due to its presence over the links, the north frame is more rigid and has a larger capacity than the south frame, this making re-centring of the north frame more difficult than in the case of the south frame.

5. NUMERICAL VALIDATION OF DESIGN METHODOLOGY FOR DUAL ECCENTRICALLY BRACED FRAMES WITH REMOVABLE LINKS

5.1. Introduction

Other structural configurations of dual eccentrically braced frames with removable links were analysed in order to check if the experimental specimen behaviour can be extended to more general, current practice structures. Two different 6 storey structures were designed: the first, like in the case of the experimental specimen, having a central EBF and two side MRFs and the second having a central MRF and two side EBFs. The experimental tests results were used to calibrate a numerical model that can be employed in further numerical simulations. The seismic performance of the two structures was assessed by means of nonlinear static (pushover) and dynamic (time-history) analyses. A series of numerical simulations were performed next, in order to validate the re-centring capability of the two structures and to study different solutions for removing links within a storey and per height of the structure and choose the most suitable one in order to be recommended.

Also incremental dynamic analyses were performed in order to compute the behaviour factor q and the over-strength of dual eccentrically braced frames with removable links, for different limit states.

5.2. Calibration of numerical model

In order to obtain a numerical model that can be used in further simulations on dual eccentrically braced frames with removable links, the model described in Chapter 3.4.1 and used in pre-test numerical simulations was calibrated based on experimental results of PsD tests.

Time-history analyses were performed using SeismoStruct [84] program, applying at each of the three levels of the model the displacements obtained from the experimental tests. The values used for material characteristics were the ones obtained from tensile tests on steel samples (Table 4-2).

The best match between numerical and experimental results was obtained by modelling the rotational springs at the ends of the force based inelastic link beam using "smooth curve" (as defined in SesmoStruct) link elements with a backbone curve defined in Fig. 5-1. The "smooth curve" model has been formulated with rules for stiffness and strength degradation and pinching.

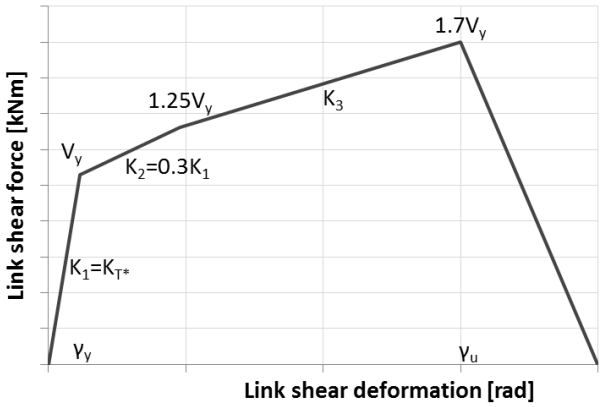

Fig. 5-1. "Smooth curve" link element backbone curve

The initial stiffness of the links from experimental tests in stories 1 and 2 is equal to the stiffness computed in order to account for bending and shear of the link and rotational deformations in the bolted connections. The links from the 3rd storey had a behaviour closer to continuous links, their initial stiffness being equal to the stiffness computed in order to account for bending and shear of the link only (without accounting for any additional connection stiffness). The links from the 3rd storey behaved this way because, even if their shear stiffness is approximately half of the one of links from the first two stories, they all had the same connection, being therefore much stiffer compared to the link in the case of the third storey links.

The ratio between the ultimate force and the yield force is 1.7 and the ultimate shear deformation γ_u=0.15 rad.

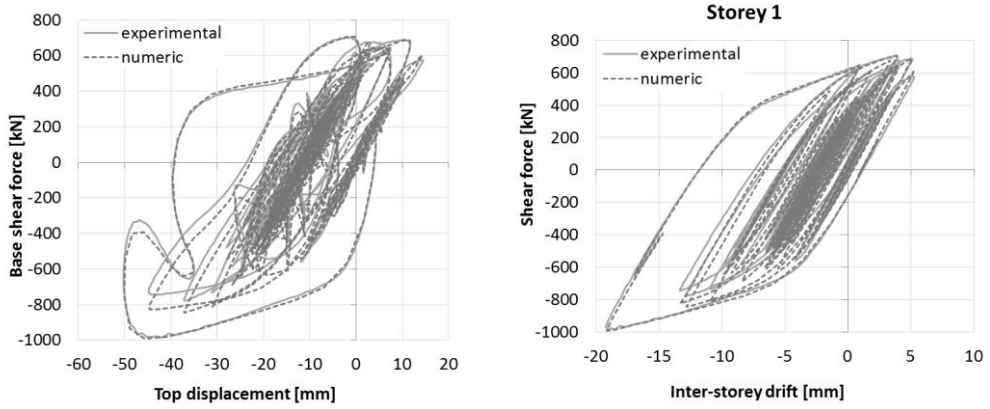

Fig. 5-2. Top displacement and first storey drift versus base shear force

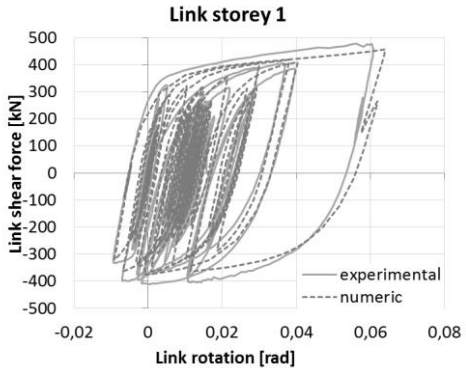

Fig. 5-3. First storey link rotation versus shear force

The results of numerical simulations and ULS experimental test were compared in terms of global top displacement and first storey drift versus base shear force (Fig. 5-2) and first storey link shear force versus rotation (Fig. 5-3). A very good match was observed. The new calibrated numerical model was than adopted for further simulations on the two 6 storey structures, with the initial stiffness computed in order to account for shear stiffness of the link and rotational deformations in the bolted connections.

5.3. Design of dual EBFs with removable links

In order to validate numerically the design methodology of current practice EBF structures with removable links and the link replacement procedure, two dual structural configurations were designed: the first, like in the case of the experimental specimen, having a central EBF (with the link being placed at mid-span) and two side MRFs, being further referred to as „Configuration A" (Fig. 5-4a) and the second having a central MRF and two side EBFs. (links placed marginally, connected to columns on one side) being further referred to as „Configuration B" (Fig. 5-4b). The links from eccentrically braced frames (EBFs) were conceived as removable (bolted links) dissipative elements because they are intended to provide the energy dissipation capacity and to be easily replaceable. The more flexible moment resisting frames provide the necessary re-centring capability to the structure.

Both structures have 3 spans of 7.5 meters and 5 bays of 7.5 meters, and 6 storeys of 3.5 meters each (4.0 m at the ground level). The main lateral load resisting system is composed of eccentrically braced frames (2 on each horizontal direction for structure A and 4 on each horizontal direction for structure B). Additionally, there are 4 moment resisting frames on each horizontal direction in case of configuration A and 2 moment resisting frames on each horizontal direction in case of configuration B, to assure the restoring forces after an earthquake.

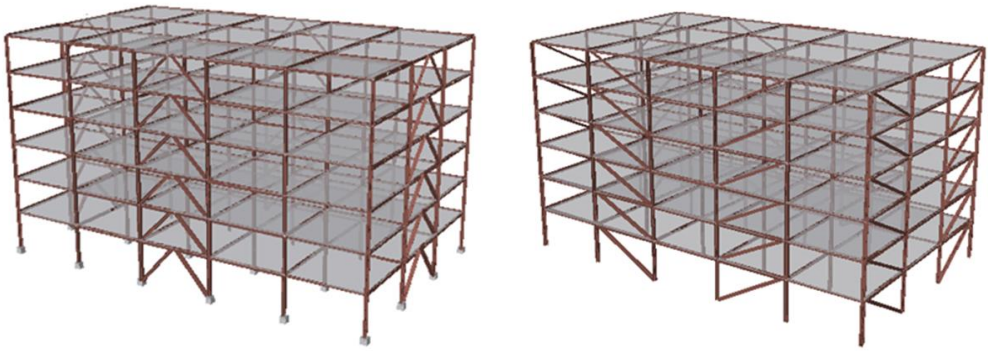

(a) (b)

Fig. 5-4. Configuration A (a) and Configuration B (b) structures

The capacity design of the structure was carried out according to EN1990 [78], EN1991 [79], EN1993 [81], EN1994 [82] and EN1998 [1]. A 4.9 kN/m^2 dead load and 3.0 kN/m^2 live load were considered. The buildings were analysed for stiff soil conditions (EC8 [1] type 1 spectrum for soil type C), characterised by 0.35g peak ground acceleration. A behaviour factor q=4 (ductility class M) and inter-storey drift limitation of 0.0075 of the storey height are used.

The Ultimate Limit State (ULS) design was performed according to Eurocode 8 [1] rules. The links were designed from the seismic design situation combination for dissipative elements [78], with a length of e=800mm, as short links ($e<e_s=1.6M_{p,link}/V_{p,link}$) which dissipate energy by yielding in shear [1], in order to ensure the practical over-strength of the link's flush end plate connection. In the global analysis, a reduced equivalent shear area A_s* was used for the links in order to account for the more flexible behaviour of bolted links, arising from the following sources [83]:

- the link web shear deformation (γ)
- the link bending deformation (γ_M)
- the rotation from the link to beam connection (θ)

The bending stiffness of the link is explicitly modelled in the global analysis; therefore, the following formulas were used:

$$A_s^* = \frac{K_T^* e}{G} \quad (3\text{-}14)$$

$$K_T^* = \frac{1}{\frac{1}{K_\gamma} + \frac{1}{K_\theta}} \quad (3\text{-}15)$$

Where:
K_T* is the equivalent stiffness of the removable link;
e is the link's length;
K_γ is the shear stiffness of the link's web;
K_θ is the stiffness component due to the rotation in the link-beam connection.

The MRFs beams were designed from the persistent design situation ULS combinations [78], while braces, beams from EBFs (eccentrically braced frames)

and columns were designed from the seismic design situation combination for non-dissipative elements [78].

For the Serviceability Limit State (SLS), overall horizontal displacement over the building height and beams deformations were checked from the fundamental SLS combinations [78], while the inter-storey drifts were checked from the seismic SLS combination [78].

The geometry of the designed elements is presented in Table 5-1 and Table 5-2.

Table 5-1. Elements sections for Configuration A

Storey	Links	EBF beams	Braces	EBF columns	MRF beams	MRF columns
1	640x260x22x12	HEA650	HEM300	HEM340	IPE450	HEB340
2	590x260x22x10	HEA600	HEM280	HEM340	IPE400	HEB340
3	540x240x22x10	HEA550	HEM260	HEB340	IPE360	HEB300
4	490x230x22x9	HEA500	HEM240	HEB340	IPE360	HEB300
5	440x230x20x8	HEA450	HEM220	HEB300	IPE300	HEB300
6	390x210x16x6	HEA400	HEM180	HEB300	IPE300	HEB300

Table 5-2. Elements sections for Configuration B

Storey	Links	EBF beams	Braces	EBF columns	MRF beams	MRF columns
1	540x260x20x9	HEA550	HEM300	HEM340	IPE600	HEB340
2	490x230x20x8	HEA500	HEM280	HEM340	IPE550	HEB340
3	440x230x20x8	HEA450	HEM260	HEM340	IPE550	HEB300
4	390x230x20x8	HEA400	HEM240	HEM340	IPE500	HEB300
5	350x230x18x8	HEA360	HEM240	HEB340	IPE500	HEB300
6	330x190x15x5	HEA340	HEM200	HEB340	IPE400	HEB300

EBFs steel structural components were designed in S355 grade steel, while MRFs steel structural components were designed in S460.

Structure B has a larger capacity than structure A because two links of configuration B have the capacity with about 40% larger than one link of configuration A, for reasons of keeping the links Class 1 sections (minimum possible web thickness for structure B links) and being able to design the link connections as elastic (to ensure their over-strength) (minimum possible section height for structure B).

The EBF beams were designed in both cases to have the same height as the links. The MRF beams are larger for configuration B for reasons of keeping the structure a dual one (the MRFs are able of resisting about 26% of the total seismic force > 25%). The EBF columns in case of configuration B have resulted in larger sections because they are made from S355 steel (as opposed to configuration A where they were S460 steel).

5.4. Numerical evaluation and investigation

5.4.1. Evaluation of seismic performance

For a structure with re-centring capability, the design objective consists in preventing yielding in members other than removable dissipative ones, up to a desired deformation. Ideally the latter should be the ultimate deformation capacity of the removable dissipative member. From a preliminary pushover analysis, it was observed that following code-based capacity design rules was not enough to

accomplish the objective stated above for the investigated structures. But, using S690 higher-strength steel in moment resisting frames (see Fig. 5-5) was shown to be efficient in avoiding yielding in their members, obtaining a larger capacity without increasing the stiffness, this being the material used in further analyses.

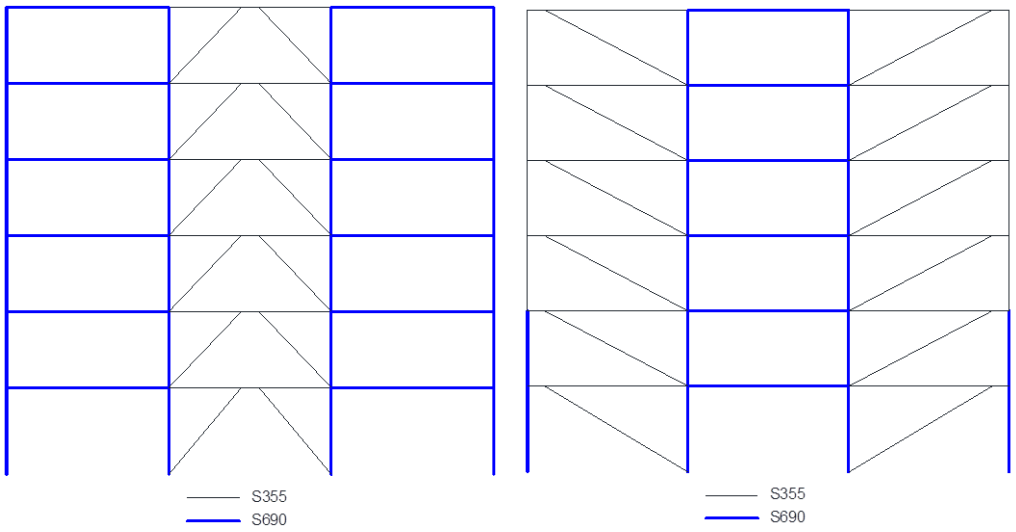

(a) (b)

Fig. 5-5. Materials used for Configuration A (a) and Configuration (b)

5.4.1.1. Static nonlinear (Pushover) analysis

Static pushover analyses were made on the calibrated numerical model in order to evaluate the seismic performance of the two structures, considering a modal (inverted triangular) lateral force distributions, determined according to EC8 [1].

Structural performance was evaluated for the limit states shown in Table 5-3, where a_{gr} is the reference peak ground acceleration of 0.35g and a_g represents the peak ground acceleration for a specific earthquake level.

Table 5-3. Limit states and corresponding scaling factors for seismic input

Limit state	Return period, years	Probability of exceedance	a_g/a_{gr}	a_g/g
Damage Limitation (DL / SLS)	95	10% / 10 years	0.59	0.207
Significant Damage (SD / ULS)	475	10% / 50 years	1.00	0.350
Near Collapse (NC)	2475	2% / 50 years	1.72	0.602

The target displacements (D_t) were computed using the N2 method for each of the three limit states above. For each limit state, the link rotation at the target

displacement was compared to the FEMA356 [87] acceptance criteria for shear links (0.005 rad at DL, 0.11 rad at SD and 0.14 rad at NC):

Table 5-4. Seismic performance assessment in case of Configuration A

	N2		FEMA acc. criteria	
Config. A	D_t [mm]	Link rotation at D_t [rad]	Link rotation [rad]	Corresponding top displacement
DL/SLS	124	0,046	0,005	52
SD/ULS	210	0,091	0,11	248
NC	362	0,290	0,14	300

Table 5-5. Seismic performance assessment in case of Configuration B

	N2		FEMA acc. criteria	
Config. B	D_t [mm]	Link rotation at D_t [rad]	Link rotation [rad]	Corresponding top displacement
DL/SLS	106	0,039	0,005	42
SD/ULS	179	0,085	0,11	224
NC	308	0,310	0,14	268

Using the N2 method approach, it can be concluded that the performance objectives are accomplished only for the SD/ULS in case of both structural configurations (see Table 5-4 and Table 5-5).

The pushover curves presented below (Fig. 3-18) illustrate the seismic performance of the structures discussed above:

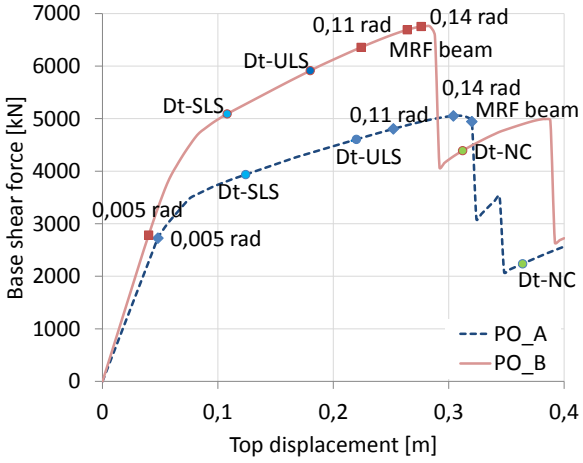

Fig. 5-6. Pushover curves

Although the performance objectives are not satisfied for SLS and NC using the N2 approach, the objective of having no yielding in the MRFs before the attainment of the ULS deformation in the removable links (0.11 rad) of the EBFs is accomplished, representing the basic design requirement for dual frames with

removable dissipative members. MRFs provide the re-centring of the specimen even until after the links ultimate deformation (0.14 rad) for configuration A.

5.4.1.2. Dynamic non-linear (Time-history) analysis

The seven seismic records employed to assess the performance of the DUAREM specimen using nonlinear time-history analysis were used also for these two configurations. They were scaled to the target spectrum (EN 1998 type 1, soil type C, a_g = 0.35g) used in designing these two structures.

This set of seismic records proved not to be the more suitable for analysing these structures, because the structures 2nd structural mode (first two periods T_1 and T_2 of the structure are marked in Fig. 5-7 and Fig. 5-8) has an important influence on the structural response, the corresponding spectral acceleration of the mean of these records being with over 40% larger than the spectral acceleration of the spectrum used in design (see Fig. 5-7).

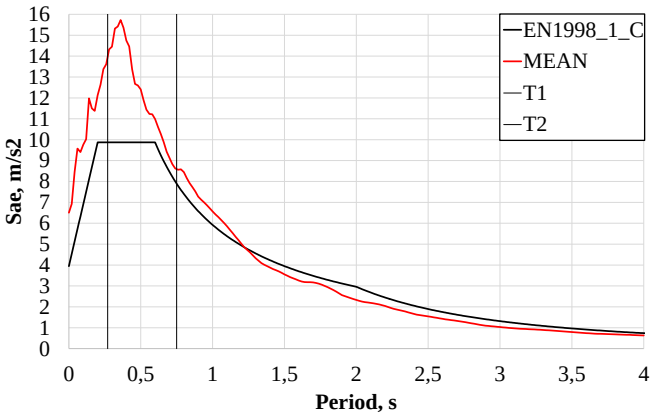

Fig. 5-7. Average response spectra of selected records (as scaled) versus target spectrum.

Therefore, another set of recorded accelerograms were used for seismic performance assessment of the structures using nonlinear time-history analysis. These recorded accelerograms were selected the same way as the ones described in Chapter 3.4.2.2. Accelerograms having closest matching with the target spectrum (EC8 type 1 elastic spectrum for soil type C) in terms of control period T_C (0.6 s), effective peak ground acceleration (EPA), and effective peak ground velocity (EPV) were then selected. Characteristics of ground motion records are given in Table 5-6.

Individual accelerograms were first scaled to the target spectrum (EC8 type 1, soil type C, a_g = 0.35g) in the $0.2T_1$ – $2T_1$ range using the equal area rule. The average spectrum was scaled to the target spectrum using EC8 criteria. Response spectra of as scaled accelerograms are shown in Fig. 5-8 and Fig. 5-9, while acceleration time-histories can be observed in Fig. 5-10.

Pre-test nonlinear dynamic simulations were performed on the calibrated 2D model described in Chapter 5.2, using the selected ground motion records.

Table 5-6. Characteristics of ground motion records selected for performance assessment.

Record code	Earthquake name	Date	Station name	Station country	Magnitude Mw
00844_H2	Spitak	07.12.1988	Gukasian	Armenia	6.8
00967_H2	Erzincan	13.03.1992	Erzincan Merkez Meteoroloji Mudurlugu	Turkey	6.7
06796_H2	South Iceland (Aftershock)	21.06.2000	Thjorsarbru	Iceland	6.4
09301_H1	Avaj	22.06.2002	Shirinsu (Bakhshdari)	Iran	6.5
16035_H2	Faial	09.07.1998	Horta	Portugal	6.1
16353_H1	Olfus	29.05.2008	Selfoss-Hospital	Iceland	6.1
17167_H1	Aigion	15.06.1995	Aigio-OTE	Greece	6.5

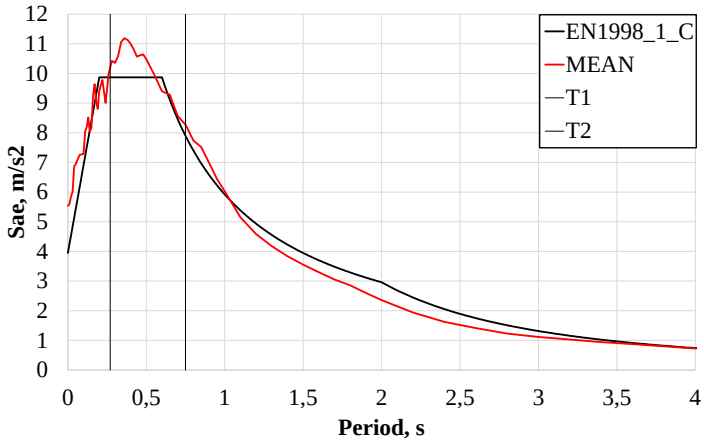

Fig. 5-8. Average response spectra of selected records (as scaled) versus target spectrum.

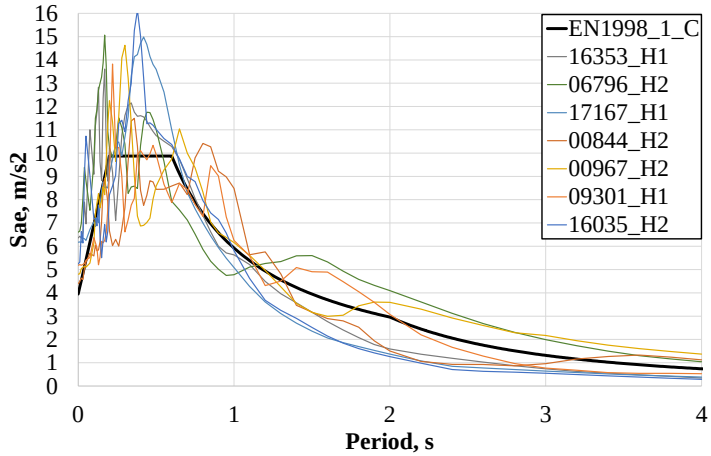

Fig. 5-9. Response spectra of selected records (as scaled) versus target spectrum

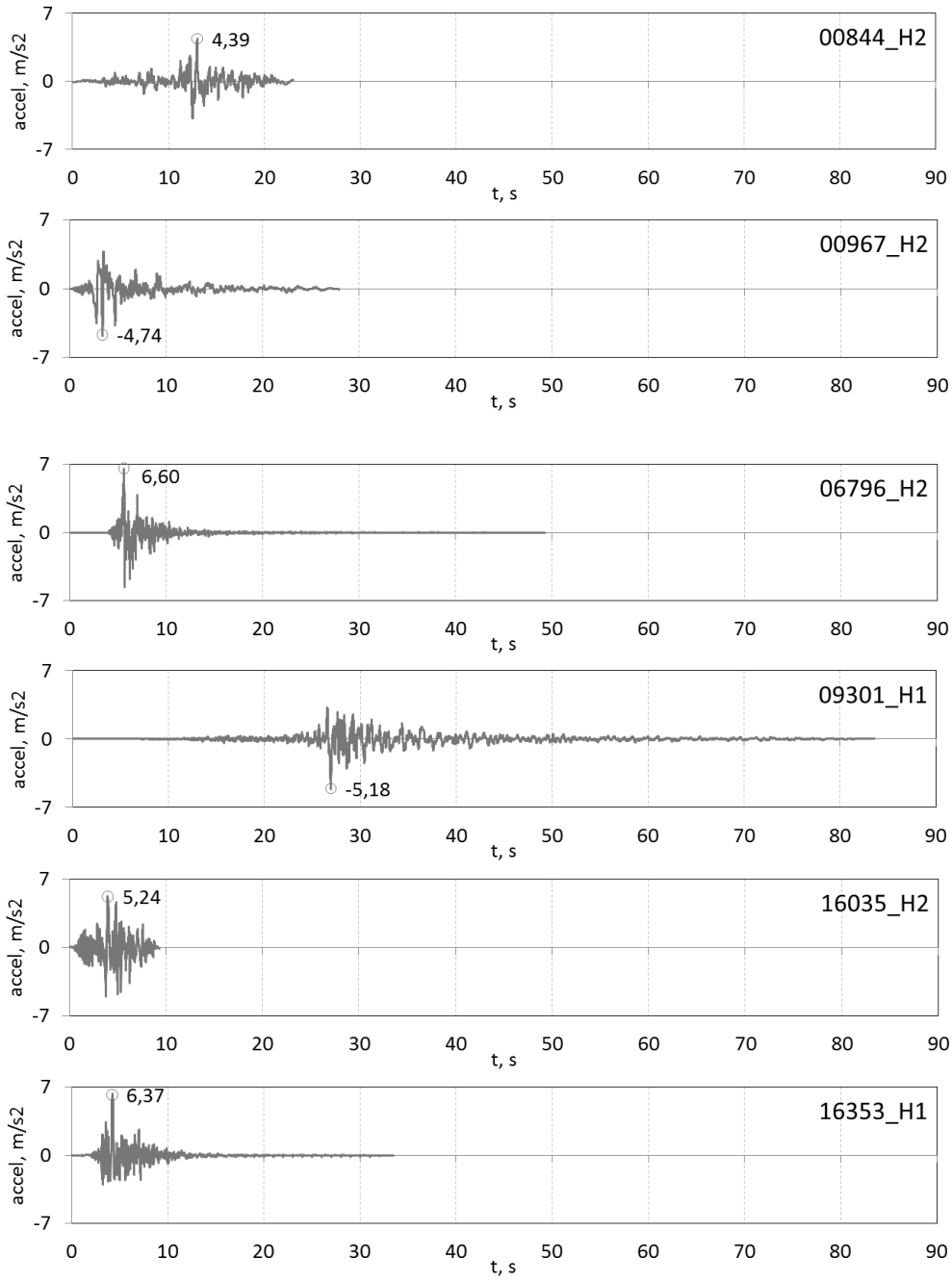
00844_H2
4,39
00967_H2
-4,74
06796_H2
6,60
09301_H1
-5,18
16035_H2
5,24
16353_H1
6,37
accel, m/s2
t, s
7
0
-7
0
10
20
30
40
50
60
70
80
90

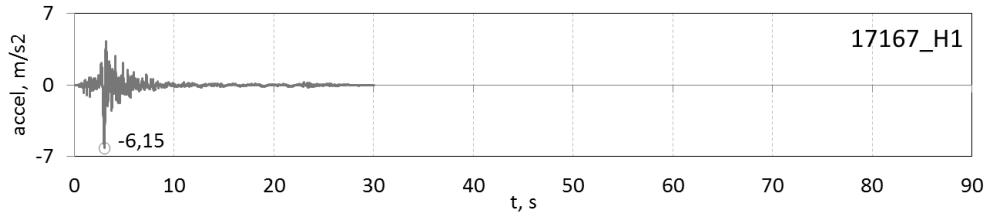

Fig. 5-10. Acceleration time histories of selected records.

Structural performance was evaluated for the limit states shown in Table 5-7, where a_{gr} is the reference peak ground acceleration (corresponding to 10% / 50 years earthquake) and a_g represents the peak ground acceleration for a specific earthquake level.

Table 5-7. Limit states and corresponding scaling factors for seismic input

Limit state	Return period, years	Probability of exceedance	a_g/a_{gr}
Damage Limitation (DL / SLS)	95	10% / 10 years	0.59
Significant Damage (SD / ULS)	475	10% / 50 years	1.00
Near Collapse (NC)	2475	2% / 50 years	1.72

At the Damage Limitation (DL) limit state all structural components except links are in the elastic range. Shear deformations in links exceed the FEMA 356 limits of 0.005 radians (0.039 rad for structure A and 0.026 rad for structure B), but this is normal, since the design carried out according to EN 1998 did not impose any limitation on yielding of structural members at DL limit state. Even so, peak inter-storey drifts are within the limits imposed (<0.75%). In these conditions, the advantage of the proposed system is obvious, since the damaged dissipative members (links) can be replaced easily due to negligible permanent drifts. Even if some structural damage is present, it can be repaired easily by replacing the bolted links.

At the Significant Damage (SD) limit state damage is still constrained to links only, which exhibit plastic deformation demands below 0.11 rad (0.092 rad for structure A and 0.078 rad for structure B). Permanent drifts are only slightly larger than at the DL limit state. Due to low permanent drifts, the structures are easily repairable at this limit state as well.

At the Near Collapse (NC) limit state the structural damage is widespread. Shear deformations in links are well over acceptable values of 0.14 rad (0.282 rad for structure A and 0.266 rad for structure B). However, due to moment resisting frames, the overall performance of the structures can be considered acceptable for this limit state. Plastic deformation demands are present in moment resisting frames (beams and columns) and braces. Even so, permanent inter-storey drifts are not very large. However, repairing of the structures is considered not to be feasible and desirable at these large levels of seismic input.

A previous design of the structure was performed considering ductility class H for the two structures, with a corresponding behaviour factor q=6 (according to EN1998). This was not a feasible version, because after assessing the structural performance of the two configurations using time-history analyses, at the ULS, link

rotations were much larger than the 0.11 rad acceptance criteria (0.21 rad for configuration A and 0.24 rad for configuration B) and yielding was observed in other elements (MRFs beams and columns and EBFs braces), the objectives for ULS not being accomplished.

5.4.2. Re-centring capability of dual EBFs with removable links

Following the same approach discussed in Chapter 3.4.3, the yield strength of the EBFs (F_y^{EBF}), as well as the yield strength of the MRFs (F_y^{MRF}) were computed using the same formulas for configuration A and the following adapted formulas for configuration B (for this case there are two EBFs and only one MRF):

$$F_y^{EBF} = 2 \cdot \frac{L}{H} V_{p,link} \quad (5\text{-}1)$$

Where $V_{p,link}$ is the shear strength of the link.

$$F_y^{MRF} = \frac{2M_{pl,b}}{H} \quad (3\text{-}16)$$

Where $M_{pl,b}$ is the beam plastic moment.

The yield strength of the MRFs represents on average 29% from the total yield strength of the system for configuration A and 26% for configuration B, both configurations being considered dual structures.

Moreover, the ultimate displacement of the EBFs (δ_u^{EBF}) at ULS (where the plastic deformation capacity of the link $\gamma_{pl,u}$ is considered to be 0.11 rad) is smaller than the yield displacement of the MRFs (δ_y^{MRF}), meaning the yielding in MRFs is prevented up to the attainment of ultimate deformation capacity in the EBFs with removable links. This was checked analytical, using the formulas from Chapter 3.4.3 for configuration A and the adapted ones presented below for configuration B, and numerical in Chapter 5.4.1.1.

$$K^{EBF} = 2 \cdot \frac{K_{link}^{EBF} \cdot K_{br}^{EBF}}{K_{link}^{EBF} + K_{br}^{EBF}} \quad (5\text{-}2)$$

Where K^{EBF} is the eccentrically braced frames stiffness, K_{link}^{EBF} (3-10) is the link's stiffness, K_{br}^{EBF} is the braces stiffness.

$$K_{br}^{EBF} = \frac{E \cdot A}{l_{br}} \cdot \cos^2 \alpha \quad (5\text{-}3)$$

Where E is the Young's modulus, A is brace cross-section area, l_{br} is the brace length.

$$K^{MRF} = \frac{2}{H^2 \cdot \left(\frac{L}{6 \cdot E \cdot I_b} + \frac{H}{12 \cdot E \cdot I_c} \right)} \quad (5\text{-}4)$$

Where K^{MRF} is the moment resisting frame stiffness, while L and H are shown in Fig. 3-23.

Table 5-8. Comparison of analytical and numerical predictions of storey displacements for configuration A

Configuration A	δ_u^{EBF}, mm	δ_y^{MRF}, mm	$\delta_y^{MRF}/\ \delta_u^{EBF}$
Analytical	49.5	101.1	2.0
Numerical	51.8	71.4	1.4

Table 5-9. Comparison of analytical and numerical predictions of storey displacements for configuration B

Configuration B	δ_u^{EBF}, mm	δ_y^{MRF}, mm	$\delta_y^{MRF}/\ \delta_u^{EBF}$
Analytical	50.2	76.2	1.5
Numerical	52.5	56.2	1.1

Table 5-8 and Table 5-9 present a comparison of yield displacements in the MRFs and ultimate displacements in the EBFs for the third storey, where largest demands are present. For the 6 storey configurations, the results from analytical method are not very close to the ones from numerical one (in case of yield displacements in MRFs), like happened for the DUAREM specimen, therefore nonlinear analyses are recommended to check the re-centring capability of the structure.

5.4.3. Link replacement investigation

As presented in Chapter 3.4.4 and proved in Chapter 4.4.4, the technically easiest way to release the forces in links is by flame cutting the web and flanges of the link if large permanent drifts occur or by unbolting otherwise, on a storey by storey basis, starting from the least loaded towards the most loaded one (from the upper storey downwards).

In order to numerically simulate the link removal order, 3D numerical models of the two structures were subjected to a modal (inverted triangular) distribution of lateral forces up to the attainment of 0.11 rad plastic rotation in links on the transversal direction, simulating the seismic action. Then the structures were unloaded, simulating the state of the structure after an earthquake and links were removed level by level, from the 6th storey downwards.

Three possibilities of links removing order within a storey were studied: 1 - firstly removing the links on the longitudinal direction and secondly the ones on the transversal direction (see Fig. 5-11a and Fig. 5-12a); 2 - vice versa (see Fig. 5-11b and Fig. 5-12b), and 3 - in a circular pattern (see Fig. 5-11c and Fig. 5-12c).

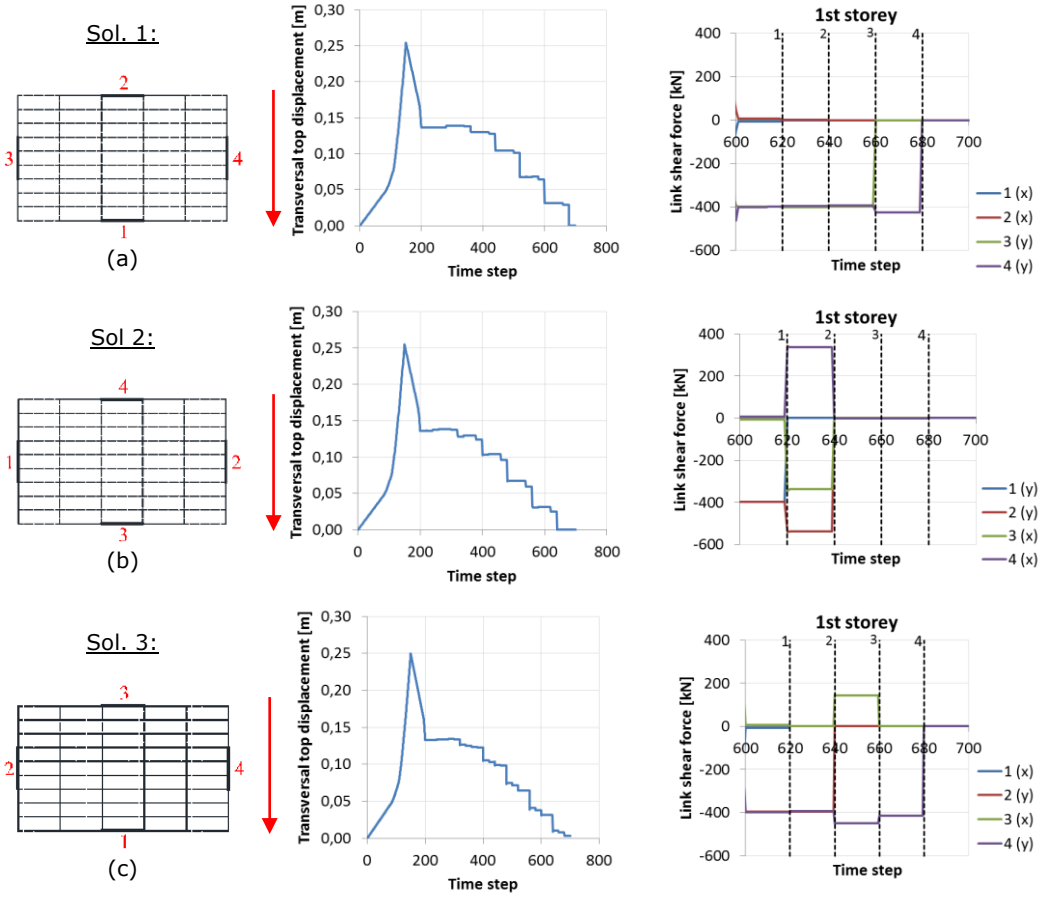

Fig. 5-11. Link removal solutions for configuration A

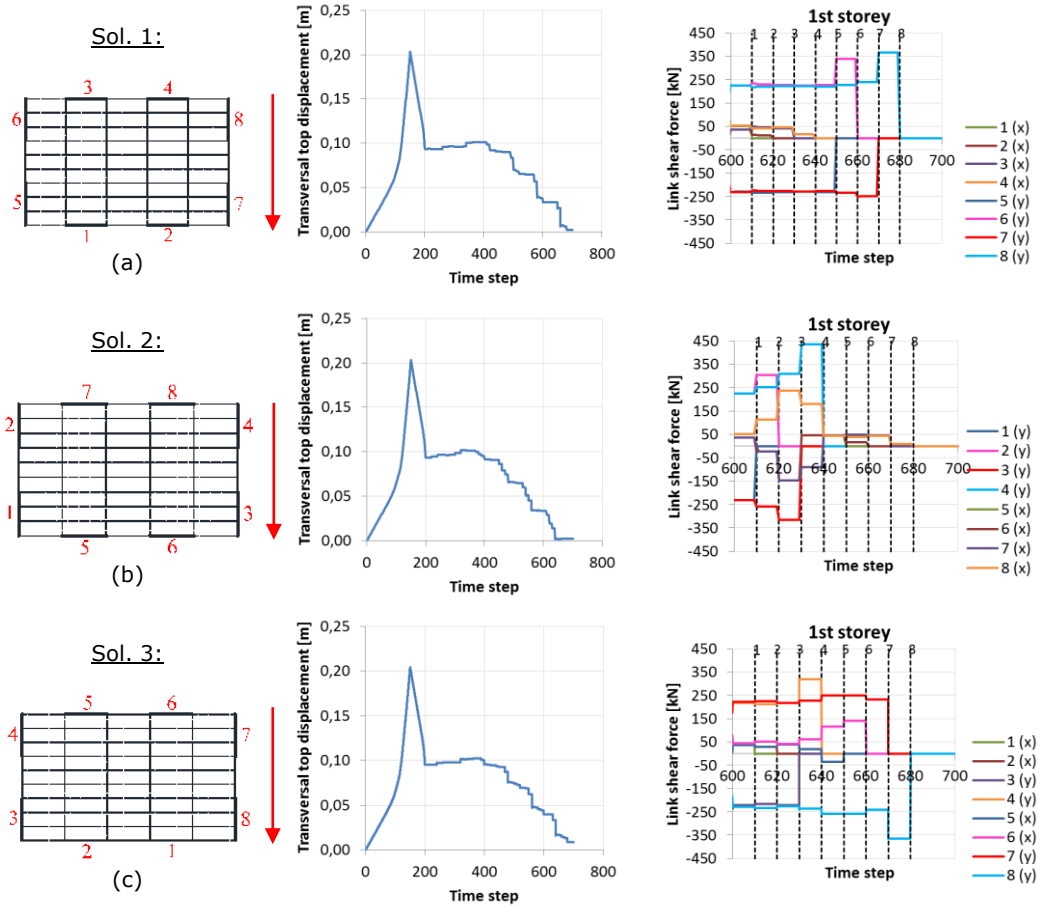

Fig. 5-12. Link removal solutions for configuration B

Very good re-centring of the two structures is observed (see Fig. 5-11 and Fig. 5-12, middle column graphs). For configuration A the residual top displacement is of 0.4 mm for solution 1, 0.3 mm for solution 2 and 3 mm for solution 3. For configuration B the residual top displacement is of 2.3 mm for solution 1, 2.2 mm for solution 2 and 8.8 mm for solution 3.

In the right column graphs from Fig. 5-11 and Fig. 5-12 is presented the link shear force time history at the first storey during the link removal order. The loading of the structure is until 150 time step, the unloading is between 150 and 200 time step and the links removal is from 200 to 700 time step (24 links from 20 to 20 for configuration A and 48 links from 10 to 10 for configuration B).

It was observed that for the first solution (firstly removing the links on the longitudinal direction and secondly the ones on the transversal direction) the residual shear force drop is about 21% (configuration A) and 16% (configuration B) smaller than for the second solution and the redistribution of forces between the links of the same storey is also smaller. This is because, when removing links using solution 1, the structure becomes more flexible (the least loaded links on the longitudinal direction are first removed and when removing the first link on the

transversal direction, only the MRFs in the other direction are still working) and the links develop smaller residual forces. When removing links using solution 2, the structure is more rigid (when removing the first link on the transversal direction, both MRFs and EBFs in the other direction are still working) and the links develop larger residual forces. The situation for the third solution is in between the other two.

Maximum top displacement on the other direction (on longitudinal direction) during the link removal are small: 9 mm for solution 1, 4 mm for solution 2 and 9 mm for solution 3 in case of configuration A and 9 mm for solution 1, 4 mm for solution 2 and 6 mm for solution 3 in case of configuration B.

On the first solution of link removal order within a storey (see Fig. 5-13), was analysed also the removal of links starting from the most loaded to the least loaded storey (from the first storey upwards). In this case, was observed a larger interaction between stories, but values of the shear force drop with 43% (configuration A) and 39% (configuration B) smaller than in the case of eliminating links from the upper one toward the lower one and smaller redistribution of forces between the links of the same storey.

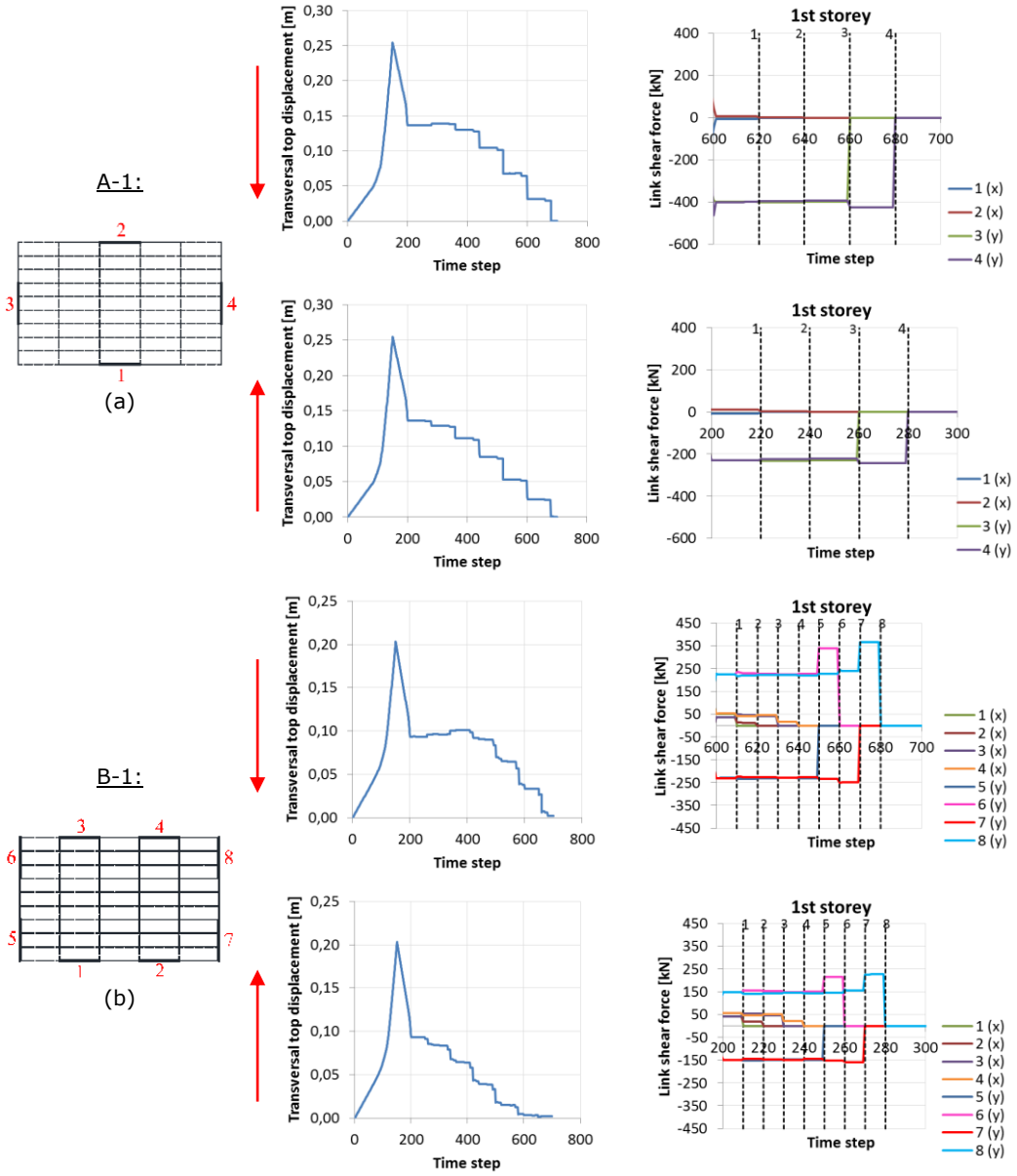

Fig. 5-13. First link removal solution

Maximum top displacement on the other direction (on longitudinal direction) during the link removal using solution 1 are also smaller when removing links from the first storey upwards: 8 mm in case of configuration A and 7 mm in case of configuration B, compared to 9 mm for both configuration when removing links from the sixth storey downwards.

The optimal link removal order is the one which results in smaller drop of force during link removal. From this perspective, within a given storey links should

be removed from the least loaded toward the most loaded. In the height-wise direction, links should be removed from the lower storey toward the upper ones (from the storeys with larger residual stresses toward the storeys with smaller ones).

5.4.4. Evaluation of behaviour factor

Incremental dynamic analyses were performed (using the seven seismic records from time-history analyses), in order to evaluate the design behaviour factor of the two structural configurations, with an increment of 0.2 of the seismic record amplifier λ. In the high interest areas (yielding rotation in links or link rotation at ULS), the increment of the seismic action amplifier was more discrete – 0.001. A 2% Rayleigh damping was employed in dynamic analyses, as used for steel structures [102], [103].

The behaviour curves for configuration A and configuration B are presented in Fig. 5-14, corresponding to the seven seismic records used and their mean.

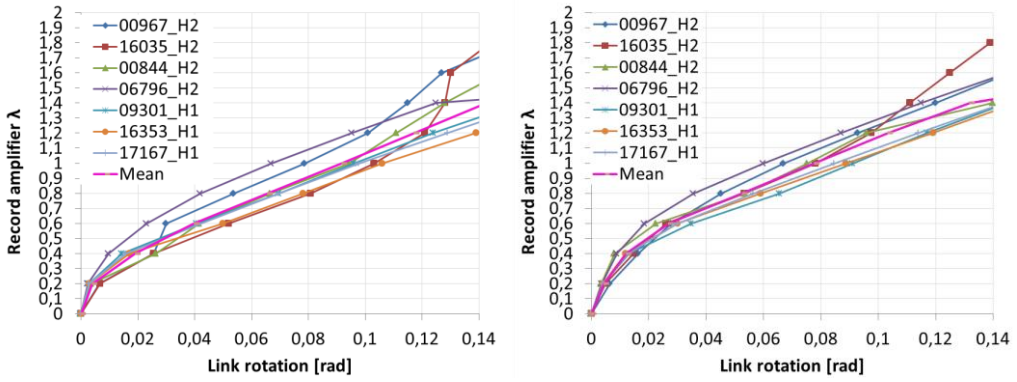

(a) (b)

Fig. 5-14. Behaviour curves for configuration A (a) and configuration B (b)

Computations were first performed for a level of the seismic action corresponding to an ultimate limit state (ULS) acceptance criterion of 0.08 radians plastic rotation in links, considered by EN 1998. A design (q_d) and an effective (q) behaviour factor were computed using the following formulas:

$$q_d = \frac{\lambda_u}{\lambda_d} \quad (5\text{-}5)$$

where λ_u is the seismic record amplifier corresponding to the ultimate link rotation (EN 1998 acceptance criteria for link rotation at ULS being of 0.08 rad) and λ_d is the seismic record amplifier corresponding to the level of seismic action used in design.

$$q = \frac{\lambda_u}{\lambda_1} \quad (5\text{-}6)$$

where λ_1 is the seismic record amplifier corresponding to yield rotation in links.

When designing the two structures, EC8 type 1 elastic response spectrum for soil type C (for 5% damping) was used in spectral analysis, reduced with a behaviour factor q=4. Thus the amplifier of the level of seismic action was considered $\lambda_{d,sp}$=0.25 (1 over 4). In order to account for dynamic nonlinear analysis type and a different damping (of 2%), the amplifier λ_d was adjusted using the following formula:

$$\lambda_d = \lambda_{d,sp} \cdot \frac{V_{d,SP}}{V_{d,TH}} \quad (5\text{-}7)$$

where $V_{d,SP}$ is the design base shear force from spectral analysis (5% damping) and $V_{d,TH}$ is the base shear force from a linear time-history analysis (2% damping) with a 0.25 amplifier.

The ratio between these two factors is represented by the design over-strength Ω_d, computed with the formula below:

$$\Omega_d = \frac{q_d}{q} \quad (5\text{-}8)$$

Also the total over-strength Ω_t of the structure was computed as the product between the structure's over-strength Ω_s and the design over-strength Ω_d, using the following formulas:

$$\Omega_t = \Omega_s \cdot \Omega_d = \frac{V_u}{V_d} \quad (5\text{-}9)$$

where V_u is the base shear force corresponding to ULS rotation of 0.08 rad in links and V_d is the design base shear force (from spectral analysis using EC8 spectrum).

$$\Omega_s = \frac{V_u}{V_1} \quad (5\text{-}10)$$

where V_1 is the base shear corresponding to yield rotation in links.

$$\Omega_d = \frac{V_1}{V_d} \quad (5\text{-}11)$$

The obtained values are presented in Table 5-10 and Table 5-11.

Table 5-10. Values at ULS (EC8) for configuration A

Record	00844H2	00967H2	06796H2	09301H1	16035H2	16353H1	17167H1	**Mean**
λ_d	0,175	0,178	0,253	0,207	0,181	0,240	0,186	**0,203**
λ_1	0,195	0,176	0,279	0,261	0,172	0,248	0,230	**0,223**
λ_u	0,904	1,010	1,093	0,886	0,794	0,815	0,874	**0,911**
q_d	5,166	5,674	4,320	4,280	4,387	3,396	4,699	**4,6**
q	4,636	5,739	3,918	3,395	4,616	3,286	3,800	**4,2**
Ω_d	1,114	0,989	1,103	1,261	0,950	1,033	1,237	**1,10**

Record	00844H2	00967H2	06796H2	09301H1	16035H2	16353H1	17167H1	**Mean**
V_d	2161	2192	2521	2360	2202	2245	2261	**2277**
V_1	2408	2167	2781	2957	2100	2320	2766	**2500**
V_u	4365	4440	5087	4318	3876	4152	4322	**4366**
Ω_d	1,114	0,989	1,103	1,253	0,954	1,033	1,223	**1,10**
Ωs	1,813	2,049	1,829	1,460	1,846	1,790	1,563	**1,76**
Ωt	2,02	2,03	2,02	1,83	1,76	1,85	1,91	**1,92**

Table 5-11. Values at ULS (EC8) for configuration B

Record	00844H2	00967H2	06796H2	09301H1	16035H2	16353H1	17167H1	**Mean**
λ_d	0,253	0,162	0,248	0,216	0,202	0,202	0,194	**0,211**
λ_1	0,269	0,171	0,266	0,235	0,207	0,223	0,216	**0,227**
λ_u	1,076	1,107	1,159	0,923	1,019	0,953	0,968	**1,029**
q_d	4,253	6,833	4,673	4,273	5,045	4,718	4,990	**5,0**
q	4,000	6,474	4,357	3,928	4,923	4,274	4,481	**4,6**
Ω_d	1,063	1,056	1,073	1,088	1,025	1,104	1,113	**1,07**
V_d	2474	2447	2650	2411	2444	2423	2441	**2470**
V_1	2624	2547	2834	2583	2504	2668	2715	**2639**
V_u	5863	6183	6190	5841	5345	5605	5657	**5812**
Ω_d	1,061	1,041	1,069	1,071	1,025	1,101	1,112	**1,07**
Ωs	2,234	2,428	2,184	2,261	2,135	2,101	2,084	**2,20**
Ωt	2,37	2,53	2,34	2,42	2,19	2,31	2,32	**2,35**

Values amounting to 4.6 for configuration A and 5 for configuration B were obtained for the design behaviour factor, being larger than 4 as considered in design. Design of eccentrically braced frames with short bolted links is thus recommended considering a medium ductility class of the structure.

Computation were also performed for levels of the seismic action corresponding to ULS (0.11 rad) (see Table 5-12 and Table 5-13) and NC (near collapse) (0.14 rad) (see Table 5-14 and Table 5-15) acceptance criteria for plastic rotation in links considered by FEMA356.

Table 5-12. Values at ULS (FEMA356) for configuration A

Record	00844H2	00967H2	06796H2	09301H1	16035H2	16353H1	17167H1	**Mean**
λ_d	0,175	0,178	0,253	0,207	0,181	0,240	0,186	**0,203**
λ_1	0,195	0,176	0,279	0,261	0,172	0,248	0,230	**0,223**
λ_u	1,182	1,326	1,302	1,124	1,070	1,023	1,079	**1,158**
q_d	6,754	7,449	5,146	5,430	5,912	4,263	5,801	**5,8**
q	6,062	7,534	4,667	4,307	6,221	4,125	4,691	**5,4**
Ω_d	1,114	0,989	1,103	1,261	0,950	1,033	1,237	**1,10**
V_d	2161	2192	2521	2360	2202	2245	2261	**2277**
V_1	2408	2167	2781	2957	2100	2320	2766	**2500**
V_u	4861	4896	5640	4665	4192	4634	4722	**4801**
Ω_d	1,114	0,989	1,103	1,253	0,954	1,033	1,223	**1,10**
Ωs	2,019	2,259	2,028	1,578	1,996	1,997	1,707	**1,94**
Ωt	2,25	2,23	2,24	1,98	1,90	2,06	2,09	**2,11**

Table 5-13. Values at ULS (FEMA356) for configuration B

Record	00844H2	00967H2	06796H2	09301H1	16035H2	16353H1	17167H1	**Mean**
λ_d	0,253	0,162	0,248	0,216	0,202	0,202	0,194	**0,211**
λ_1	0,269	0,171	0,266	0,235	0,207	0,223	0,216	**0,227**
λ_u	1,270	1,328	1,377	1,149	1,379	1,140	1,174	**1,260**

Record	00844H2	00967H2	06796H2	09301H1	16035H2	16353H1	17167H1	**Mean**
q_d	5,020	8,198	5,552	5,319	6,827	5,644	6,052	**6,1**
q	4,721	7,766	5,177	4,889	6,662	5,112	5,435	**5,7**
Ω_d	1,063	1,056	1,073	1,088	1,025	1,104	1,113	**1,07**
V_d	2474	2447	2650	2411	2444	2423	2441	**2470**
V_1	2624	2547	2834	2583	2504	2668	2715	**2639**
V_u	6656	6683	6802	6200	5896	6052	6188	**6354**
Ω_d	1,061	1,041	1,069	1,071	1,025	1,101	1,112	**1,07**
Ωs	2,537	2,624	2,400	2,400	2,355	2,268	2,279	**2,41**
Ωt	2,69	2,73	2,57	2,57	2,41	2,50	2,54	**2,57**

Table 5-14. Values at NC (FEMA356) for configuration A

Record	00844H2	00967H2	06796H2	09301H1	16035H2	16353H1	17167H1	**Mean**
λ_d	0,175	0,178	0,253	0,207	0,181	0,240	0,186	**0,203**
λ_1	0,195	0,176	0,279	0,261	0,172	0,248	0,230	**0,223**
λ_u	1,523	1,707	1,477	1,315	1,756	1,207	1,273	**1,465**
q_d	8,703	9,590	5,838	6,353	9,702	5,029	6,844	**7,4**
q	7,810	9,699	5,294	5,038	10,209	4,867	5,535	**6,9**
Ω_d	1,114	0,989	1,103	1,261	0,950	1,033	1,237	**1,10**
V_d	2161	2192	2521	2360	2202	2245	2261	**2277**
V_1	2408	2167	2781	2957	2100	2320	2766	**2500**
V_u	5337	5766	6099	4931	5861	5016	5206	**5459**
Ω_d	1,114	0,989	1,103	1,253	0,954	1,033	1,223	**1,10**
Ωs	2,22	2,66	2,19	1,67	2,79	2,16	1,88	**2,22**
Ωt	2,47	2,63	2,42	2,09	2,66	2,23	2,30	**2,40**

Table 5-15. Values at NC (FEMA356) for configuration B

Record	00844H2	00967H2	06796H2	09301H1	16035H2	16353H1	17167H1	**Mean**
λ_d	0,253	0,162	0,248	0,216	0,202	0,202	0,194	**0,211**
λ_1	0,269	0,171	0,266	0,235	0,207	0,223	0,216	**0,227**
λ_u	1,4	1,565	1,578	1,374	1,81	1,35	1,38	**1,494**
q_d	5,534	9,660	6,363	6,361	8,960	6,683	7,113	**7,2**
q	5,204	9,152	5,932	5,847	8,744	6,054	6,389	**6,8**
Ω_d	1,063	1,056	1,073	1,088	1,025	1,104	1,113	**1,07**
V_d	2474	2447	2650	2411	2444	2423	2441	**2470**
V_1	2624	2547	2834	2583	2504	2668	2715	**2639**
V_u	7171	7161	7381	6501	6857	6553	6705	**6904**
Ω_d	1,061	1,041	1,069	1,071	1,025	1,101	1,112	**1,07**
Ωs	2,73	2,81	2,60	2,52	2,74	2,46	2,47	**2,62**
Ωt	2,90	2,93	2,79	2,70	2,81	2,70	2,75	**2,79**

Larger values were obtained: 5.8 for configuration A and 6.1 for configuration B at ULS and 7.4 for configuration A and 7.2 for configuration B at NC.

5.5. Design flowchart

A flowchart that *briefly* illustrates the design of eccentrically braced frames with removable links and re-centring capability is shown in Fig. 5-15.

Firstly, a capacity design can be performed, according to Eurocodes. The structural elements are to be designed from the ULS load combinations (both fundamental and seismic) and the structure's drifts, beam deflections and top

displacement should be checked from the SLS load combinations (both fundamental and seismic). The dissipative behaviour concept is recommended, considering a medium ductility class, with a corresponding behaviour factor q=4 (when designing such structures considering high ductility class, with a behaviour factor q=6, the obtained link rotations are much larger than the acceptance criteria, thus not being recommended). A global dissipative behaviour of the structure should be achieved, checking that the individual values of the ratios Ω_i for each dissipative member not to exceed the minimum value Ω by more than 25%.

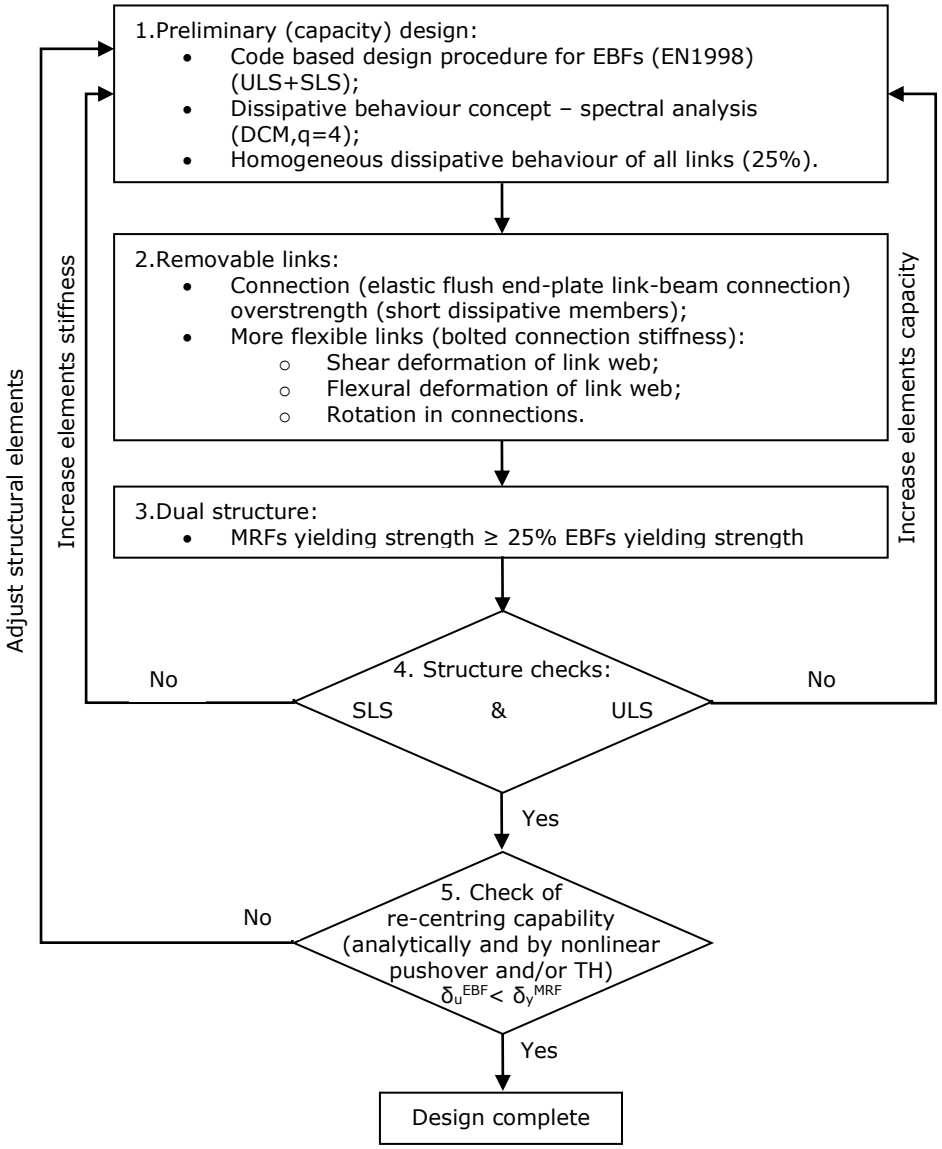

Fig. 5-15. Design flowchart for EBFs with removable links and re-centring capacity

The dissipative elements should be designed as removable. This can be done by using a flush end-plate link-beam connection that should be kept elastic (using a design bending moment and shear force computed with formulas (3-3) and (3-4)). In order to achieve the connection over-strength, very short dissipative members should be used (with a recommended length e around $0.8M_{p,link}/V_{p,link}$).

The issue of permanent (residual) deformations of the structure after a damaging earthquake, which can lead to difficulties in replacing removable links, can be solved by realising a structure as a dual one, by combining eccentrically braced frames (EBFs) with moment-resisting frames (MRFs). If the more flexible MRFs are kept elastic (a possible way to favour this is to realise some members from high-strength steel) and the plastic deformations are constrained to removable dissipative members only, the MRFs would provide the restoring force necessary to re-centre the structure upon removal of damaged removable links. Therefore, the duality of the structure should be checked by verifying that the MRFs should be able to resist at least 25% of the total seismic force.

After fulfilling all the above conditions to design eccentrically braced frames with removable links, the structures should be re-checked. If it doesn't verify at ULS, the elements capacity should be increased, still meeting all the requirements described above. If the SLS conditions are not verified, the structural stiffness should be increased.

In order to verify the re-centring capability of eccentrically braced frames with removable links structures, the ultimate displacement of the EBFs (δ_u^{EBF}) at ULS (corresponding to the plastic deformation capacity of the link) is smaller than the yield displacement of the MRFs (δ_y^{MRF}), meaning the yielding in MRFs is prevented up to the attainment of ultimate deformation capacity in the EBFs with removable links. This can be done analytically (using formulas) or by nonlinear static and/or dynamic analyses. Because, for structures with more than 3 stories (2 structural configurations with 6 stories were studied in this thesis), an acceptable agreement between the results computed analytically and the ones obtained from nonlinear analyses wasn't obtained, there is recommended to use pushover and time-history analysis in order to check the re-centring capability.

If following code-based capacity design rules is not enough to accomplish the objective stated above for obtaining re-centring structures, MRFs structural members should be adjusted, by increasing the strength without increasing the stiffness (in order not to attract larger forces). Using higher-strength steel in moment resisting frames can be efficient in avoiding yielding in their members, prior to attaining the ultimate deformation in the EBFs. After elements adjustment (if necessary), all the above conditions should be re-checked.

When all the conditions for designing eccentrically braced frames with removable links and re-centring capability are accomplished, the design can be considered complete.

5.6. Concluding remarks

To check if the experimental specimen behaviour can be extended to more general structures, other current practice structural configurations of dual eccentrically braced frames with removable links were analysed.

The numerical model used in numerical simulations was calibrated using the results of experimental tests. A greater link over-strength of 1.7 resulted, together

with neglecting the slip in the link connections (mentioned in the numerical model description in Chapter 3).

Using the same capacity design rules as for the experimental specimen, two dual structural configurations were designed: the first (configuration A) having a central EBF (with the link being placed at mid-span) and two side MRFs, and the second (configuration B) having a central MRF and two side EBFs. (links placed marginally, connected to columns on one side). For a structure with re-centring capability, the design objective consists in preventing yielding in members other than removable dissipative ones, up to a desired deformation. Ideally the latter should be the ultimate deformation capacity of the removable dissipative member. Because following code-based capacity design rules was not enough to accomplish this objective for the investigated structures, a higher-strength steel was used in moment resisting frames to avoid yielding in their members, obtaining a larger capacity without increasing the stiffness.

To evaluate the seismic performance of the specimen in the inelastic domain, static nonlinear analyses were performed together with using the N2 method, as well as dynamic nonlinear analyses. Although the performance objectives are not satisfied for SLS and NC using the N2 approach, the objective of having no yielding in the MRFs before the attainment of the ULS deformation in the removable links (0.11 rad) of the EBFs is accomplished, representing the basic design requirement for dual frames with removable dissipative members. MRFs provide the re-centring of the specimen even until after the links ultimate deformation (0.14 rad) for configuration A. Performing time-history analyses on the calibrated model of the two structural configurations, structural performance similar to experimental specimen was obtained for the evaluated limit states: DL (SLS), SD (ULS) and NC.

At DL limit state all structural components except links are in the elastic range. Shear deformations in links exceed the FEMA 356 limits of 0.005 radians, but this is normal, since the design carried out according to EN 1998 did not impose any limitation on yielding of structural members at DL limit state. Even so, peak inter-storey drifts are within the limits imposed. In these conditions, the advantage of the proposed system is obvious, since the damaged dissipative members (links) can be replaced easily due to negligible permanent drifts. Even if some structural damage is present, it can be repaired easily by replacing the bolted links.

At SD limit state damage is still constrained to links only, which exhibit plastic deformation demands below 0.11 rad. Permanent drifts are only slightly larger than at the DL limit state. Due to low permanent drifts, the structures are easily repairable at this limit state as well.

At NC limit state the structural damage is widespread. Shear deformations in links are well over acceptable values of 0.14 rad. However, due to moment resisting frames, the overall performance of the structures can be considered acceptable for this limit state. Plastic deformation demands are present in moment resisting frames (beams and columns) and braces. Even so, permanent inter-storey drifts are not very large. However, repairing of the structures is considered not to be feasible and desirable at these large levels of seismic input.

As proved previously, the technically easiest way to release the forces in links is by flame cutting the web and flanges of the link if large permanent drifts occur or by unbolting otherwise, on a storey by storey basis, starting from the least loaded towards the most loaded one (from the upper storey downwards). Three possibilities of links removing order within a storey were studied for the two studied

structures: 1 - firstly removing the links on the longitudinal direction and secondly the ones on the transversal direction; 2 - vice versa, and 3 - in a circular pattern. Very good re-centring was obtained. It was observed that for the first solution the residual shear force drop is smaller than for the second solution and the redistribution of forces between the links of the same storey is also smaller. The situation for the third solution is in between the other two. On the first solution of link removal order within a storey, was analysed also the removal of links starting from the most loaded to the least loaded storey (from the first storey upwards) and was observed a larger interaction between stories, but values of the shear force drop smaller than in the case of eliminating links from the upper one toward the lower one and smaller redistribution of forces between the links of the same storey. Thus, considering the optimal link removal order is the one which results in smaller drop of force during the process, within a given storey links should be removed from the least loaded toward the most loaded and in the height-wise direction, links should be removed from the lower storey toward the upper ones (from the storeys with larger residual stresses toward the storeys with smaller ones).

To evaluate the design behaviour factor of the two structural configurations, incremental dynamic analyses were performed. Computations were performed for a level of the seismic action corresponding to an ultimate limit state (ULS) acceptance criterion of 0.08 radians plastic rotation in links, considered by EN 1998 and for levels of the seismic action corresponding to ULS (0.11 rad) and NC (0.14 rad) acceptance criteria for plastic rotation in links considered by FEMA356. Close values of the design behaviour factor were obtained for the two structural configurations, 4.6 and 5, being larger than 4 as considered in design according to EN1998, for medium ductility class.

A flowchart was proposed to design eccentrically braced frames with removable links and re-centring capability, using capacity code-based design, as well as nonlinear analyses.

6. CONCLUSIONS OF PHD STUDY. CONTRIBUTIONS OF AUTHOR. FUTURE RESEARCH ACTIVITIES

6.1. Conclusions of PhD study

Chapter 1: Introduction

An introduction was made to the research topic. The scope and the objectives of the thesis were shown, as well as the research framework.

Chapter 2: Seismic resistant structural systems which constrain plastic deformations in safety fuses

A state-of-the-art of seismic resistant structural systems which constrain plastic deformations in safety fuses was presented.

Different strategies can be employed in order to reduce damage to structures under moderate to strong earthquakes. The most radical solutions are base isolation and various implementations of active and semi-active structural control. Other strategies rely on supplemental damping conferred to the structure through various devices based on viscous, friction, or yielding dampers. More or less efficient for reduction of structural damage, all these solution have the disadvantage of requiring specialised knowledge at the design stage and during erection, need for careful maintenance and high initial cost. Also, solutions providing self-centring of the structure exist, but are technically demanded (post-tensioned strands, shape memory alloy devices, etc.).

Alternatively, a conventional design can be employed, but with the dissipative members realised to be removable (e.g. through bolted connections), allowing replacement of the dissipative elements damaged as a result of a moderate to strong earthquake, and reducing the repair costs. For the structure to be repairable, in addition to constraining inelastic deformations to removable dissipative members, the permanent (residual) drifts should be eliminated. This solution provides re-centring capability (as opposed to self-centring), through removable dissipative members and dual (rigid-flexible) structural configuration.

Chapter 3: Structural design and numerical investigation of experimental specimen

In order to achieve the objectives of the DUAREM project, a dual frame (eccentrically braced frames with removable bolted links combined with moment resisting frames) prototype structure was firstly conceived, designed and analysed. The links from eccentrically braced frames (EBFs) were conceived as removable (bolted links) dissipative elements because they are intended to provide the energy dissipation capacity and to be easily replaceable. The more flexible moment resisting frames provide the necessary re-centring capability to the structure.

Considering that in the transversal direction of the prototype structure the lateral force resisting system is located on the perimeter frames only, and in order

to reduce the cost of the experimental mock-up, the latter is composed of the two end frames only with columns fixed at the base.

The seismic performance of the specimen in the inelastic domain was evaluated, performing static nonlinear analyses together with using the N2 method, as well as dynamic nonlinear analyses. Although the performance objectives were not satisfied for SLS and NC using the N2 approach, the objective of having no yielding in the MRFs before the attainment of the ULS deformation in the removable links (0.11 rad) of the EBFs is accomplished, representing the basic design requirement for dual frames with removable dissipative members. MRFs provide the re-centring of the specimen even until after the links ultimate deformation (0.14 rad).

Pre-test nonlinear dynamic simulations were also performed on the experimental mock-up, using the seven selected ground motion records and structural performance was evaluated for three limit states: DL (SLS), SD (ULS) and NC. At the Damage Limitation limit state all structural components except links are in the elastic range. Shear deformations in links exceed the FEMA 356 limits, but this is normal, since the design carried out according to EN1998 did not impose any limitation on yielding of structural members at DL limit state. Even so, permanent inter-storey drifts are very low and peak inter-storey drifts are within the limits imposed. In these conditions, the advantage of the proposed system is obvious, since the damaged dissipative members (links) can be replaced easily due to negligible permanent drifts. Even if some structural damage is present, it can be repaired easily by replacing the bolted links. At the Significant Damage limit state damage is still constrained to links only, which exhibit plastic deformation demands very close to the acceptable 0.11 rad. Permanent drifts are only slightly larger than at the DL limit state. Due to low permanent drifts, the structure is easily repairable at this limit state as well. At the Near Collapse limit state the structural damage is widespread. Shear deformations in links are well over acceptable values. However, due to moment resisting frames, the overall performance of the structure can be considered acceptable for this limit state. Plastic deformation demands are present in moment resisting frames (beams and columns) and braces. Even so, permanent inter-storey drifts are not very large. However, repairing of the structure is considered not to be feasible and desirable at these large levels of seismic input.

Residual forces and deformations are present in the links after they have experienced plastic excursions during an earthquake. Removing a damaged link involves redistribution of residual forces to other parts of the structure, more precisely from eccentrically braced frame to moment resisting ones. The technically easiest way to release the residual forces in links is believed to be by flame cutting the web and flanges of the link. This operation is necessary only if large permanent deformations are present in the link. Direct unbolting might be feasible if permanent deformations are small.

There were concerns that a sudden release of link shear force may occur during flame cutting of the link that might be dangerous to the operating personnel. Consequently, the solution was improved by introducing a temporary bracing system consisting of tension braces and dampers. During removal of links through flame cutting, the forces locked in the links are transferred to the temporary bracing system and smoothly released through the dampers.

Link removal procedure was numerically performed on a storey-by-storey basis. Once all links from a storey are removed, all structural components from that storey are in the elastic range of response. Therefore, as brace forces are released

through dampers, the structure recovers its initial (plumb) position, becoming free of any locked-in forces and new link can be installed.

Chapter 4: Experimental evaluation of re-centring dual eccentrically braced frames with removable links

Tests on material samples

In order to evaluate material characteristics, tensile tests were performed at Politehnica University Timisoara (CEMSIG Research Centre), on steel samples prepared from the additional material received from JRC associated to each structural member of the test specimen and link-beam connection bolts. All the materials have fulfilled the product standards demands.

Tests on full-scale specimen

The validation of re-centring capability and link replacement procedure in a dual eccentrically braced structure, together with assessing its seismic performance, was realised through a pseudo-dynamic testing programme of a full-scale model performed at the European Laboratory for Structural Assessment (ELSA) facility at JRC in Ispra, Italy.

The first set of tests were represented by the snap-back tests. These were performed to simulate the snap due to a sudden release of forces, prior to the instalment of the actuators which were used for pseudo-dynamic tests, assessing on one side the amplitude of the free vibrations, and on the other side the effectiveness of dampers in limiting such vibrations. The results show a very small maximum displacement and confirm that the dampers were not activated due to the small size of displacements imposed on the frame. The transverse displacements were also small.

In order to assess the seismic performance of the full-scale specimen and validate the link replacement procedure, a pseudo-dynamic testing programme was proposed, composed of the sequence of the following tests: DL/SLS tests (Full-operation FO1 earthquake and DL earthquake), followed by the first set of links replacement, SD/ULS tests (Full-operation FO2 earthquake, SD earthquake and a pushover test), followed by the second set of links replacement and NC tests (Full-operation FO3 earthquake and NC earthquake).

DL tests

The structure manifested an elastic response, in the non-dissipative elements, as well as in the dissipative ones (including the links), during the first FO1 test. This means that there were no residual top displacements or any inter-storey drift in the structure, while the maximum top displacement was also small.

During DL test, no yield was observed in the elements outside the links. Small maximum plastic deformations occurred in links. Minor cracks were observed in the concrete slab. The structure exhibited a low residual top displacement of in the S frame and slightly higher in the N frame. Also, a low residual inter-storey drift was observed.

First link replacement

Because the structure exhibited a low residual top displacement after the DL test and low residual drift was observed, the removal of the first set of damaged links was performed by simply unscrewing the bolts, one level at a time, starting from the lower level. The dampers where not installed because a smooth transition of forces from the link to the frame was expected. The low value of the residual top displacement at the end of the DL test decreased after the elimination of the damaged links. Better re-centring was observed in the south frame, where the link is not connected to the concrete slab. An additional low re-centring was also verified during the replacement with a new set of unused links A very small residual drift that is lower than the erection tolerance was observed at the end of this procedure, the structure being almost re-centred.

SD tests

The structure behaved similarly to the FO1 test, during the FO2 test. This means that the structure exhibited an elastic response, in the non-dissipative elements, as well as in the dissipative ones (including the links) and there were no residual top displacements or inter-storey drifts of the structure.

Because after the SD test, the residual displacement was still small, a monotonic pushover test was performed, starting from the end of the SD test position. This was done to obtain a larger residual displacement than would be necessary to validate the feasibility of the link removal process and re-centre the structure. During this test, no yield was observed in the elements outside the links. Higher maximum plastic deformations occurred in the links. More visible cracks were observed in the concrete slab. After the completion of this test, the structure exhibited a significantly larger residual top displacement. Larger residual inter-storey drift was observed.

Second link replacement

Because the PO1 test caused the structure to exhibit a significantly larger residual top displacement, removal of the links required that they be flame cut (firstly the link web and after, the flanges), from the top storey downwards. The residual top displacement at the end of the PO1 test was reduced after the elimination of the damaged links. Again, better re-centring was observed in the south frame, where the link is not connected to the concrete slab. A new set of unused links was then mounted into the structure, thus readying the structure for the next upper input level of the seismic record. An additional low re-centring was also observed after the replacement of the links. A small residual drift that was lower than erection tolerance was observed, the structure being mostly re-centred.

NC tests

The structure behaved similarly to the first two FO tests, during the FO3 test. The structure exhibited an elastic response in the non-dissipative elements, as well as in the dissipative ones outside the links, as well as a very small residual deformation in the links. There was no residual top displacement or inter-storey drift in the structure.

The NC test was started, but had to be stopped prematurely because the available actuator capacity was not sufficient to execute the test with the imposed null torsion at every floor. It was then decided to continue with pushover tests.

The last pushover test produced extensive plastic behaviour throughout the entire structure. First of all, very large maximum plastic deformations occurred in the links, specifically, with failure occurring inside the link element very close to the welding with the end plate and also between the webs and flanges of the first two levels. At the point of maximum displacements the links from the first two floors had already failed and fallen down. The first link to fall was the one from the first floor on the south frame, followed by the link on the opposite frame. Significant damage was also observed in the column bases zones and at the end of the MRF beams, just outside the haunch. The concrete slab was heavily compromised in the north frame.

Concrete slab influence

One of the critiques to the removable link solution is related to the interaction between the removable links and the concrete slab. The floor layout of the test specimen was designed to allow the investigation of two different solutions to the interaction between a removable link and the reinforced concrete slab. The solution for the south frame involved disconnecting the removable link from the reinforced concrete slab, by extending the slab only up to an additional secondary beam placed in parallel with the beam containing the link. The solution for the north frame involved using a conventional reinforced concrete slab (not connected to the link with shear studs) such that it would accept damage to it.

The concrete slab increases the link's shear capacity. Due to its presence over the links, the north frame is more rigid and has a larger capacity than the south frame, this making re-centring of the north frame more difficult than in the case of the south frame.

Chapter 5: Numerical validation of design methodology for dual eccentrically braced frames with removable links

To check if the experimental specimen behaviour can be extended to more general structures, other current practice structural configurations of dual eccentrically braced frames with removable links were analysed.

The numerical model used in numerical simulations was calibrated using the results of experimental tests. A greater link over-strength of 1.7 resulted, together with neglecting the slip in the link connections (mentioned in the numerical model description in Chapter 3).

Using the same capacity design rules as for the experimental specimen, two dual structural configurations were designed: the first (configuration A) having a central EBF (with the link being placed at mid-span) and two side MRFs, and the second (configuration B) having a central MRF and two side EBFs. (links placed marginally, connected to columns on one side). For a structure with re-centring capability, the design objective consists in preventing yielding in members other than removable dissipative ones, up to a desired deformation. Ideally the latter should be the ultimate deformation capacity of the removable dissipative member. Because following code-based capacity design rules was not enough to accomplish this objective for the investigated structures, a higher-strength steel was used in

moment resisting frames to avoid yielding in their members, obtaining a larger capacity without increasing the stiffness.

To evaluate the seismic performance of the specimen in the inelastic domain, static nonlinear analyses were performed together with using the N2 method, as well as dynamic nonlinear analyses. Although the performance objectives are not satisfied for SLS and NC using the N2 approach, the objective of having no yielding in the MRFs before the attainment of the ULS deformation in the removable links (0.11 rad) of the EBFs is accomplished, representing the basic design requirement for dual frames with removable dissipative members. MRFs provide the re-centring of the specimen even until after the links ultimate deformation (0.14 rad) for configuration A. Performing time-history analyses on the calibrated model of the two structural configurations, structural performance similar to experimental specimen was obtained for the evaluated limit states: DL (SLS), SD (ULS) and NC.

At DL limit state all structural components except links are in the elastic range. Shear deformations in links exceed the FEMA 356 limits of 0.005 radians, but this is normal, since the design carried out according to EN 1998 did not impose any limitation on yielding of structural members at DL limit state. Even so, peak inter-storey drifts are within the limits imposed. In these conditions, the advantage of the proposed system is obvious, since the damaged dissipative members (links) can be replaced easily due to negligible permanent drifts. Even if some structural damage is present, it can be repaired easily by replacing the bolted links.

At SD limit state damage is still constrained to links only, which exhibit plastic deformation demands below 0.11 rad. Permanent drifts are only slightly larger than at the DL limit state. Due to low permanent drifts, the structures are easily repairable at this limit state as well.

At NC limit state the structural damage is widespread. Shear deformations in links are well over acceptable values of 0.14 rad. However, due to moment resisting frames, the overall performance of the structures can be considered acceptable for this limit state. Plastic deformation demands are present in moment resisting frames (beams and columns) and braces. Even so, permanent inter-storey drifts are not very large. However, repairing of the structures is considered not to be feasible and desirable at these large levels of seismic input.

As proved previously (numerically and experimentally), the technically easiest way to release the forces in links is by flame cutting the web and flanges of the link if large permanent drifts occur or by unbolting otherwise, on a storey by storey basis, starting from the least loaded towards the most loaded one (from the upper storey downwards). Three possibilities of links removing order within a storey were studied for the two studied structures: 1 - firstly removing the links on the longitudinal direction and secondly the ones on the transversal direction; 2 - vice versa, and 3 - in a circular pattern. Very good re-centring was obtained. It was observed that for the first solution the residual shear force drop is smaller than for the second solution and the redistribution of forces between the links of the same storey is also smaller. The situation for the third solution is in between the other two. On the first solution of link removal order within a storey, was analysed also the removal of links starting from the most loaded to the least loaded storey (from the first storey upwards) and was observed a larger interaction between stories, but values of the shear force drop smaller than in the case of eliminating links from the upper one toward the lower one and smaller redistribution of forces between the links of the same storey. Thus, considering the optimal link removal order is the one which results in smaller drop of force during the process, within a given storey links

should be removed from the least loaded toward the most loaded and in the height-wise direction, links should be removed from the lower storey toward the upper ones (from the storeys with larger residual stresses toward the storeys with smaller ones).

To evaluate the design behaviour factor of the two structural configurations, incremental dynamic analyses were performed. Computations were performed for a level of the seismic action corresponding to an ultimate limit state (ULS) acceptance criterion of 0.08 radians plastic rotation in links, considered by EN 1998 and for levels of the seismic action corresponding to ULS (0.11 rad) and NC (0.14 rad) acceptance criteria for plastic rotation in links considered by FEMA356. Close values of the design behaviour factor were obtained for the two structural configurations, 4.5 and 5, being larger than the 4 as considered in design according to EN1998, for medium ductility class.

A flowchart was proposed to design eccentrically braced frames with removable links and re-centring capability, using capacity code-based design, as well as nonlinear analyses.

6.2. Contributions of the author

The main contribution of the author is represented by the design of a coherent experimental program with the aim to validate the re-centring capability and link replacement procedure in a dual eccentrically braced structure with removable links, together with assessing its seismic performance. This was realised through a pseudo-dynamic testing programme of a full-scale model performed at the European Laboratory for Structural Assessment (ELSA) facility at JRC in Ispra, Italy. A record of the main contributions of the author is further shown:

- Design of a full-scale dual eccentrically braced frames with removable links experimental specimen with the aim of validating re-centring capability and link replacement procedure through experimental tests;
- Performing pre-test numerical simulations of link removal procedure in order to propose solutions for link elimination order height-wise and within a level in a multi-storey building;
- Performing pre-test numerical simulations in order to obtain the safety of link removal procedure and numerical testing of using some safety systems (braces with dampers) during the process;
- Validation of re-centring capability of experimental specimen and of link replacement feasibility after an earthquake through experimental tests of a full-scale structure;
- Verification and numerical validation of seismic performance of proposed system and link replacement procedure on more general, current practice structures;
- Behaviour factor evaluation at ultimate limit state and near collapse limit state in order to assess the application of code provisions in designing the proposed system.

6.3. Dissemination of results

The dissemination of results was performed in the first place in the research project DUAREM within several scientific and technical reports.

The main results and conclusions of the research have been presented and published in several conferences and national or international journals. A list of the most important papers is presented below:

- A. Stratan, **A. Ioan**, D. Dubina, "Re-centring capability of dual eccentrically braced frames with removable bolted links", Proceedings of the 7th International Conference on Behaviour of Steel Structures in Seismic Areas (STESSA2012), pp. 723-728, 9-11 January 2012, Santiago, Chile (Thomson Reuters Web of Science);
- **A. Ioan**, "Seismic response of dual steel eccentrically braced frames with removable links", Mathematical Modelling in Civil Engineering. Dec. 2011, Issue 4, p101-110 (EBSCO database);
- **A. Ioan**, A. Stratan and D. Dubina, "Numerical simulation of bolted links removal in eccentrically braced frames", Pollack Periodica, Volume 8, Issue 1, 1 April 2013, Pages 15-26 (Scopus database);
- **A. Ioan**, A. Stratan, D. Dubina, M. Poljanšek, F. J. Molina, F. Taucer, P. Pegon, G. Sabău, „Experimental validation of re-centring capability of eccentrically braced frames with removable links" – Engineering Structures Journal (ISI) – sent on December 28th ,2014 (pending acceptation);
- **A. Ioan**, A. Stratan, D. Dubina, "Seismic performance of re-centring capability of dual eccentrically braced frames with replaceable links", The 8th International Conference on Behaviour of Steel Structures in Seismic Areas (STESSA2015), 1-3 July 2015, Tongji University, Shanghai, China – sent on February 16th, 2015 (pending acceptation);
- A. Stratan, **A. Ioan**, D. Dubina, M. Poljanšek, F. J. Molina, P., Pegon F. Taucer, "Large-scale tests on a re-centring dual eccentrically braced frame", The 8th International Conference on Behaviour of Steel Structures in Seismic Areas (STESSA2015), 1-3 July 2015, Tongji University, Shanghai, China – sent on March 2nd, 2015 (pending acceptation);
- **A. Ioan**, A. Stratan, D. Dubina, "Re-centring dual eccentrically braced frames with removable links" - Proceedings of the Romanian Academy - series A: Mathematics, Physics, Technical Sciences, Information Science. (accepted to be published);
- G.A. Sabău, M. Poljansek, F. Taucer, P. Pegon, F.-J. Molina, D. Tirelli, B. Viaccoz, A. Stratan, **A. Ioan**-Chesoan, D. Dubina, Final Official Report of "Full-scale experimental validation of dual eccentrically braced frame with removable links" (DUAREM) SERIES Project, ISBN 978-92-79-44717-4 (PDF), ISSN 1831-9424 (online), 147pp., 2014

In addition, the author was involved in research activities from which the results were published within the following papers:

- **A. Ioan**, " Numerical Simulation of pseudo-dynamic full-scale test on a three storey - one span - three bays steel frame", Bauhaus Summer School (6-7 August 2012, Weimar, Germany) – „Modal validation and simulation" booklet (http://nbn-resolving.de/urn:nbn:de:gbv:wim2-20130805-19969), pp. 272-280;
- **A. Ioan**, A. Stratan, D. Dubina, F. Taucer and M. Poljansek, "Pre-test numerical simulations and experimental program on dual eccentrically

braced frame with removable links", International Workshop "High Strength Steel in Seismic Resistant Structures - HSS-SERF", 28-29 June 2013, Naples, Italy;

- A. Stratan, **A. Ioan**, D. Dubina, M. D'Aniello, G. La Manna Ambrosino, R. Landolfo, F. Taucer, M. Poljansek, " Pre-test numerical simulation and experimental program on a dual eccentrically braced frame with replaceable links", XXIV Giornate italiane della Costruzione in Acciaio, 30 September – 2 October 2013, Torino, Italy;
- **A. Ioan**, A. Stratan, D. Dubina, F. Taucer, M. Poljansek, J. Molina, P. Pegon, M. D'Aniello, L. Landolfo, "Experimental program for large-scale tests on a re-centring dual eccentrically braced frame", EUROSTEEL 2014 (7th European Conference on Steel and Composite Structures), 10-12 September 2014, Napoli, Italy;
- **A. Ioan**, A. Stratan and D. Dubina, "Link replacement order in high-rise re-centring dual eccentrically braced frames", EUROSTEEL 2014 (7th European Conference on Steel and Composite Structures), 10-12 September 2014, Napoli, Italy.
- **A. Ioan**, A. Stratan, D. Dubina and F. Taucer, "Dual Steel Eccentrically Braced Frames with Bolted Links – Simulation of Safe Removal Process", First International Conference for PhD students in Civil Engineering (CE-PhD) 4-7 November 2012, Cluj-Napoca, Romania;
- D. Dubina, A. Stratan, F. Dinu and **A. Ioan**, "Sisteme structurale cu componente disipative de siguranta seismica", AICPS Review, no. 1-2 ISSN 2067-4546, pp. 41-50, 2013;
- **A. Ioan**, " Pre-testarea numerica a unui cadru cu bare disipative demontabile supus la incercari pseudo-dinamice", AICPS Review, no. 3, ISSN 2067-4546, pp. 63-71, 2013;
- A. Stratan, **A. Ioan**, D. Dubina, M. Poljansek, J. Molina, P. Pegon and F. Taucer, "Dual eccentrically braced frames with removable links: Experimental validation of technical solution through large-scale pseudo-dynamic testing", 5CNIS&1CNISS (5th National Conference of Earthquake Engineering and 1st National Conference on Earthquake Engineering and Seismology), 19-20 June 2014, Bucharest, Romania.

6.4. Future research activities

The research of the proposed system can continue with some future activities like:

- Extending the numerical study on other structural configurations (different number of stories, spans, symmetrical/unsymmetrical configurations, etc.) in order to obtain the generality of application conditions for the proposed system;
- Development of performance based design methodology;
- Proposal of design recommendations.

6.5. Acknowledgements

The research leading to these results has received funding from the European Community's Research Fund for Coal and Steel (RFCS) under grant agreement n° RFSR-CT-2009-00024 "High strength steel in seismic resistant building frames" and from the European Community's Seventh Framework Programme [FP7/2007-2013] for access to the European Laboratory for Structural Assessment of the European Commission – Joint Research Centre under grant agreement n° 227887 and was partially supported by the strategic grant POSDRU/159/1.5/S/137070 (2014) of the Ministry of National Education, Romania, co-financed by the European Social Fund – Investing in People, within the Sectorial Operational Programme Human Resources Development 2007-2013.

ANNEX A

Frame and plan drawings for experimental specimen erection, together with corresponding details, are presented in the following figures:

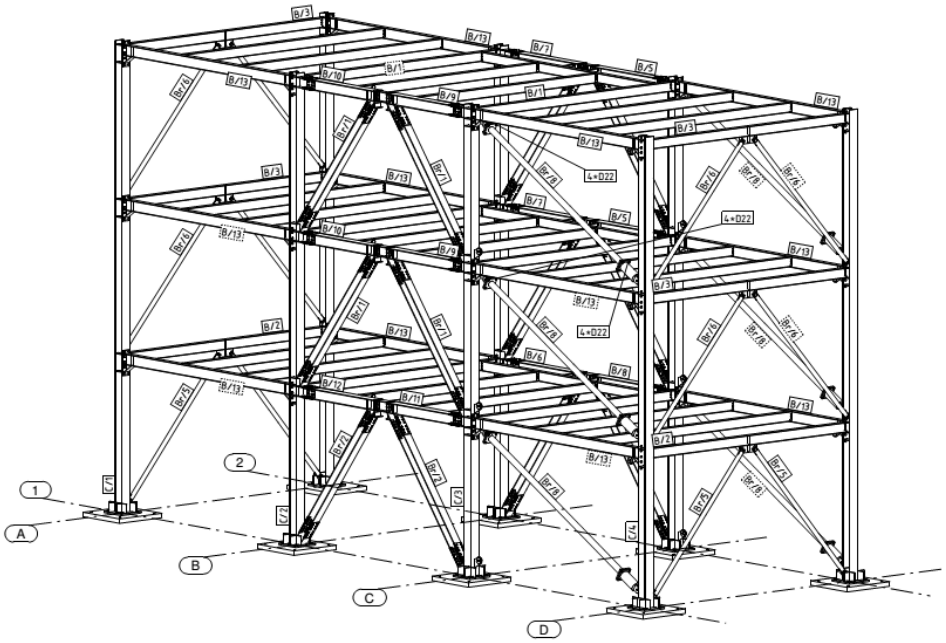

Fig. A-1. 3D view of the specimen

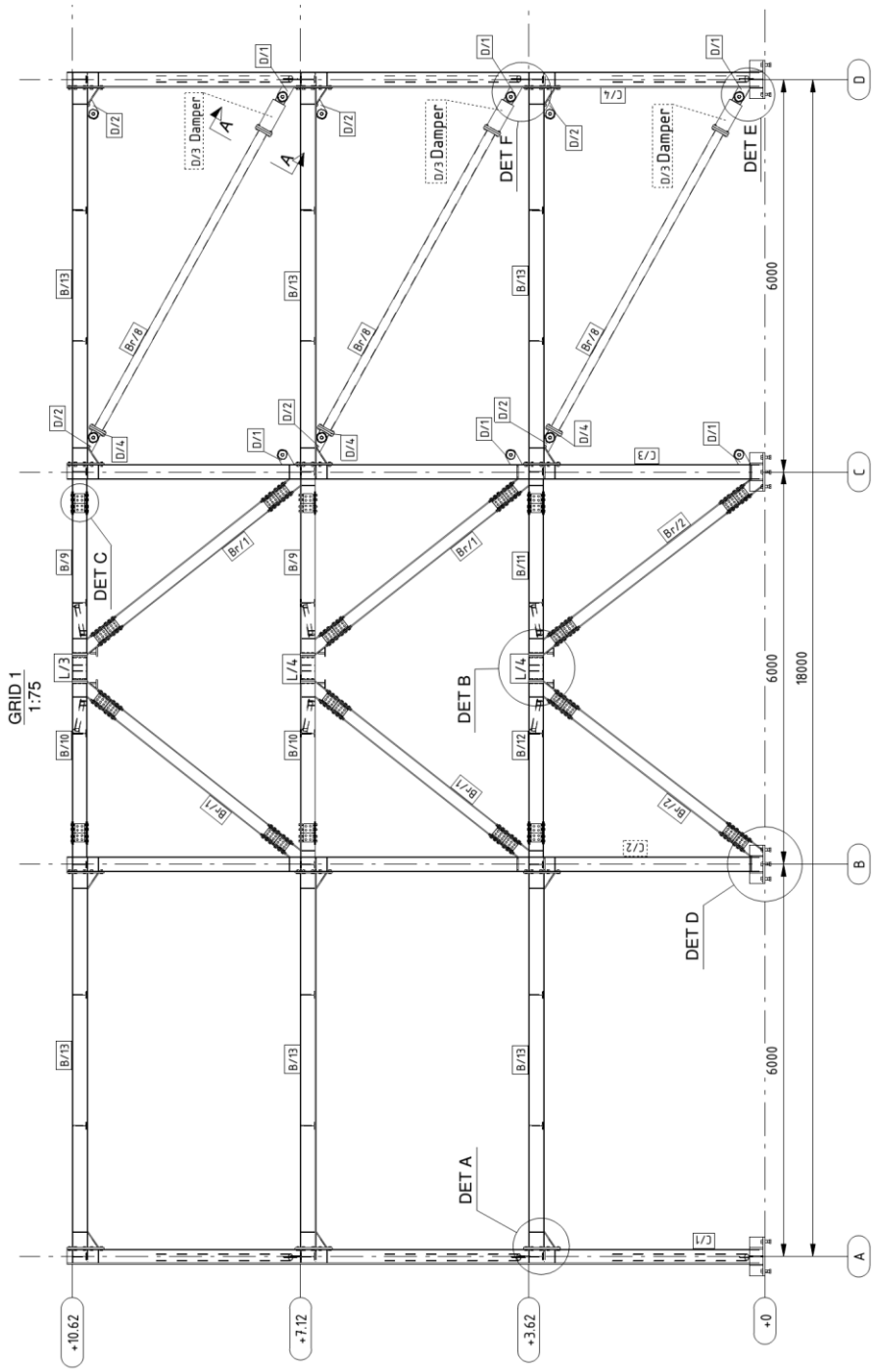

Fig. A-2. North frame view

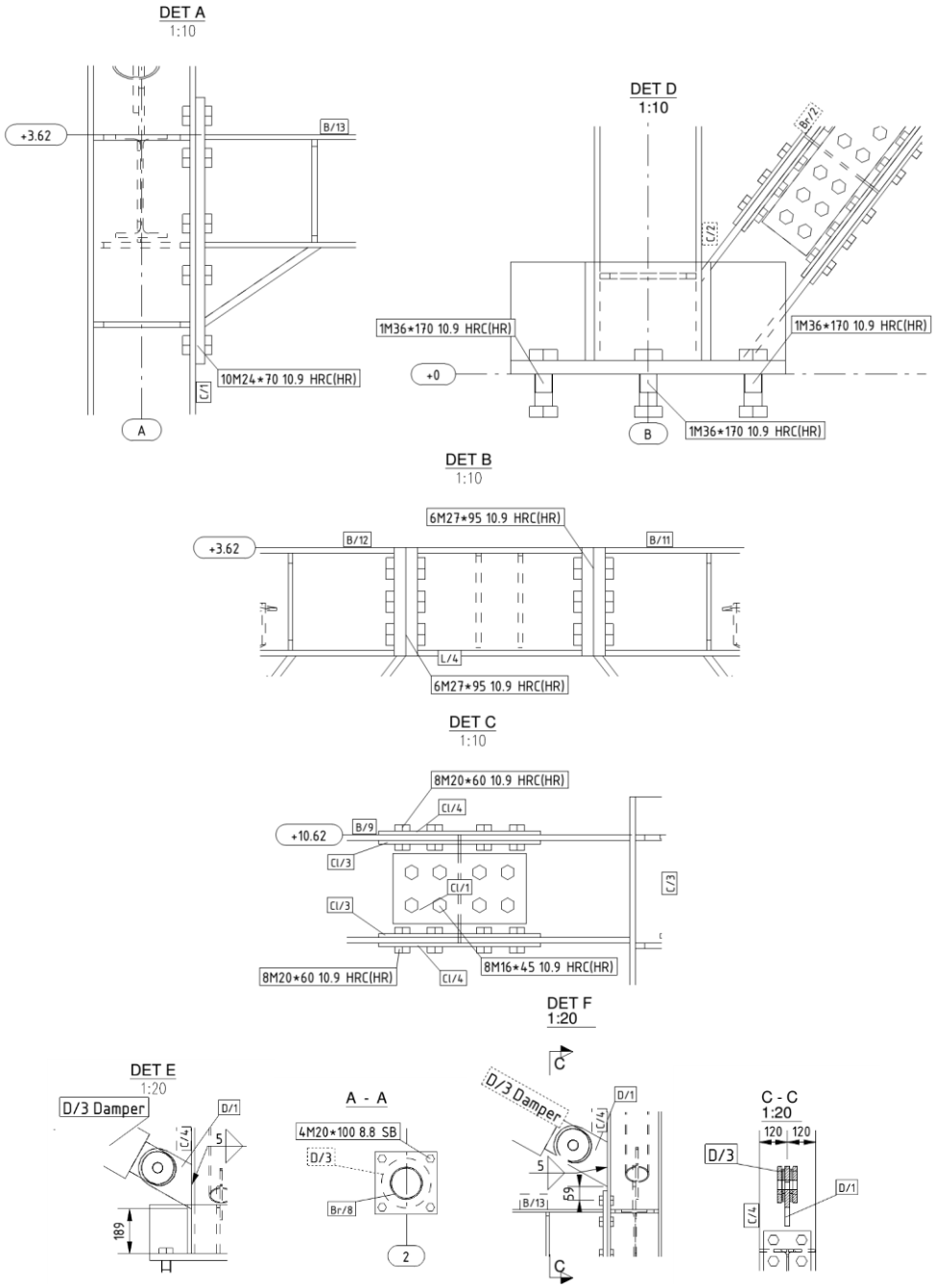

Fig. A-3. North frame details

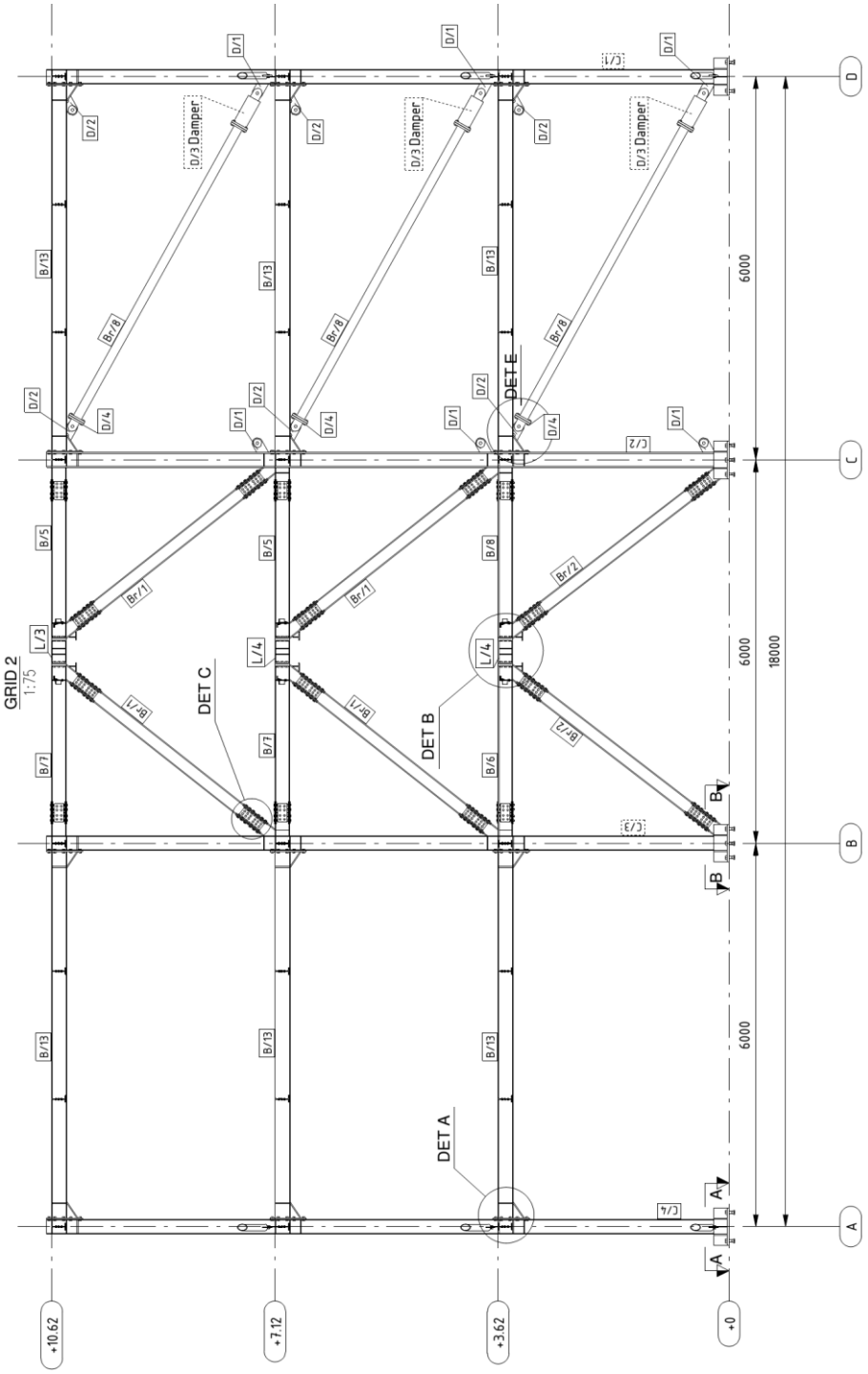

Fig. A-4. South frame view

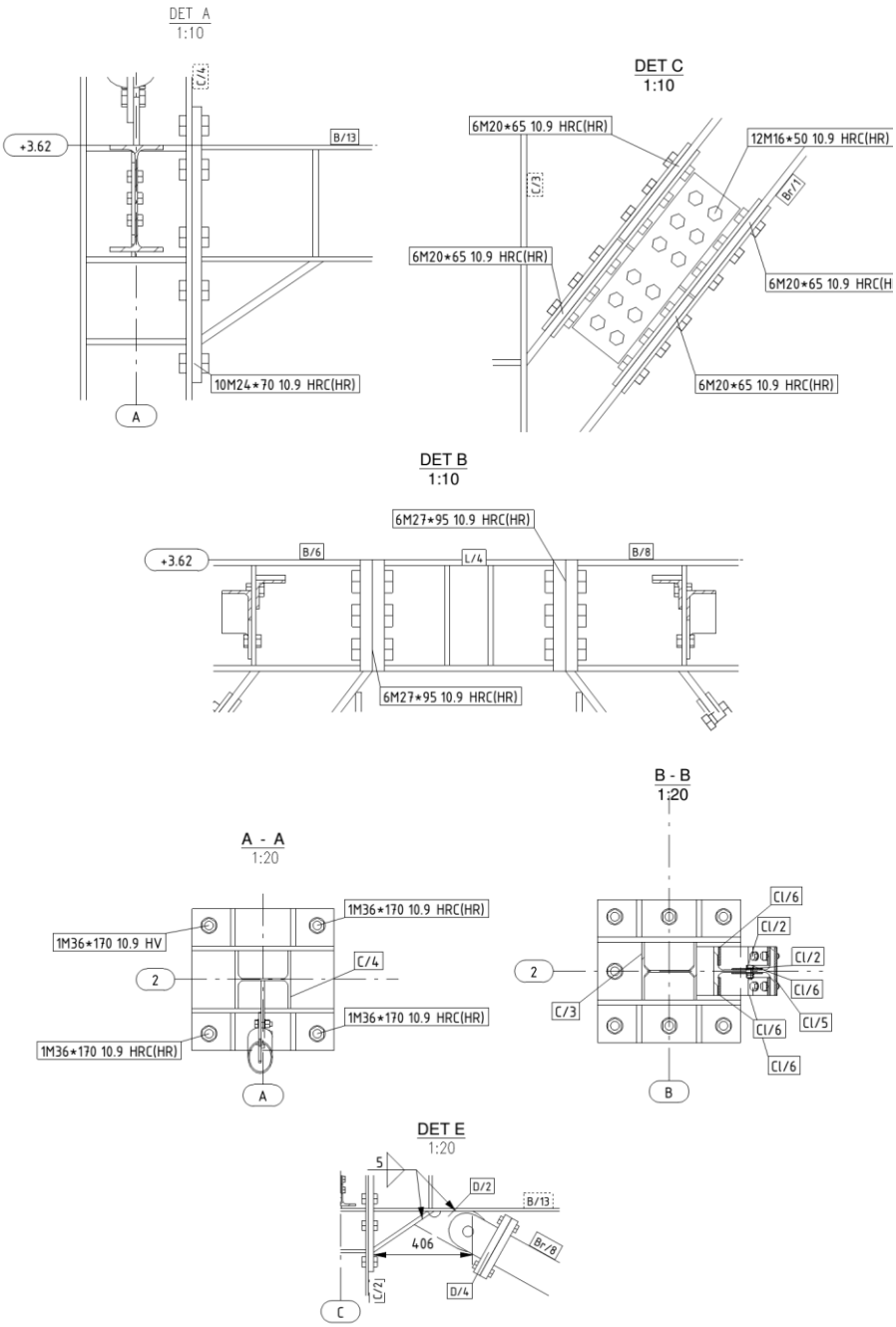

Fig. A-5. South frame details

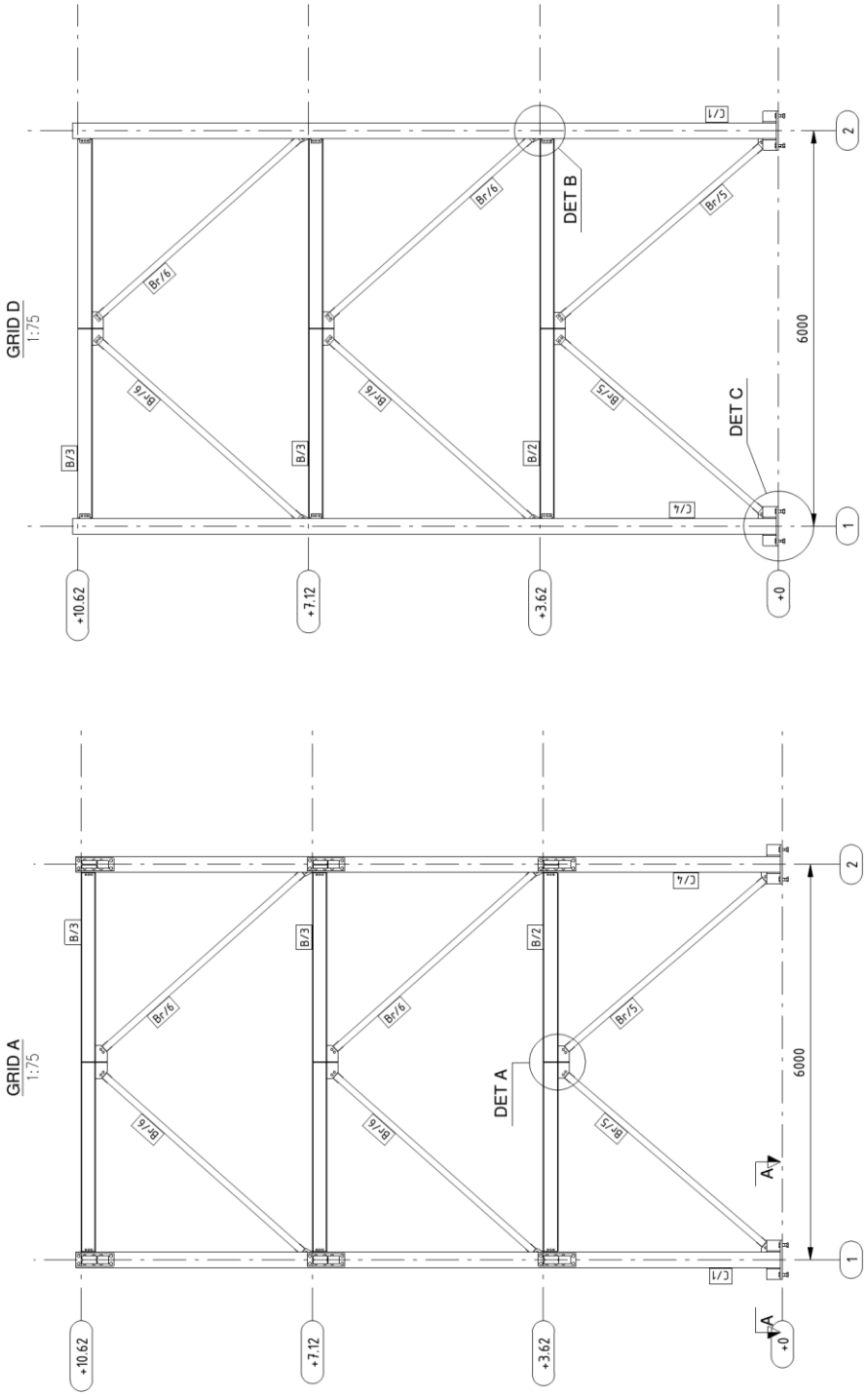

Fig. A-6. Transversal end frames view

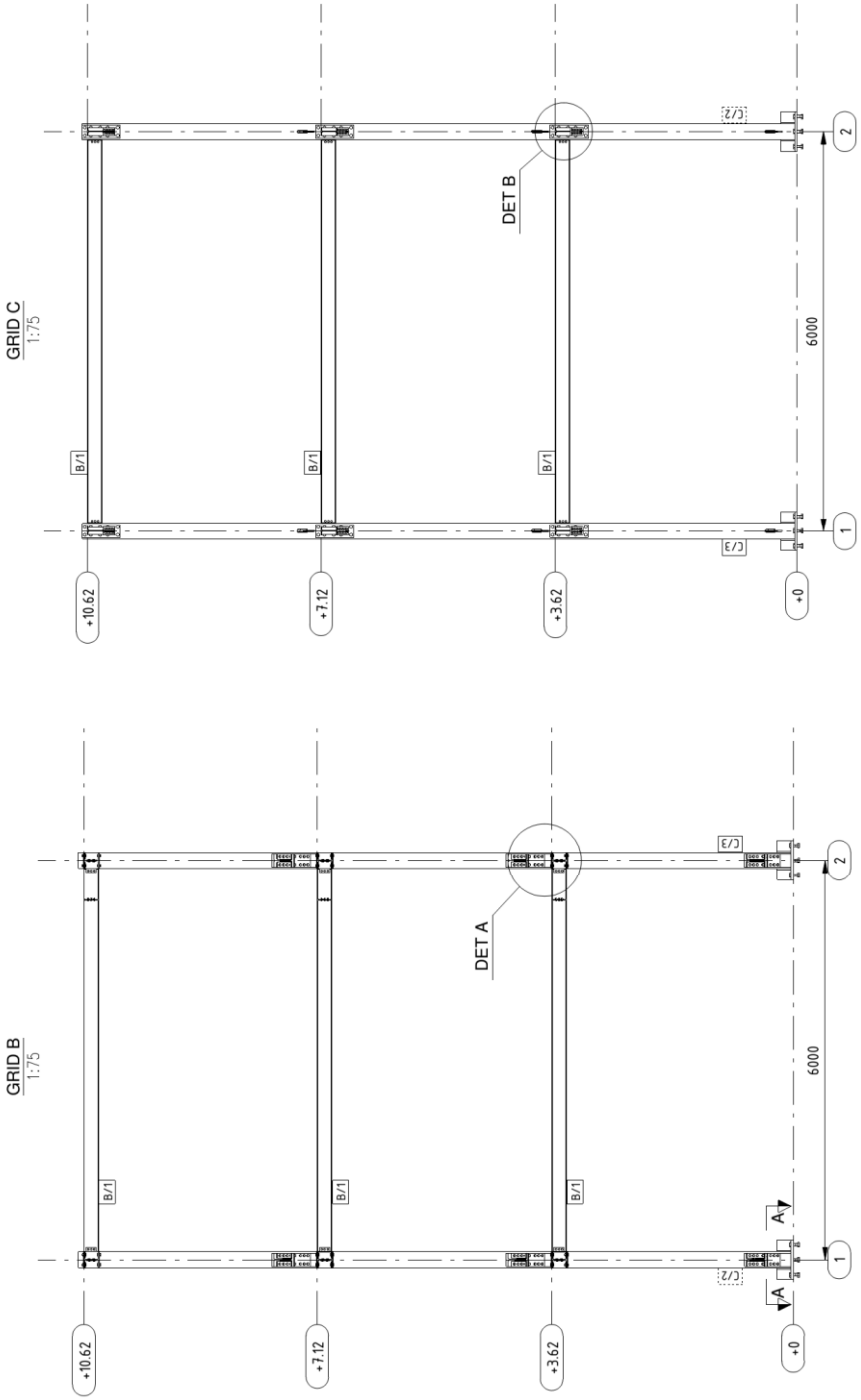

Fig. A-7. Transversal current frames view

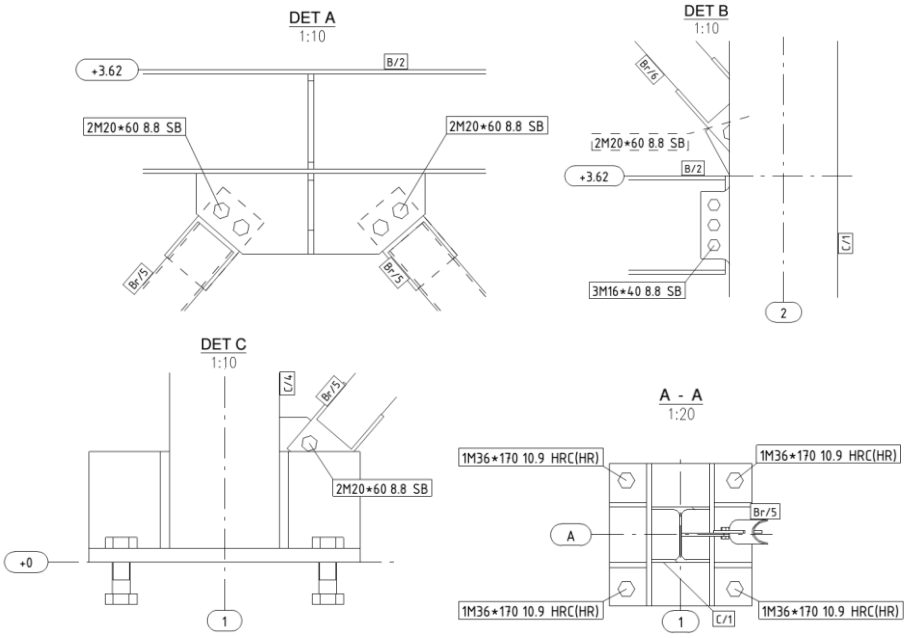

Fig. A-8. Transversal end frames details

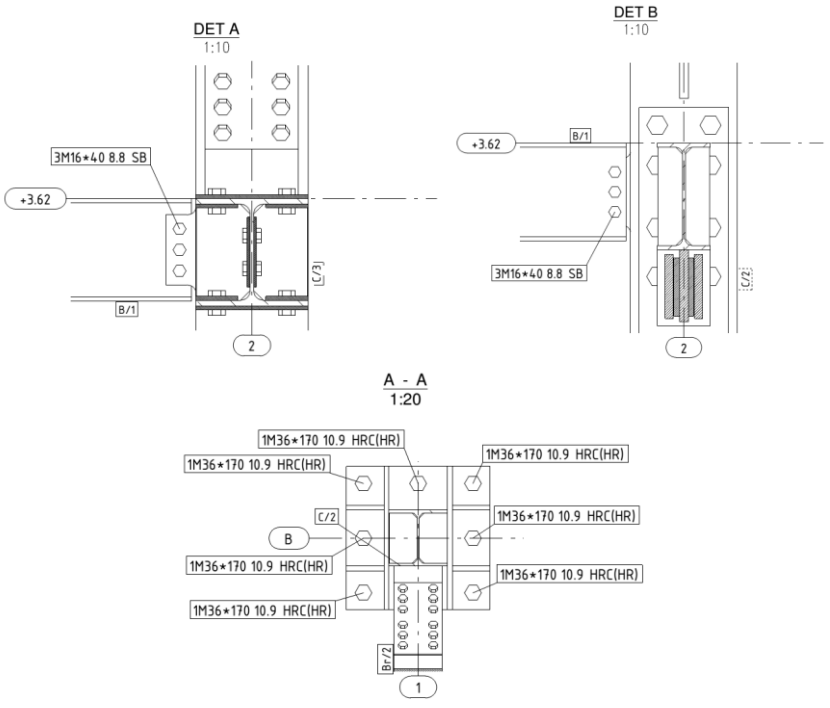

Fig. A- 9. Transversal current frames details

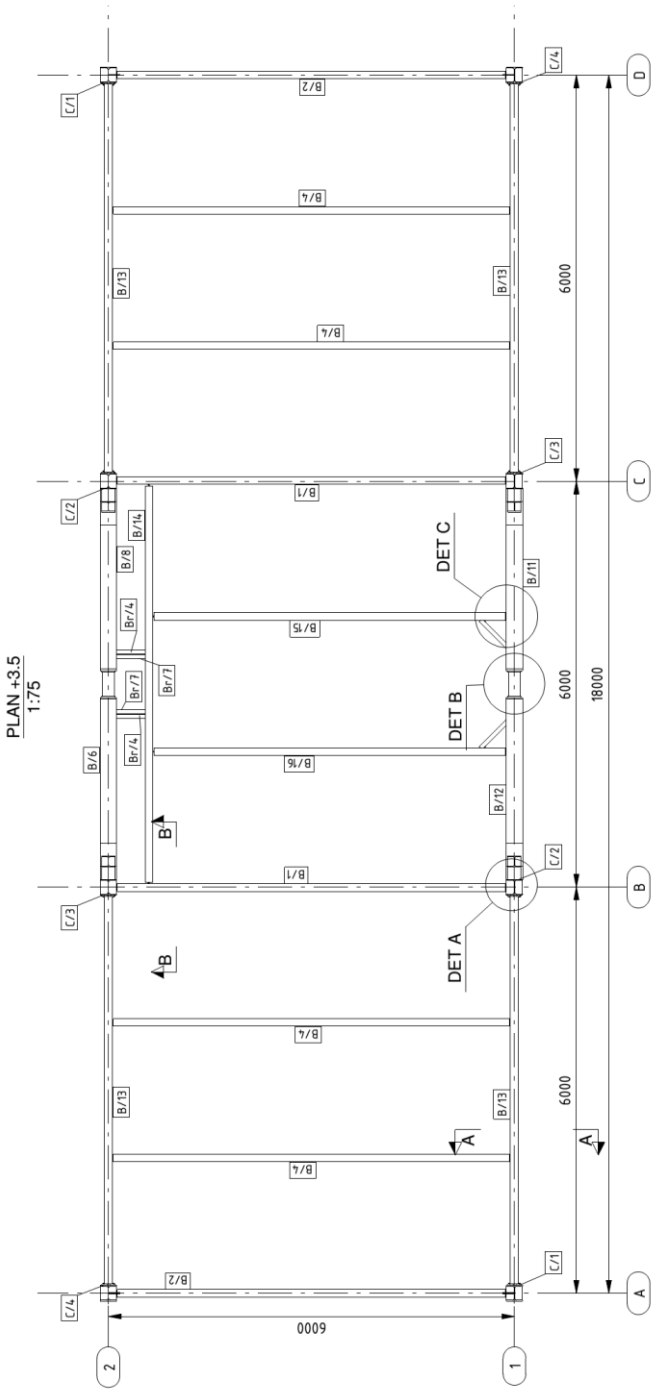

Fig. A-10. First floor plan

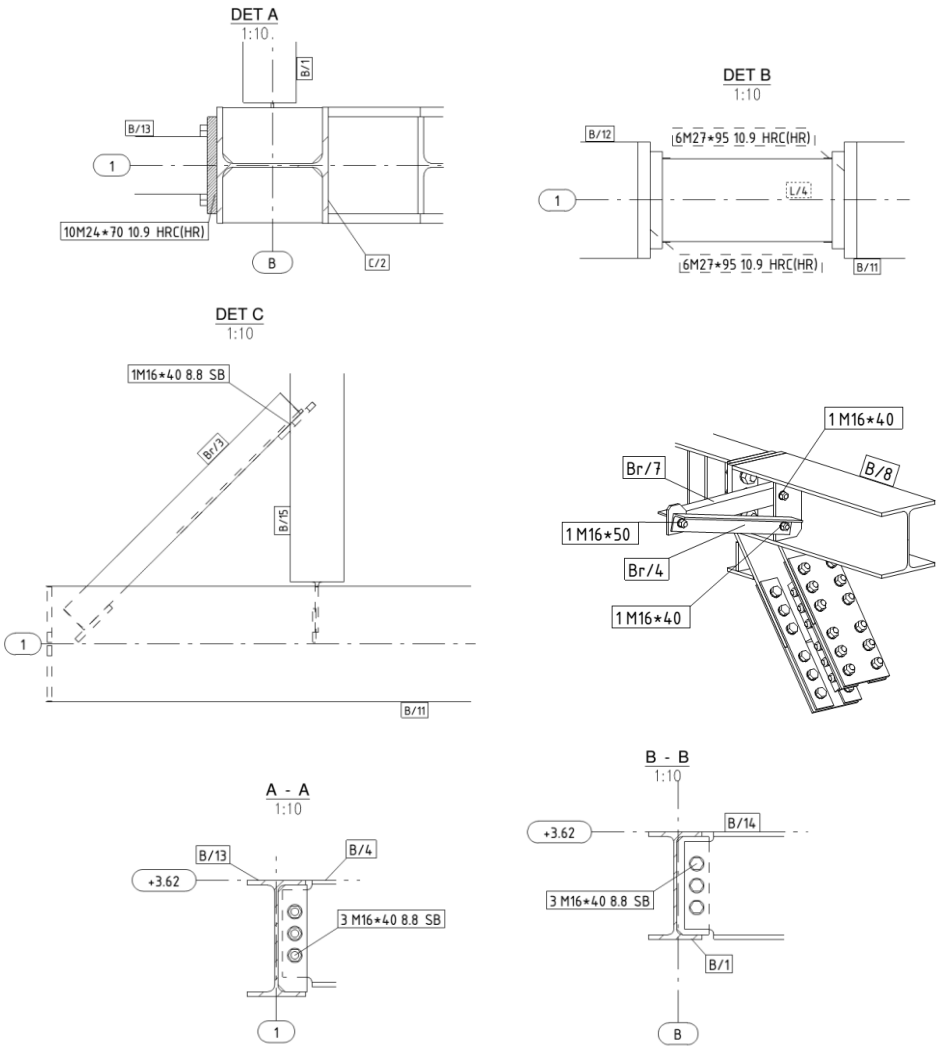

Fig. A-11. First floor plan details

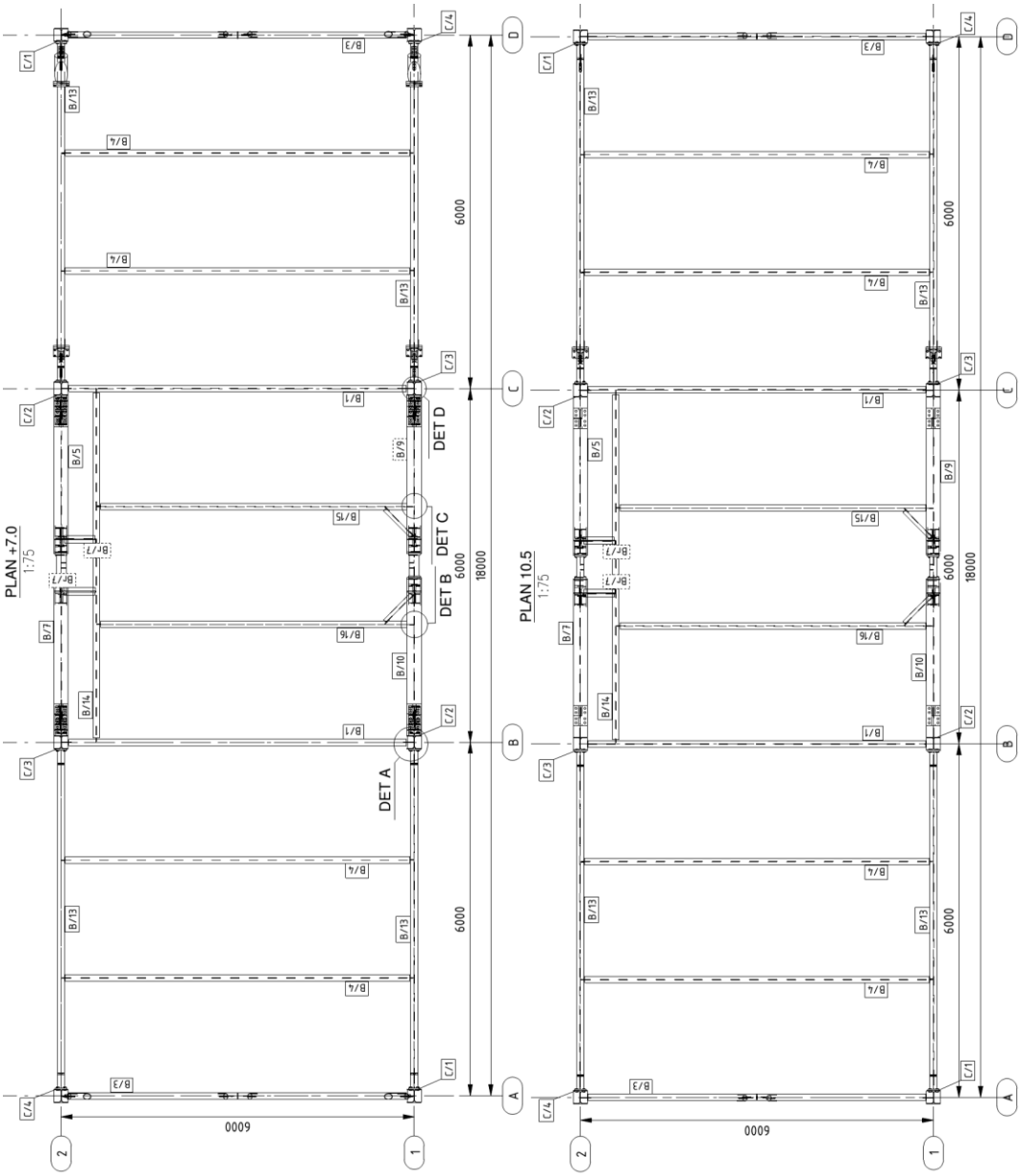

Fig. A-12. Second and third floors plans

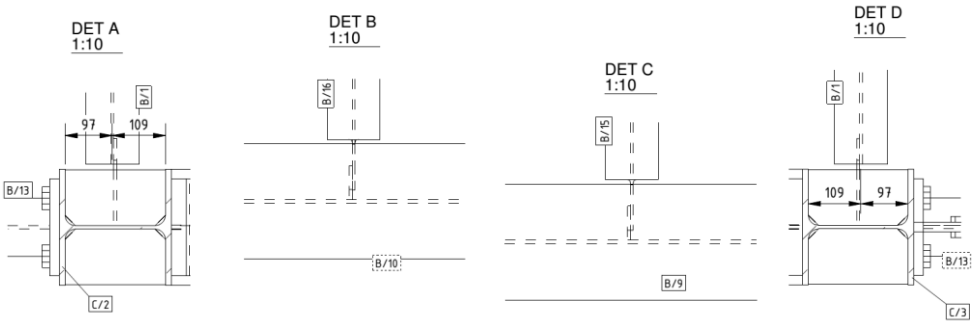

Fig. A-13. Second and third floors plans details

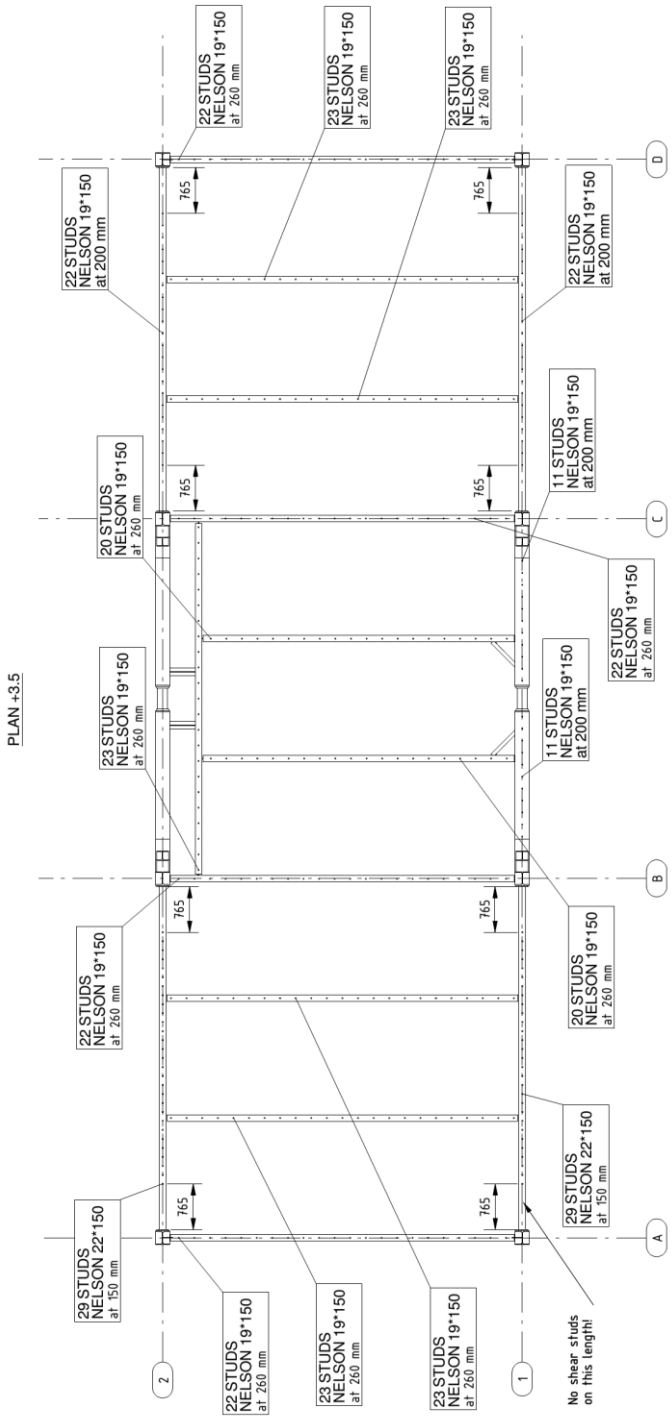

Fig. A-14. Shear studs plan

ANNEX B

General views with the position of the displacement transducers (Heidenhains, inclinometers and other transducers) as well as Strain gauges positions on the N and S frames are illustrated in the following figures:

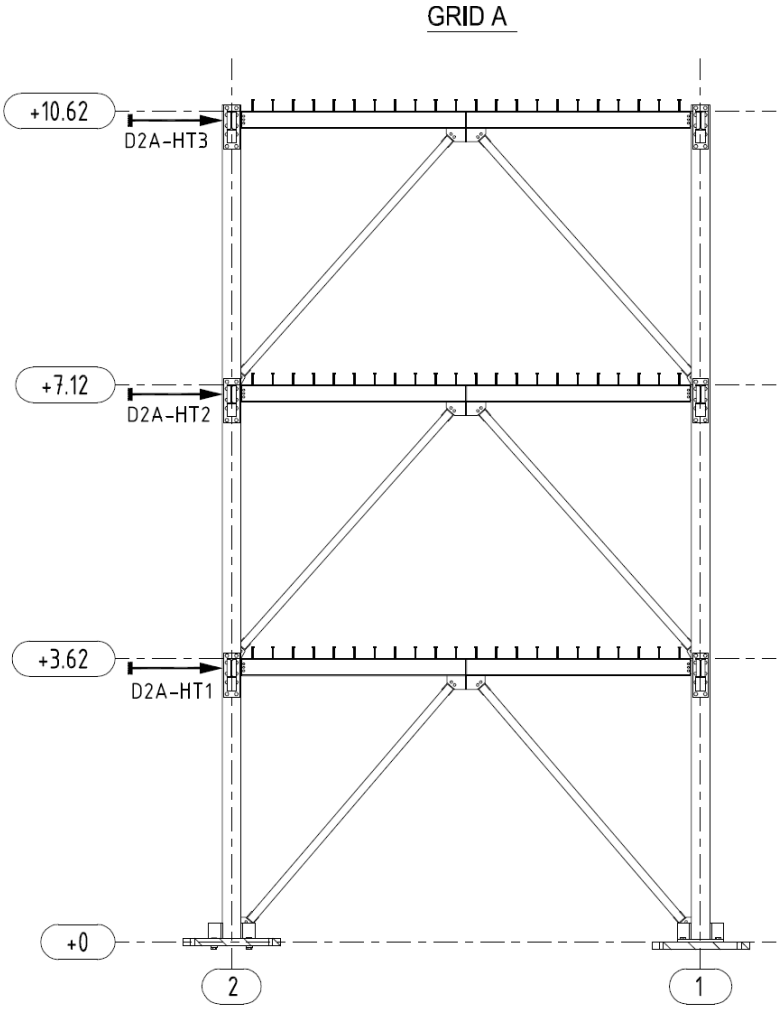

Fig. B-1. General view with the position of the transversal global displacement transducers

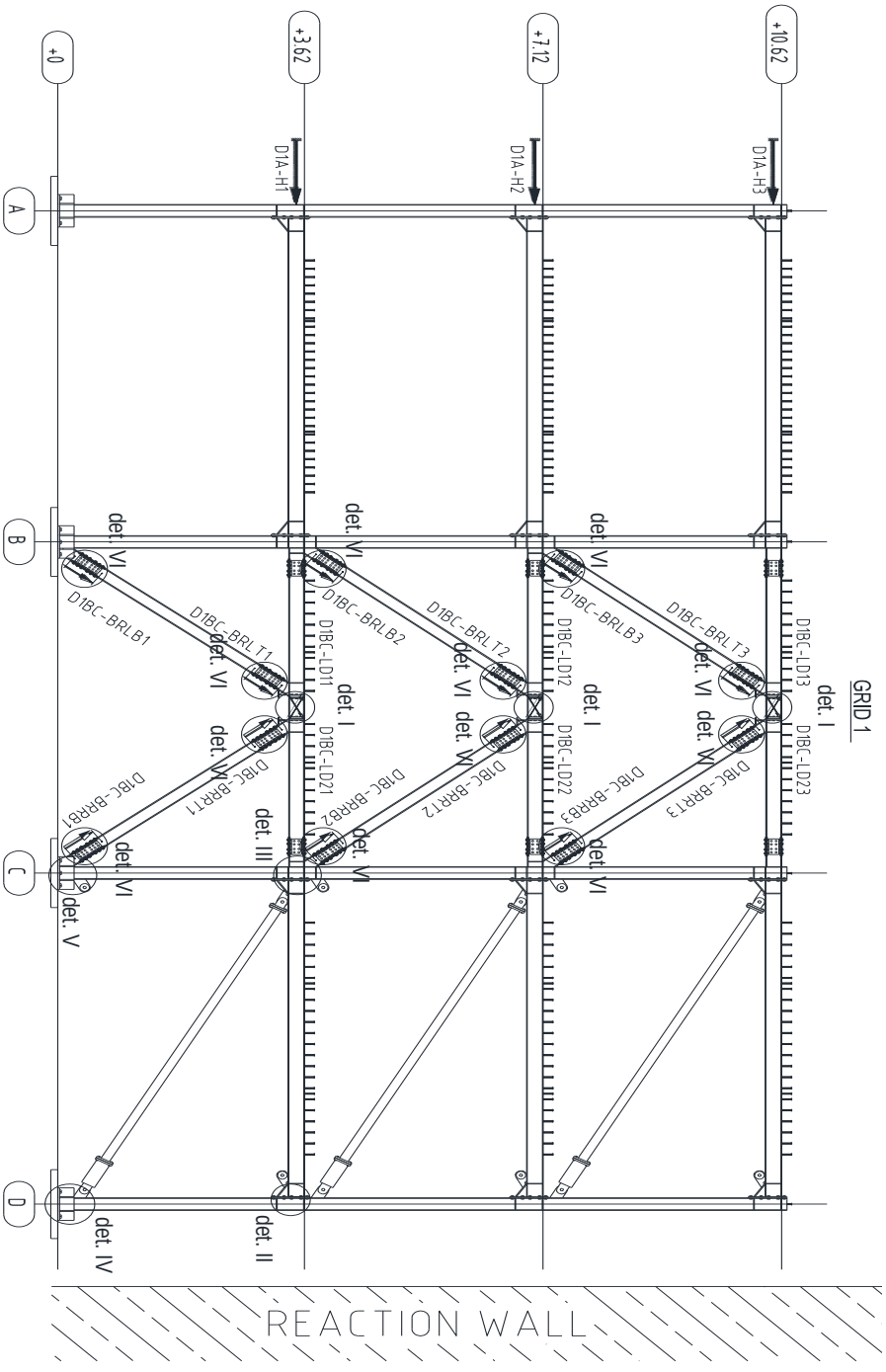

Fig. B-2. General view with the position of the displacement transducers (Heidenhains, inclinometers and other transducers) on the northern side

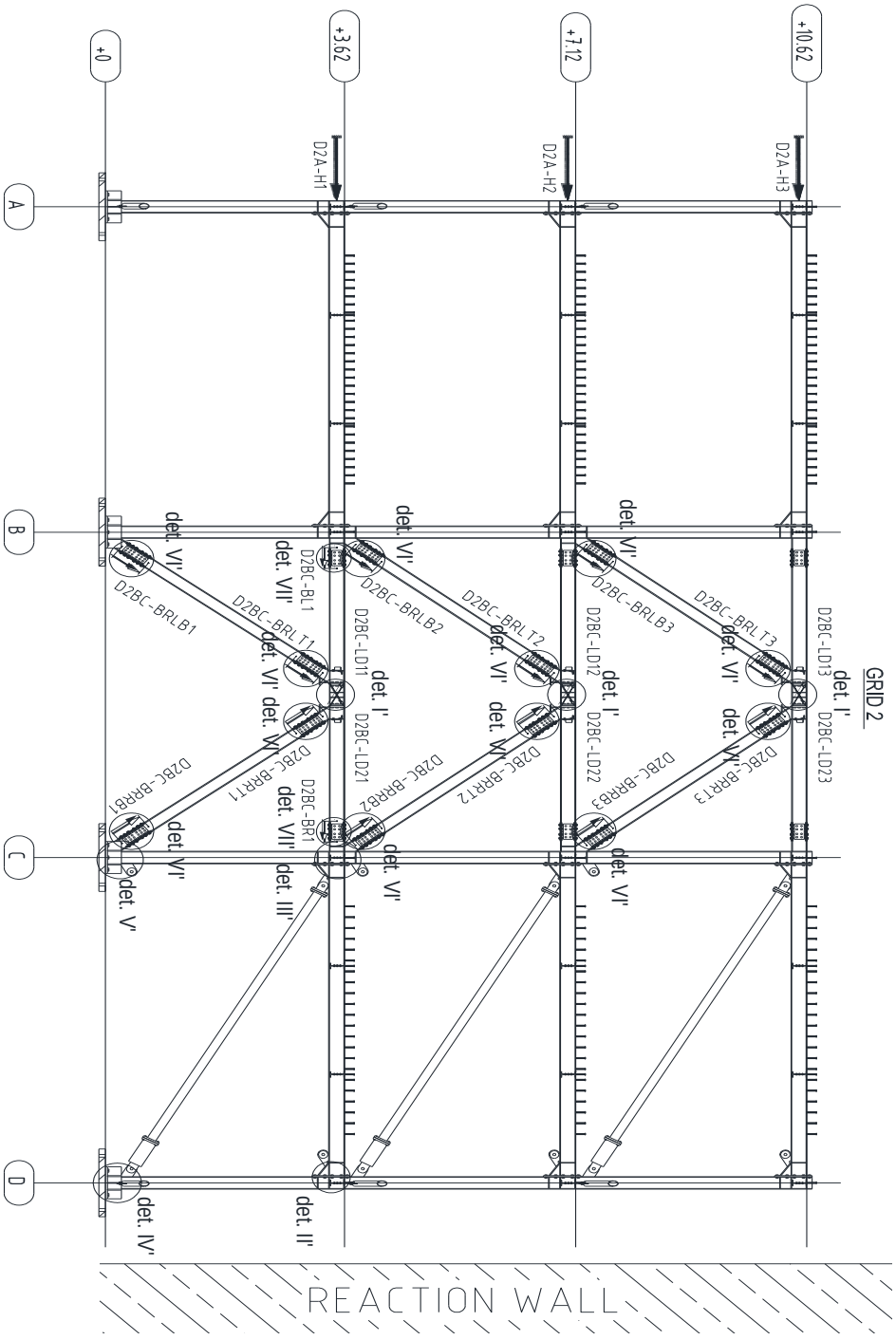

Fig. B-3. General view with the position of the displacement transducers (Heidenhains, inclinometers and other transducers) on the southern side

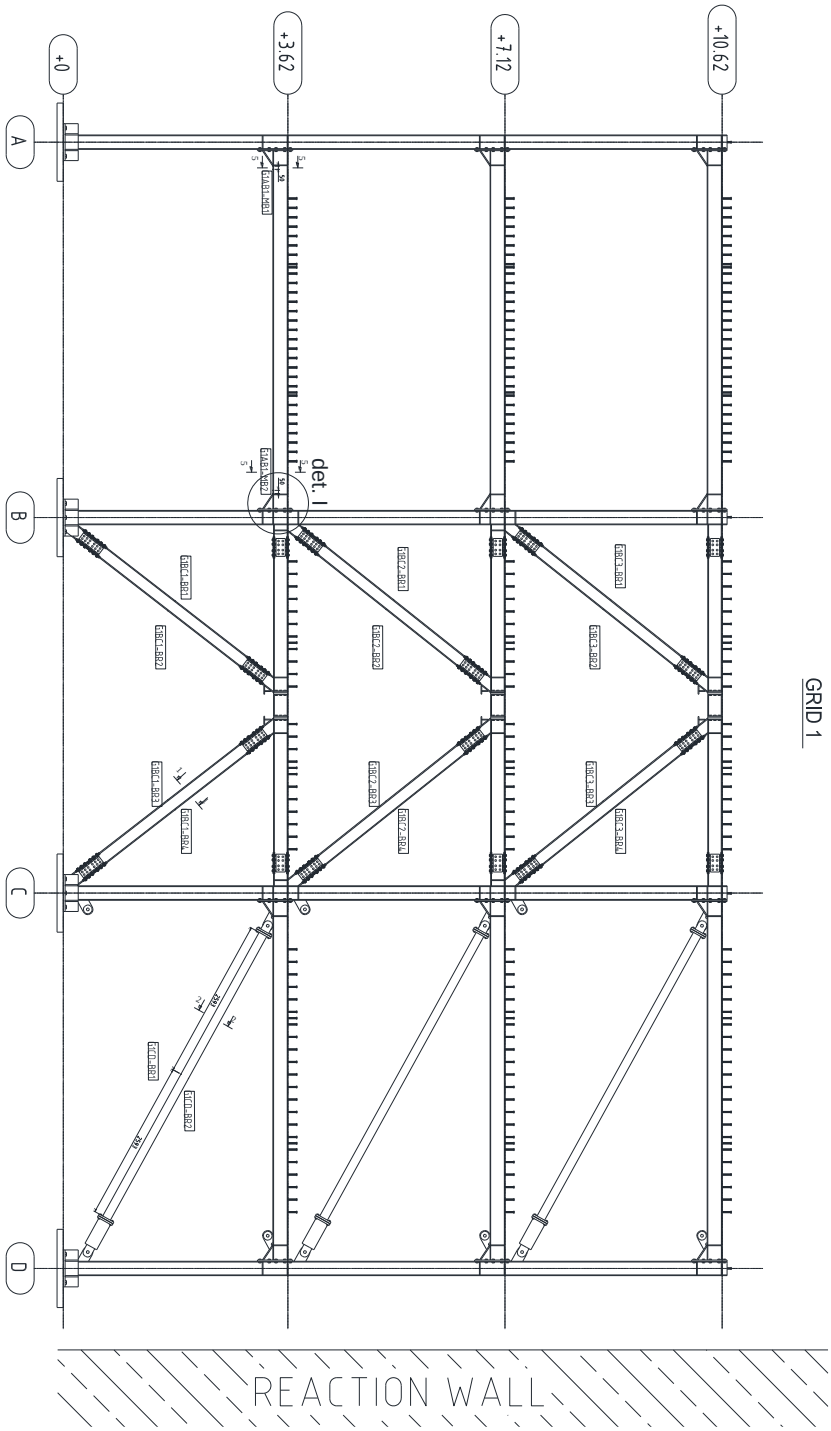

Fig. B-4. Strain gauges positions - N frame

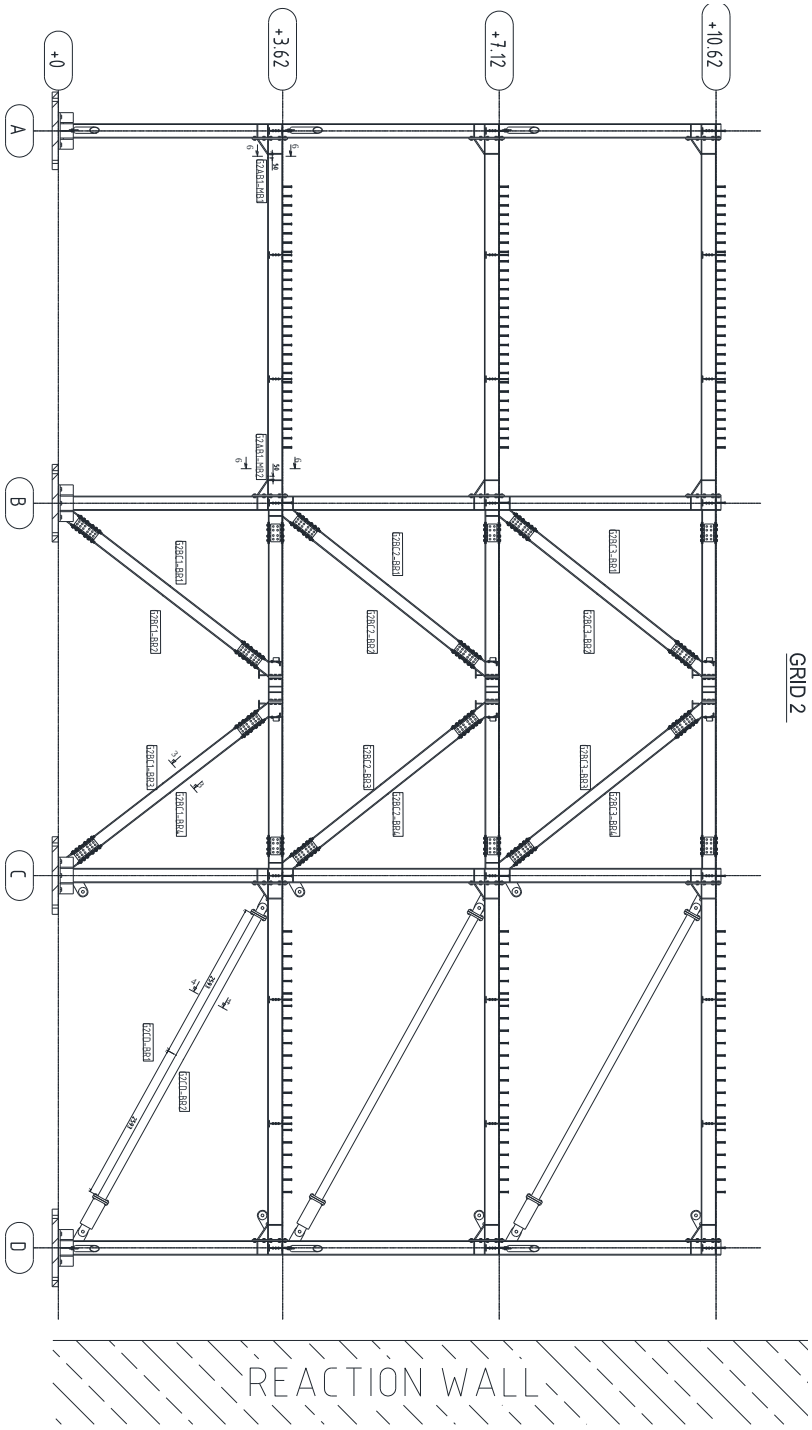

Fig. B-5. Strain gauges positions - S frame

ANNEX C

C.1. Snap-back test results

The frequencies measured during the snap back tests were obtained by means of two methodologies. The first one, based on modal filtering, involved the use of readings from displacement transducers placed in the longitudinal direction, resulting in frequencies equal to 2.6, 5.1 and 7.5 Hz for the first longitudinal, first transverse and second longitudinal modes, respectively, with a damping ratio of approximately 5% (Fig. C-1). The second method, based on automatic modal parameter selection, used readings from accelerometers and displacement transducers placed in the longitudinal and transverse direction (Fig. C-2 and Fig. C-3) with a higher sampling rate than that used in the first method. The modal frequencies and damping obtained for the first 16 modes are given in Fig. C-4, highlighting the main global modes. The mode shapes and frequencies for the first three longitudinal, two torsional and two transverse modes are given in Fig. C-5, Fig. C-6 and Fig. C-7, respectively.

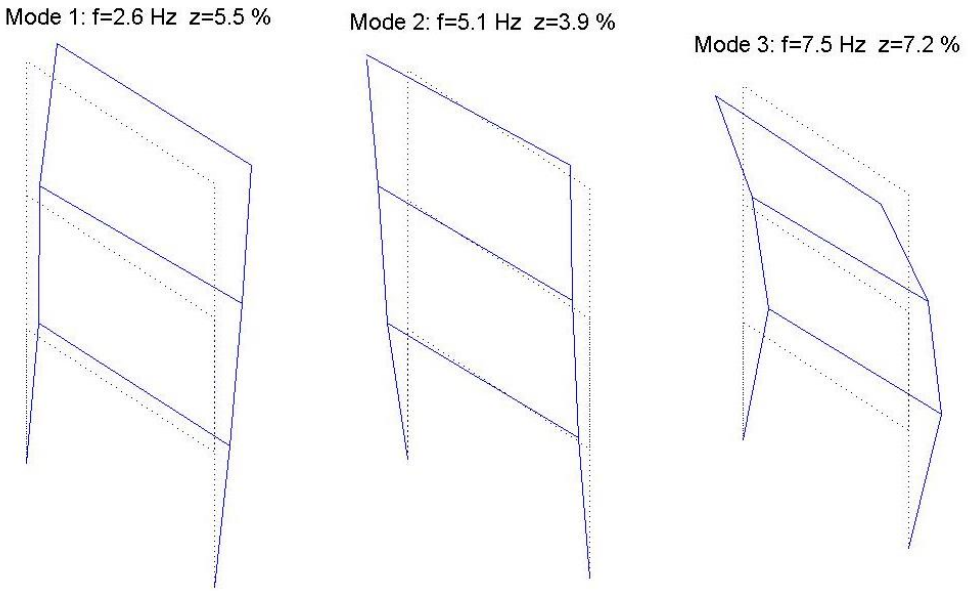

Fig. C-1. Mode shapes for snap back with ALGA dampers from LVDT readings [97]

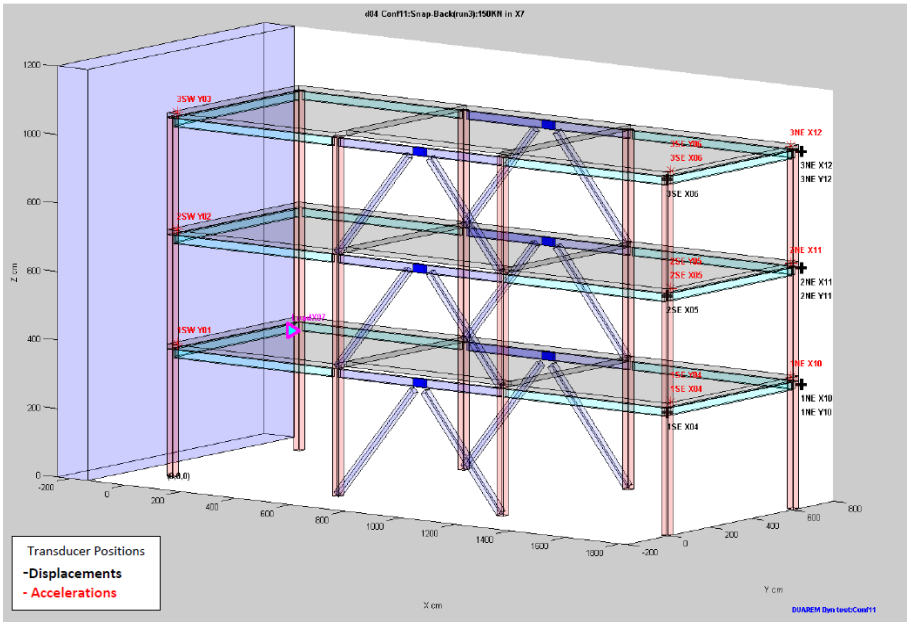

Fig. C-2. Location of transducers for the snap back test [97]

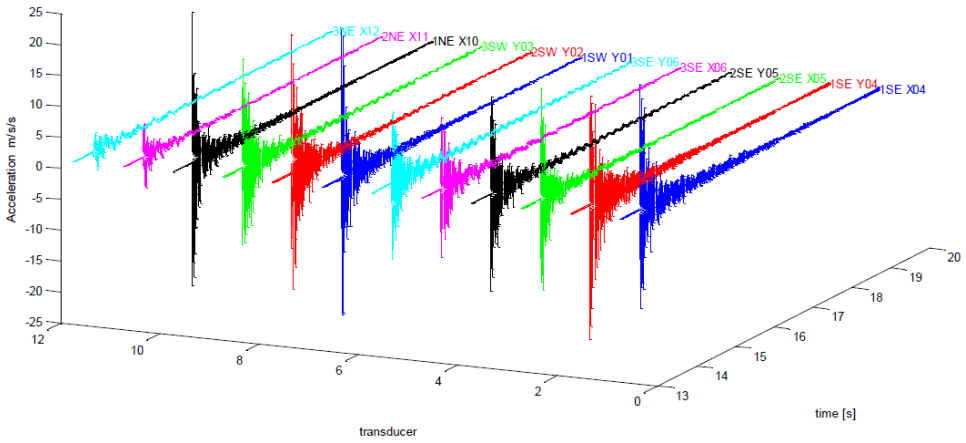

Fig. C-3. Accelerations measured during the snap back test [97]

It is possible to see that the two methods are in agreement with the frequencies of the first and second modes in the longitudinal direction, while there is a discrepancy in the identification of the frequency of the first transverse mode. The reason for this is that the first transverse mode is coupled with the first torsional mode, and the method based on displacement readings only in the longitudinal direction may not be sufficiently accurate for decoupling these two modes and identifying them separately.

The displacements of the frame during the snap back were also measured with a high speed camera using the target points shown in Fig. 4-15. After the snap back the seismic links were remounted on the frame and ready for the first PsD test.

DUAREM
16 Highest modes/FRF.
Minimum of. 3 values/mode
Dispersion limits=0.1 to 3 (%)
Results from Output: Acce.

Mode shapes representation: global modes

Solution Number:1

Mode Nb.	Freq. Hz)	Damp. (%)	Fre.Disp. (%)
01	2.653	8.07	1.43
02	2.891	2.78	0.0931
03	3.124	2.11	0.3
04	5.163	3.12	0.999
05	5.344	1.71	1.8
06	7.424	5.53	1.77
07	7.886	3.82	0.319
08	8.213	1.46	0.148
09	8.497	4.27	1.04
10	9.183	1.44	0.69
11	11.66	4.03	1.43
12	11.96	2.94	2.28
13	12.23	2.28	1.45
14	13.05	1.17	0.0138
15	13.87	3.11	2.05
16	13.97	2.78	1.47
17	14.40	1.05	2.05
18	16.28	0.579	0.175
19	16.85	0.466	0.716

Frequencies (Hz)		
Longitudinal	Torsional	Transverse
2.65		
		3.12
	5.16	
7.42		
11.7		
	12.2	
		14.0

Fig. C-4. Snap back test with dampers: Frequencies and damping for the first 16 modes and identification of the main global modes [97]

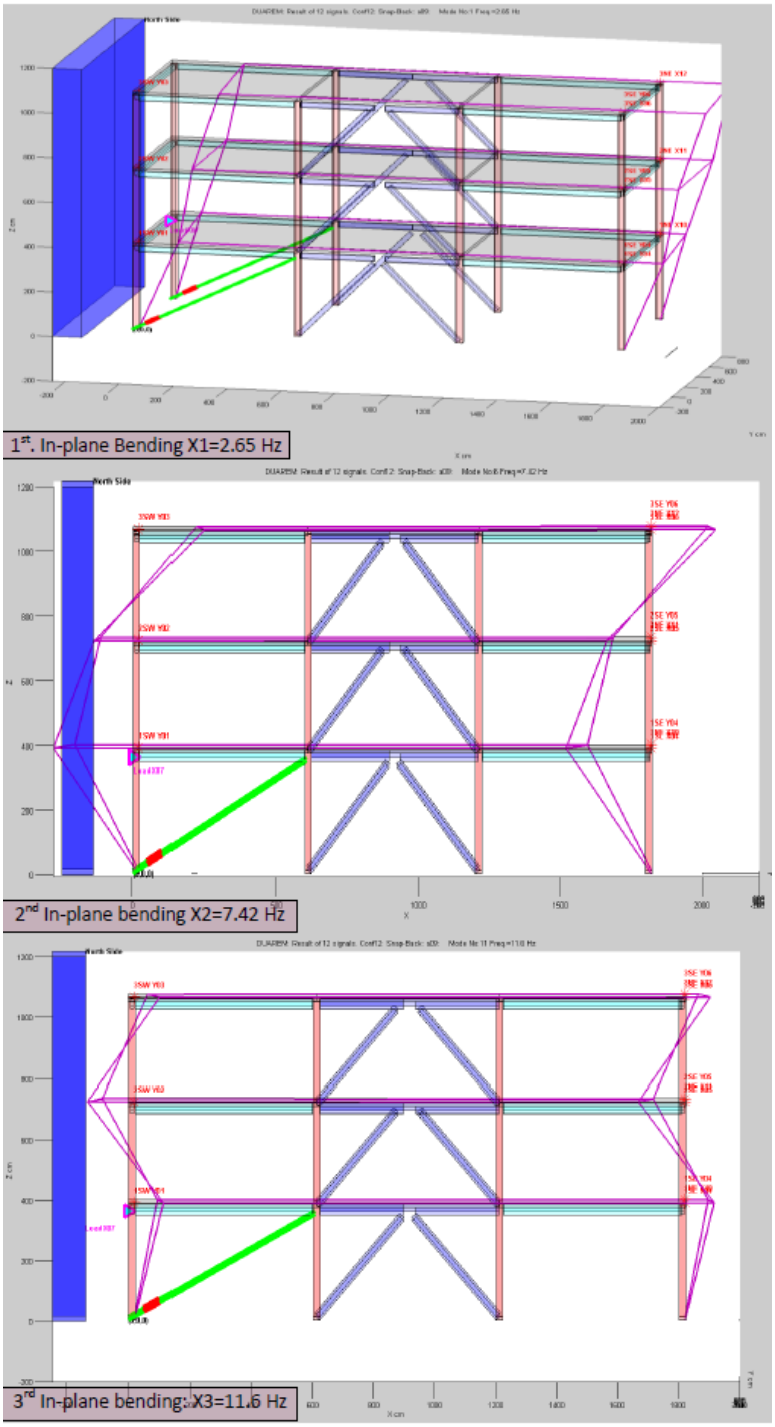

Fig. C-5. Snap back test: First three modes in the longitudinal direction [97]

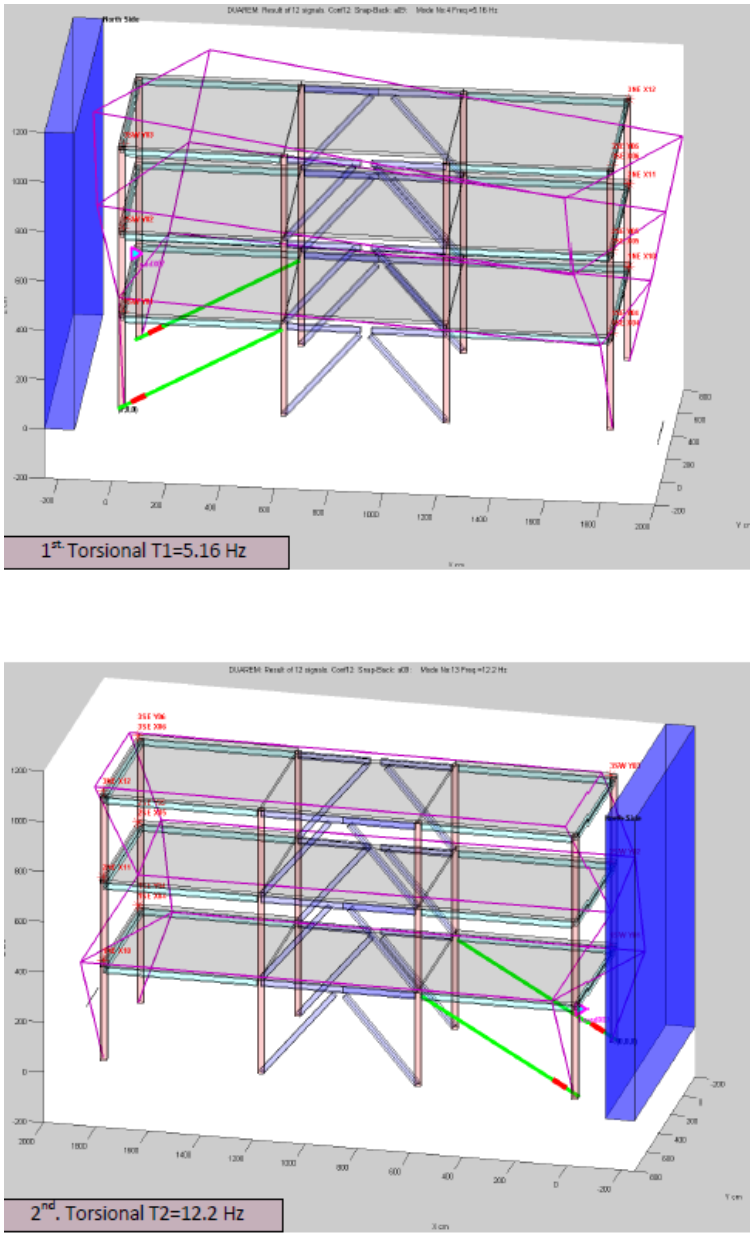

Fig. C-6. Snap back test: First two torsional modes [97]

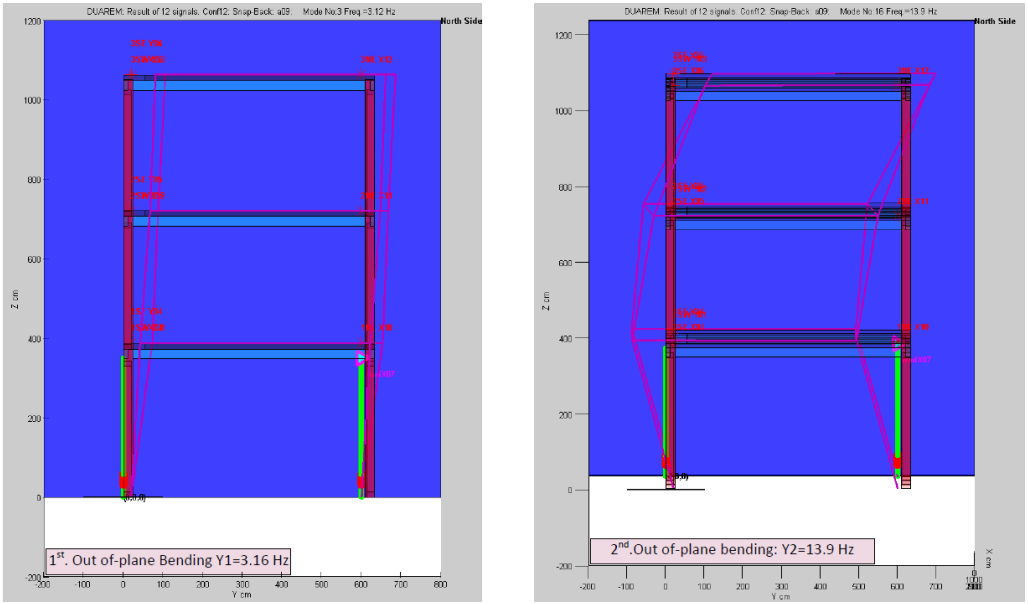

Fig. C-7. Snap back test: First two modes in the transverse direction [97]

C.2. FO1 test results

Some additional results for the first Full Operation test are presented in the following figures:

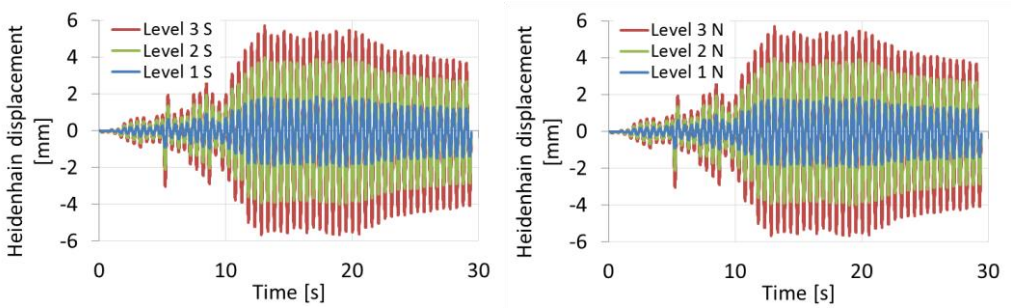

Fig. C-8. FO1 test - Heidenhain displacements for the S and N frames

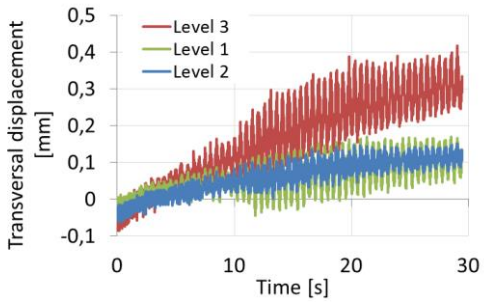

Fig. C-9. FO1 test – Transversal displacement

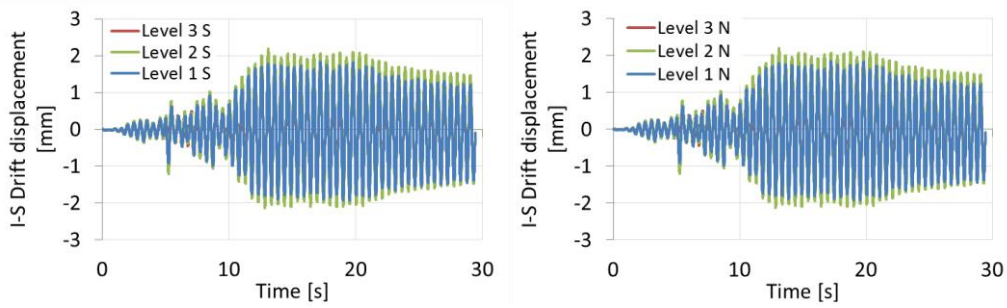

Fig. C-10. FO1 test – Inter-storey drift for the S and N frames

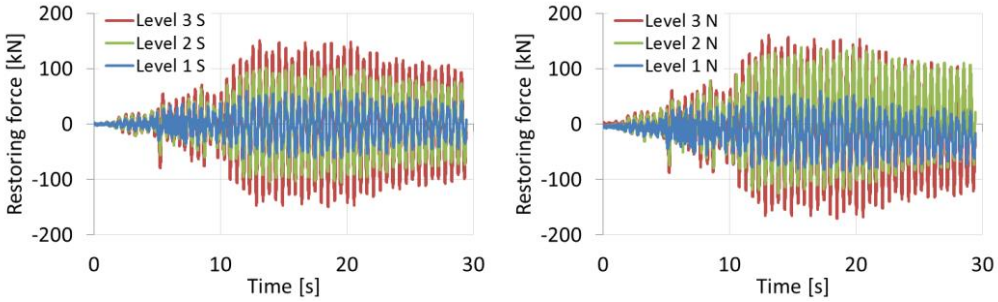

Fig. C-11. FO1 test – Restoring forces for the S and N frames

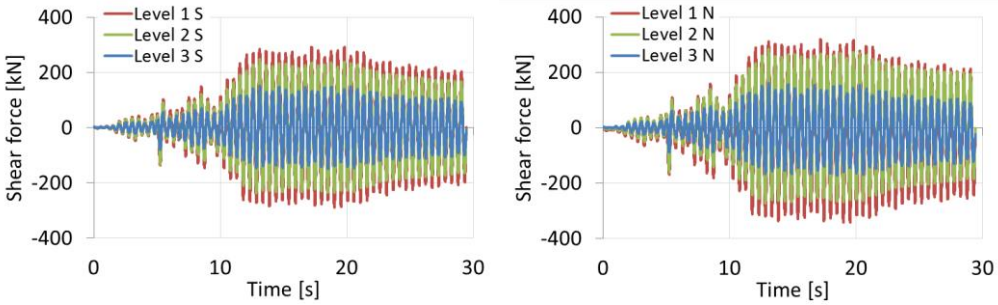

Fig. C-12. FO1 test – Shear forces for the S and N frames

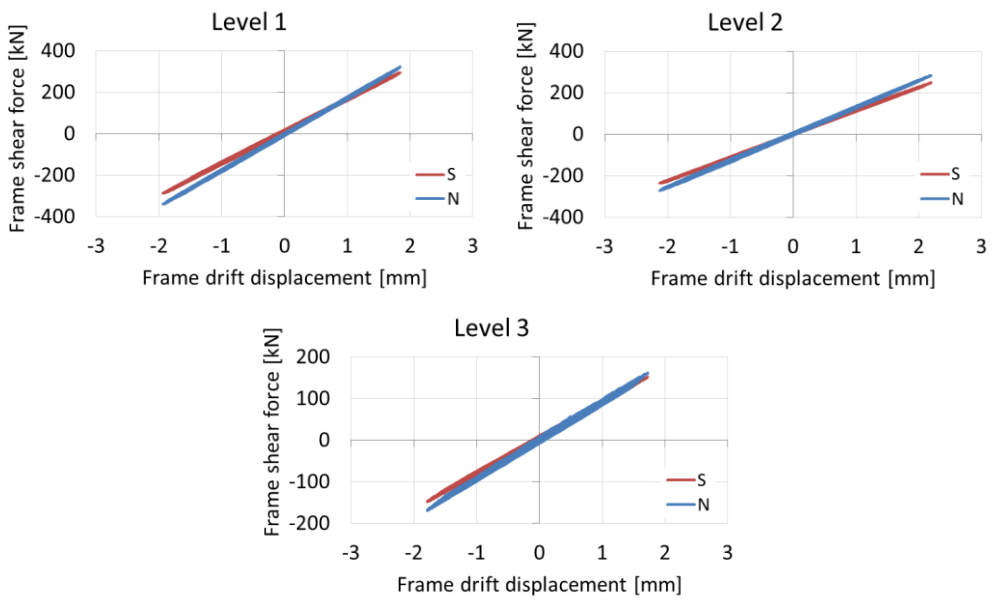

Fig. C-13. FO1 test – Frame shear force vs. frame drift displacement

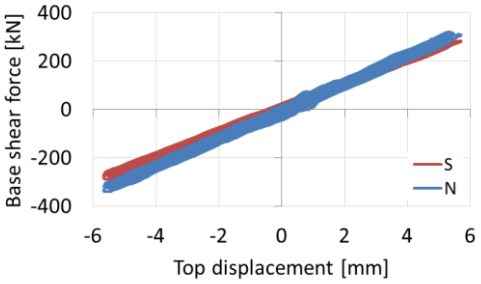

Fig. C-14. FO1 test – Base shear force vs. top displacement

C.3. DL/SLS test results

Some additional results for the Damage Limitation/Serviceability Limit State test are presented in the following figures:

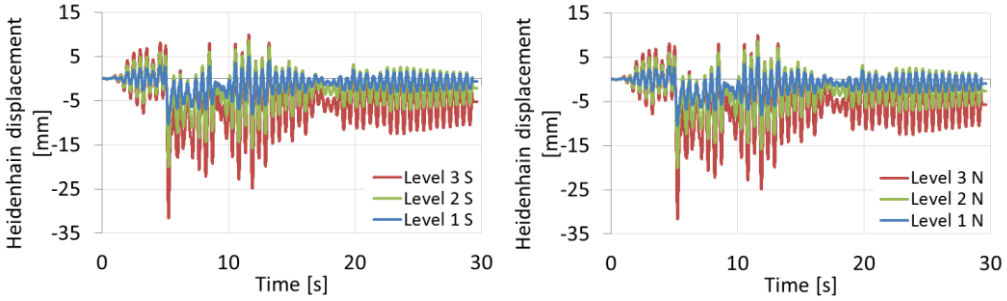

Fig. C-15. DL/SLS test - Heidenhain displacements for the S and N frames

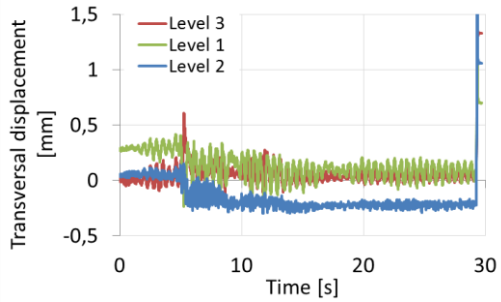

Fig. C-16. DL/SLS test – Transversal displacement

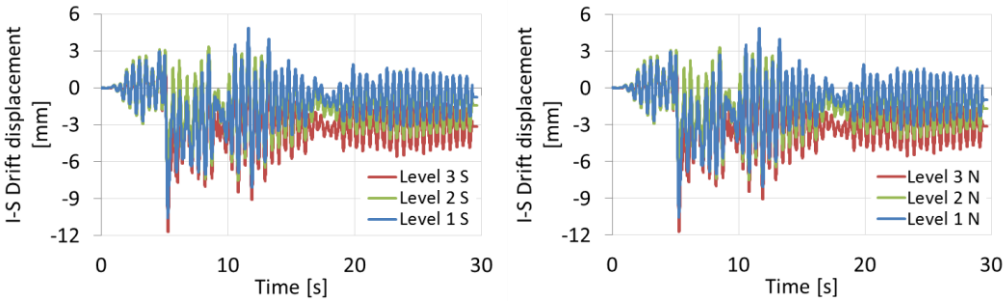

Fig. C-17. DL/SLS test – Inter-storey drift for the S and N frames

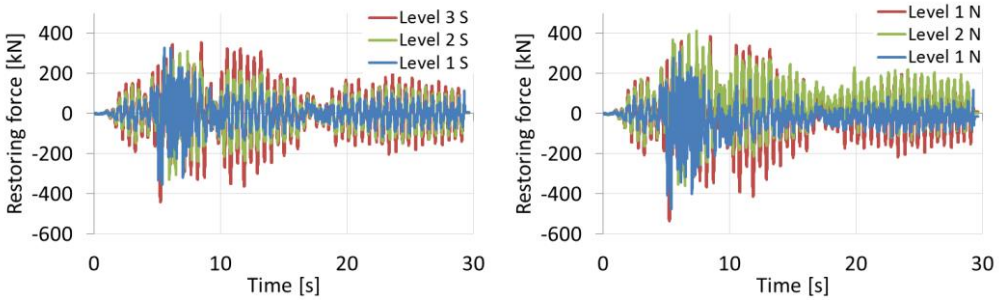

Fig. C-18. DL/SLS test – Restoring forces for the S and N frames

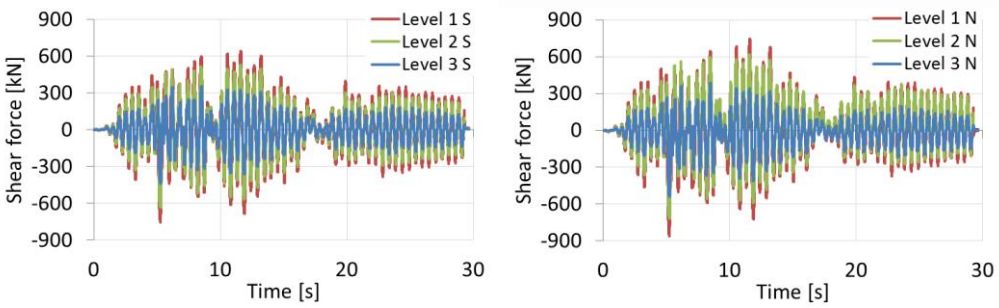

Fig. C-19. DL/SLS test – Shear forces for the S and N frames

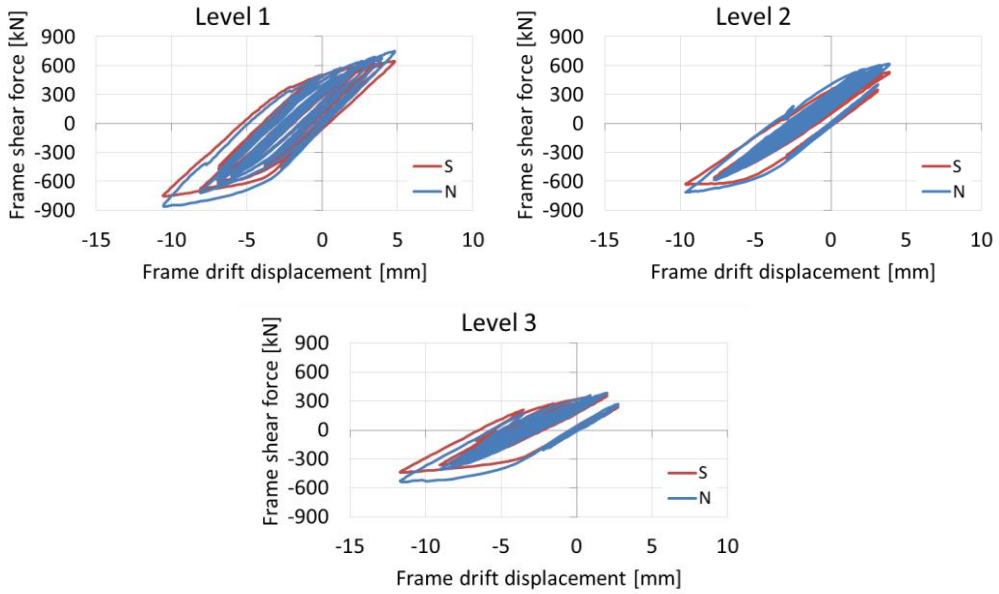

Fig. C-20. DL/SLS test – Frame shear force vs. frame drift displacement

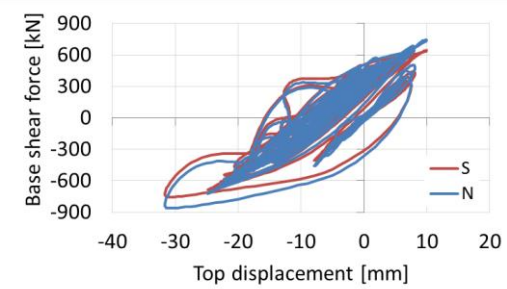

Fig. C-21. DL/SLS test – Base shear force vs. top displacement

C.4. SD/ULS test results

Some additional results for the Significant Damage/Ultimate Limit State test are presented in the following figures:

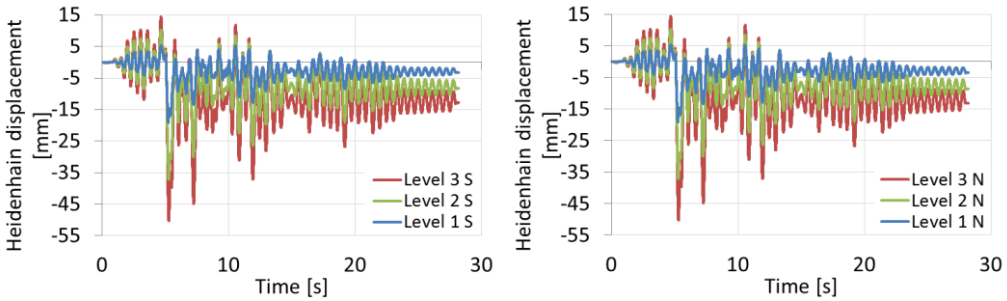

Fig. C-22. SD/ULS test - Heidenhain displacements for the S and N frames

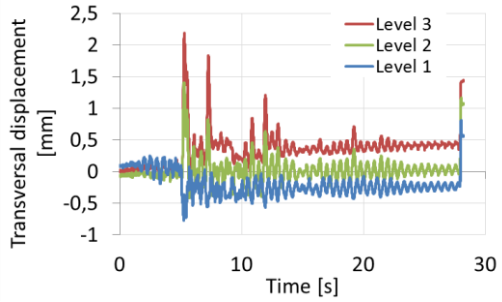

Fig. C-23. SD/ULS test - Transversal displacement

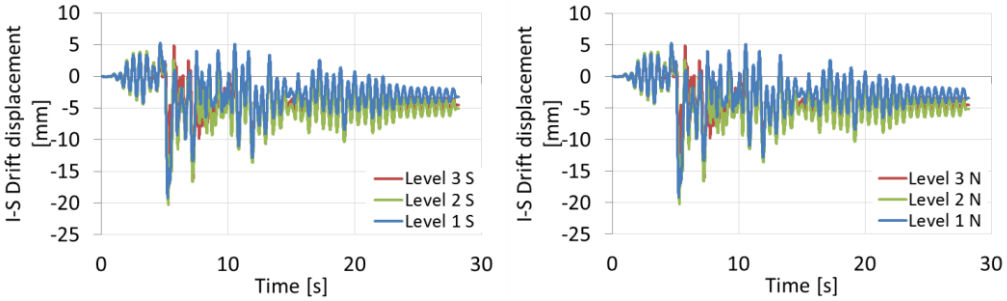

Fig. C-24. SD/ULS test - Inter-storey drift for the S and N frames

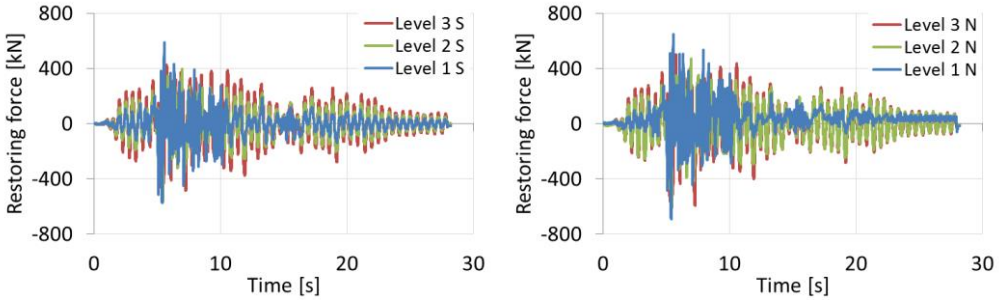

Fig. C-25. SD/ULS test - Restoring forces for the S and N frames

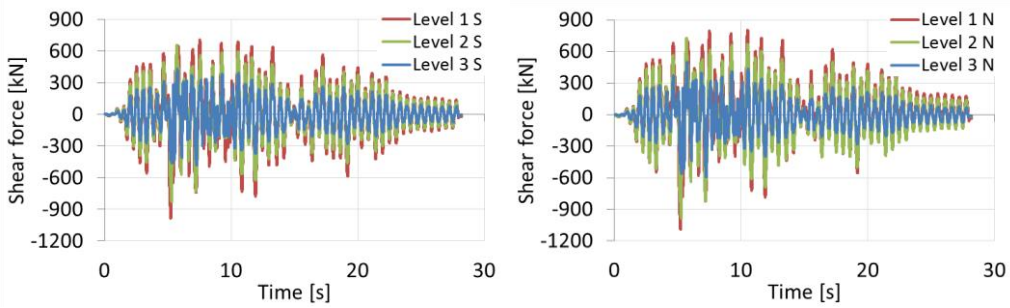

Fig. C-26. SD/ULS test - Shear forces for the S and N frames

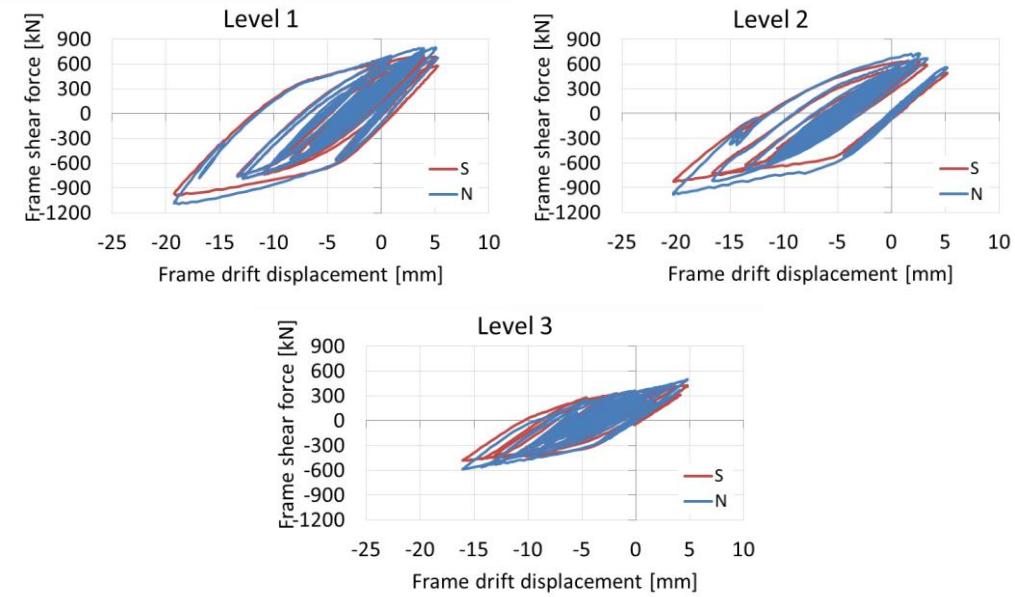

Fig. C-27. SD/ULS test - Frame shear force vs. frame drift displacement

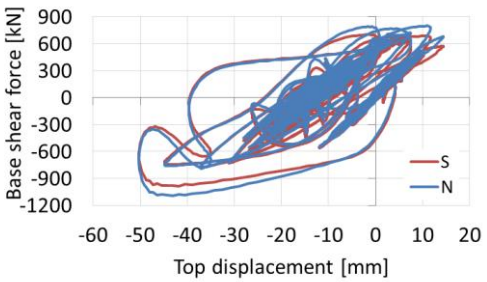

Fig. C-28. SD/ULS test - Base shear force vs. top displacement

C.5. PO1 test results

Some additional results for the first Push-Over test are presented in the following figures:

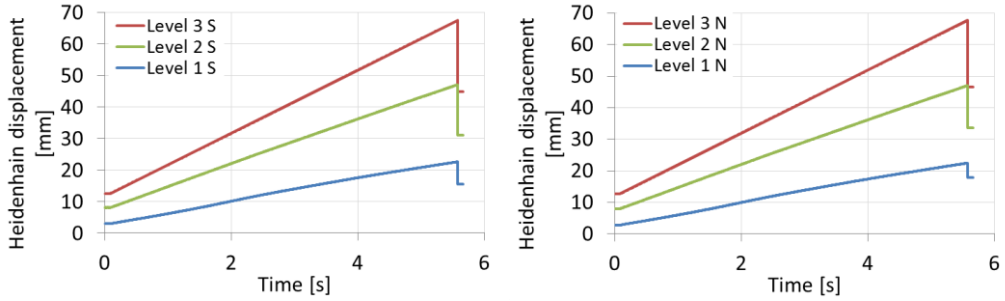

Fig. C-29. PO1 test - Heidenhain displacements for the S and N frames

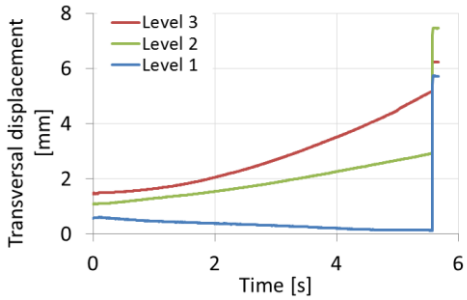

Fig. C-30. PO1 test - Transversal displacement

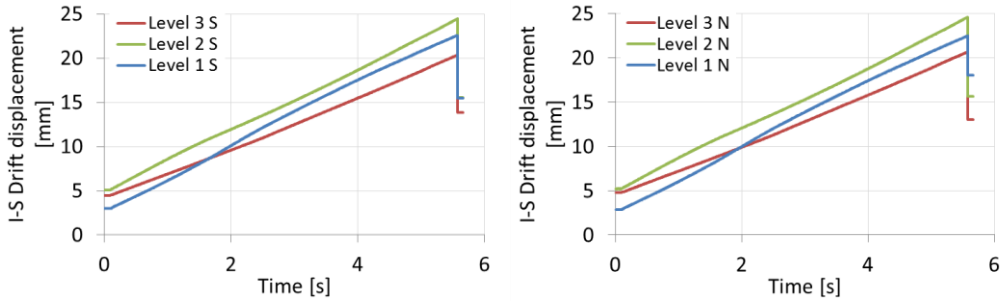

Fig. C-31. PO1 test - Inter-storey drift for the S and N frames

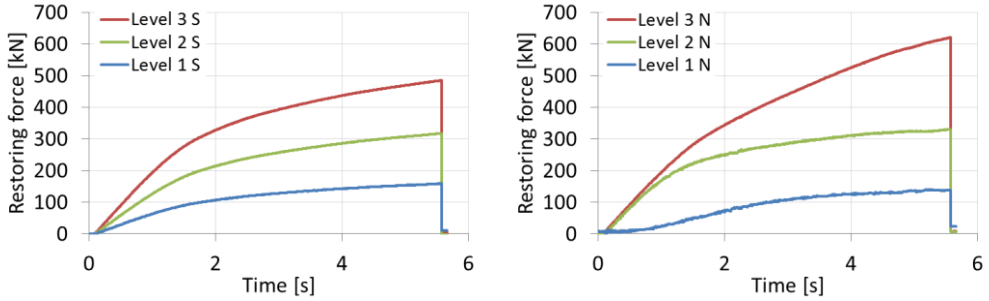

Fig. C-32. PO1 test - Restoring forces for the S and N frames

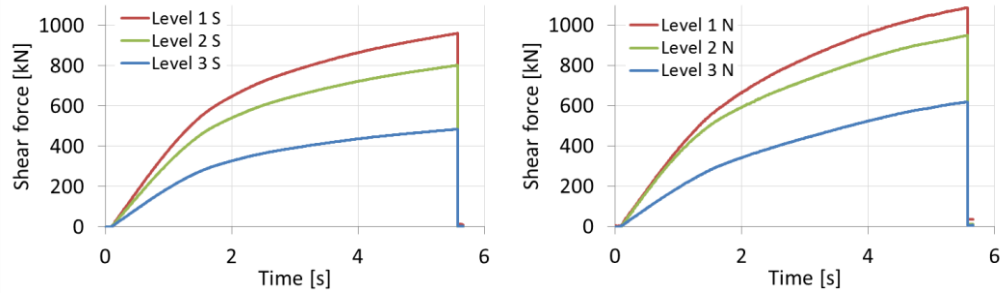

Fig. C-33. PO1 test - Shear forces for the S and N frames

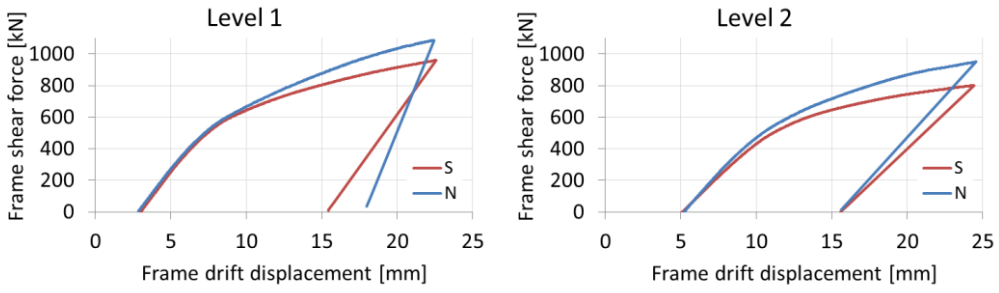

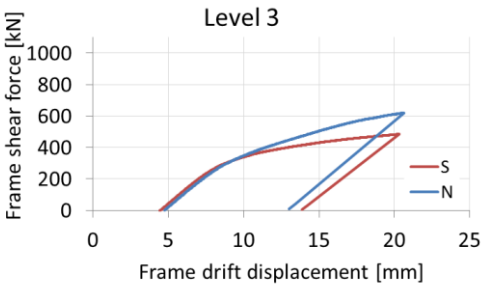

Fig. C-34. PO1 test - Frame shear force vs. frame drift displacement

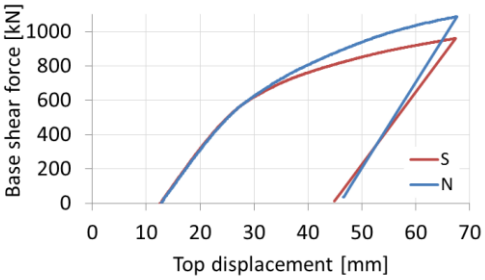

Fig. C-35. PO1 test - Base shear force vs. top displacement

C.6. NC test results

Some additional results for the Near Collapse test are presented in the following figures:

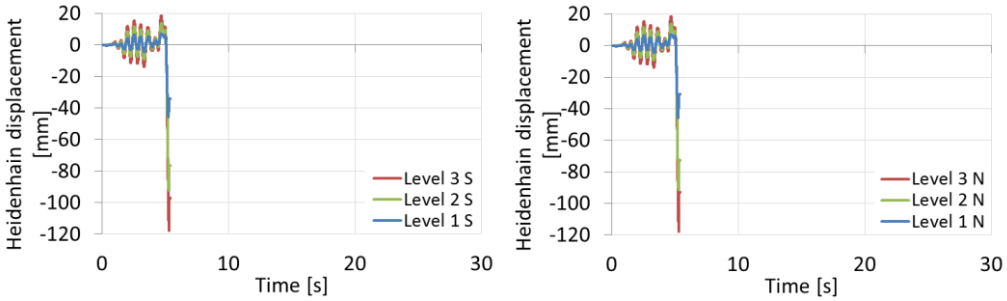

Fig. C-36. NC test - Heidenhain displacements for the S and N frames

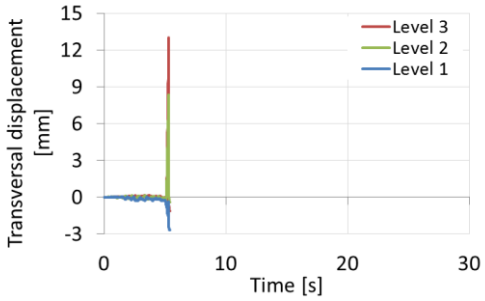

Fig. C-37. NC test - Transversal displacement

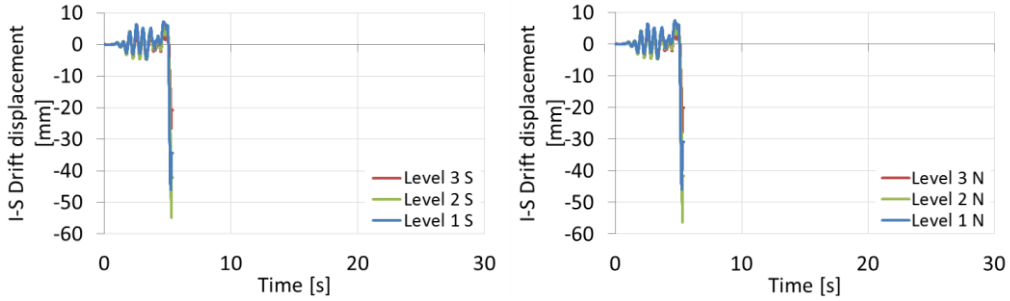

Fig. C-38. NC test - Inter-storey drift for the S and N frames

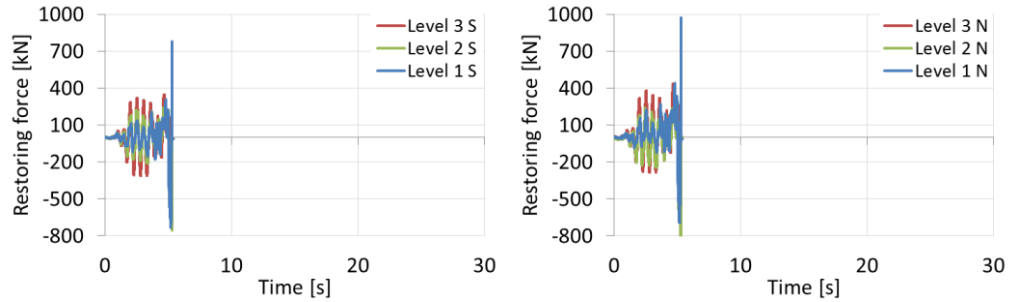

Fig. C-39. NC test - Restoring forces for the S and N frames

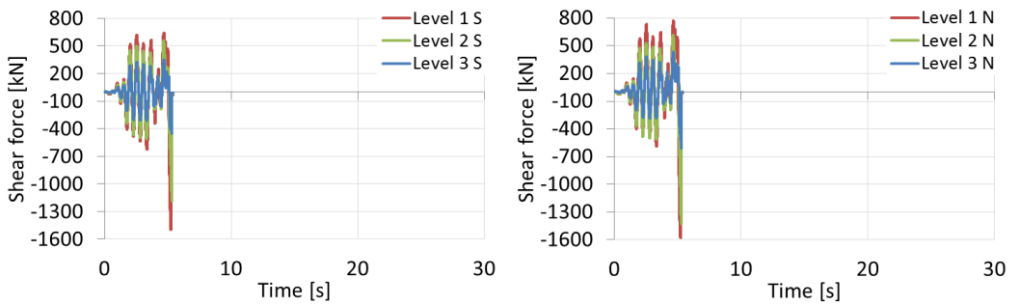

Fig. C-40. NC test - Shear forces for the S and N frames

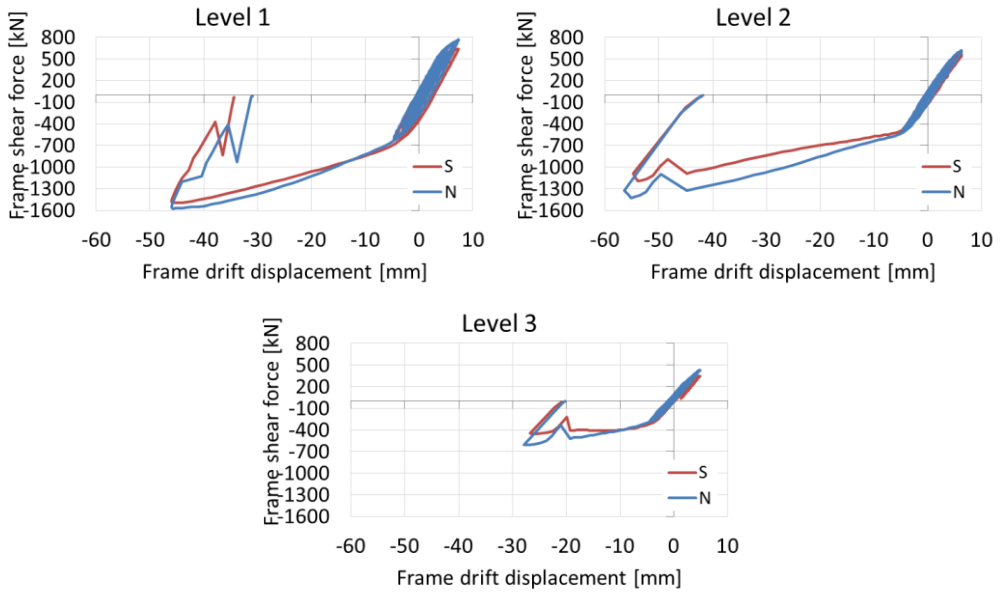

Fig. C-41. NC test - Frame shear force vs. frame drift displacement

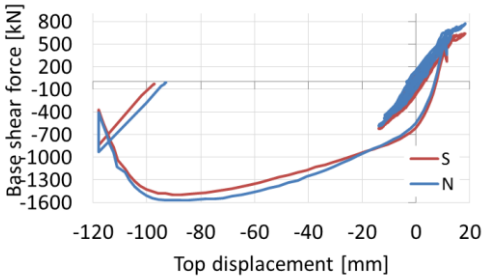

Fig. C-42. NC test - Base shear force vs. top displacement

C.7. PO2 test results

Some additional results for the Push-Over test, after the NC one, are presented in the following figures:

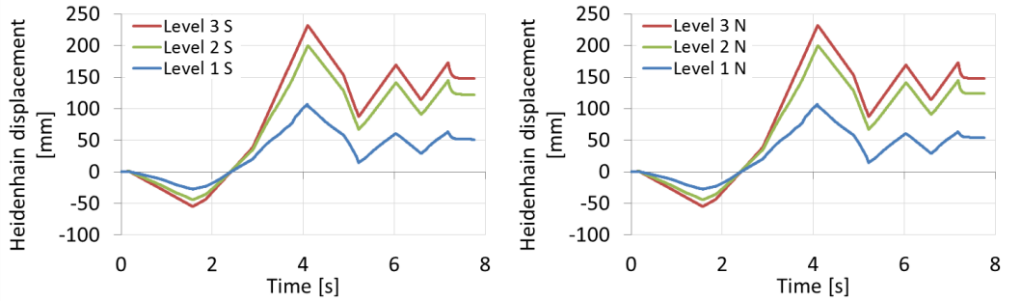

Fig. C-43. PO2 test - Heidenhain displacements for the S and N frames

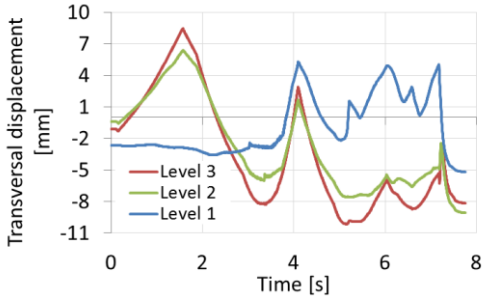

Fig. C-44. PO2 test - Transversal displacement

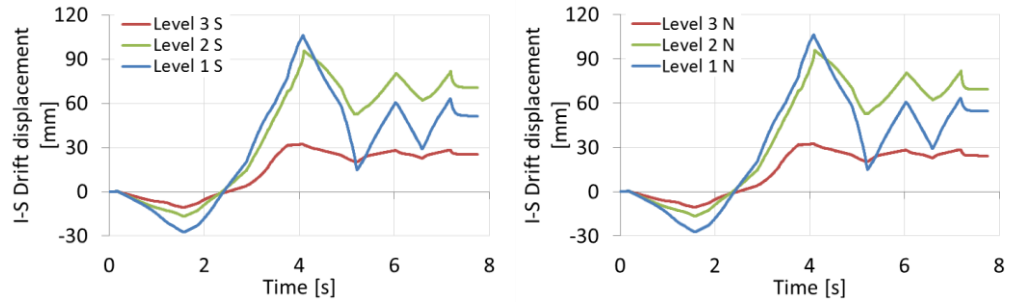

Fig. C-45. PO2 test - Inter-storey drift for the S and N frames

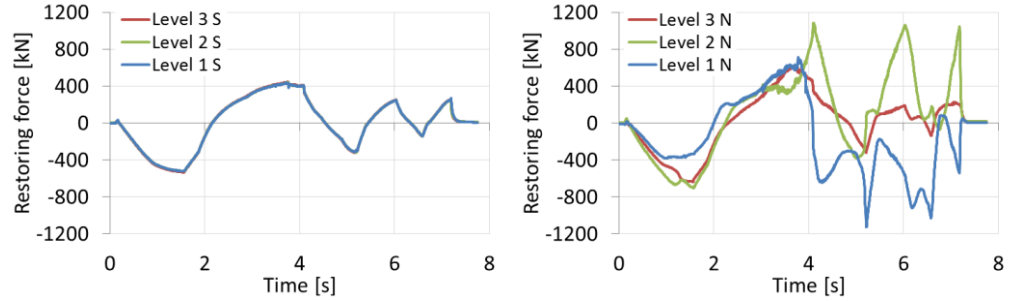

Fig. C-46. PO2 test - Restoring forces for the S and N frames

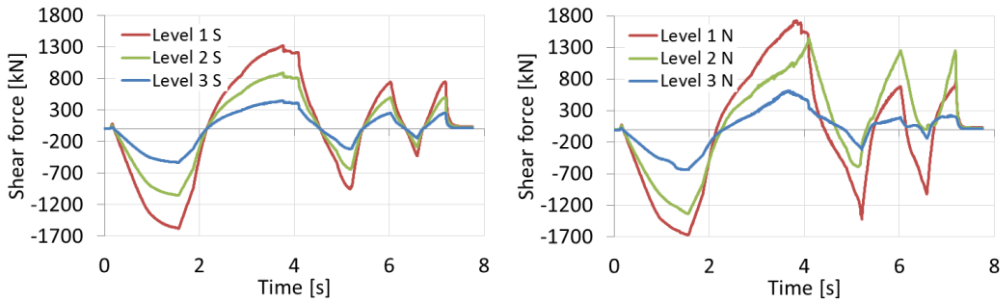

Fig. C-47. PO2 test - Shear forces for the S and N frames

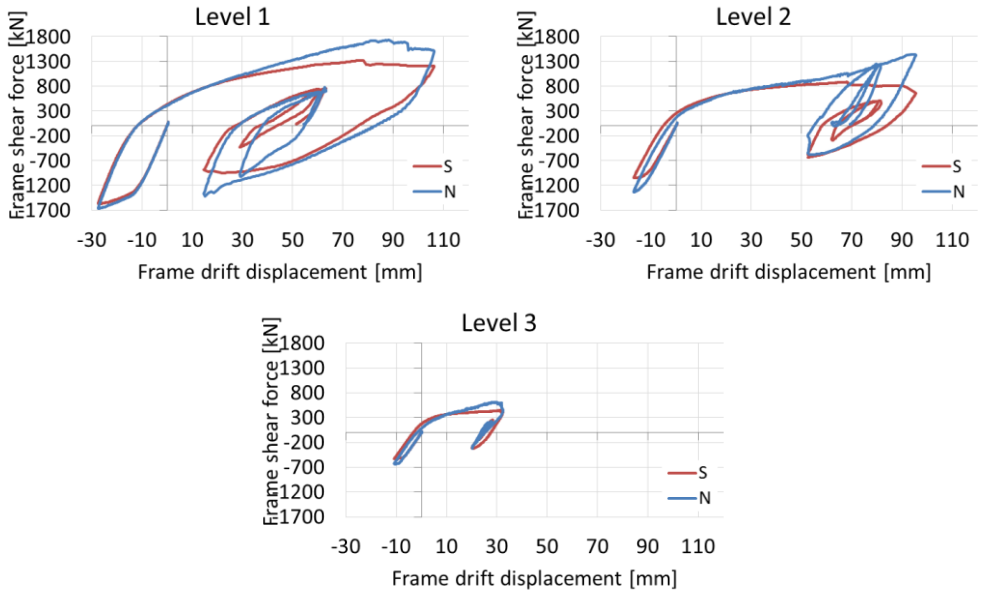

Fig. C-48. PO2 test - Frame shear force vs. frame drift displacement

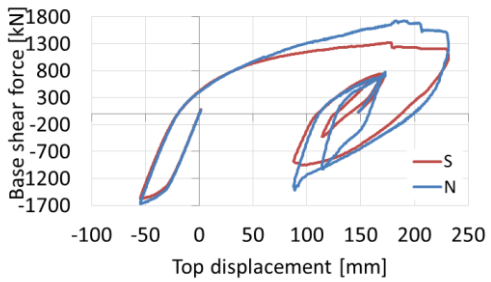

Fig. C-49. PO2 test - Base shear force vs. top displacement

C.8. PO3 test results

Some additional results for the final cyclic Push-Over test are presented in the following figures:

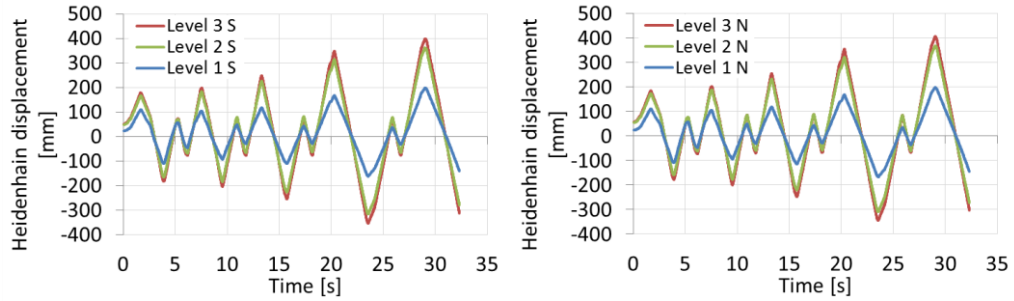

Fig. C-50. PO3 test - Heidenhain displacements for the S and N frames

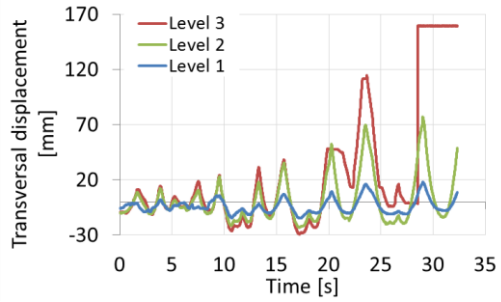

Fig. C-51. PO3 test - Transversal displacement

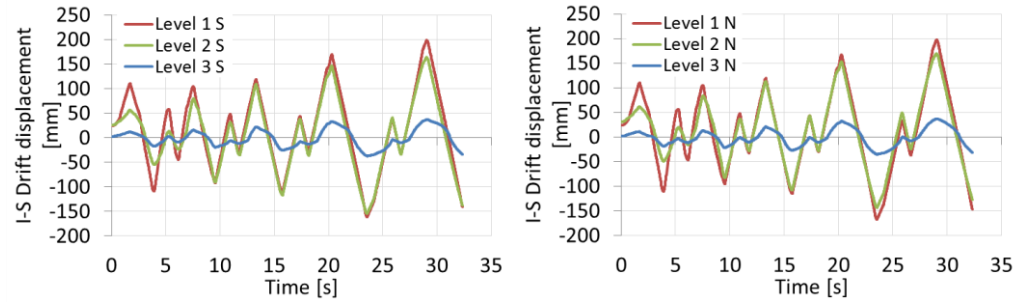

Fig. C-52. PO3 test - Inter-storey drift for the S and N frames

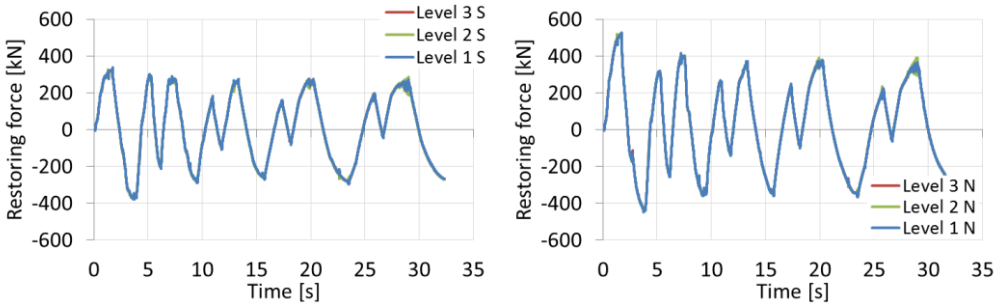

Fig. C-53. PO3 test - Restoring forces for the S and N frames

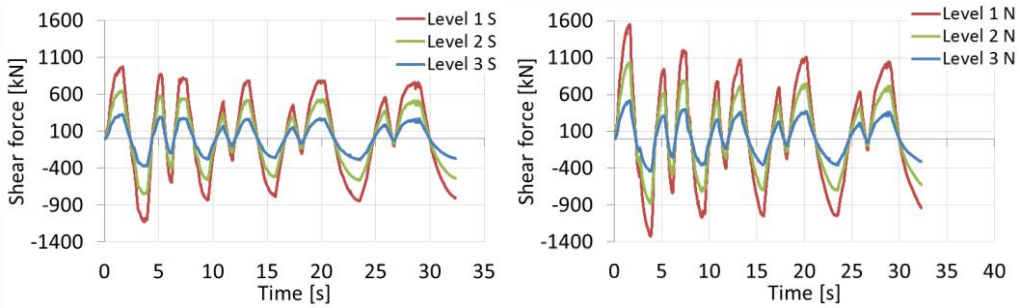

Fig. C-54. PO3 test - Shear forces for the S and N frames

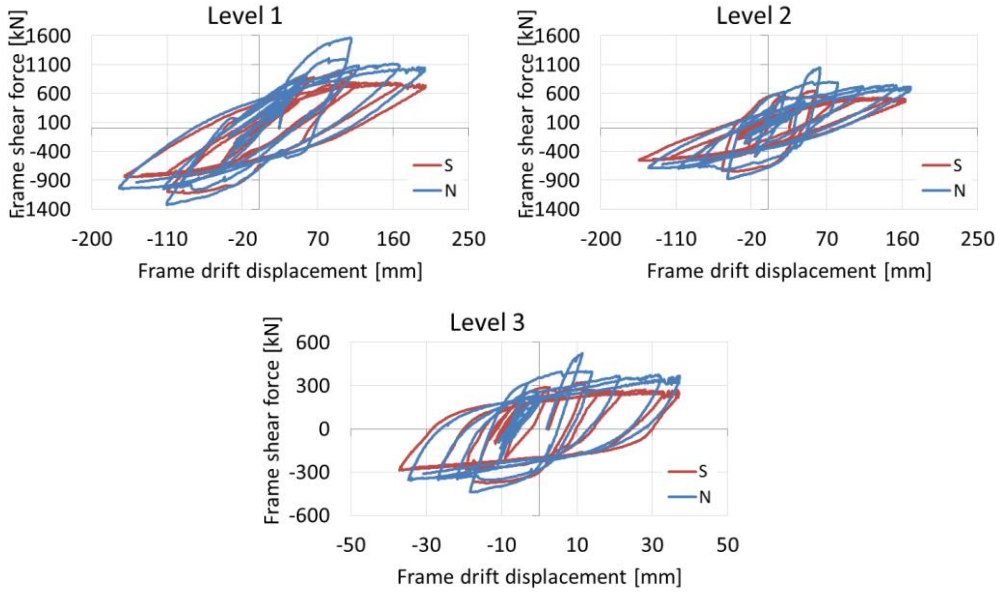

Fig. C-55. PO3 test - Frame shear force vs. frame drift displacement

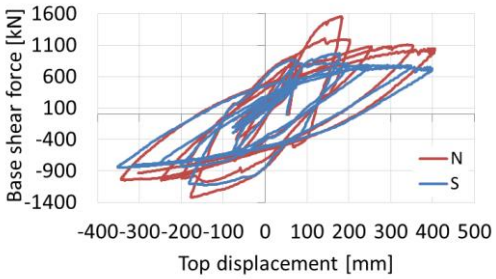

Fig. C-56. PO3 test - Base shear force vs. top displacement

C.9. All tests results

Maximum and residual values for all the PsD tests are presented in the following tables:

Table C-1. Maximum link rotation

TEST	Maximum link rotation [rad]					
	S			N		
	1	2	3	1	2	3
FO1	0,001	0,001	0,001	0,001	0,001	0,001
DL	0,028	0,018	0,032	0,026	0,020	0,031
FO2	0,002	0,001	0,001	0,002	0,002	0,001
SD	0,061	0,057	0,050	0,055	0,058	0,049
PO1	0,074	0,075	0,066	0,069	0,075	0,064
FO3	0,002	0,001	0,001	0,002	0,002	0,001
NC	0,164	0,185	0,094	0,152	0,186	0,092
PO2	0,240	0,198	0,110	0,247	0,194	0,102
PO3	0,172	0,282	0,128	0,173	0,379	0,124

Table C-2. Residual link rotation

TEST	Residual link rotation [rad]					
	S			N		
	1	2	3	1	2	3
FO1	0,000	0,000	0,000	0,000	0,000	0,000
DL	0,003	0,006	0,013	0,003	0,008	0,014
FO2	0,000	0,000	0,000	0,000	0,000	0,000
SD	0,013	0,021	0,019	0,011	0,022	0,019
PO1	0,066	0,065	0,060	0,053	0,065	0,056
FO3	0,001	0,001	0,001	0,001	0,001	0,001
NC	0,145	0,171	0,089	0,131	0,167	0,085
PO2	0,146	0,115	0,009	0,177	0,124	0,008
PO3	0,145	0,112	0,004	0,173	0,117	0,000

Table C-3. Maximum link shear force

TEST	Maximum link shear force [kN]					
	S			N		
	1	2	3	1	2	3
FO1	181	164	97	-200	170	-107
DL	-399	-398	-230	-472	-433	-288
FO2	160	149	97	-156	-137	-92
SD	478	-477	-250	-556	-546	-311
PO1	-447	-469	-245	-559	-556	-307
FO3	156	127	88	-176	-161	97
NC	-604	-619	-271	-694	-720	-375
PO2	-603	-614	292	-757	742	-377
PO3	257	492	-334	514	814	-446

Table C-4. Residual link shear force

TEST	Residual link shear force [kN]					
	S			N		
	1	2	3	1	2	3
FO1	13	16	6	-4	3	-21
DL	10	1	15	5	8	16
FO2	24	29	21	6	0	-10
SD	18	30	22	4	11	5
PO1	74	26	46	102	-15	34
FO3	14	4	7	-22	-24	11
NC	186	85	23	152	88	-13
PO2	-12	-84	53	-95	-100	78
PO3	22	72	-9	72	62	-48

Table C-5. EBF braces and MRF beams yielding

TEST	Maximum brace strain	Maximum MRF beam strain	Residual brace strain	Residual MRF beam strain
	Yield at 0.00181	Yield at 0.00186	Yield at 0.00181	Yield at 0.00186
FO1	0,00000	-	0,00000	-
DL	0,00045	-	-0,00004	-
FO2	0,00018	0,00015	0,00006	0,00003
SD	-0,00054	0,00101	0,00006	0,00017
PO1	0,00060	0,00127	0,00027	0,00089
FO3	0,00022	0,00014	0,00009	0,00004
NC	-0,00085	**-0,00543**	-0,00046	**-0,00543**
PO2	-0,00098	**-0,00563**	0,00027	**-0,00566**
PO3	-0,00104	**-0,00738**	-0,00025	**-0,00521**

Table C-6. EBF braces and beams deformations

TEST	Braces maximum deformation [mm]		Braces residual deformation [mm]		EBF beams maximum deformation [mm]	EBF beams residual deformation [mm]
	S	N	S	N		
FO1	-0,150	-0,160	-0,068	-0,052	-0,075	-0,017
DL	-0,328	0,388	-0,214	0,179	-0,169	0,016
LR1	-0,212	0,231	-0,148	0,216	0,148	0,138
FO2	-0,103	-0,130	-0,070	0,035	-0,058	0,010

TEST	Braces maximum deformation [mm]		Braces residual deformation [mm]		EBF beams maximum deformation [mm]	EBF beams residual deformation [mm]
	S	N	S	N		
SD	-0,340	-0,430	-0,098	0,058	-0,218	-0,023
PO1	-0,341	-0,457	-0,067	-0,083	-0,180	-0,034
FO3	-0,127	-0,152	0,080	-0,107	-0,070	-0,034
NC	-0,525	-0,606	0,095	-0,104	-0,216	0,120
PO2	0,678	-0,694	0,484	-0,248	-0,373	-0,243
PO3	24,444	1,853	-	**1,658**	-0,195	0,082

Table C-7. Joint zones rotations

TEST	Maximum joint zone rotations [mrad] - S				Maximum joint zone rotations [mrad] - N			
	Beam-column marginal	Beam-column middle	Column base marginal	Column base middle	Beam-column marginal	Beam-column middle	Column base marginal	Column base middle
FO1	1	-1	1	-1	-1	3	-1	1
DL	4	-5	3	4	3	-9	-4	-4
LR1	-1	-6	0	0	0	3	0	0
FO2	-1	1	1	1	1	2	-1	-1
SD	8	-9	6	8	-7	-12	-7	-7
PO1	9	-12	8	9	-9	-20	-8	-9
FO3	1	1	1	-1	-1	3	1	1
NC	21	-25	15	17	-22	-31	-15	-15
PO2	22	32	-27	-26	25	55	27	27
PO3	65	-89	65	67	-69	-84	-66	-63

Table C-8. Maximum longitudinal displacements

TEST	Peak longitudinal displacements (heidenhains) [mm]					
	S			N		
	1	2	3	1	2	3
FO1	-1,9	-4,0	5,7	-1,9	-4,0	5,7
DL	-10,6	-20,0	-31,7	-10,5	-20,0	-31,6
LR1	-2,0	-3,3	-6,4	-1,2	-3,0	-6,2
FO2	-1,7	3,4	5,0	-1,6	3,4	5,0
SD	-19,2	-37,1	-50,3	-19,2	-37,1	-50,3
PO1	-22,6	-47,0	-67,4	-22,5	-47,0	-67,6
LR2	-15,9	-31,4	-45,1	-17,8	-33,5	-46,6
FO3	1,8	3,8	5,4	1,8	3,8	5,4
NC	-45,9	-92,4	-118,0	-45,9	-91,4	-118,1
PO2	106,4	199,6	231,6	106,5	199,6	231,6
PO3	198,7	362,5	399,4	198,1	368,1	405,3

Table C-9. Residual longitudinal displacements

TEST	Residual longitudinal displacements (heidenhains) [mm]					
	S			N		
	1	2	3	1	2	3
FO1	-0,1	-0,2	-0,4	-0,1	-0,2	-0,4
DL	-0,7	-2,2	-5,3	-1,0	-2,6	-5,8
LR1	0,4	0,7	-0,1	-1,0	-2,7	-5,0
FO2	0,1	0,2	0,2	0,1	0,2	0,2
SD	-3,2	-8,3	-12,8	-3,5	-8,7	-13,2

TEST	Residual longitudinal displacements (heidenhains) [mm]					
	S			N		
	1	2	3	1	2	3
PO1	-15,5	-31,0	-44,9	-18,0	-33,6	-46,6
LR2	-2,2	-4,4	-8,8	-4,0	-9,7	-16,0
FO3	-1,1	-2,4	-3,5	-1,1	-2,4	-3,5
NC	-34,3	-76,5	-97,2	-31,0	-72,7	-92,9
PO2	51,4	122,0	147,5	54,4	123,7	147,9
PO3	-140,4	-278,2	-312,1	-146,3	-272,9	-303,8

Table C-10. Transversal displacements

TEST	Peak transversal displacements [mm]			Residual transversal displacements [mm]		
	1	2	3	1	2	3
FO1	0,170	0,152	0,418	0,134	0,133	0,334
DL	1,373	1,689	1,756	0,698	1,059	1,327
LR1	2,210	6,785	11,484	1,954	6,019	9,122
FO2	0,123	-0,152	-0,141	0,004	-0,119	-0,098
SD	0,807	1,406	2,193	0,578	1,081	1,444
PO1	5,737	7,467	6,242	5,720	7,455	6,230
LR2	10,742	21,188	26,899	-0,362	5,541	11,038
FO3	0.123	0.205	0.297	0.026	0.198	0.170
NC	-2,678	8,373	13,036	-2,678	-0,392	-1,117
PO2	7.943	-8.693	9.574	-2.510	-8.693	-7.050
PO3	18,268	77,138	159,616	9,021	49,000	159,479

Table C-11. Maximum inter-storey drifts

TEST	Peak inter-storey drifts [mm]					
	S			N		
	1	2	3	1	2	3
FO1	-2	2	-2	-2	2	-2
DL	-11	-10	-12	-11	-10	-12
LR1	-2	-2	-4	-1	-2	-3
FO2	-2	-2	2	-2	-2	2
SD	-19	-20	-16	-19	-20	-16
PO1	-23	-24	-20	-22	-25	-21
LR2	-16	-15	-14	-18	-16	-13
FO3	2	2	-2	2	2	-2
NC	-46	-55	-27	-46	-56	-28
PO2	106	96	32	106	96	32
PO3	199	164	37	198	170	37

Table C-12. Residual inter-storey drifts

TEST	Residual inter-storey drifts [mm]					
	S			N		
	1	2	3	1	2	3
FO1	0	0	0	0	0	0
DL	-1	-1	-3	-1	-2	-3
LR1	0	0	-1	-1	-2	-2
FO2	0	0	0	0	0	0
SD	-3	-5	-5	-3	-5	-5
PO1	-15	-16	-14	-18	-16	-13

TEST	Residual inter-storey drifts [mm]					
	S			N		
	1	2	3	1	2	3
LR2	-2	-2	-4	-4	-6	-6
FO3	-1	-1	-1	-1	-1	-1
NC	-34	-42	-21	-31	-42	-20
PO2	51	71	25	54	69	24
PO3	-140	-138	-34	-146	-127	-31

Table C-13. Frame forces

TEST	Frame forces [kN]					
	S			N		
	1	2	3	1	2	3
FO1	65	106	151	-85	139	-170
DL	-353	-330	-440	-475	413	-537
LR1	-12	-7	-12	-12	-12	-9
FO2	67	-100	135	59	-145	148
SD	587	-563	-484	-690	-609	-591
PO1	-159	-317	-485	-141	-330	-620
LR2	-	-	-	-	-	-
FO3	-63	-102	143	58	-136	-150
NC	780	-754	-457	975	-858	-609
PO2	-523	-523	-533	-1129	1081	-637
PO3	-379	-377	-378	526	525	523

Table C-14. Frame shear forces

TEST	Frame shear forces [kN]					
	S			N		
	1	2	3	1	2	3
FO1	293	249	151	-341	284	-170
DL	-755	-634	-440	-863	-718	-537
LR1	-29	-17	-12	-26	-20	-9
FO2	-242	199	135	-261	-239	148
SD	-984	-829	-484	-1092	-988	-591
PO1	-961	-802	-485	-1088	-950	-620
LR2	-	-	-	-	-	-
FO3	269	228	143	-284	-249	-150
NC	-1495	-1190	-457	-1575	-1427	-609
PO2	-1579	-1056	-533	1726	1442	-637
PO3	-1128	-754	-378	1558	1042	523

REFERENCES

[1] EN1998-1-1, Eurocode 8, Design of structures for earthquake resistance - Part 1, General rules, seismic actions and rules for buildings, CEN, European Committee for Standardization, 2004;

[2] Stratan A., „Dual multi-storey steel frame buldings in seismic areas behaviour study", PhD Thesis, 2003;

[3] A. Ioan, A. Stratan and D. Dubina, „Numerical simulation of bolted links removal in eccentrically braced frames", Pollack Periodica, vol. 8, no.1, ISSN 1788-1994, pp. 15-26, 2013;

[4] Constantinou M. C., Symans M. D., "Experimental study of seismic response of buildings with supplemental fluid dampers." Struct. Des. Tall Build., 2(2), 93–132, 1993a;

[5] Whittaker A. S., Aiken I. D., Bergman D., Clark P. W., Cohen J., Kelly J. M., Scholl R. E., "Code requirements for design and implementation of passive energy dissipation systems." Proc., ATC-17–1 Seminar on Seismic Isolation, Passive Energy Dissipation, and Active Control, Vol. 2, ATC, Redwood City, Calif., 497–508, 1993;

[6] Marshall J. D., "Development, Analysis and Testing of a Hybrid Passive Control Device for Seismic Protection of Framed Structures" PhD Thesis, Faculty of Virginia Polytechnic Institute and State University, Blacksburg, Virginia, 2008;

[7] DesRoches R., Smith B., "Shape Memory Alloys in Seismic Resistant Design and Retrofit: A Critical Review of Their Potential and Limitations." Journal of Earthquake Engineering, 8(3), 415-429, 2004;

[8] Wilson J. C., Wesolowsky M. J., "Shape Memory Alloys for Seismic Response Modification: A State-of-the-Art Review." Earthquake Spectra, 21(2), 569-601, 2005;

[9] Aiken I. D., Kelly J. M., Pall A. S., "Seismic Response of a Nine-Story Steel Frame with Friction-Damped Cross-Bracing." Earthquake Engineering Research Center, University of California, Berkeley, Berkeley, CA, 1988;

[10] Symans M. D., Charney F. A., Whittaker A. S., Constantinou M. C., Kircher C. A., Johnson M. W., McNamara R. J., "Energy Dissipation Systems for Seismic Applications: Current Practice and Recent Developments", Journal of Structural Engineering, 134:1(3), 3–21, 2008;

[11] Chang, C., Pall, A., and Louie, J. 2006 . "The use of friction dampers for seismic retrofit of the Monterey County Government Center." Proc., 8th U. S. National Conf. on Earthquake Engineering, EERI, Oakland, Calif., Paper No. 951.;

[12] Shao, D., Pall, A., and Soli, B. 2006 . "Friction Dampers for seismic upgrade of a 14-story patient tower with a 36-foot tall soft story." Proc. of 8th U. S. National Conf. on Earthquake Engineering, EERI, Oakland, Calif., Paper No. 90.;

[13] Housner G.W. et al., "Structural control: past, present, and future." J. Engrg. Mech., ASCE, 123:897–971, 1997;

[14] Guangqiang Yang B.S., "Large-scale magnetorheological fluid damper for vibration mitigation: modeling, testing and control", PhD Thesis, University of Notre Dame, Indiana, 2001;

[15] Fisco N.R., Adeli H. , "Smart structures: Part I—Active and semi-active control", Scientia Iranica A, 18 (3), 275–284, 2011;

[16] Zapateiro De la Hoz M.F., "Semiactive control strategies for vibration mitigation in adaptronic systems equipped with magnetorheological dampers", PhD Thesis, Girona University, Spain, 2009;

[17] Spencer BF, Dyke SJ, Sain MK, Carlson JD. (1997) —Phenomenological Model of Magnetorheological Damper‖, Journal of Engineering Mechanics, Vol. 123, No. 3, March, pp. 230-238;

[18] Spencer BF, Yang G, Carlson JD, Sain MK. (1998) "'Smart' Dampers for Seismic Protection of Structures: A Full-Scale Study." Proc., 2nd World Conf. Struct. Control, Vol.1, 417-426;

[19] Dyke, S.J., Spencer Jr., B.F., Jr.,Sain, M.K., and Carlson, J.D. (1996a). "Modeling and control of magnetorheological dampers for seismic response reduction." Smart Mat. and Struct., 5:565–575;

[20] Dyke, S.J., Spencer Jr., B.F., Sain, M.K., and Carlson, J.D. (1996b). "Seismic response reduction using magnetorheological dampers." Proc. IFAC World Cong., vol. L, Int. Fed. of Automatic Control, pp. 145–150;

[21] Djajakesukma S. L., B. Samali B., Nguyen H., "Study of a semi-active stiffness damper under various earthquake inputs" Earthquake Engineering and Structural Dynamics Journal, 31:1757–1776, 2002;

[22] Yalla S.K., Kareem A., "Semiactive Tuned Liquid Column Dampers: Experimental Study" Journal of Structural Engineering, 129:7, 960-971, 2003;

[23] KITAGAWA Y., TAMAI H., TAKESHITA M., "Characteristics of piezoelectric dampers and their application to tall buildings as a smart structural system" 13th Worl Conference on Earthquake Engineering, Vancouver, Canada, 1-6 Aug., 2004;

[24] Garlock M, Sause R, Ricles J. Behavior and design of post-tensioned steel frames. J Struct Eng ASCE 2007;133(3):389–99;

[25] Ricles J, Sause R, Garlock M, Zhao C. Post-tensioned seismic resistant connections for steel frames. J Struct Eng ASCE 2001;127(2);

[26] Christopoulos C, Filiatrault A, Uang C-M, Folz B. Posttensioned energy dissipating connections for moment-resisting steel frames. J Struct Eng ASCE 2002;128(9): 1111–20;

[27] Garlock M, Ricles J, Sause R. Experimental studies on full-scale post-tensioned steel connections. J Struct Eng ASCE 2005;131(3);

[28] Chou CC, Chen JH, Chen YC, Tsai K-C. Evaluating performance of post-tensioned steel connections with high-strength strands. Earthquake Eng Struct Dyn 2006;35 (9):1167–85;

[29] Wolski M, Ricles J, Sause R. Experimental study of a self-centering beam–column connection with bottom flange friction device. J Struct Eng ASCE 2009;135(5): 479–88;

[30] Kim H-J, Christopoulos C. Seismic design procedure and seismic response of posttensioned self-centering steel frames. Earthquake Eng Struct Dyn 2009;38: 355–76;

[31] Kim H-J, Christopoulos C. Numerical models and ductile ultimate deformation response of posttensioned self-centering moment connections. Earthquake Eng Struct Dyn 2009;38:1–21;

[32] Uma SR, Pampanin S, Christopoulos C. Development of probabilistic framework for performance-based seismic assessment of structures considering residual deformations. J Earthquake Eng ASCE 2010;14(7):1092–111;

[33] Garlock MM, Ricles JM, Sause R, Peng SW, Zhao C, Lu L-W. Post-tensioned seismic resistant connections for steel frames. Proceedings of the structural stability research council conference workshop; 1998;

[34] Rojas P, Ricles JM, Sause R. Seismic performance of post-tensioned steel MRFs with friction devices. J Struct Eng ASCE 2005;131(4):529–40;

[35] Lin Y-C, Ricles J, Sause R, Seo C-Y. Earthquake simulations on a self-centering steel moment resisting frame with web friction devices. Proceedings of the ASCE structures congress, 2009;

[36] Kim H-J, Christopoulos C. Friction damped post-tensioned self-centering steel moment-resisting frames. J Struct Eng ASCE 2008;134(11):1768–79;

[37] Herning, G., Garlock, M.E.M., Vanmarcke, E., "Reliability-based evaluation of design and performance of steel self-centering moment frames". Journal of Constructional Steel Research 67 (2011), pp. 1495–1505;

[38] Chi, H., Liu, J., "Seismic behavior of post-tensioned column base for steel self-centering moment resisting frame". Journal of Constructional Steel Research 78 (2012), pp. 117–130;

[39] Roke, D., Jeffers, B., „Parametric study of self-centering concentrically-braced frame systems with friction-based energy dissipation", Stessa 2012 – Mazzolani & Herrera (eds), Taylor & Francis Group, London, pp. 691-696;

[40] Christopoulos, C., Tremblay, R., Kim, H.-J., Lacerte, M. (2008). „Self-Centering Energy Dissipative Bracing System for the Seismic Resistance of Structures: Development and Validation". JOURNAL OF STRUCTURAL ENGINEERING 134:1 (96);

[41] Braconi, A., Morelli, F., Salvatore, W. (2012). "Development, design and experimental validation of a steel self-centering device (SSCD) for seismic protection of buildings". Bull Earthquake Eng (2012) 10:1915–1941;

[42] Miller, D.J., Fahnestock, L.A., Eatherton, M.R., "Development and experimental validation of a nickel–titanium shape memory alloy self-centering buckling-restrained brace", Engineering Structures 40 (2012), pp. 288–298;

[43] Plumier, A., Doneux, C., Castiglioni, C., Brescianini, J., Crespi, A., Dell'Anna, S., Lazzarotto, L., Calado, L., Ferreira, J., Feligioni, S., Bursi, O., Ferrario, F., Sommavilla, M., Vayas, I., Thanopoulos, P., Demarco, T., „Two INnovations for Earthquake Resistant Design The INERD Project" – Final Report, 2004;

[44] Vayas, I., Karydakis, Ph., Dimakogianni, D., Dougka, G., Castiglioni, C.A., Kanyilmaz, A., Calado, L., Proença, J.M., Espinha, M., Hoffmeister, B., Rauert, T., Kalteziotis, O., „FUSEIS - Dissipative Devices for Seismic Resistant Steel Frames" - Design Guide, 2012;

[45] Ko, E., Field, C., „The Unbonded Brace™: From research to Californian practice";

[46] Wada, A., Saeki, E., Takeuchi, T., and Watanabe, A., 1998, "Development of Unbonded Brace," Nippon Steel's Unbonded Braces (promotional document), pp. 1–16, Nippon Steel Corporation Building Construction and Urban Development Division, Tokyo, Japan;

[47] PROHITECH, WP6 Report, Set-up of Advanced Reversible Mixed Technologies for Seismic Protection, edited D.Beg., P.Skuber. L.Pavlocic, University of Ljubljana Faculty of civil and geodetic engineering Slovenia;

[48] Brown, A.P.,Ian D. Aiken., F. Jeff Jafarzadeh, 2001, "Buckling Restrained Braces Provide the Key to the Seismic Retrofit of the Wallace F. Bennett Federal Building", to appear in Modern Steel Constructio;

[49] Bordea, S., "DUAL FRAME SYSTEMS OF BUCKLING RESTRAINED BRACES" – PhD Thesis, 2010;

[50] AISC/SEAOC Recommended Provisions for BRBF, Structural Engineers Association of Northern California - Seismology and Structural Standards Committee, Recommended Provisions for Buckling-Restrained Braced Frames (2001);

[51] Kiggins, S., Uang, C.-M. (2006). "Reducing Residual Drift of Buckling-Restrained Braced Frames as a Dual System." Engineering Structures, 28(11), 1525-1532;

[52] D. Vian, and M. Bruneau, 2004 "Testing of Special LYS steel plate shear walls," 13th World Conference on Earthquake Engineering, Vancouver, B.C., Canada, August 1-6, 2004, Paper No. 978, 2004;

[53] Shishkin, Driver and Grondin, 2005, Analysis of steel plate shear walls using the modified strip model, Department of Civil and Environmental Engineering University of Alberta Edmonton, Alberta, Canada, Structural Engineering Report No. 261, 2005;

[54] M.M. Alinia, M. Dastfan (2006), Behavior of thin steel plate shear walls regarding frame members, Journal of Constructional Steel Research 62 (2006) 730–738;

[55] Chih-Han Lin 1, Keh-Chyuan Tsai 2, Ying-Cheng Lin 3, Kung-Juin Wang 4, Wang-Da Hsieh 5, Yuan-Tao Weng 4, Bing Qu 6 and Michel Bruneau 7, 4th International Conference on Earthquake En gineering Taipei, Taiwan, October 12- 13, 2006, Paper No. 155;

[56] Mehdi H.K. Kharrazi, Helmut G.L. Prion, Carlos E. Ventura (2008), Implementation of M-PFI method in design of steel plate walls, Journal of Constructional Steel Research 64 (2008) 465–479;

[57] S. Sabouri-Ghomi and M. Gholhaki (2008), Ductility of thin steel plate shear walls, Asian Journal of Civil Engineering (Building and Housing), Vol. 9, No. 2 (2008), pg. 153-166;

[58] A. K. Bhowmick, R. G. Driver, G. Y. Grondin, 2009, Seismic analysis of steel plate shear walls considering strain rate and P- delta effects, Journal of Constructional Steel Research 65, 1149-1159, 2009;

[59] H.R. Habashi, M.M. Alinia, Characteristics of the wall_frame interaction in steel plate shear walls, Journal of Constructional Steel Research 66 (2010) 150_158;

[60] Alinia, M.M., Dastfan, M. "Cyclic behaviour, deformability and rigidity of stiffened steel shear panels", Journal of Constructional Steel Research 63 554–563, 2007;

[61] Celebi, M. (1997). "Response of Olive View Hospital to Northridge and Whittier Earthquakes", J. of Structural Engineering, ASCE, . v. 123 Apr. 97, p. 389-96, 1997;

[62] Neagu, C., "MULTI-STOREY BUILDING FRAMES STIFFENED WITH DISSIPATIVE SHEAR WALLS"- PhD Thesis, 2011;

[63] Bruneau M., "Self-centring steel plate shear walls", Steel Innovations Conference, Christshurch, New Zeeland, 21-22 Febr, 2013;

[64] David, S.O., Koboevic, S., "SEISMIC PERFORMANCE OF ECCENTRICALLY BRACED FRAMES DESIGNED FOR CANADIAN CONDITIONS"- The 14 th World Conference on Earthquake Engineering October 12-17, 2008, Beijing, China;

[65] nexus.globalquakemodel.org;

[66] web.iku.edu.tr;

[67] Choi, J., Stojadinovic, B., Goel, S.C., "Development of free flange moment connection." Report No. UMCEE 00-15, Department of Civil and Environmental Engineering, The University of Michigan, Ann Arbor, MI, 2002;

[68] OKAZAKI, T., ENGELHARDT, M.D., NAKASHIMA, M., SUITA, K., "EXPERIMENTAL STUDY ON LINK-TO-COLUMN CONNECTIONS IN STEEL ECCENTRICALLY BRACED FRAMES", 13th World Conference on Earthquake Engineering Vancouver, B.C., Canada, August 1-6, 2004;

[69] Clifton C., Bruneau M., MacRae G., Leon R., Fussell A., "Steel structures damage from the Christchurch earthquake series of 2010 and 2011". BULLETIN OF THE NEW ZEALAND SOCIETY FOR EARTHQUAKE ENGINEERING, Vol. 44, No. 4, December 2011;

[70] Bruneau M., Anagnostopoulou M., MacRae G., Clifton C., Fussell A., "Preliminary Report On Steel Building Damage From The Darfield Earthquake Of September 4, 2010", Bulletin of the New Zealand Society for Earthquake Engineering, Vol. 43, No. 4, pp.351-359, 2010;

[71] Mansour, N., "DEVELOPMENT OF THE DESIGN OF ECCENTRICALLY BRACED FRAMES WITH REPLACEABLE SHEAR LINKS"- PhD Thesis, 2010;

[72] Ghobarah, A., Ramadan, T., „Bolted link-column joints in eccentrically braced frames". Engineering Structures, Vol.16 No.1, 1994, pp. 33-41;

[73] Balut, N., Gioncu, V., "Suggestion for an improved 'dog-bone' solution". STESSA 2003, Proc. of the Conf. on Behaviour of Steel Structures in Seismic Areas, 9-12 June 2003, Naples, Italy, Mazzolani (ed.), A.A. Balkema Publishers, p. 129-134;

[74] Stratan, A., Dubina, D., "Bolted links for eccentrically braced steel frames". Proc. of the Fifth AISC / ECCS International Workshop "Connections in Steel Structures V. Behaviour, Strength & Design", June 3-5, 2004. Ed. F.S.K. Bijlaard, A.M. Gresnigt, G.J. van der Vegte. Delft University of Technology, The Netherlands, pp. 223-232;

[75] Dubina, D., Stratan, A., Dinu, F., "Dual high-strength steel eccentrically braced frames with removable links". Earthquake Engineering & Structural Dynamics, Vol. 37, No. 15, p. 1703-1720, 2008;

[76] Vargas, R., Bruneau, M., "Seismic design of multi-story buildings with metallic structural fuses". Proceedings of the 8th U.S. National Conference on Earthquake Engineering, April 18-22, 2006, San Francisco, California, USA. Paper No. 280;

[77] Kiggins, S., Uang, C.-M., "Reducing residual drift of buckling-restrained braced frames as a dual system". Engineering Structures, 28 (2006) 1525–1532;

[78] EN1990, Eurocode, Basis of structural design, CEN, European Committee for Standardization, 2002;

[79] EN1991-1-1, Eurocode 1, Actions on structures - Part 1-1: General actions Densities, self-weight, imposed loads for buildings, CEN, European Committee for Standardization, 2002;

[80] EN1992-1-1, Eurocode 2, Design of concrete structures - Part 1-1: General rules and rules for buildings, CEN, European Committee for Standardization, 2004;

[81] EN1993-1-1, Eurocode 3, Design of steel structures - Part 1-1: General rules and rules for buildings, CEN, European Committee for Standardization, 2005;

[82] EN1994-1-1, Eurocode 4, Design of composite steel and concrete structures Part 1-1: General rules and rules for buildings, CEN, European Committee for Standardization, 2004;

[83] Stratan A., Ciutina A., Dogariu A., Guidelines for designing steel eccentrically braced frames with removable bolted links, 2008;

[84] SeismoSoft, SeismoStruct v6.5 - A computer program for static and dynamic nonlinear analysis of framed structures, www.seismosoft.com;

[85] Stratan A, Dubina D. Bolted links for eccentrically braced steel frames. Proc. of the Fifth AISC / ECCS International Workshop "Connections in Steel Structures V. Behaviour, Strength & Design", June 3-5, 2004. Ed. Bijlaard FSK, Gres-nigt AM, van der Vegte GJ. Delft University of Technology, The Netherlands, pp. 223-232;

[86] Fajfar P., "A nonlinear analysis method for performance-based seismic design", Earthquake Spectra, 16(3):573-592, 2000;

[87] FEMA 356, "Prestandard and commentary for the seismic rehabilitation of buildings", Federal Emergency Management Agency and American Society of Civil Engineers, Washington DC, USA, 2000;

[88] Stratan A., Dinu F., Dubina D., "Replacement of bolted links in dual eccentrically braced frames", 14th European Conference on Earthquake Engineering, August 30 – September 3, 2010, Ohrid, Republic of Macedonia;

[89] Akkar S, Sandıkkaya MA, Şenyurt M, Azari Sisi A, Ay BÖ, Traversa P, Douglas J, Cotton F, Luzi L, Hernandez B, Godey S. (2014). Reference database for seismic ground-motion in Europe (RESORCE), Bulletin of Earthquake Engineering, DOI: 10.1007/s10518-013-9506-8, Volume 12, Issue 1, pp 311-339;

[90] Stratan, A., Dubina, D., "Bolted links for eccentrically braced steel frames". Proc. of the Fifth AISC / ECCS International Workshop "Connections in Steel Structures V. Behaviour, Strength & Design", June 3-5, 2004. Ed. F.S.K. Bijlaard, A.M. Gresnigt, G.J. van der Vegte. Delft University of Technology, The Netherlands, pp. 223-232;

[91] Dubina, D., Stratan, A., Dinu, F., "Dual high-strength steel eccentrically braced frames with removable links". Earthquake Engineering & Structural Dynamics, Vol. 37, No. 15, p. 1703-1720, 2008;

[92] NEHRP (2003). NEHRP Recommended provisions for new buildings and other structures (FEMA 450). Part 1: Provisions and Part 2: Commentary. Building Seismic Safety Council, National Institute of Building Sciences, Washington, D.C.;

[93] P100-1/2013 (2013). Seismic design code – Part 1: Rules for buildings (in Romanian);

[94] Stratan, A., Ioan, A., Dubina, D. (2012). Re-centring capability of dual eccentrically braced frames with removable bolted links. STESSA 2012 (Behaviour of Steel Structures in Seismic Areas) Conference, 9-11 January 2012, Santiago, Chile, pp. 723-728;

[95] Ioan, A., Stratan, A., Dubina, D. (2013). Numerical Simulation of bolted links removal in eccentrically braced frames. Pollack Periodica - Vol. 8, No.1, 2013, p. 15-26;

[96] ISO 6892-1, International Standard, Metallic materials – Tensile testing – Part 1: Method of test at room temperature, 2009;

[97] DUAREM – Full-scale experimental validation of dual eccentrically braced frame with removable links - TA Project Final Report – G. Sabau, M. Plojansek, F. Taucer, D. Tirelli, A. Ioan, A. Stratan, D. Dubina, 2014;

[98] EN 1090-2, European Standard, Execution of steel structures and aluminium structures - Part 2: Technical requirements for steel structures, 2008;

[99] ISO 2768-1: General tolerances – Part 1: Tolerances for linear and angular dimensions without individual tolerance indications, 2001;

[100] Pegon P, Molina FJ, Magonette G. Continuous pseudo-dynamic testing at ELSA in "Hybrid Simulation; Theory, Implementation and Applications", Eds. Saouma VE, Sivaselvan MV, Taylor & Francis/Balkema Publishers, 2008, 79-88;

[101] Stratan A., „Dual multi-storey steel frame buldings in seismic areas behaviour study", PhD Thesis, 2003;

[102] Richards P., Uang C., "Testing Protocol for Short Links in Eccentrically Braced Frames." Journal of Structural Engineering, 132(8), 1183–1191, 2006;

[103] Sullivan T., Quaini M., Maleyb T., Calvi G.M., "Deformed shapes of steel moment resisting frames subjected to earthquake actions" Eurosteel 2011, 31 Aug. – 2 Sept., Budapest, Hungary, 2011;